# QUANTITATIVE MASS SPECTROMETRY-BASED (CHEMO-)PROTEOMICS FOR THE CHARACTERIZATION OF MEP PATHWAY INHIBITORS

**Dissertation**

Zur Erlangung des Grades

des Doktors der Naturwissenschaften

der Naturwissenschaftlich-Technischen Fakultät

der Universität des Saarlandes

von

**M. Sc. Lorenzo Bizzarri**

Saarbrücken

2025

| | |
|---|---|
| **Tag des Kolloquiums:** | 27.02.2025 |
| **Dekan:** | Prof. Dr.-Ing. Dirk Bähre |
| **Berichterstatter:** | Prof. Dr. Anna K. H. Hirsch<br>Prof. Dr. Rolf Müller |
| **Akad. Mitglied:** | Dr. Stefan Boettcher |
| **Vorsitz:** | Prof. Dr. Martin Empting |

Die vorliegende Arbeit wurde von Januar 2021 bis Juli 2024 unter Anleitung von Dr. Hannes Hahne, Mitbegründer und Gesellschafter der OmicScouts GmbH und Univ.- Prof. Dr. Anna K. H. Hirsch in der Fachrichtung Pharmazeutische und Medizinische Chemie der Naturwissenschaftlich-Technischen Fakultät der Universität des Saarlandes, sowie am Helmholtz-Institut für Pharmazeutische Forschung Saarland (HIPS) in der Abteilung Drug Design and Optimization (DDOP) angefertigt.

*"Non c'è uomo più libero di colui che ha deciso di mettersi in cammino, perché il viaggio non è solo percorrere terre, ma conquistare se stessi."*

*Anonimo*

# Acknowledgements

First and foremost, I wish to express my deepest gratitude to Dr. Hannes Hahne for the incredible opportunity to undertake my PhD within his company and for the invaluable time and guidance he provided throughout my journey.

I extend my sincere thanks to Prof. Dr. Anna K. H. Hirsch for supervising my research and offering invaluable insights that greatly enriched my work.

I am also deeply grateful to Prof. Dr. Rolf Müller and Dr. Andreas Kany for being part of my thesis committee meetings, offering thoughtful feedback and guidance.

A special acknowledgment goes to my first internal supervisor and dear friend, Dr. Jonas Lohse. Thank you for your wise counsel and constant support from the very beginning of this adventure. Your guidance has been a cornerstone of my progress, and I will carry your advice forward in my career.

I would also like to thank everyone involved in the MepAnti project for their exceptional collaboration and dedication throughout our PhD. I hold cherished memories of our time together, and I sincerely hope our paths cross again. My heartfelt appreciation goes to Victor Gawriljuk, Camilla Ornago, Lucia D'Auria, Thibaut Quennesson, Maria Braun Cornejo, Gabriella Ines Bianchino, Bruna Schuck, and Vidhisha Sonawane. A special mention to Patricia Bravo for your unwavering dedication and the supportive partnership we shared, navigating challenges that turned into meaningful accomplishments. A big thank you to Antoine Lacour and Daan Willocx for their wonderful camaraderie; the time spent with you was both fun and uplifting. You all made difficult moments easier to bear, and working with you was immensely fulfilling.

To my colleagues at OmicScouts, thank you for the support and the many laughs we shared, particularly Dominik, Johanna, Catalina, Janine, Theresa, and Leonie.

I am also grateful to my flatmates in Freising: Andreas, Austin, and Gaon. The joyful times we spent together will be dearly missed.

To my lifelong friends, Lorenzo Marta, Filippo Bossi, Daniele, Luisa, Filippo Castrini, and Lorenzo Arrais, thank you for your unwavering support and true friendship. You have been pillars of strength over the years, and our shared memories are among my most treasured. I hope this friendship continues to thrive for years to come.

To my family, my mother Valentina, my sister Arianna, and my father Stefano. Your constant love and support have been my anchor. Thanks to your encouragement, I have achieved my goals, and for that, I am eternally grateful.

Lastly, to Clarissa. Your support through these years, in both good and challenging times, has been invaluable. Even when distance separated us, I felt your unwavering presence. I owe you so much, perhaps everything, and I am beyond thankful to have you by my side as I reach this milestone.

# Publications of the Author Included in This Thesis

Publication A: Bizzarri, L.; Sonawane, V.; Haupenthal, J; Lohse, J.; Reiling, N; Hirsch, A. K. H.; Hahne, H. Comprehensive Proteomic Profiling of Human Pathogens and CRISPRi-Driven Gene Modulation in *Mycobacterium tuberculosis*. Manuscript in preparation.

Contribution see Chapter 3.1

Publication B: Bizzarri, L.; Willocx, D.; Cornejo, B. M.; Lohse, J.; Hirsch, A. K. H.; Hahne, H. Affinity-Based Chemoproteomics for Bacterial Target Identification. Manuscript in preparation.

Contribution see Chapter 3.2

Publication C: Bizzarri, L.; Steinbrunn, D.; Quennesson, T.; Lacour, A.; Bianchino, G. I.; Bravo, P.; Chaignon, P.; Lohse, J.; Mäser, P.; Seemann, M.; Calenbergh, S. Van; Hirsch, A. K. H.; Hahne, H. Studying Target–Engagement of Anti-Infectives by Solvent-Induced Protein Precipitation and Quantitative Mass Spectrometry. *ACS Infect. Dis.* 2024. https://doi.org/10.1021/acsinfecdis.4c00417.

Contribution see Chapter 3.3

Publication D: Bravo, P.;⊥ Bizzarri, L.;⊥ Steinbrunn, D.; Lohse, J.; Hirsch, A. K. H.; Mäser, P.; Rottmann, M.; Hahne, H. Integral Solvent-Induced Protein Precipitation for Target-Engagement Studies in *Plasmodium Falciparum*. *ACS Infect. Dis.* 2024. https://pubs.acs.org/doi/10.1021/acsinfecdis.4c00418.

Contribution see Chapter 3.4. (⊥ these authors contributed equally).

# Publications of the Author Not Included in This Thesis

Willocx, D.; Bizzarri, L.; Alhayek, A.; Kannan, D.; Bravo, P.; Illarionov, B.; Rox, K.; Lohse, J.; Fischer, M.; Kany, A. M.; Hahne, H.; Rottmann, M.; Witschel, M.; John, A. O.; Hamed, M. M.; Diamanti, E.; Hirsch, A. K. H. Targeting *Plasmodium Falciparum* IspD in the Methyl-d-Erythritol Phosphate Pathway: Urea-Based Compounds with Nanomolar Potency on Target and Low-Micromolar Whole-Cell Activity. *J. Med. Chem.* 2024. https://pubs.acs.org/doi/10.1021/acs.jmedchem.4c00212.

Bravo, P; Bizzarri, L; Wiedemar, N.; Pessecker, A; Brancucci, N; Albisetti, A; Gumpp, C; Fischli, C; Curtrufello, R; Diamanti, E; Mostafa, H; Witschel, M; Hahne, H; A. K. H., Hirsch, Mäser, P; Rottmann, M. Hydroxy Benzamides: Mechanisms of Action and Resistance in *Plasmodium falciparum*. Manuscript in preparation.

# Summary

A critical bottleneck in early drug discovery of new agents for both bacterial and malarial pathogens is the challenge of accurately identifying protein targets, confirming target–engagement, and evaluating selectivity profiles. To that end, quantitative mass spectrometry-based proteomics (LC-MS/MS) is a powerful tool for acquiring comprehensive and unbiased information on protein expression and protein–drug interactions on a proteome-wide scale.

As part of the MepAnti research program, global proteomic profiling was conducted on six human pathogens (*Mycobacterium tuberculosis*, *Escherichia coli*, *Klebsiella pneumoniae*, *Pseudomonas aeruginosa*, *Staphylococcus aureus*, and *Plasmodium falciparum*) to assess the detectability and abundance of the 2-*C*-methyl-D-erythritol 4-phosphate (MEP) pathway enzymes using LC-MS/MS. Subsequently, compound–protein interactions were characterized across multiple chemical classes developed within the MepAnti Consortium. Initially, we employed conventional probe-based chemoproteomics. However, this method can present challenges, as the protein targets may not be effectively enriched due to potential losses in activity and selectivity during the probe-design process. To overcome these limitations, integral solvent-induced protein precipitation (iSPP) was evaluated and subsequently employed. This biophysical proteomics approach measures changes in protein stability in response to solvent-induced precipitation in the presence of ligands, facilitating the identification of compound–protein targets. iSPP is a modification-free approach, eliminating the need for compound functionalization, and is suitable for application to hard-to-culture pathogens characterized by slow growth rates and limited protein yields.

Overall, this thesis underscores the pivotal role of chemo- and biophysical proteomics in advancing early-stage drug discovery for anti-infective agents.

# Zusammenfassung

Ein entscheidender Engpass in der frühen Wirkstoffentwicklung für bakterielle und malariabedingte Krankheitserreger ist die präzise Identifizierung von Protein-Zielen, die Bestätigung der Zielbindung (Target Engagement) und die Bewertung der Selektivitätsprofile. Die quantitative, massenspektrometrie-basierte Proteomik (LC-MS/MS) ist ein effizientes Werkzeug, um umfassende und unverfälschte Informationen über Proteinexpression und Protein-Wirkstoff-Interaktionen auf proteomweiter Ebene zu gewinnen.

Im Rahmen des MepAnti-Forschungsprogramms wurde eine globale Proteomprofilierung an sechs humanpathogenen Organismen (*Mycobacterium tuberculosis*, *Escherichia coli*, *Klebsiella pneumoniae*, *Pseudomonas aeruginosa*, *Staphylococcus aureus* und *Plasmodium falciparum*) durchgeführt, um die Nachweisbarkeit und Häufigkeit der Enzyme des 2-*C*-Methyl-D-Erythritol-4-phosphat (MEP)-Stoffwechsels mittels LC-MS/MS zu bewerten. Im Anschluss daran wurden Wirkstoff-Protein-Interaktionen über mehrere chemische Klassen hinweg charakterisiert, die innerhalb des MepAnti-Konsortiums entwickelt wurden. Zunächst wurde die klassische, auf Sonden basierende Chemoproteomik eingesetzt. Allerdings können bei dieser Methode Herausforderungen auftreten, da die Zielproteine aufgrund möglicher Aktivitäts- und Selektivitätsverluste während des Sondendesigns nicht effektiv angereichert werden könnten. Um diese Einschränkungen zu überwinden, wurde die integral solvent-induced protein precipitation (iSPP) evaluiert und anschließend eingesetzt. Dieser biophysikalische proteomische Ansatz misst Änderungen in der Protein-Stabilität als Reaktion auf lösungsmittelinduzierte Präzipitation in Anwesenheit von Liganden und erleichtert die Identifizierung von Wirkstoff-Protein-Zielen. iSPP ist eine modifikationsfreie Methode, die keine Wirkstofffunktionalisierung erfordert und sich für schwer zu kultivierende Krankheitserreger mit langsamen Wachstumsraten und begrenzten Proteinausbeuten eignet.

Zusammenfassend unterstreicht diese Dissertation die zentrale Rolle von chemo- und biophysikalischer Proteomik bei der Förderung der Wirkstoffentwicklung in der Frühphase für Antiinfektiva.

# List of Abbreviations

| | |
|---|---|
| °C | degree Celsius |
| ABPP | activity-based protein profiling |
| ABPs | activity-based probes |
| ACTs | artemisinin combination therapies |
| AMR | antimicrobial resistance |
| ART | artemisinin |
| AUC | area under the curve |
| BCA | bicinchoninic acid |
| CDP-ME | 4-diphosphocytidyl-2-C-methylerythritol |
| CETSA | cellular thermal-shift assay |
| CID | collision-induced dissociation |
| CuAAC | copper-catalyzed azide-alkyne cycloaddition |
| DDA | data-dependent acquisition |
| DIA | data-independent acquisition |
| DMADP | dimethylallyl diphosphate |
| DMSO | dimethyl sulfoxide |
| DTT | dithiothreitol |
| *Ec* | *Escherichia coli* |
| ESI | electron spray ionization |
| FA | formic acid |
| HPLC | high-pressure liquid chromatography |
| HTS | high-throughput screening |
| IAA | iodoacetamide |
| $IC_{50}$ | half-maximal inhibitory concentration |
| IDP | isopentenyl diphosphate |
| IspD | 4-diphosphocytidyl-2C-methyl-D-erythritol synthase |
| $K_m$ | Michaelis constant |
| LC | liquid chromatography |
| LC-MS/MS | liquid chromatography-tandem mass spectrometry |
| LFQ | label-free quantification |
| MEP: | 2-C-methylerythritol-D-erythritol-4-phosphate |
| MIC | minimum inhibitory concentration |
| µM | micromolar |
| MoA | mechanism of action |
| MS | mass spectrometry |
| m/z | mass-to-charge ratios |
| NGS | next-generation sequencing |
| PAL | photoaffinity labeling |
| PBP | penicillin-binding protein |
| *Pf* | *Plasmodium falciparum* |
| PSM | peptide-spectrum match |
| PTM | post-translational modification |
| RT | retention time |
| SAR | structure–activity relationship |
| SPE | solid-phase extraction |
| SPP | solvent-induced protein precipitation |
| TCEP | tris(2-carboxyethyl)phosphine |
| TIC | total ion chromatogram |
| TMT | tandem mass tags |
| TPP | thermal protein profiling |
| WHO | World Health Organization |

# Table of Contents

# 1. INTRODUCTION

## 1.1 Anti-infectives

### 1.1.1 Emerging Antimicrobial Resistance

Antibiotic therapy to treat bacterial infections stands as one of the most impactful medical advancements and breakthroughs in human history. Before the discovery of antibiotics, infections accounted for more than half of all deaths worldwide.[1] The advent of antibiotics, alongside other infection-control measures, greatly reduced mortality rates by directly eliminating infections and enabling life-saving medical procedures.[2]

Similar to bacterial infections, malaria is one of the most critical infectious diseases, exerting its greatest toll in sub-Saharan Africa, where it accounts for 95% of malaria cases and deaths globally. Young children and pregnant women are the most vulnerable and affected by this disease.[3] The large majority of these cases and nearly all fatalities are caused by *Plasmodium falciparum*, the most virulent human malaria parasite.[4] Due to advancements in malaria control and elimination, such as rapid diagnosis, promotion of mosquito nets and insecticides, artemisinin-based combination therapies, and development of vaccines, there has been a 40% decrease in malaria incidence and a 60% reduction in mortality rate in the African regions between 2000 and 2022.[3]

However, the effectiveness of treatments for these infectious diseases is gradually diminishing due to the emergence of antimicrobial resistance (AMR). Recognized by the World Health Organization (WHO) as one of the primary global threats, AMR is a rapidly escalating global challenge. It occurs as bacteria, fungi, viruses, and parasites evolve over time, acquiring new mechanisms to evade antimicrobial treatments. The development of resistance against anti-infectives is closely associated with the misuse of anti-infective drugs and/or incomplete drug regimens, with genetic mutations serving as the primary AMR mechanism.[2,5–7]

Specifically, antibiotic resistance has underscored the urgent need to prudently manage the use of antibiotics, as well as the implementation of policies aimed at reducing their usage in food animal production across various nations.[8] Unfortunately, due to scientific and economic challenges, the pace at which new antibiotics are brought to market and delivered to health-care workers and patients is at its lowest point in 80 years.[2] Over the past two decades, only two new antibiotic classes (lipopeptides and oxazolidinones) have been developed and approved by international drug agencies (US Food and Drug Administration and European Medicines Agency), both effective against Gram-positive bacteria. The quinolones, discovered in 1962, represent the most recent novel drug class identified to be active against Gram-negative bacteria.[9] Consequently, there is widespread concern that due to the lack of innovation in the antibiotic drug-discovery and development pipeline, we may be approaching a post-antibiotic era. In this scenario, infections that were routinely treated with drugs discovered in the 20$^{th}$ century may become untreatable in the 21$^{st}$ century.[2]

Current antibiotics target crucial processes in the bacterial life cycle, including cell wall synthesis, DNA replication, and protein biosynthesis.[9,10] This redundancy leads to selection pressure on bacteria, thereby promoting the development of resistance.[11] Notably, extensive surveys assessing various antibiotics against numerous commensal bacteria revealed that almost all the tested drugs adversely affect gut commensals.[12] This disruption of the gut microbiome, known as gut dysbiosis, has been associated with both Gram-positive-only and broad-spectrum antibiotics.[13] Such perturbations can increase susceptibility to colonization by opportunistic pathogens like *Clostridioides difficile*[14] and elevate the risk of gastrointestinal, renal, and hematological abnormalities.[15,16]

Likewise, many challenges are emerging in the fight against malaria in Africa, such as climate change, poverty, inadequate health services and coverage, increased outdoor transmission, emergence of new vectors, and the growing threat of resistance to antimalarial drugs and insecticides. [5] In 2022 alone, there were 249 million cases of malaria worldwide, resulting in an estimated 608,000 deaths. [3] Drug-resistant *P. falciparum* has emerged for virtually all antimalarial drugs, including chloroquine, quinoline, sulfadoxine–pyrimethamine, mefloquine, and the crucial artemisinin (ART), pivotal in the current first-line treatment of artemisinin combination therapies (ACTs).[17] However, the efficacy of ACT is compromised if resistance develops to both artemisinins and their partner drugs within ACTs.

As a result, emerging drug resistance has prompted an urgent search for new anti-infective drugs and novel drug targets. Specifically, there is a pressing need for drugs featuring a novel mechanism of action. Blocking the biosynthesis of various essential metabolites can be bactericidal and has drawn close attention from many research groups. The validation of multiple targets across various biosynthetic pathways has greatly propelled this strategy.[18]

### 1.1.2 Methylerythritol Phosphate Pathway as Source of Drug Targets

Comprising over 55,000 molecules, isoprenoids, also known as terpenoids, represent one of the largest classes of natural products known to date.[19] Regardless of complexity, all members of this group share common five-carbon isoprene building blocks, namely, isopentenyl diphosphate (IDP) and dimethylallyl diphosphate (DMADP). Isoprenoids have been identified across the three domains of life (bacteria, archaea and eukaryotes) and play essential roles in a variety of ubiquitous cellular processes. Among others, they are responsible for transcription and post-translational modifications, cell-wall biosynthesis, electron transport, photosynthesis, intracellular signaling, secreted defense mechanisms, and protein degradation.[19]

For many years, the mevalonate pathway was universally acknowledged as the sole source of isoprenoid building blocks starting from the condensation of two molecules of acetyl-coenzyme A (CoA). In the early 1990s, an alternative pathway, the Methylerythritol Phosphate (MEP) pathway, was discovered by the research groups of Rohmer[20,21] and Arigoni.[22] This pathway was shown to utilize entirely different starting materials, namely, pyruvate and D-glyceraldehyde 3-phosphate (Figure 1). Following the discovery of the MEP pathway, extensive research has been conducted to investigate the taxonomic distribution of both pathways.[23] These studies have revealed that while the mevalonate pathway is used by humans, animals, archaebacteria, and fungi, the MEP pathway serves as the exclusive source of IDP and DMADP for green algae and numerous pathogenic bacteria and apicomplexan protozoa, including important human pathogens such as *Mycobacterium tuberculosis*, *Klebsiella pneumoniae*, *Pseudomonas aeruginosa* and *P. falciparum*.[24] Interestingly, higher plants use both pathways.

The distinct distribution of these pathways among organisms, coupled with the essential role of the MEP pathway in several infectious-disease-causing organisms,[24,25] has motivated scientists to focus on targeting the enzymes of the MEP pathway on the way to the development of novel anti-infective agents as well as novel and more potent herbicides.[26]

The MEP pathway consists of seven enzymes and has unveiled a series of unusual and even unprecedented enzymatic reactions, such as the two single-electron reduction and concomitant hydroxy-group elimination reactions catalyzed by the [4Fe-4S] cluster-containing metalloenzymes IspG and IspH. Interestingly, according to Wang and Dowd,[25] the MEP enzymes DXS, DXR, and

IspF have emerged as promising drug targets for tuberculosis. Each of these enzymes is deemed essential for bacterial viability in *M. tuberculosis* and exhibits druggable binding pockets.[25,27]

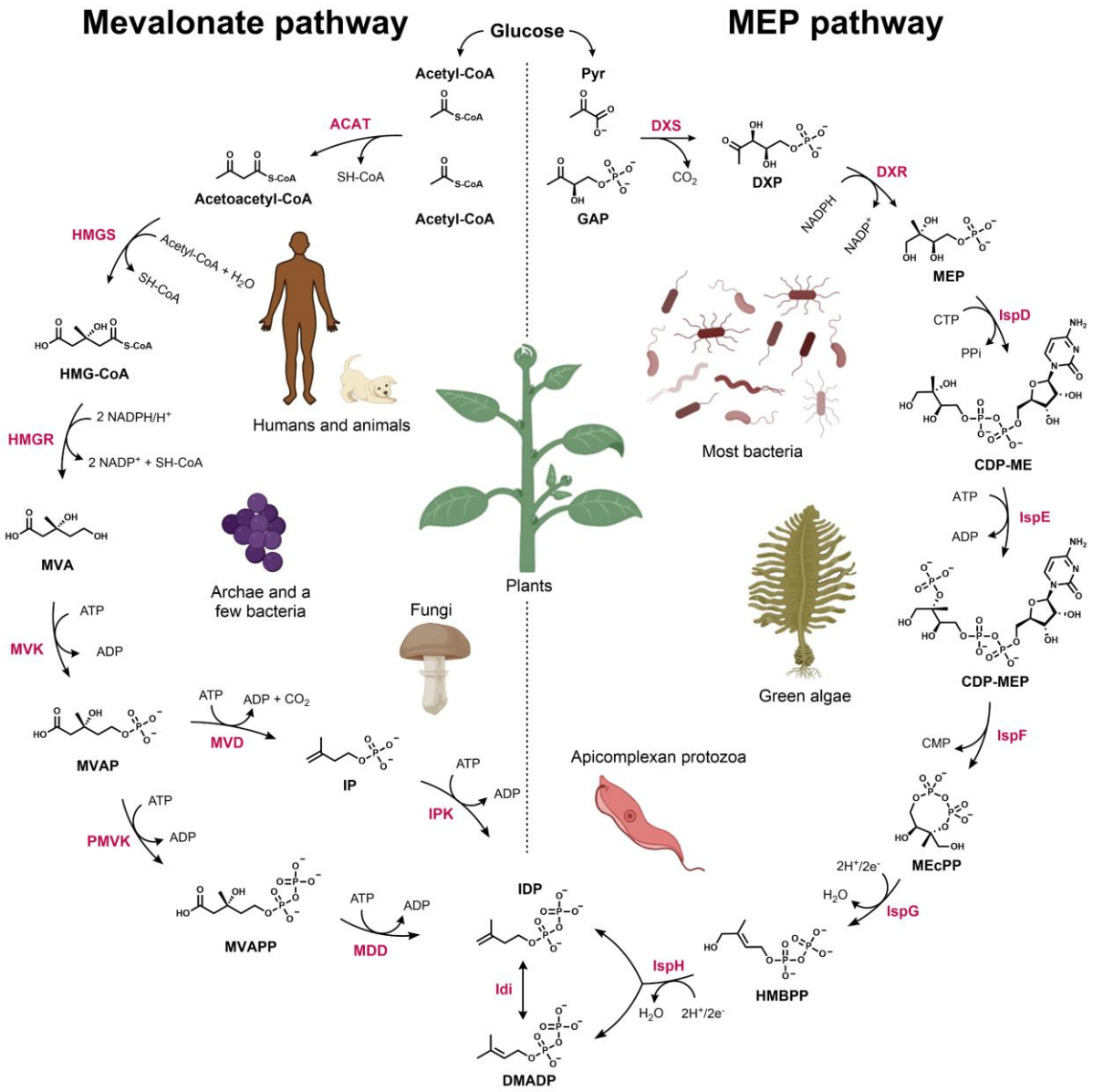


**Figure 1**. Isoprenoid precursor biosynthetic pathways. Isoprenoids are essential metabolites in all kingdoms of life. Their biosynthesis occurs by two distinct pathways: Methylerythritol Phosphate (MEP) (right) and Mevalonate (left). The Mevalonate pathway is found in higher, complex organisms including animals and fungi, as well as in archaea and some bacteria. Most other prokaryotes and the eukaryotic apicomplexa, including many major pathogens, make use of the MEP pathway. Plants show compartmentalized isoprenoid biosynthesis in their cytosol (Mevalonate) and plastids (MEP). Figure created with ChemDraw.

Nevertheless, despite the important functions served by the MEP pathway and its enzymes, only a few inhibitors have been reported so far. Importantly, fosmidomycin,[28–30] a potent inhibitor of the second enzyme of the pathway, DXR, has undergone phase II clinical trials as antimalarial chemotherapeutic agent in combination with clindamycin and piperaquine,[31–33] validating the enzymes of the MEP pathway as viable drug targets.

## 1.2 Proteomics and Quantitative Mass Spectrometry

Proteomics[34] offers a distinct approach to genomic and transcriptomic technologies, allowing for the comprehensive analysis of biological processes at the protein level. Proteins are the primary biochemically active components in biological systems,[35] and the majority of small molecule drugs and biologics exert their effects on protein targets. These proteins do not function independently; instead, they are part of cellular pathways and networks, forming intricate physical and functional connections with various other proteins and cellular components.[36] Thus, analytical methods to assess the activities and functions of proteins[37,38] are highly valuable for drug discovery. These methods help to elucidate the effects of drug candidates on their protein targets and determine how to specifically interfere with disease phenotypes.[36]

The two key challenges in proteomics are the vast number of proteins within a cell and their wide dynamic range (difference between most and least abundant proteins) of expression, which spans four to five orders of magnitude in prokaryotes, six to seven orders in eukaryotic cells and tissues, and up to twelve orders of magnitude in body fluids.[39–41] Additionally, proteins undergo post-translational modifications (PTMs), which significantly increase the diversity of distinct protein entities, known as proteoforms, in a sample. Proteoforms refer to the different isoforms of a protein product derived from a single gene. These variations arise not only from PTMs but also from alternative splicing and other processing events. This diversity adds complexity to sample handling and analysis, as it results in a wide range of protein forms with distinct structural and functional characteristics. In contrast to eukaryotic proteins (including *P. falciparum*), most PTMs occur on a relatively smaller subset of bacterial proteins, and the majority of these modified proteins exhibit low, substoichiometric levels of modification.[42] Consequently, analyzing their structure and function poses significant challenges. However, growing evidence suggests that protein PTMs play crucial roles in various cellular processes in bacteria.[42]

The two primary methods for detecting and quantifying proteins are (1) affinity reagent-based techniques, such as ELISA, Western blotting, or immunohistochemistry staining, and (2) mass spectrometry (MS)-based identification and quantification, primarily utilized in research and discovery proteomics. The assays in (1) have limitations in their dynamic range and the number of proteins they can quantify, with potential challenges in achieving broad proteome coverage and sensitivity.[43] While these techniques are highly specific to target proteins, their ability to detect and quantify a wide range of proteins simultaneously is limited. These methods heavily rely on specific antibodies, leading to low throughput and the requirement for prior hypotheses to select proteins of interest. However, recent advancements in affinity-based proteomics technologies, such as Olink's Proximity Extension Assay (PEA)[44] and Somalogic's Slow Off-rate Modified Aptamer-based (SOMAmer)[45] platform, have addressed some of these limitations by enabling the simultaneous quantification of thousands of proteins with high sensitivity and specificity, even from small sample volumes. Additionally, emerging platforms like Nautilus Biotechnology offer an innovative approach by analyzing proteins at the single-molecule level,[46,47] allowing for the direct measurement of individual protein molecules with unprecedented sensitivity and a broader dynamic range. This technology uses massively parallel readouts to capture and quantify a vast number of proteins simultaneously, potentially offering deeper insights into the proteome than traditional methods.

(2) offers an alternative to affinity reagent-based techniques, emerging as a powerful tool for studying drug-protein interactions, protein-protein interactions (PPIs), PTMs, and disease biomarkers, among others.[35,36,48] MS-based bottom-up proteomics allows comprehensive analysis of highly complex proteomes in a hypothesis-free manner, enabling the identification and quantification of thousands of proteins within a single experiment.[49–52] Over the past two decades, technological advancements

have dramatically improved proteomic depth and throughput. Firstly, there has been a substantial enhancement in instrumentation, characterized by the introduction of robust and high-throughput liquid chromatography (LC) systems,[53] alongside the development of new types of mass spectrometers that enable peptide separation by ion mobility.[54–56] Secondly, these advances have been accompanied by the development of high-throughput data- acquisition techniques[57–61] and a spread of computational methods for proteomics data analysis.[62–64]

### 1.2.1 Basics of Bottom-up Proteomics

Bottom-up proteomics, which identifies and quantifies proteins by measuring peptides, is the predominant proteomic method for analyzing complex biological samples. In contrast, top-down proteomics involves analyzing intact proteins directly. While bottom-up proteomics offers greater sensitivity and broader proteome coverage, top-down measurements provide more detailed information on protein isoforms and PTMs.[38,65]

The following paragraphs provide insights into classical bottom-up workflows. Various preparation steps can be performed, depending on the sample type and the experiment's objectives. Certain steps are elucidated further, with particular attention given to the methodologies employed in this study.

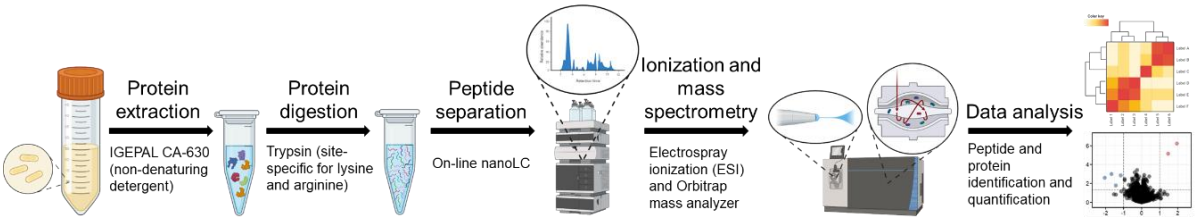


**Figure 2**. Bottom-up proteomics workflow for biochemical assays. Proteins are extracted from biological samples (e.g., mammalian cells, tissues, bacteria) and then digested enzymatically using the protease Trypsin. The resulting peptide mixture is separated by an on-line liquid chromatography setup (nanoLC) and peptides are ionized via nano electrospray ionization (nano-ESI). Mass-to-charge ratios (m/z) of peptide precursors and fragments are measured by tandem mass spectrometry via orbitrap mass-analyzer. Peptide and protein identification and label-free quantification is performed using DIA-NN or MaxQuant, depending on the acquisition method. Figure created with Biorender.com.

#### Protein extraction and digestion

Proteomic sample preparation generally begins with the extraction of proteins from their cellular context (Figure 2), which can vary depending on the type of sample (e.g., tissues, body fluids, cell lines) and the downstream assays (native or denaturing lysis conditions). In addition to mechanical methods for cell disruption, non-mechanical methods such as chemical lysis can be employed. Commonly used detergents include sodium dodecyl sulfate (SDS, denaturing) and non-ionic IGEPAL CA-630 (non-denaturing, chemically equivalent to Nonidet P-40 or NP-40), which contain both hydrophilic and hydrophobic moieties that allow them to integrate into the phospholipid bilayer of cells, causing membrane disruption.[66,67] While detergents often comprise multiple advantages, such as an increased yield of membrane proteins, they can also impair enzymatic digestion, hinder chromatographic separation, and suppress ionization,[68] necessitating their removal during sample preparation for MS-based proteomics. As an alternative to detergents, chaotropic reagents like urea or guanidine (denaturing) can be used for chemical lysis. These reagents interact with water molecules surrounding the cell membrane, reducing hydrophobicity and causing membrane disruption. In this study, biochemical assays necessitating native protein conditions were conducted using the non-denaturing detergent IGEPAL CA-630 in combination with sonication as extraction methods. Upon protein extraction, the protein amount is measured using a commercial assay such as the bicinchoninic

acid (BCA) assay;[69] the amount of material necessary varies widely depending on the technology and application, from nanograms to milligrams.

The proteins are then rendered chemically inert through a two-step process involving disulfide bond reduction followed by thiol alkylation. This is typically achieved using agents such as dithiothreitol (DTT) or tris(2-carboxyethyl)phosphine (TCEP) for reduction, and iodoacetamide (IAA) for alkylation. By converting disulfides and thiols to thioethers, this process prevents the formation of thiol oxidation products or disulfide bonds during the subsequent workflow, thereby simplifying the analysis.[70]

The reduced and alkylated proteins are then subjected to enzymatic digestion, where specific peptide bonds are hydrolyzed. Trypsin is a commonly used protease due to its high efficiency and sequence specificity, cleaving peptide bonds C-terminally at lysine (K) and arginine (R) residues. The positive charges of these basic amino acids make tryptic peptides ideal for MS as it is based on the manipulation of charged ions. Besides trypsin digestion, considered the 'gold standard' for proteomics, other sequence specific proteases, such as Glu-C and Lys-C are also used and can be advantageous in certain cases.[71] Traditionally, enzymatic digestion for bottom-up proteomics was performed either in-solution or in-gel. In-gel digestion is robust and effective at removing interfering contaminants, but it is time-consuming and requires numerous manual handling steps.[72] Conversely, the in-solution protocol is easily automatable and scalable, but it does not easily remove interfering substances from the lysis buffer, necessitating additional peptide cleanup.[73] Filter-based methods such as S-Trap,[74] which was utilized in this work, address these issues by facilitating the removal of detergents and enabling protein digestion within a single spin column. An alternative approach involves utilizing magnetic beads, as demonstrated by the single-pot, solid-phase-enhanced sample preparation (SP3) method.[75] The SP3 method is particularly beneficial for processing samples with limited input and is highly amenable to automation, making it ideal for large-scale, high-throughput experiments.[76–78] This technique facilitates the capture of proteins on magnetic beads, allowing for effective removal of contaminants, such as detergents, through successive washing steps prior to protein digestion.

The digested peptides are then cleaned using methods such as solid-phase extraction (SPE), which involves a C18-coated solid phase using alternating mobile phases for trapping, washing, and elution steps. This step, often referred to as "desalting," removes buffer salts and contaminants that can adversely affect the ionization/desolvation process and suppress signal.[79] The eluent is then evaporated and the peptides are resuspended in an aqueous buffer compatible with liquid chromatography-tandem mass spectrometry (LC-MS/MS) analysis, such as 0.1% formic acid (FA) in high-performance liquid chromatography(HPLC)-grade water.

In this type of experiment, LC-MS/MS performs three essential functions: it separates and concentrates the peptides into distinct chromatographic peaks, collects data that allows for the determination of the peptides' amino acid sequences, and gathers data that facilitates the relative quantification of the peptides.

**High-Performance Liquid Chromatography**

At this stage, the peptides are ready for LC-MS/MS analysis. The sample is loaded into the autosampler of an on-line nano-HPLC instrument (e.g., 4 μL containing 0.1−1 μg of peptide), which is connected to a mass spectrometer. The use of nano-LC is crucial in proteomics due to its ability to handle very small sample volumes with high sensitivity and resolution, allowing for the detection and analysis of low-abundance peptides that would be challenging to identify with conventional HPLC.

In proteomics, nano-HPLC is almost always conducted in reversed-phase mode, wherein the column is packed with a hydrophobic stationary phase, often silica coated with linear hydrocarbon chains 18 carbons in length (referred to as C18).[70] The solvents, or mobile phase, consist of a mixture of two solutions pumped by their respective gradient pump: an aqueous buffer (often 0.1% formic acid in water) and an organic solvent (often acetonitrile with small amounts of formic acid, e.g., 0.1%, and water, e.g., 5%). This approach relies on the direct interaction between hydrophobic peptide residues and the non-polar stationary phase. The analyte is dissolved in the acidic mobile phase, leading to a net positive charge on most tryptic peptides, a prerequisite for the commonly applied positive MS mode. Additionally, it results in protonated hydroxyl groups of the silica beads, which enhances peptide separation. However, a drawback of this approach is that polar peptides are not retained by the stationary phase. To address this issue, ion-pairing reagents like formic acid are added to the mobile phase to increase separation via indirect ion pairing effects. As a result, peptides are partially separated based on their hydrophobicities and elute at different times (retention times, RTs) during the gradient. The gradient can be adjusted to optimize separation and chromatographic peak shape: a longer gradient allows more time to detect more peptides, whereas a shorter gradient enables more runs during the experiment and can enhance signal by sharpening chromatographic peaks.

**Peptide Ionization**

As the gradient progresses, peptides eluting from the reversed-phase column flow through a thin capillary known as the emitter. Since the mass spectrometer acquires mass-to-charge (m/z) ratios of ions, peptides must be transferred into the gas phase before entering the mass spectrometer for analysis. One widely and gentle used ionization method is electrospray ionization (ESI), which efficiently generates highly stable ions.[80] As a high voltage is applied between the emitter and the mass spectrometer, the charged molecules are pulled from the liquid towards the counter electrode. However, surface tension also acts to pull the liquid back towards the emitter to minimize surface area. When a specific voltage is applied, a Taylor Cone forms, resulting in the release of droplets towards the counter electrode. During flight, solvents evaporate until the repulsive forces of the remaining charges exceed the surface tension (known as the Rayleigh limit) of the droplet. This leads to Coulomb fission, causing the droplet to burst and form multiple nanodroplets containing charged peptides.[81] In proteomics, nano-ESI is typically used due to its ability to generate highly sensitive ionization from very low sample volumes, which is essential for detecting low-abundance peptides. Unlike standard ESI, which operates at higher flow rates and is suitable for larger sample volumes, nano-ESI operates at much lower flow rates, enhancing ionization efficiency and signal sensitivity.

The ionizability, or propensity to become a gas-phase ion, varies widely among peptides.[82] Those with insufficient ionizability may go undetected as charge-neutral species are not influenced by electromagnetic fields. Thus, they may deviate from their intended path, for instance, during desolvation or at the first bend in the flight path inside the spectrometer. A given peptide can typically adopt different charge states upon ionization, each one usually corresponding to a protonation state (z, indicating how many protons are bound to the peptide). These different charge states result in different m/z values. For example, an ionized peptide with $z = 1$ will have an m/z value of $[M + H]$, where M is the mass of the neutral peptide and H is the mass of a proton, whereas the same peptide with $z = 2$ will have an m/z value of $[M + 2H]/2$. Due to this variability, different charge state-specific versions of a peptide are isolated separately and serve as separate precursors in fragmentation reactions; hence, they are referred to as different "precursors".

**Precursor m/z Acquisition**

The spectrometer repeatedly and quickly acquires spectra to detect ionized peptides. The spectrum acquisition events are called "MS1 scans." The acquisition of any mass spectrum requires a mass-analyzer, which resolves ions according to their m/z values, and a detector, which measures an electrical signal. The signal generated by a peptide is related to the peptide's ionizability, charge state, and abundance, and the abundance-signal relationship is generally linear over some range of values.[83] Several mass-analyzers are effective for proteomics; four popular examples are the time-of-flight (TOF),[84–86] the orbitrap,[87,88] the quadrupole,[70] and the novel Asymmetric Track Lossless (Astral),[89,90] the latter of which is emerging as a powerful option due to its high throughput and resolution. Each mass-analyzer bears different properties regarding mass resolution, mass accuracy, sensitivity, scan speed, dynamic range, and m/z range.[91] Depending on the research question and sample type, specific mass-analyzers are favored and very often combined in one machine.

In MS instruments based on TOF mass-analyzers, ions generated by an ionization source are accelerated into a flight tube by a pulsed electric field. Since all ions receive the same amount of kinetic energy, their velocities depend solely on their m/z ratios: lighter ions travel faster, while heavier ions move more slowly. As the ions travel through the field-free drift region of the TOF analyzer, they separate based on their flight times. These flight times are measured with high precision when the ions reach the detector at the end of the flight tube. By calculating the time it takes for ions to reach the detector, the instrument can determine their m/z ratios. The process is extremely fast, allowing the TOF analyzer to acquire data rapidly, which is crucial for analyzing complex mixtures of peptides and proteins in proteomics. In addition to standalone TOF analyzers, hybrid instruments like Q-TOF combine a quadrupole for precursor ion selection with TOF for mass analysis, enhancing both the sensitivity and accuracy of proteomic experiments.[92] This makes TOF analyzers particularly useful for tasks like peptide-mass fingerprinting and the analysis of PTMs.

Novel mass-analyzer architectures are being developed to meet the growing demands of proteomics. One such advancement is the Astral mass-analyzer, a TOF-like instrument released by Thermo Fisher Scientific in 2023. The Astral employs a unique ion trapping approach, offering high mass resolution and accuracy, which makes it suitable for large-scale proteomics studies.[89] Its high throughput and ability to analyze low-abundance peptides further enhance its utility for both discovery-based and targeted proteomics. Another key feature of Astral technology is its ability to process data at an extremely high speed, making it particularly well-suited for large-scale proteomics studies where thousands of peptides must be analyzed simultaneously.

The Q Exactive Plus Hybrid Quadrupole-Orbitrap Mass Spectrometer[93] (Thermo Fisher Scientific) was utilized in this study (Figure 3A). This instrument incorporates a quadrupole, a collision cell for fragmentation, and an orbitrap mass-analyzer. The quadrupole consists of four parallel metal rods, with opposing rods electrically connected. By applying different Alternating Current (AC) and Direct Current (DC) voltages, the trajectories of ions traveling through the quadrupole can be stabilized or destabilized. Consequently, the quadrupole is frequently used as a prefilter to select ions with specific m/z ratios.[94] For an MS1 scan, all ions within a wide m/z range, such as 400−1600, are allowed to pass through the quadrupole. The ions are then trapped in the C-trap, which utilizes an electromagnetic field to accumulate and store ions before directing them simultaneously and instantaneously into the orbitrap.[95] The orbitrap consists of two barrel-like outer electrodes and a coaxial inner spindle-like electrode. Once inside the orbitrap, ions orbit the central spindle while oscillating along its axis at frequencies proportional to their m/z values. This axial oscillation is crucial for m/z measurements. As the ions move, they induce a fluctuating current, which is processed via Fourier transform to determine

m/z values and intensities.[87,88,96] This method of mass analysis is notable for its high m/z resolution and accuracy. Upon completion of the measurement, an MS1 spectrum is generated. As peptides are sprayed into the mass spectrometer, MS1 spectra are repeatedly acquired, many times per minute and sometimes multiple times per second. Each MS1 spectrum can trigger MS2 acquisition events, which occur before the subsequent MS1 spectrum is recorded.

**Tandem Mass Spectrometry**

MS1 acquisition measures m/z values and intensities of ionized peptides but does not provide sufficient information to determine peptide identities or sequences unambiguously. Although m/z values are typically measured with high accuracy (to at least three decimal places), the number of potential peptides within the allowed m/z error range is usually too large to identify peptides based solely on m/z. Moreover, peptides with a different amino acid sequence but the same mass cannot be distinguished. To obtain the necessary identification information, peptides are fragmented (typically at peptide bonds) and the fragments are analyzed by MS. The resulting spectra are referred to as "MS2 spectra" and the two consecutive MS1 and MS2 spectra acquired as "tandem MS" (LC-MS/MS setup).

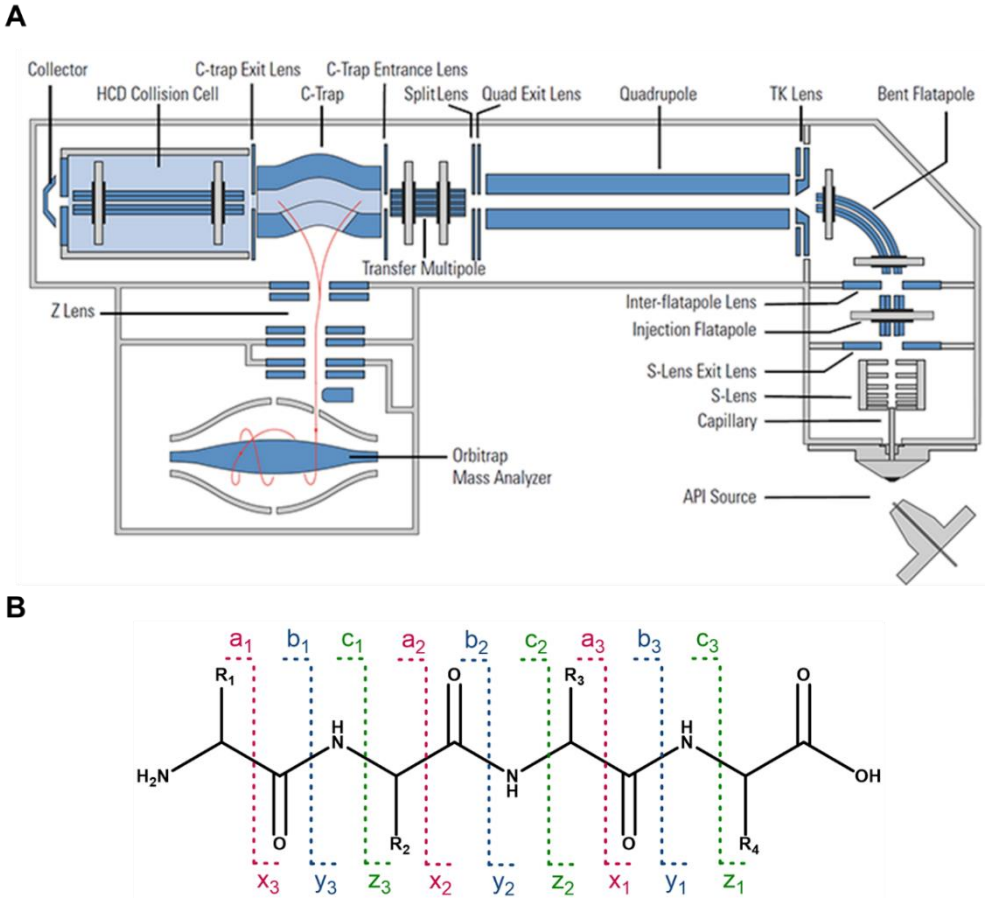


**Figure 3**. (A) Schematic of the Q Exactive Plus Hybrid Quadrupole-Orbitrap Mass Spectrometer. The quadrupole mass-analyzer acts as mass filter. Precursor ions are fragmented sequentially in the higher-energy CID (HCD) collision cell. Precursor and fragment ions are analyzed in the orbitrap and their m/z values determined. Adapted from Thermo Fisher Scientific. (B) Peptide fragmentation nomenclature according to Roepsdorf and Fohlmann[97] modified by Johnson et al.[98] Fragment ions which can be obtained are a, b and c ions (amino-terminus), and x, y, and z ions (carboxy-terminus). Collision-induced dissociation (CID) tends to preferentially generate b and y ions. Scheme created with ChemDraw.

After each MS1 scan, the mass spectrometer can select specific ions from the MS1 spectrum for reaccumulation and fragmentation while continuing its operation. Since many nonpeptide contaminant

ions have a charge of +1 and because fragmentation of peptides with z = +1 is often less informative, ions of charge +2 or greater are typically selected for fragmentation. Each selected precursor ion is then fragmented sequentially using collision-induced dissociation (CID) in the higher-energy CID (HCD) cell or collision cell, where they collide with inert gas molecules (usually nitrogen, $N_2$).[99] During these collisions, the peptides acquire vibrational energy until the breakage of chemical bonds. CID tends to preferentially cleave C–N bonds between carbonyl carbons and amide nitrogens (i.e., peptide bonds), resulting in fragments whose m/z values are predictable, known as b- and y- ions which are more common for trypsin-generated peptides (Figure 3B).[97,98] b-ions include the N terminus of the peptide, while y-ions include the C terminus. The resulting fragments are analyzed and detected similarly to the MS1 process, generating an MS2 spectrum that reveals the peptide's amino-acid sequence.

Data-acquisition methods in mass spectrometry are crucial for determining how peptide ions are selected and analyzed, ultimately influencing the quality and depth of proteomic data. The two primary approaches, data-dependent acquisition (DDA) and data-independent acquisition (DIA), each have unique strengths and limitations. For mass spectrometers operated in DDA, the MS1 scan first measures the m/z values and intensities of intact peptide precursor ions. The mass spectrometer then automatically selects the most intense precursors for further fragmentation and MS2 spectrum acquisition in real-time. This process continues for a predefined number or time range, but the stochastic nature of precursor selection can limit reproducibility. Alternatively, in DIA, which was the primary acquisition method utilized in this study, precursor ions are isolated using pre-defined m/z windows for further fragmentation. This approach facilitates accurate label-free proteome quantification, reduces the number of missing values, and increases throughput.[59–61,100] The DIA mode is also cost-effective and straightforward, with low compression of quantitative ratios. Other data-acquisition methods, such as targeted MS approaches like Selected Reaction Monitoring (SRM) and Parallel Reaction Monitoring (PRM), offer high specificity and sensitivity for quantifying known targets but are generally less suitable for comprehensive proteome-wide analysis. The selection of an appropriate acquisition method depends on the specific goals and constraints of the study. Acquisition methods are further discussed in Section 1.2.2 Protein Quantification.

### 1.2.2 MS Data Analysis

Central to all proteomics projects is the raw data obtained from the MS,[101] and suboptimal analysis outcomes can often be attributed to their poor quality. Consequently, evaluating the quality of raw MS data is a crucial initial step in data analysis, although it is frequently overlooked. Data quality is typically assessed through visual examination of the raw MS data, which can reveal various issues related to both sample integrity and instrument performance.[102] Additionally, numerous computational quality control methods have been developed and are well-documented in the literature.[103]

Inspecting the total ion chromatogram (TIC) can unveil various problems (Figure 4), including poor peak separation (evidenced by very broad peaks), unstable spray or MS failure (indicated by intensity drops), and errors in sample preparation (manifested as low intensity, sparse peaks, or unexpected overall shape).[104,105] Another significant issue is the saturation of the entire LC-MS system, which can occur due to overloading or contamination.

Depending on the acquisition mode, measurement time, and the mass-analyzer utilized for data generation, typically thousands of MS1 and MS2 spectra are captured. To extract peptide information

from these spectra, search engines are employed. Subsequently, this peptide information is utilized for protein identification and quantification.

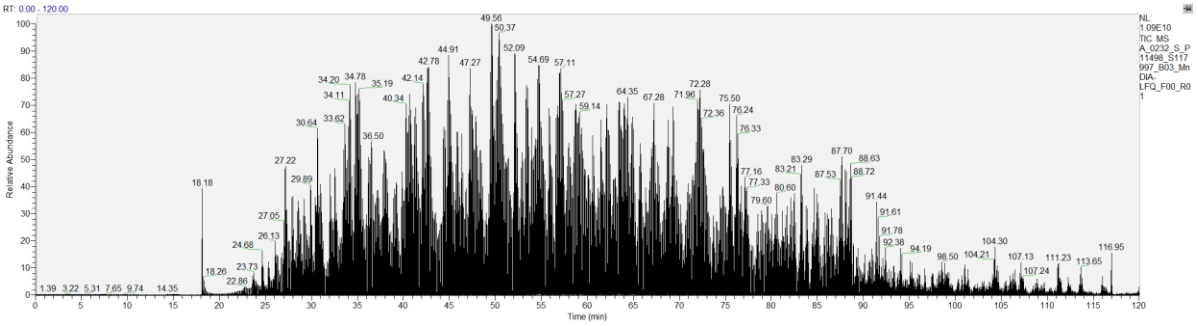


**Figure 4.** Typical chromatogram from an LC-MS/MS run. Each point on the plot represents an acquisition of a spectrum. The x-axis is the time (retention time, RT) at which the spectrum was acquired. The y-axis is the total electrical signal from all ions in the spectrum (total ion chromatogram, TIC), scaled to the TIC of the highest point in the chromatogram. Sample: *Klebsiella pneumoniae* proteins digested with trypsin. Peptides (1.0 µg) analyzed on Q Exactive Plus (Thermo Fisher Scientific) equipped with an orbitrap mass-analyzer with a Dionex UltiMate 3000 nano System (Thermo Fisher Scientific) using a 120-minute method. Peptides were separated using a linear gradient from 2% solvent B (0.1% FA, 5% DMSO in HPLC-MS grade acetonitrile) in solvent A (0.1% FA, 5% DMSO in HPLC-MS grade water) to 32% Buffer B in Buffer A. Plot generated in XCalibur Qual Browser (Thermo Fisher Scientific).

## Protein Identification

DIA and DDA are fundamentally distinct approaches in mass spectrometry, each requiring specialized strategies for protein identification and analysis. In DDA, the mass spectrometer selects the most intense precursor ions for fragmentation and analysis in real-time, often leading to variability in protein identification due to the stochastic nature of precursor selection. Conversely, DIA systematically fragments all precursor ions within predefined m/z windows, offering more consistent and comprehensive data, but requiring different computational methods to deconvolute the complex spectra. Given these differences, specialized software packages are required to process the raw data generated by each method. For instance, MaxQuant,[106] and Proteome Discoverer (Thermo Fisher Scientific),[107] are widely used for DDA data. In contrast, software like DIA-NN[63] is specifically designed to handle DIA data. These tools ensure accurate and reliable generation of peptide and protein lists from MS experiments, tailored to the specific acquisition approach used.

The most common approach for peptide identification is known as database search. In this method, users load raw data files into the selected software alongside a reference proteome, typically in FASTA[108] format. Reference proteomes for numerous species are widely available on UniProt.org and are frequently used in such analyses.[109] The search engine performs an *in silico* enzymatic cleavage of the proteins in the proteome database to predict all possible peptides and their corresponding charge-specific MS2 spectra, which serve as reference spectra for these peptides (Figure 5A). Search parameters, such as the chosen protease and mass tolerance, are specified to narrow the search space. The predicted peptides and their predicted spectra are then compared with the experimental spectra to generate peptide-spectrum matches (PSMs).

The high quality of the PSM is represented by numerical score(s) produced by the search algorithm based on how well the observed spectrum matches the peptide. To estimate the likelihood that a PSM is a false match, software packages use these scores and incorporate a target-decoy approach.[110,111] In this method, the experimental spectra are also searched against a database of reversed or scrambled peptide sequences (Figure 5B). Hits to this decoy database are inherently false, allowing for the

calculation of a false discovery rate (FDR), which is commonly set at 1% to minimize incorrect identifications.

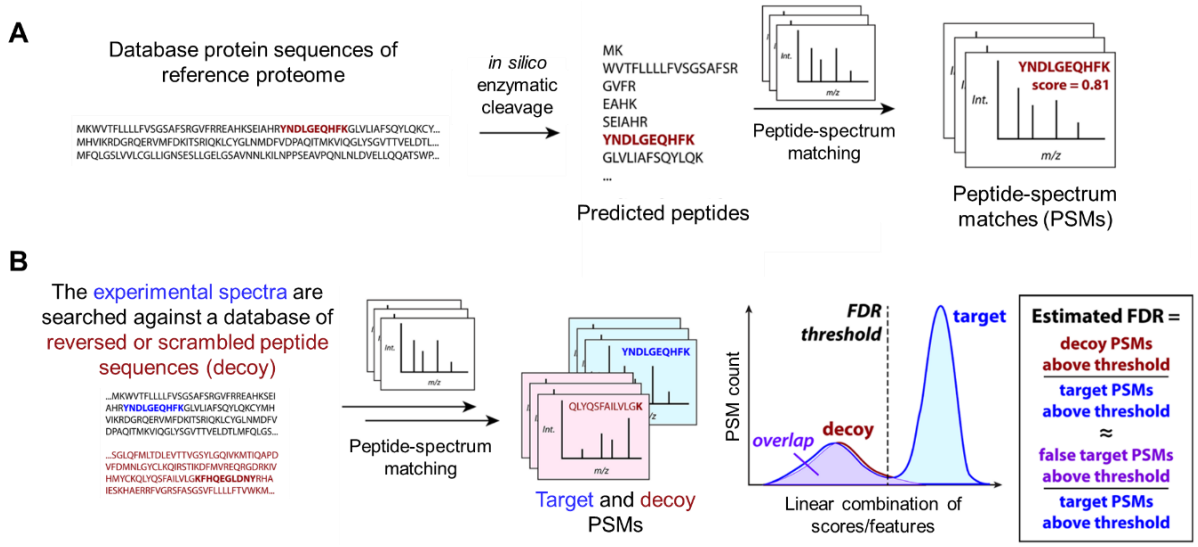


**Figure 5.** (A) Overview of database search. *In silico* enzymatic cleavage = computational prediction of digestion products. (B) Target-decoy search. PSM = peptide-spectrum match. FDR = false discovery rate. Adapted from Shuken SR.[70]

In bottom-up proteomics, the inherent ambiguity in peptide identification necessitates reporting results as protein groups rather than individual proteins. This arises because proteins are enzymatically cleaved into peptides, and the observed peptide set may represent multiple protein proteoforms, making it challenging to definitively assign all peptides to a single protein. Consequently, protein inference relies on peptide-to-protein grouping algorithms, which attempt to map detected peptides back to their corresponding proteins. This is particularly complex in eukaryotic systems, where a single gene can produce multiple proteoforms through alternative splicing or PTMs. In contrast, this issue is less pronounced in bacterial systems, where the one gene–one protein paradigm generally applies.

Another significant limitation of this method is its dependency on a comprehensive protein sequence database. Since peptide matching requires the presence of the corresponding protein sequence in the database, any protein not included in the user-supplied FASTA file cannot be identified, regardless of its actual presence in the sample. This underscores the importance of an accurate and complete database for effective protein identification, especially when dealing with less-characterized organisms or novel protein isoforms.

## Protein Quantification

In addition to protein identification, quantifying protein abundance is a crucial aspect of proteomic research. Depending on the experiment and sample type, various quantification methods are available, broadly classified into label-free and label-based approaches. In label-free quantification (LFQ), such as those employed in both DDA and DIA, protein identification relies on MS2 spectra, while MS1 spectrum information is used for quantification.[112] A common LFQ technique involves measuring the peak intensity of peptides across different samples, as peptide intensity is directly correlated with protein abundance. This method, often referred to as intensity-based LFQ, allows for relative quantification across multiple samples. However, a considerable drawback of label-free methods is that samples from a single experiment are only combined during the final data processing stage. Consequently, sample preparation and MS measurement must be conducted individually for each sample, making the process both time-consuming and prone to variability and errors. Despite these

challenges, LFQ remains a widely used approach in proteomics due to its flexibility and applicability to a broad range of experimental designs.

To enhance reproducibility and throughput, several multiplexing techniques have been developed based on labeling reagents to quantify multiple biological samples within the same mass spectrum.[113] These methods involve labeling peptides with groups of atoms that are chemically identical but differ in isotopic composition, resulting in different m/z values for either the peptides or their fragments. This isotopic labeling preserves important chemical properties such as retention time, ionizability, and fragmentation patterns, allowing for accurate comparative analysis of multiple samples simultaneously.

In metabolic labeling methods such as stable isotope labeling with amino-acids in cell culture (SILAC), the entire proteome is labeled using amino-acids that contain heavy isotopes.[114,115] During sample preparation, proteins labeled with natural "light" isotopes are combined with those labeled with heavy isotopes (Figure 6). Comparisons between the light and heavy proteins are then performed using MS1 spectra, enabling accurate quantification of protein abundance across different conditions.

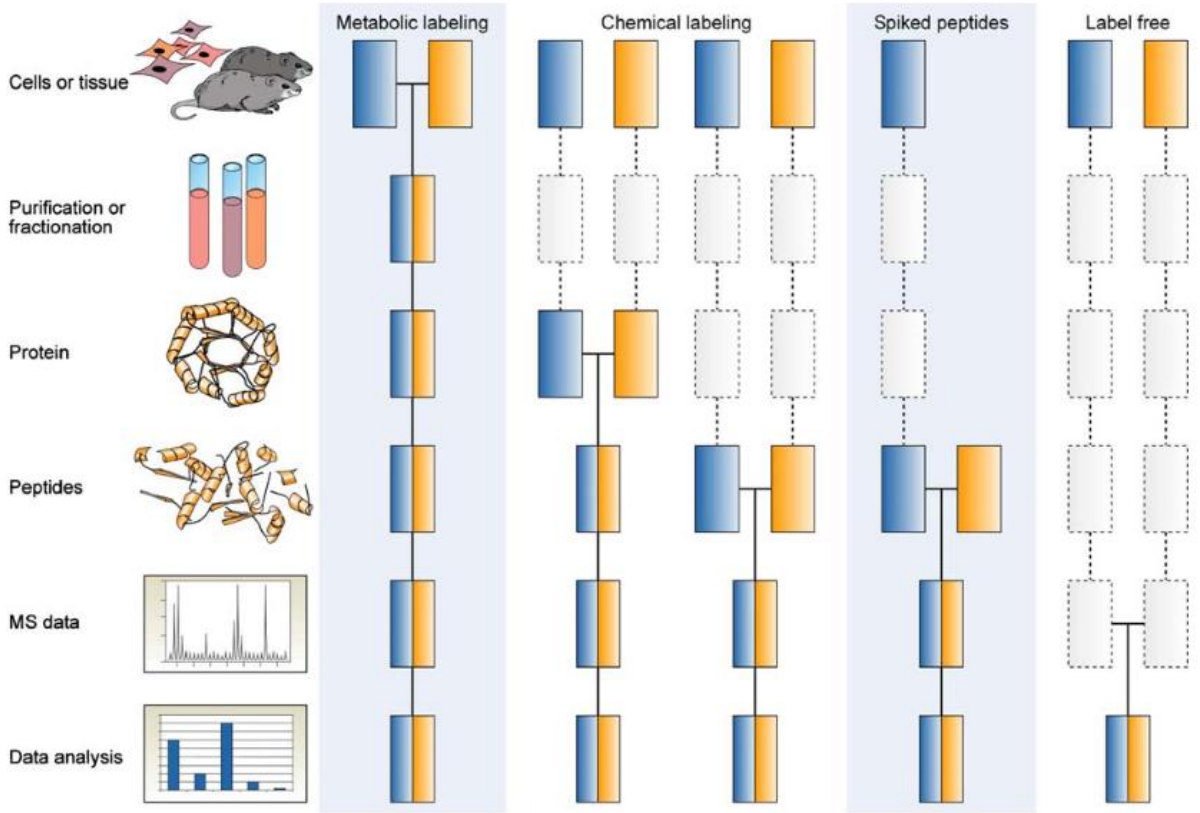


**Figure 6.** Common quantitative mass spectrometry workflows. Boxes in blue and yellow represent two experimental conditions. Horizontal lines indicate when samples are combined. Dashed lines indicate points at which experimental variation and thus quantification errors can occur. Adapted from Bantscheff et al.[116]

In chemical labeling methods such as tandem mass tags (TMT), succinimide chemistry is employed to label the amino termini and lysine residues of peptides after digestion.[117–120] These labeled peptides are then combined before LC-MS/MS analysis. Since TMT reagents have the same nominal mass, they do not increase the complexity of MS1 spectra. Upon precursor selection and subsequent fragmentation, the TMT reporter ions are cleaved off, allowing for both relative quantification and peptide identification based on MS2 scans. However, the process of precursor selection can suffer from the coisolation of coeluting precursors, which can lead to ratio distortion of the TMT reporter ions.

This phenomenon, known as coisolation interference, can compromise the accuracy of quantification.[121,122]

With LFQ, each run analyzes a single biological sample. SILAC typically allows for the analysis of two to three biological samples per run. TMT significantly increase throughput, enabling the analysis of up to 18 different biological samples in a single run.[117] Generally, the quantities of a particular peptide across different samples can be used for comparative analysis. Conversely, due to varying ionizabilities among different peptides, these quantities are relative, and MS-derived quantities of different peptides cannot be accurately compared directly. Each method—LFQ, SILAC, and TMT—has its own set of advantages and disadvantages (Figure 6).[70] The choice of method depends on the specific experimental setup and conditions, balancing factors like throughput, accuracy, and complexity.

## 1.3 Elucidating the Mechanisms of Action of Antimicrobial Agents

The target profiles of small molecule compounds are often not fully elucidated, even for those already in clinical use or in clinical evaluation. However, target identification (or target deconvolution) is a crucial determinant of success in drug discovery, as it is essential for understanding a drug's mechanism of action (MoA) and its potential as an anti-infective agent. Clinical trials are typically expensive and complex, and the likelihood of failure is higher without clear mechanistic insights.[123] This is particularly important following phenotypic screenings, where compounds are tested for a specific biological response. In such cases, target deconvolution is necessary to elucidate the MoA underlying the observed phenotypic effects.[124] Determining the full spectrum of targets associated with a bioactive molecule can accelerate optimization and assist the identification of unwanted off-target side effects. This enables early minimization of potential toxicities in the drug discovery process.[125] Similarly, target–engagement studies are essential for confirming the interaction of a drug with its specific protein targets. These studies provide direct evidence that the compound binds to its intended target within the cellular context, thereby validating its MoA.

To address the urgent need for new antimicrobials, researchers have adopted the screening of diverse natural and synthetic molecule libraries, utilizing two primary methodologies for drug discovery that differ in their approaches to compound selection and optimization (Figure 7).[126–128] Target-based strategies can identify small molecules that bind to recombinant target proteins by high-throughput screening (HTS).[129] This approach includes developing biochemical or biophysical assays to monitor modulation of target activity and identify potential hits. Here, molecules are screened for activity against a validated pathogen target, such as an essential protein, well established prior to conducting the screen. Preferably, the target should be novel in order to minimize the chances of pre-existing resistance. Upon hit validation, lead compounds are selected and further optimized for potency, selectivity, pharmacodynamic and pharmacokinetic properties, and then tested for efficacy in cellular or in vivo disease models. Target-based biochemical screens have been conducted against various malaria targets, resulting in improved molecules with both phenotypic and biochemical activity.[130] One such validated target in *P. falciparum* is the dihydrofolate reductase–thymidylate synthase (DHFR-TS). The drug candidate P218 was optimized against this target using a structure-guided enzymatic inhibition assay.[131] These target-based approaches have become particularly attractive due to the enhanced comprehension of the molecular mechanisms driving disease pathology and the advancements in HTS technologies. Furthermore, significant progress has been made in biophysical methods for assessing compound-target interactions during the lead optimization phase.[128]

In contrast, virtual screening techniques offer a cost-effective alternative to HTS, as they do not require expensive reagents. However, predicted active compounds must be subsequently acquired, and extensive downstream validation is necessary to confirm their binding affinity to the target and functional inhibition of the pathogens. Virtual pharmacophore screens have been utilized to identify new chemical starting points active against *Plasmodium* targets, including the DNA minor groove,[132] DHODH,[133] falcipain 2,[134] β-haematin formation,[135,136] and metalloaminopeptidases.[137] Despite their potential, this approach has yet to yield novel compounds with potent cell-based activity. Nonetheless, pharmacophore models, whether based on the protein target or a ligand binder, remain valuable tools for optimizing compounds identified through phenotypic and biochemical screens.

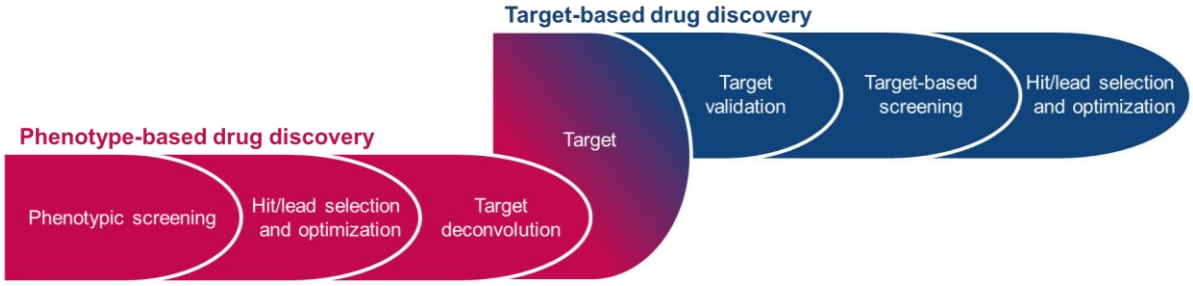


**Figure 7**. The diagram shows the early phase of drug discovery, focused on the identification of targets and lead molecules. In the phenotype-based approach, lead molecules are obtained first, followed by target deconvolution to identify the molecular targets that underlie the observed phenotypic effects. In the target-based approach, molecular targets are identified and validated before lead discovery starts; assays and screens are then used to find a lead.

Recently, there has been a shift towards phenotypic-based screenings because they more closely mimic physiological conditions compared to assays that target isolated proteins.[36,138] Here, a cellular assay is employed to screen a compound library, where the measured outcome is a cellular response, such as cell death. Numerous antimalarials currently in development have been discovered through phenotypic screening.[130] Notable examples include ganaplacide (KAF156), cipargamin (KAE609), cabamiquine (M5717, DDD107498, MMV643121), and ZY-19489. Another example is the identification of antimicrobial compounds that alter ATP synthesis in *M. tuberculosis*, where the observed phenotype is the intracellular ATP concentration.[139] However, since multiple cellular pathways can lead to reduced ATP levels, further experiments are required to unveil the precise target(s).

Phenotypic-based screens have uncovered promising antimicrobial agents, yet they are target-agnostic. Thus, a major challenge lies in unraveling the molecular mechanisms behind their activity, along with assessing potential safety concerns associated with their targets. Therefore, robust methodologies are crucial for thoroughly understanding both the molecular MoA (specific binding partner and biochemical consequences) and mode of action (disrupted physiological processes) of novel antimicrobial agents.[140]

### 1.3.1 Traditional Approaches for Target Identification

Genetic strategies have traditionally been the most widely used approaches for target identification for antibiotics. These strategies rely on the concept that identifying gene mutations causing resistance can reveal the target of the compound. While identifying and characterizing drug-resistant clones is often straightforward and effective, this method is typically limited to model microbial systems and may not always be successful due to multiple ways resistance can arise to a drug. Nevertheless, this approach has been useful in identifying targets of several well-known natural products. For instance, the

detection of mutations in the rpoB gene, which encodes the β-subunit of RNA polymerase, revealed the target of rifampicin.[141] Similarly, sequencing analysis of coumarin-resistant mutants identified gyrB and parE as the targets of novobiocin.[142] This method also identified the target of bedaquiline, a diarylquinoline antibiotic that kills *M. tuberculosis*. Bedaquiline-resistant strains display mutations in the gene encoding AtpE, a component of the F0 subunit of ATP synthase, thus pinpointing AtpE as the target.[143]

With the advent of next-generation sequencing (NGS), mapping drug-resistant mutations through sequencing and annotating microbial genomes has become comprehensive, rapid, and cost-effective.[144] Recent research on the naturally produced antimycobacterial compound pyridomycin demonstrates the enduring relevance of genomics in target identification, enhanced by NGS. In this study,[145] whole-genome sequencing of pyridomycin-resistant *M. tuberculosis* mutants and subsequent genetic confirmation identified InhA, the NADH-dependent enoyl-acyl carrier protein reductase, as the primary target of pyridomycin. In *P. falciparum*, the approach led to the discovery of various anti-malarial targets, including ATP4, eEF2, PI4K, and AcAS[146,147] and most tRNA synthetase inhibitors (KRS, cIRS, PRS and FRS).[130]

Although whole-genome sequencing offers a rapid route to identify drug targets, there are cases where generating mutants resistant to a particular drug is not feasible. Furthermore, sequencing resistant mutants may reveal alternative resistance pathways, distinct from mutations in target genes. For example, mutations in regulatory regions can lead to the overexpression of multidrug efflux pumps and transporters.[148,149]

Moreover, resistance does not always emerge readily, which, while advantageous for antimicrobial development, complicates target identification using selection-based methods. Fortunately, there are strategies to enhance resistance rates, thereby increasing the likelihood of favorable mutations arising in the genome. For instance, ethyl methane sulfonate is commonly employed to induce guanine alkylation, significantly elevating resistance frequency to antimicrobials.[150]

Another approach involves cloning and expressing protein libraries to investigate compound–protein interactions, such as in phage display or yeast-three-hybrid experiments. These in vitro technologies are cost- and labor-intensive and necessitate prior knowledge about the target space.[124] Despite providing a comprehensive view of the molecular target space of compounds, these methods entirely decouple the compound–target interaction from its biological relevance.

Macromolecular assays are also conventional methods. These assays assess the impact of newly identified antimicrobial compounds on the synthesis of macromolecules by monitoring the incorporation of radiolabeled precursors into major biosynthetic pathways. Typically, this approach determines whether a compound specifically inhibits DNA, RNA, protein, or cell wall biosynthesis. While macromolecular assays have been informative and utilized for years by the pharmaceutical community, they do have drawbacks. For instance, their utility diminishes when dealing with compounds that act through novel mechanisms, as they only report on a small fraction of potential MoAs. Nonetheless, macromolecular assays can effectively report on off-target effects and distinguish compounds that affect all processes simultaneously, suggesting non-specific MoA.[128,151] A classic example of successful macromolecular analysis is the naturally-produced lipopeptide daptomycin. Analysis of its effect on macromolecular synthesis revealed a minor decrease in peptidoglycan synthesis in bacteria and a more significant impact on lipid biosynthesis,[152] uncovering daptomycin's ability to disrupt multiple functional aspects of the cell membrane. Similar assays have been used to deduce the MoA of many other natural products with antibacterial activities.[152–154] Despite their limitations in resolution and throughput, improvements have been made to enhance these

assays. Originally designed for large culture formats, they have now been adapted for use with microplates, addressing issues of low throughput.[128] In summary, while macromolecular assays are limited by low resolution and throughput, they serve as valuable starting points for investigating the MoA of novel compounds.

Recently, biochemical assays, such as bioluminescence resonance energy transfer (BRET) have also been utilized in bacteria.[155] BRET technology can be used to measure interactions between compound and target protein, or between two different proteins in their native cellular environment. However, the requirement for an engineered version of the target protein fused to a luciferase (BRET donor) and a modified version of a known target ligand containing a luciferase-compatible fluorophore (BRET acceptor) restricts its applicability.

### 1.3.2 Chemical and Biophysical Proteomic Methods for Antimicrobial Drug Discovery

The following section provides an overview of various proteomics and chemoproteomics-based approaches for drug target deconvolution developed to date.

Chemoproteomics is a subfield of chemical biology, an interdisciplinary research area that intersects medicinal chemistry, biochemistry, and cell biology, requiring the design and synthesis of chemical probes and techniques to study the interactions between lead compounds and proteins on a proteome-wide scale.[156,157] Chemical probes are commonly employed as bait to capture target proteins within cell extracts under close-to-physiological conditions or intact cells. The interaction between the bait and its targets can be either covalent, as in activity-based protein profiling (ABPP), or noncovalent, as in affinity-based profiling.[156]

ABPP is a powerful chemoproteomics technique that employs activity-based probes (ABPs) to comprehensively measure endogenous enzymatic activity within complex proteomes.[158] This method has been extensively utilized to characterize human disease states and identify druggable targets across various disease conditions. Recently, ABPP has also been applied in microbiology, including functional studies of pathogenic bacteria and complex microbiome.[159–161]

ABPs function by covalently modifying active-site nucleophiles in an activity-dependent manner. An ABP typically consists of three components: (1) an electrophilic warhead that forms a covalent bond with the nucleophilic target, (2) a linker that provides specificity, and (3), optionally, a tag for visualization or enrichment of the labeled enzymes. Commonly, (3) is an alkyne-based tag, which allows for the addition of an azide-containing fluorophore or biotin via copper-catalyzed or copper-free alkyne-azide cycloaddition (CuAAC)[162] following probe labeling. Consequently, the labeled proteins can be separated by gel electrophoresis and visualized via the fluorophore tag, or enriched through affinity purification using the affinity tag. Subsequently, the proteins are digested, and their targets identified by LC-MS/MS.[163]

ABPP has been adapted to profile specific reactive cysteine[164] and lysine[165] residues, which are critical for the catalytic activity of many enzymes. For instance, iodoacetamide alkyne and sulfotetrafluorophenyl ester alkyne are used to label these residues, respectively. However, these probes not only label active site residues but also cysteines and lysines that have other functional roles, such as serving as metal ligands or forming redox-active disulfides.[166] For example, Deng and colleagues utilized a cysteine-reactive ABP to identify oxidation-sensitive cysteines in *Pseudomonas aeruginosa* and *Staphylococcus aureus*, thereby mapping pathogen responses to oxidative stress induced by hydrogen peroxide.[167]

A method akin to ABPP is photoaffinity labeling (PAL), where a chemical probe initially binds reversibly to its target proteins and subsequently forms a covalent bond upon photoactivation of a crosslinker, such as diazirine.[168] Similarly to ABPP, PAL probes typically include an additional handle, enabling stable enrichment of target proteins via click chemistry or streptavidin–biotin interaction.[169] A notable example is the identification of the major staphylococcal autolysin Atl and an ABC transporter protein as novel interactors of a vancomycin-based PAL probe.[170] However, the clear identification of enriched protein target(s) is often hindered by low abundant proteins and low photo-labeling yields. This low efficiency complicates the detection of true target interactions.

Additionally, both ABPP and PAL approaches are not ideal for screening the binding affinities of reversible ligands in competitive experiments, as the covalent binding of the probe significantly influences the binding equilibrium between the drug and the protein.

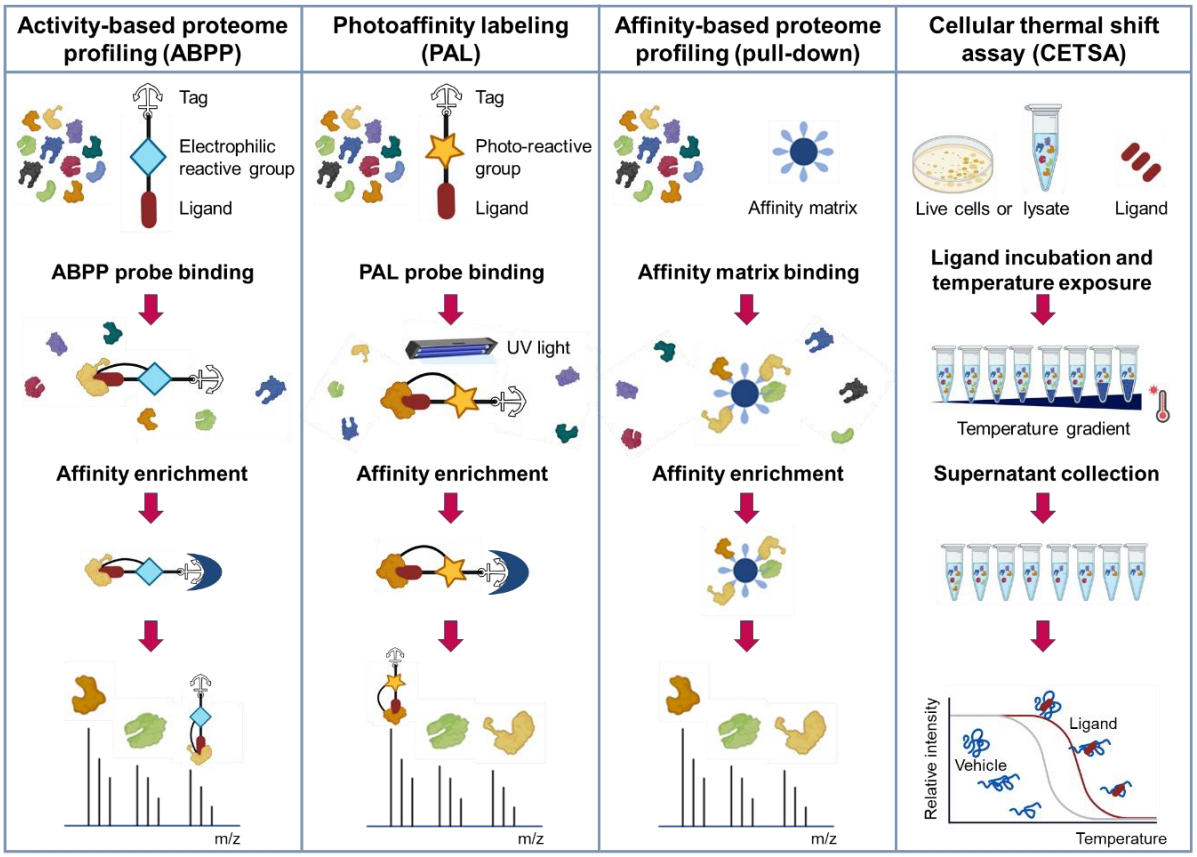


**Figure 8.** Schematic representation of various proteomic methods employed in target deconvolution studies. **Activity-based proteome profiling (ABPP)** utilizes a covalent probe bearing an electrophilic group that covalently reacts with the active sites of target proteins, enabling subsequent enrichment via an affinity tag. **Photoaffinity labeling (PAL)** employs a probe that initially binds reversibly to the target protein; upon UV irradiation, a photoreactive group forms a covalent bond with the target, facilitating its identification. **Affinity-based proteome profiling (pull-down)** utilizes affinity matrices to selectively enrich target proteins from cell lysates, based on reversible interactions with the probe. Bound proteins are captured and retained for analysis. The cellular thermal shift assay (CETSA) measures thermal stability of proteins in the presence or absence of a ligand, providing insights into protein-ligand interactions. Image created with BioRender.com.

To that end, the use of affinity matrices for affinity-based profiling has demonstrated significant advantages. In this approach, probes bearing a tag are immobilized on a solid support, such as sepharose or agarose beads, to enrich and isolate their target proteins from complex cell lysates. Typically, a linkable version of the ligand of interest is designed to ensure that the binding properties of the ligand to its target proteins are minimally affected. The experimental setup is prone to high background noise resulting from non-specific binding, further challenging the accurate identification of the protein targets. This can be improved by evaluating the optimal coupling density of the affinity

matrix to enhance the signal-to-noise ratio and by conducting dose-dependent competitive experiments with the non-modified ligand. In such experiments, specific binders can be identified by their dose-dependent behavior, significantly reducing false-positive target selection.

The success of affinity purification is best represented by the classic pull-down experiments identifying penicillin-binding proteins (PBPs) as targets of β-lactam antibiotics.[171–173] Another notable example is the interaction of immobilized vancomycin derivatives with bacterial transglycosylases.[174]

All the methods mentioned above require the functionalization of small molecules while retaining their activity, a process that can be both challenging and time-consuming to execute.[175]

In 2013, the cellular thermal shift assay (CETSA)[176,177] was published, offering a novel proteomics approach with many advantages. Unlike other methods, CETSA does not require prior modification of the binding partners or the use of additional chemical probes that could interfere with the binding equilibrium, and it can be performed within the biological environment. In CETSA, cells or cell lysates are incubated with a ligand and then subjected to a temperature gradient. Heat induces unfolding (denaturation) of the proteins by increasing the kinetic energy of the protein molecules, which results in the disruption of non-covalent interactions that stabilized their three-dimensional structures. The unfolding exposes hydrophobic regions that were previously buried inside the proteins, which tend to aggregate to minimize their exposure to the aqueous environment, leading to subsequent precipitation. The interaction with the ligand prior to denaturation, causes (de)stabilization of the target protein(s), leading to a shift in their melting behavior. The fundamental principle of CETSA is based on the thermodynamic stabilization; the binding of a ligand often results in a more favorable energy state for the protein–ligand complex compared to the unbound protein. This lower-energy state translates to a higher thermal stability because more energy (heat) is required to disrupt the interactions and unfold the protein. The same principle has been leveraged for over a decade to systematically screen recombinant proteins against potential inhibitors using the thermal shift assay (TSA).[178]

All proteins possess a specific melting temperature ($T_M$, temperature where half of the protein population is in the folded state and the other half is unfolded), which is altered by ligand-binding. Initially, CETSA experiments used antibody-based detection through western blotting for readouts. This approach enables the verification of target engagement and potency but is limited in its ability to identify novel or unexpected targets.

Thermal proteome profiling (TPP), as introduced by Savitski et al. in 2014,[179] combines the principles of CETSA[176] with multiplexed quantitative mass spectrometry-based proteomics, using TMTs.[118–120,180] In TPP experiments cells or lysates are subjected to a range of temperatures, the soluble fractions of the proteome are then collected and quantified by LC-MS/MS at each temperature point of the gradient. This approach generates complete melting curves for thousands of proteins and assigns $T_M$ values to them, enabling proteome-wide, agnostic target deconvolution studies. Beyond identifying protein–drug interactions, TPP serves as a potent tool for detecting many physiological alterations in protein states, including interactions with metabolites, PTMs, protein–protein and protein–DNA interactions, and chaperone–client interactions.[179,181–183]

Recently, Mateus et al.[184] applied TPP to *E. coli* both in cells and in lysate, confirming the known targets of the antimicrobial drugs ampicillin and ciprofloxacin. Additionally, TPP has been successfully established in *P. falciparum*. Dobrescu et al.[185] utilized TPP to investigate the mode of action of quinoline-quinazoline-based inhibitors as potential antimalarials. Their study identified the eukaryotic translation initiation factor 3 (EIF3i) subunit I as the primary target protein stabilized by their

inhibitors, a protein not previously characterized in malaria parasites. This adaptation of TPP to bacteria and *P. falciparum* holds promise for accelerating the discovery of new anti-infectives, as it enables the identification of targets for new compounds and provides insights into their resistance mechanisms.

TPP experiments can vary in their configurations and formats, depending on how samples are multiplexed with TMT for MS analysis.[186] The traditional approach[179] is commonly referred to as temperature range TPP (TPP-TR), indicating the multiplexing of a range of temperatures within the same mass spectrometry experiment. During data analysis, the resulting data are depicted as melting curve for individual proteins. The melting curves are then used to calculate the $T_M$. Such experiments are useful for comparing multiple conditions, such as drug *vs.* vehicle or gene knock-out vs. wild type. Moreover, TPP-TR is useful for assessing thermal proximity coaggregation (TPCA), where interacting proteins (e.g., in the same complex) tend to exhibit similar melting curves due to co-melting.[187]

In the compound concentration range TPP (TPP-CCR) approach,[179] samples from a single temperature point but from multiple compound concentrations are multiplexed. These data are represented as dose-response curves and can be used to estimate compound affinity and rank compounds or targets.

An extension of this approach is the two-dimensional TPP (2D-TPP), where a TPP-CCR experiment is conducted at multiple temperatures.[188] This format broadens the list of potential target proteins, as thermal stabilization of a specific protein is typically observed only at temperatures close to its $T_M$.

Recently, the proteome integral solubility alteration (PISA) assay was introduced by Gaetani et al.[189] to increase the throughput of the TPP readout. Unlike constructing complete melting curves, PISA employs TMT-based quantitative proteomics to estimate, or integrate, the area under a protein's melting curve (AUC). Instead of individually TMT labeling the soluble fractions from each temperature point, PISA pools the soluble fractions of multiple samples exposed to the temperature gradient, allowing a single TMT reporter to represent an entire integrated melting curve. Ultimately, any alteration in protein stability can be quantified as a fold change in the abundance of soluble proteins in a compound-incubated sample compared to a vehicle-incubated control after denaturation and centrifugation. Thus, an increase in $T_M$ will result in a rise in the AUC and an increase in the soluble protein abundance relative to controls (stabilized protein with a positive $\log_2$ fold change). Conversely, a decrease in $T_M$ will result in a decrease in the AUC and a reduction in the soluble protein abundance relative to controls (destabilized protein with a negative $\log_2$ fold change). Overall, compressing entire denaturation curves into a single TMT channel allows the simultaneous assessment of multiple compounds at various concentrations with multiple replicates in a single experiment.[189] Thanks to its enhanced scalability, PISA offers increased throughput compared to the traditional TPP. This advancement, combined with the relatively straightforward data analysis compared to the complex generation of complete melting curves, facilitates large-scale studies, including chemical library screening.[186,190,191]

Regrettably, not all proteins exhibit detectable thermal shifts, which can be attributed to factors such as protein size, binding kinetics with high off-rates, or other reasons.[179] Consequently, while CETSA and TPP offer an unbiased experimental setup, the insights they provide may not encompass the entire target space of a given ligand.

TPP and CETSA belongs to a broader category of recently developed biophysical proteomics tools that focus on alterations in proteome stability.[192] Importantly, heat is not the only way to induce unfolding of the proteome. Various agents, including salt, acid, organic solvents, and some chemical denaturants, also disrupt protein folding, leading to aggregation and precipitation. Therefore, there are other approaches relying on different principles, such as differential proteolytic access upon ligand

binding, as seen in limited proteolysis (LiP) methods, [193–196] or inferring protein stability from rates of oxidation, as in the case of SPROX. [197] Additionally, Fast Photochemical Oxidation of Proteins (FPOP)[198,199] uses hydroxyl radicals generated by laser-induced photolysis to map solvent-accessible regions of proteins, providing insights into protein structure and dynamics. A recent addition to that toolbox is the solvent-induced protein precipitation.

### 1.3.3 Integral Solvent-Induced Protein Precipitation (iSPP)

In 2020, Zhang and colleagues[200] introduced a novel biochemical method known as solvent-induced protein precipitation (SPP), which was validated in human cell lysates under close-to-physiological conditions. SPP is a LC-MS/MS-based proteome stability assay designed for target–engagement studies and selectivity profiling of compounds. Similar to the aforementioned stability assays, SPP is a modification-free approach that does not require compound functionalization. The method is based on the chemical denaturation of proteins, achieved by exposing cell lysates to increasing concentrations of organic solvents.

Organic solvents induce protein denaturation by altering the overall polarity of the solvent environment. Proteins in aqueous solutions are surrounded by a hydration shell of water molecules that stabilize their structure. Organic solvents disrupt this shell, thereby affecting hydrogen bonding and electrostatic interactions that maintain the protein's structure, leading to destabilization and denaturation. Furthermore, proteins possess hydrophobic cores stabilized by hydrophobic interactions. Organic solvents, being less polar than water, can penetrate these hydrophobic regions, disrupting the interactions and causing protein unfolding. Upon denaturation, the exposed hydrophobic regions of proteins aggregate, resulting in proteins precipitation. The primary differences between solvent- and heat-induced denaturation are related to (1) solvent polarity; organic solvents change the polarity of the environment, disrupting hydrogen bonds and hydrophobic interactions in a different manner than heat, (2) direct interaction; organic solvents can directly interact with non-polar side chains of amino-acids, altering their behavior and causing protein unfolding, and (3) disruption of hydration; organic solvents disrupt the hydration shell around proteins, a mechanism not typically associated with heat denaturation.

As observed with other protein stability-based methods, ligand binding to target protein(s) often leads to a more favorable energy state for the protein-ligand complex compared to the unbound protein. This lower energy state translates to higher stability, as more energy (in the form of a higher concentration of organic solvents in SPP) is required to disrupt the interactions and unfold the protein.

Similar to TPP, SPP experiments can be conducted with various configurations and formats. In these experiments, data is often presented as denaturation curves for each protein when all organic solvent concentrations across the gradient are measured at the LC-MS/MS. These denaturation curves enable the calculation of melting concentrations ($C_M$), which represent the concentration of organic solvents at which a protein reaches equilibrium between its folded and unfolded states, based on the assumption that an unfolded protein precipitates. Recently, Van Vranken and colleagues successfully applied the compressed PISA approach to SPP assays in human cell lysates.[201] However, this method reported a drawback as the approach can lead to a compression of the observable effect size, making it difficult to detect stabilized proteins. To address this issue, it is crucial to select a gradient that is tailored to the region where the most substantial solubility changes occur in the known target proteins. This adjustment is critical as it greatly influences the observed stabilization outcomes in target–engagement studies.

To that end, we developed an assay based on SPP-PISA principles, hereafter referred to as integral SPP (iSPP), in the three Gram-negative bacteria *E. coli*, *K. pneumoniae*, *P. aeruginosa*, the Gram-positive bacterium *S. aureus*, and the parasite *P. falciparum*.

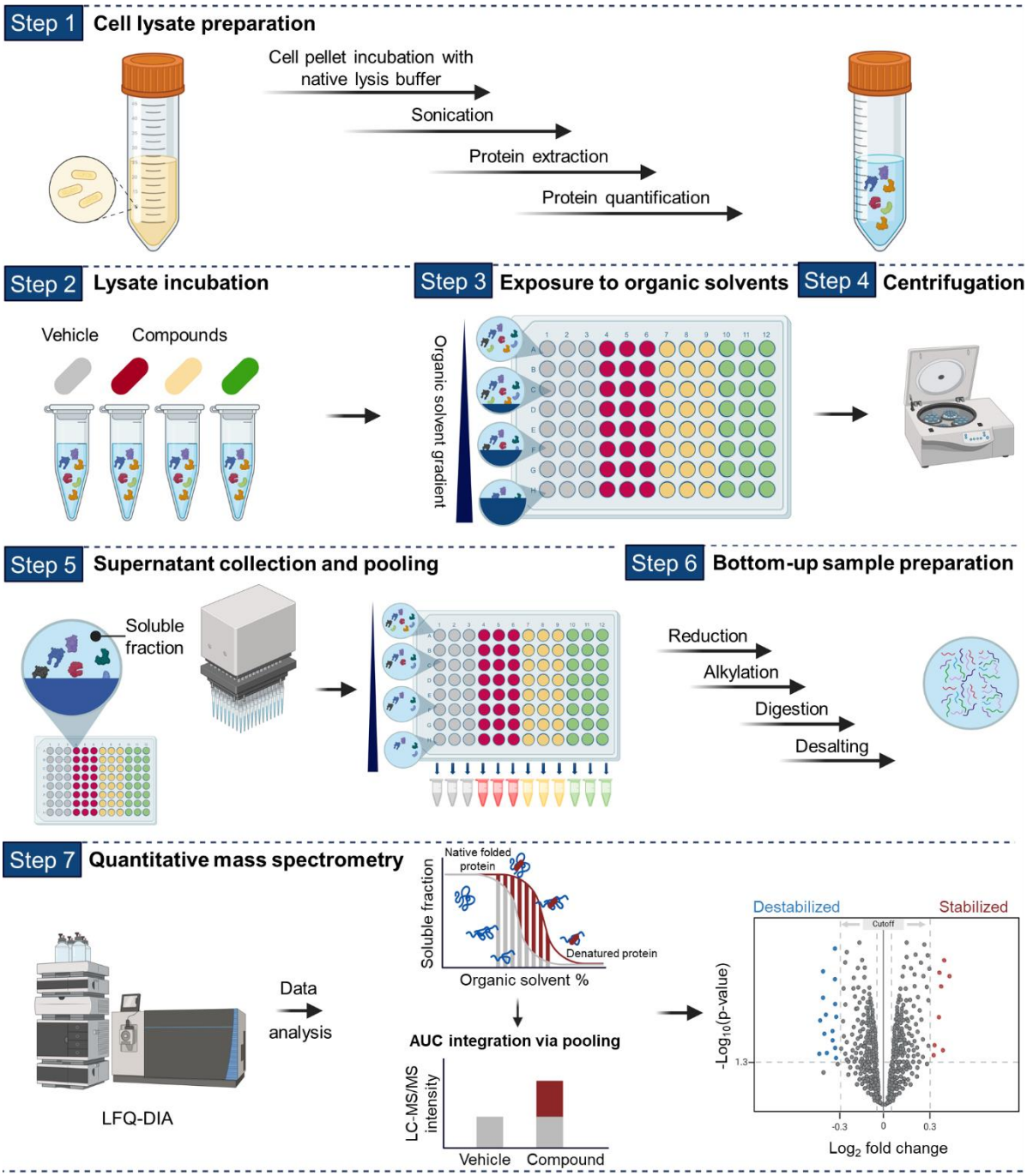


**Figure 9.** Schematic representation of the iSPP approach for target–engagement studies. Workflow graphic created with BioRender.com.

The optimized iSPP assay presented in chapters 3.3 and 3.4 (1) requires a minimal total protein experimental input material (20 µg per data point) which is well-suited for hard-to-culture pathogens characterized by slow growth rates and limited protein yields. A typical experimental design—such as four distinct conditions, one vehicle control and three distinct drugs, each in triplicate, distributed across eight solvent concentrations—requires about 2.0 mg of total protein extract. (2) It utilizes a target-specific, empirically chosen solvent concentration range for target–engagement studies to

maximize the observable effect size in the area-under-the-denaturation-curve readout of the known protein targets of the compounds of interest. For target deconvolution studies, a generalized gradient is employed. (3) It employs LFQ-DIA quantitative MS as a sensitive and versatile alternative to TMT labeling, differing from approaches used in previous SPP studies.[200–202] DIA was employed for LC-MS/MS identification and quantification to streamline the protocol by eliminating the need for peptide labeling and the subsequent sample fractionation required before LC-MS/MS.

The adaptability and robustness of iSPP in validating the protein targets of model anti-infectives and small molecules in early drug discovery stages are further discussed in the next chapters.

# 2. AIMS OF THE THESIS

Due to the increasing emergence of AMR to commonly used therapies, the development of novel anti-infectives is urgently needed. Despite the rapid emergence of resistance, the development of new antimicrobials requires substantial time and is at its lowest point in decades. A key obstacle in early drug discovery is the lack of techniques for determining and confirming the MoA of new anti-infectives, particularly those identified from phenotypic screenings.

The primary objective of this thesis was to advance the goals of the MepAnti Consortium by aiding in the discovery and characterization of novel anti-infective agents targeting the MEP pathway, which is absent in humans but essential in green algae and numerous pathogenic bacteria and apicomplexan protozoa, including important human pathogens. To achieve this, quantitative proteomics (LC-MS/MS) was employed to evaluate the measurability and abundance of MEP pathway enzymes across multiple pathogenic species (Chapter 3.1). This analysis provided a foundation for subsequent efforts to characterize inhibitors of the MEP pathway. Subsequently, chemoproteomics, specifically affinity matrices for affinity-based profiling, was investigated (Chapter 3.2). Despite their potential, these methods proved to be inadequate for our objectives. Their limitations highlight a critical challenge within chemoproteomics: the dependence on functionalized chemical probes that must retain their activity after modification. This process can be both challenging and time-consuming. Consequently, the complexities involved in designing and synthesizing such probes can lead to major issues with selectivity and affinity, ultimately resulting in inadequate enrichment of the target proteins. These findings underscored the need for alternative approaches in the MepAnti project to effectively identify and characterize novel anti-infectives, particularly when the functionalization of chemical probes does not yield the desired specificity or efficacy.

To that end, the aim of this work evolved to establish and validate a novel modification-free proteome stability assay suitable for target deconvolution and confirmation in microbial pathogens under close-to-physiological conditions. The assay, named iSPP, was adapted and optimized for key pathogens associated with deaths due to AMR, including *E. coli*, *K. pneumoniae*, *P. aeruginosa*, *S. aureus*, and *P. falciparum*. The primary goal was to validate the assay using well-established anti-infectives and then apply it to confirm the targets of novel small molecules directed against enzymes of the MEP pathway. Detailed results are presented in Chapters 3.3 and 3.4.

# 3. RESULTS

## 3.1 Chapter A: Comprehensive Proteomic Profiling of Human Pathogens and CRISPRi-Driven Gene Modulation in *Mycobacterium tuberculosis*

Lorenzo Bizzarri, Vidhisha Sonawane, Jörg Haupenthal, Jonas Lohse, Norbert Reiling, Anna K. H. Hirsch, Hannes Hahne

Contributions: Lorenzo Bizzarri, Jonas Lohse and Hannes Hahne conceived the proteomic profiling project; Lorenzo Bizzarri conducted protein extraction for *Escherichia coli*, performed the proteomics experiments and analyzed the resulting data from LC-MS/MS measurements; Vidhisha Sonawane and Norbert Reiling conceived the CRISPRi project and executed the *Mycobacterium tuberculosis* cell culture and lysate preparation; Jörg Haupenthal prepared cell cultures and provided lysates for *Klebsiella pneumoniae*, *Pseudomonas aeruginosa*, and *Staphylococcus aureus*; Lorenzo Bizzarri wrote the manuscript with contributions from all authors; Anna K. H. Hirsch and Hannes Hahne coordinated the project.

All authors have given approval to the final version of the manuscript.

This manuscript will be submitted upon completion of the remaining experiments, specifically the target validation of compounds directed toward the MEP enzymes modulated by CRISPRi.

# Comprehensive Proteomic Profiling of Human Pathogens and CRISPRi-Driven Gene Modulation in *Mycobacterium tuberculosis*

Lorenzo Bizzarri,[a,b] Vidhisha Sonawane,[c] Jörg Haupenthal,[b,d] Jonas Lohse,[a] Norbert Reiling,[c] Anna K. H. Hirsch,*[b,d] Hannes Hahne*[a]

[a]OmicScouts GmbH, Lise-Meitner-Straße 30, D-85354 Freising, Germany.
[b]Saarland University, Department of Pharmacy, Campus E8.1, D-66123 Saarbrücken, Germany
[c]RG Microbial Interface Biology, Research Center Borstel Leibniz Lung Center, Parkallee 1-40, Borstel, D-23845, Sülfeld, Germany
[d]Helmholtz Institute for Pharmaceutical Research (HIPS), Helmholtz Centre for Infection Research (HZI), Saarland University, Campus E8.1, D-66123 Saarbrücken, Germany

## ABSTRACT

Our study employed quantitative proteomics (LC-MS/MS) to perform a comprehensive proteomic profiling of multiple human pathogens. High proteome coverage was achieved for *Mycobacterium tuberculosis*, *Escherichia coli*, *Klebsiella pneumoniae*, *Pseudomonas aeruginosa*, *Staphylococcus aureus*, and *Plasmodium falciparum*. Notably, the seven 2-*C*-methyl-D-erythritol-4-phosphate (MEP) pathway enzymes were detected and quantified by LC-MS/MS in all MEP-utilizing organisms. We further utilized CRISPR interference (CRISPRi) in *M. tuberculosis* to modulate the expression of key enzymes involved in this pathway (*dxs1* and *dxr*), as well as *rpoB*, which encodes the β-subunit of the DNA-dependent RNA polymerase (RNAP) complex. Our primary objective was to use CRISPRi as a powerful tool for target validation of compounds directed toward the proteins encoded by these knockdown genes. To achieve this, we first validated the downregulation of the repressed genes at the protein level by using LC-MS/MS, which revealed dose-dependent reductions in protein abundance. These findings demonstrate the utility of CRISPRi-mediated gene knockdown for validating potential drug targets, highlighting its potential in the discovery of novel antimicrobial therapies against multidrug-resistant *M. tuberculosis*. Additionally, our findings confirmed the identification and detectability of MEP enzymes, facilitating future studies and aiding the identification of potential anti-infective targets.

## INTRODUCTION

Proteomics is the large-scale study of proteins, encompassing their expression, modifications, and interactions within a biological system.[1] Utilizing techniques like liquid chromatography-tandem mass spectrometry (LC-MS/MS), proteomics enables the quantitative and qualitative analysis of protein abundance and function, providing a powerful platform to assess the expression levels of proteins.[2] This approach allows for a systematic evaluation of protein dynamics across various pathogenic species. Our initial work focused on leveraging LC-MS/MS to evaluate the measurability and abundance of enzymes in the 2-*C*-methyl-D-erythritol-4-phosphate (MEP) pathway across various pathogenic species. This pathway is crucial for the biosynthesis of isoprenoids in multiple human pathogens, making it an attractive target for novel anti-infectives.[3] Our analysis was specifically conducted on the acid-fast bacillus *Mycobacterium tuberculosis*, the three Gram-negative bacteria *Escherichia coli*, *Klebsiella pneumoniae*, and *Pseudomonas aeruginosa* and the protozoan parasite *Plasmodium falciparum*. Additionally, the Gram-positive bacterium *Staphylococcus aureus* was included in the study, despite its reliance on the mevalonate pathway. The inclusion of *S. aureus* provided a broader comparative framework across organisms utilizing distinct isoprenoid biosynthetic pathways.

In addition to identifying enzymes of the MEP pathway, this comprehensive proteomic characterization offered an in-depth analysis of the global protein expression patterns within these organisms, serving as a powerful tool for the identification and quantification of their complete proteomes.[4–7] Full proteome analysis represents a robust approach for defining protein expression profiles, enabling the identification and quantification of global protein landscapes. This assessment is particularly crucial for downstream (chemo-)proteomics assays, as it establishes the extent of proteome coverage achievable within the targeted organisms.[8] High proteome coverage is vital for ensuring broad protein representation, which in turn enhances the reliability and interpretability of subsequent analyses. Moreover, this initial characterization is essential to verify whether the specific proteins of interest can be consistently detected and quantified via LC-MS/MS.

Subsequently, we performed a proteomic analysis to assess the efficiency of gene knockdown achieved through CRISPR interference (CRISPRi) in *M. tuberculosis*. CRISPRi is a modified version of the CRISPR/Cas9 system, which has revolutionized genetic engineering by enabling precise, targeted gene editing across a wide range of organisms.[9] The CRISPR/Cas9 system functions by utilizing a small guide RNA (sgRNA) to direct the Cas9 endonuclease to a specific genomic sequence.[10] Upon binding to the target site, the Cas9 protein induces a double-stranded break in the DNA. The cell's endogenous repair mechanisms, either through non-homologous end joining or homology-directed repair, then attempt to repair the break, resulting in gene disruption or the potential integration of new genetic material.[11]

Conversely, CRISPRi has emerged as a powerful tool for targeted gene repression without inducing DNA cleavage. CRISPRi utilizes a catalytically inactive form of the Cas9 protein (dCas9), which is guided by a specific small guide RNA (sgRNA) that binds to the genomic locus of interest. Along with sgRNA, the target specificity is also assisted by a protospacer adjacent motif (PAM). PAMs are 2–8 base pair sequences located immediately downstream of a sgRNA target sequence. This binding creates a steric hindrance, effectively blocking the progression of RNA polymerase and thereby inhibiting transcription. Unlike the conventional CRISPR/Cas9 system, which generates double-stranded DNA breaks, CRISPRi achieves gene knockdown without altering the genomic sequence, providing a safer and more controlled approach for transcriptional repression.[12]

The dCas9 system is particularly well-suited for studies in *M. tuberculosis*, a pathogen where fine-tuned gene regulation provides critical insights into essential metabolic pathways and potential drug targets. CRISPRi has been optimized and widely applied to studies of gene function and antibiotic mechanism of action in *M. tuberculosis*.[13–15] CRISPRi can be inducibly activated by tetracycline (Tet) analogs, such as anhydrotetracycline (Atc), allowing concentration dependent gene knockdown. Atc functions by interacting with a Tet repressor protein (TetR)-based promoter system. Upon addition of Atc to the growth medium, it binds to TetR, causing its dissociation from the promoter region controlling dCas9 expression. This allows the transcription of the dCas9 gene, leading to the formation of the dCas9-sgRNA complex, which subsequently binds to the target gene, inhibiting its transcription. The dose-dependent nature of this system allows for a graded level of gene repression, where increasing concentrations of Atc induce higher expression of dCas9, resulting in stronger repression of the target gene. By enabling dose-dependent repression, CRISPRi allows researchers to explore the effects of partial gene knockdown, which is particularly relevant for studying essential genes that cannot be fully knocked out without causing lethality.[16]

In our study, we employed CRISPRi to downregulate three specific genes in *M. tuberculosis*—*rpoB*, *dxs1*, and *dxr*. The first gene, *rpoB*, encodes the β-subunit of RNA polymerase, a well-characterized target of antibiotics in the rifamycin class.[17] Given its established role, *rpoB* was used as a control

to validate the functionality of the CRISPRi system in our experiments. The other two genes, *dxs1* and *dxr*, encode the first and second enzymes of the MEP pathway, respectively. The genome of *M. tuberculosis* has two homologs of *dxs*: *dxs1* (Rv2682c) and *dxs2* (Rv3379c).[18] A similar phenomenon is seen in *Streptomyces coelicolor*, where both homologous enzymes are fully functional.[19] However, in *M. tuberculosis*, only Dxs1 functions as an active 1-deoxy-D-xylulose 5-phosphate (DXP) synthase.[18,20] Dxs2 cannot compensate for the loss of Dxs1, as it lacks DXP synthase activity. This inactivity is attributed to an N-terminal truncation in Dxs2, which eliminates a critical histidine residue essential for catalytic function.[18]

By targeting *dxs1*, *dxr* and *rpoB* with CRISPRi, we aimed to downregulate these genes and consequently their encoded proteins in a controlled and reproducible manner to explore the essentiality of the MEP pathway in *M. tuberculosis* and validate the target of novel compounds as our ultimate goal.

Notably, CRISPRi is not only a versatile tool for gene repression but also serves as a valuable method for target validation in drug discovery. By selectively downregulating the expression of key metabolic and essential genes, CRISPRi allows us to investigate how reduced protein levels influence bacterial viability and drug susceptibility.[12] This approach is particularly beneficial for identifying potential drug targets and understanding the mechanisms of action of novel antimicrobial compounds. Target validation through CRISPRi is often conducted by evaluating the minimum inhibitory concentration (MIC) of specific compounds in both wild-type and gene-repressed strains. If a compound induces a shift in the MIC value in presence of Atc—such as a lower MIC in the CRISPRi-treated strain compared to the wild-type—it suggests enhanced drug susceptibility, indicating that the compound interacts with the protein encoded by the gene of interest. Conversely, if the MIC value remains unchanged, it implies that the compound does not target the downregulated protein. This approach provides a robust method for determining whether a compound affects its intended target, a critical step in the development of new therapeutics. In the context of *M. tuberculosis*, where multidrug resistance is a growing concern, CRISPRi-based target validation offers a powerful strategy to identify and verify new drug targets, as well as to confirm the specificity of potential antimicrobial agents.

In our research, we aimed to establish a foundation for future target identification studies using CRISPRi. To achieve this, we conducted a global proteomics analysis to compare the proteomes of *M. tuberculosis* strains in which *rpoB*, *dxs1*, or *dxr* had been repressed via CRISPRi, to those of wild-type strains not subjected to CRISPRi treatment. By assessing the abundance levels of the targeted proteins across varying concentrations of Atc, we were able to evaluate both the specificity and efficacy of the CRISPRi-mediated knockdown. The proteomics data confirmed a decrease in the abundance of all three target proteins—RpoB, Dxs1, and Dxr—in the CRISPRi-treated samples compared to the wild-type strains. Importantly, the downregulation displayed a clear dose-dependent pattern, with increasing concentrations of Atc leading to greater reductions in protein levels. This demonstrates that CRISPRi can be effectively used to quantitatively modulate gene expression, providing a reliable platform for future studies aimed at drug-target validation. Moreover, the results highlight the utility of proteomics as a robust method for validating differential expression levels of target proteins following CRISPRi-mediated repression. By enabling the precise quantification of protein abundance in response to gene knockdown, proteomics offers critical insights into the functional consequences of reduced protein expression, further strengthening its role in drug-target validation and mechanistic studies.

## RESULTS AND DISCUSSION

### Proteomic Characterization of Human Pathogens

The global proteomic characterization by LC-MS/MS led to the identification of 3062 proteins in *M. tuberculosis* (strain H37Rv), 2752 proteins in *E. coli* (strain K12), 3196 in *K. pneumoniae* (strain ATCC13883), 4139 in *P. aeruginosa* (strain PA01), 1849 in *S. aureus* (strain Newman), and 3450 proteins in *P. falciparum* (strain NF54, derived from asynchronous culture). These identifications correspond to predicted full proteome coverages of 76%, 62%, 56%, 74%, 64%, and 58%, respectively, based on the UniProt database.[21] Such coverage ranks among the highest reported in the literature for LC-MS/MS-based analyses, indicating close-to the entirety of the estimated expressed proteome for each organism.[22–35]

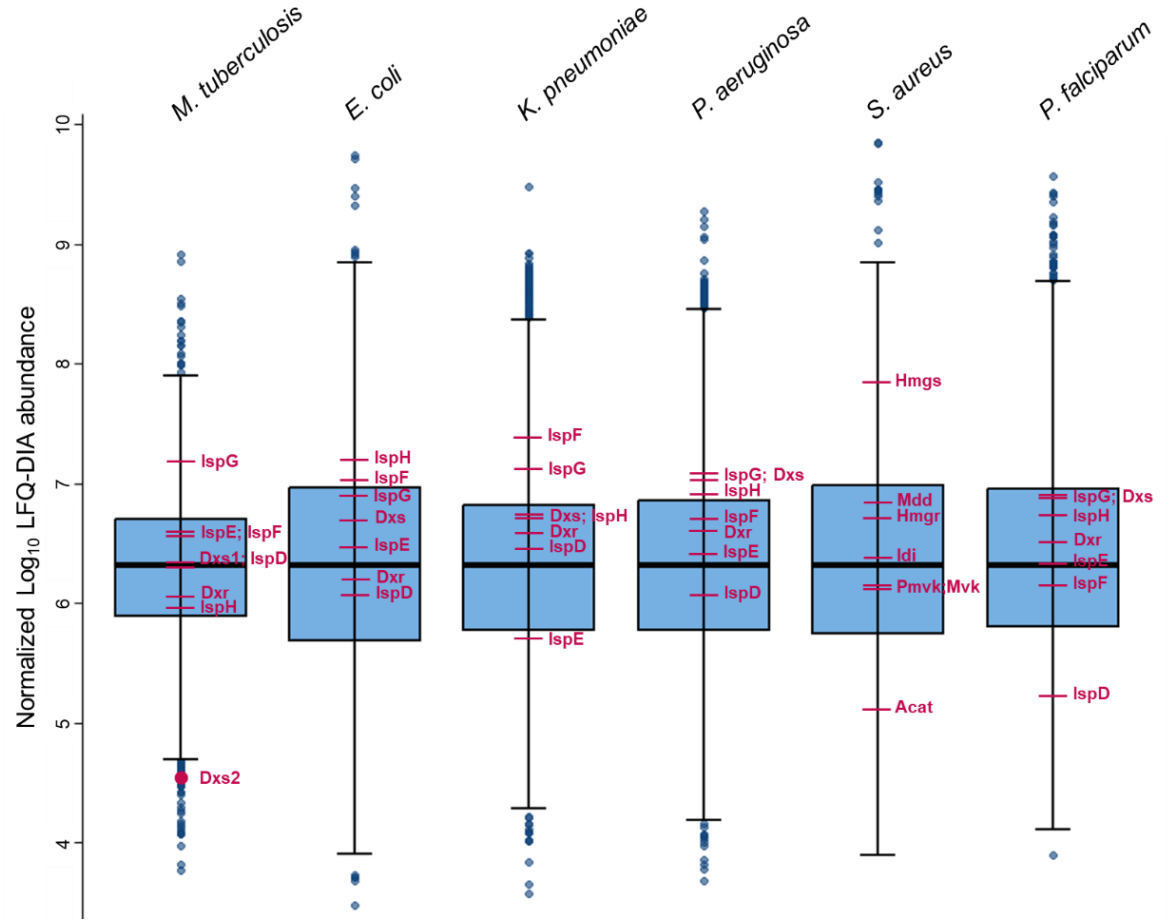


**Figure 1.** Global proteomic characterization by LC-MS/MS of the *Mycobacterium tuberculosis*, *Escherichia coli*, *Klebsiella pneumoniae*, *Pseudomonas aeruginosa*, *Staphylococcus aureus*, and *Plasmodium falciparum* proteomes. All quantified proteins are sorted by the normalized log10 LFQ-DIA abundance. The enzymes of the MEP pathway are highlighted, while the mevalonate pathway enzymes are highlighted for *S. aureus*.

For all organisms except *M. tuberculosis*, a native lysis buffer with the non-denaturing detergent IGEPAL CA-630 was used to extract proteins in their native state and solubilize membrane proteins. In contrast, due to the biosafety level 3 (BSL-3) classification of *M. tuberculosis*, the cell pellets were inactivated by heat and then resuspended in a harsh lysis buffer containing the anionic detergent SDS. This harsher lysis method was necessary to ensure complete inactivation of cells. This more aggressive approach is known to disrupt cell membranes more effectively, allowing for a more complete release of cellular contents.[22] Consequently, harsher lysis conditions often result in higher proteome coverage because they facilitate the extraction of proteins that might be inaccessible or only partially

recovered under milder conditions. Given this, the high coverage observed in our study, particularly under predominantly native lysis conditions, underscores the effectiveness of our proteomic approach.

Notably, the seven MEP enzymes were identified in all species that utilize this pathway for isoprenoid biosynthesis, as illustrated in Figure 1.

These enzymes were generally observed at medium to high abundance, with the exception of 2-*C*-methyl-D-erythritol 4-phosphate cytidylyltransferase (IspD) in *P. falciparum*, which was detected at a considerably lower abundance. Among them, 1-deoxy-D-xylulose 5-phosphate synthase (Dxs1) is particularly critical as it catalyzes the rate-limiting step of the MEP pathway, regulating the overall flux of substrates toward isoprenoid precursor biosynthesis and serving as a potential target for drug development against relevant pathogens. Dxs1 displayed comparable abundance levels across the selected species, with the highest level observed in *P. aeruginosa*.

Conversely, IspD fell within the lowest 10% of abundant proteins, indicating its low representation within the proteome of *P. falciparum*. This differential abundance of IspD in *P. falciparum* is noteworthy, as it suggests potential challenges in targeting this enzyme for drug development within this particular organism. The low abundance may reflect regulatory mechanisms that downregulate IspD expression under certain conditions or highlight a limitation inherent to bottom-up proteomics. For instance, the ionization efficiency during nano-ESI can vary between peptides, potentially leading to underrepresentation of certain proteins, especially if their peptides exhibit poor ionization properties. Additionally, specific peptides of IspD may have been less efficiently detected due to issues such as suboptimal chromatographic separation or incomplete digestion during sample preparation. [36,37] Nonetheless, by confirming the presence and quantifiability of all seven MEP pathway enzymes across these pathogens we provide a solid foundation for subsequent (chemo-)proteomic investigations. These studies are essential for the exploration of potential inhibitors of the MEP pathway through target identification and validation, critical steps in advancing the development of novel anti-infective agents.

**Proteomic Evaluation of CRISPRi-Induced Gene Knockdown in *M. tuberculosis***

We designed the CRISPRi experiments to target three specific genes in *M. tuberculosis* (strain H37Rv): *rpoB*, *dxs1*, and *dxr*. These genes encode the β-subunit of RNA polymerase (RpoB), and two key enzymes in the MEP pathway, Dxs1 and Dxr, respectively. The experiments were conducted using three different concentrations of Atc: 0 ng/mL, 1.95 ng/mL, and 500 ng/mL. The 0 ng/mL condition served as the control, where no gene repression was expected, while 1.95 ng/mL represented a low Atc concentration with the potential for limited repression, and 500 ng/mL was chosen to induce strong gene repression. All conditions were prepared in duplicate. Following growth, the resulting cell pellets were inactivated by heat, resuspended in SDS lysis buffer, and processed for bottom-up proteomics analysis via LC-MS/MS. This approach enabled the identification of 3144 proteins, corresponding to approximately 79% proteomic coverage relative to the *M. tuberculosis* H37Rv UniProt reference database.[21]

The proteomics results demonstrated a reduction in RpoB levels in the CRISPRi-treated samples, thereby validating the effectiveness of the CRISPRi system. The downregulation of RpoB provided a proof of concept, confirming that our CRISPRi system can efficiently repress gene expression in *M. tuberculosis*. Furthermore, a dose-dependent reduction in Dxs1 and Dxr protein levels was observed in response to increasing concentrations of Atc, indicating that CRISPRi was able to downregulate these key enzymes in the MEP pathway (Figure 2). In combination with additional phenotypic analyses and qPCR experiments, these results collectively demonstrate that CRISPRi effectively downregulates

target proteins. This is particularly relevant, as the MEP pathway plays a crucial role in bacterial isoprenoid biosynthesis,[38] and these findings provide direct evidence for the applicability of CRISPRi in studying essential metabolic pathways in *M. tuberculosis*.

In addition to target-specific effects, global proteomic changes were assessed through the generation of volcano plots, comparing protein abundance across two different Atc concentrations (1.95 ng/mL and 500 ng/mL compared to 0 ng/mL). As illustrated in Figure 3, Dxs1 and Dxr were among the most significantly downregulated proteins at the highest Atc concentration (500 ng/mL). In contrast, RpoB exhibited a comparatively lower level of repression, suggesting that that the sensitivity of this gene to Atc-mediated repression may not be fully captured in the proteomics setup, suggesting that additional independent experiments may be required.

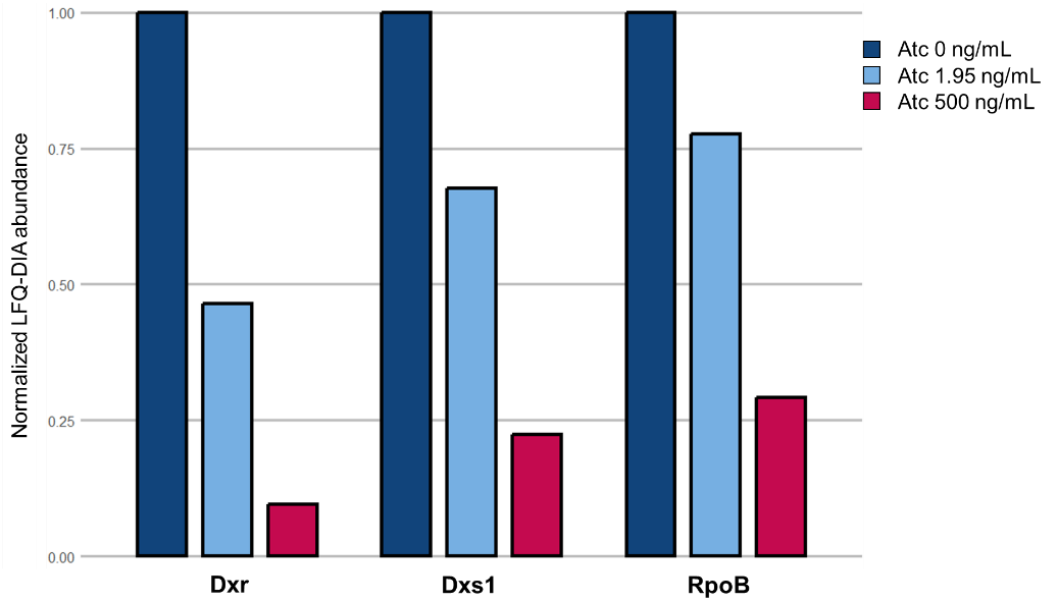


**Figure 2.** Normalized LFQ-DIA abundance of the proteins encoded by dxr, dxs1, and rpoB across three anhydrotetracycline (Atc) concentrations (0 ng/mL in dark blue, 1.95 ng/mL in light blue, and 500 ng/mL in red). For each protein, its relative abundance compared to the lowest Atc concentration (0 ng/mL) is shown. The bar chart illustrates the dose-dependent downregulation of these proteins following CRISPRi-mediated gene repression showing a clear decrease in protein abundance with increasing Atc concentrations, demonstrating the effectiveness of CRISPRi in modulating gene expression in *Mycobacterium tuberculosis*.

Dxs1 catalyzes the rate-limiting step of the MEP pathway and, alongside its downregulation (Figure 3C), additional proteins were observed to be downregulated, including Alpha-crystallin (Acr). Acr is a heat-shock protein predominantly expressed during the dormant or latent phase of *M. tuberculosis* infection.[39] It plays a critical role in protecting the bacteria from environmental stresses such as hypoxia and nutrient deprivation, promoting bacterial survival in a non-replicative state. The observed downregulation of Acr may be a consequence of the metabolic stress caused by Dxs1 repression, which could disrupt cellular energy homeostasis. Since Acr is linked to the bacteria's ability to cope with unfavorable conditions, its downregulation might indicate a cellular shift away from survival strategies in response to impaired metabolic function. Additionally, Hypoxic response protein 1 (Hrp1) and Ferredoxin (FdxA) were affected by Dxs1 repression. Hrp1 is integral to the bacterial response to hypoxic environments, such as those found in granulomas during infection.[40] Ferredoxins, including FdxA, are essential for electron transfer reactions in various metabolic processes such as nitrogen fixation, respiration, and the biosynthesis of key cofactors.[41] Their downregulation may be attributed to the metabolic reprogramming triggered by the inhibition of Dxs1. The MEP pathway is essential for the biosynthesis of quinones and other molecules involved in electron transport. Therefore, disruption

of this pathway could decrease the demand for electron transfer activities and impair the bacterial capacity for energy generation under low-oxygen conditions, reducing the need for a full hypoxic response, and consequently leading to decreased expression of FdxA and Hrp1.

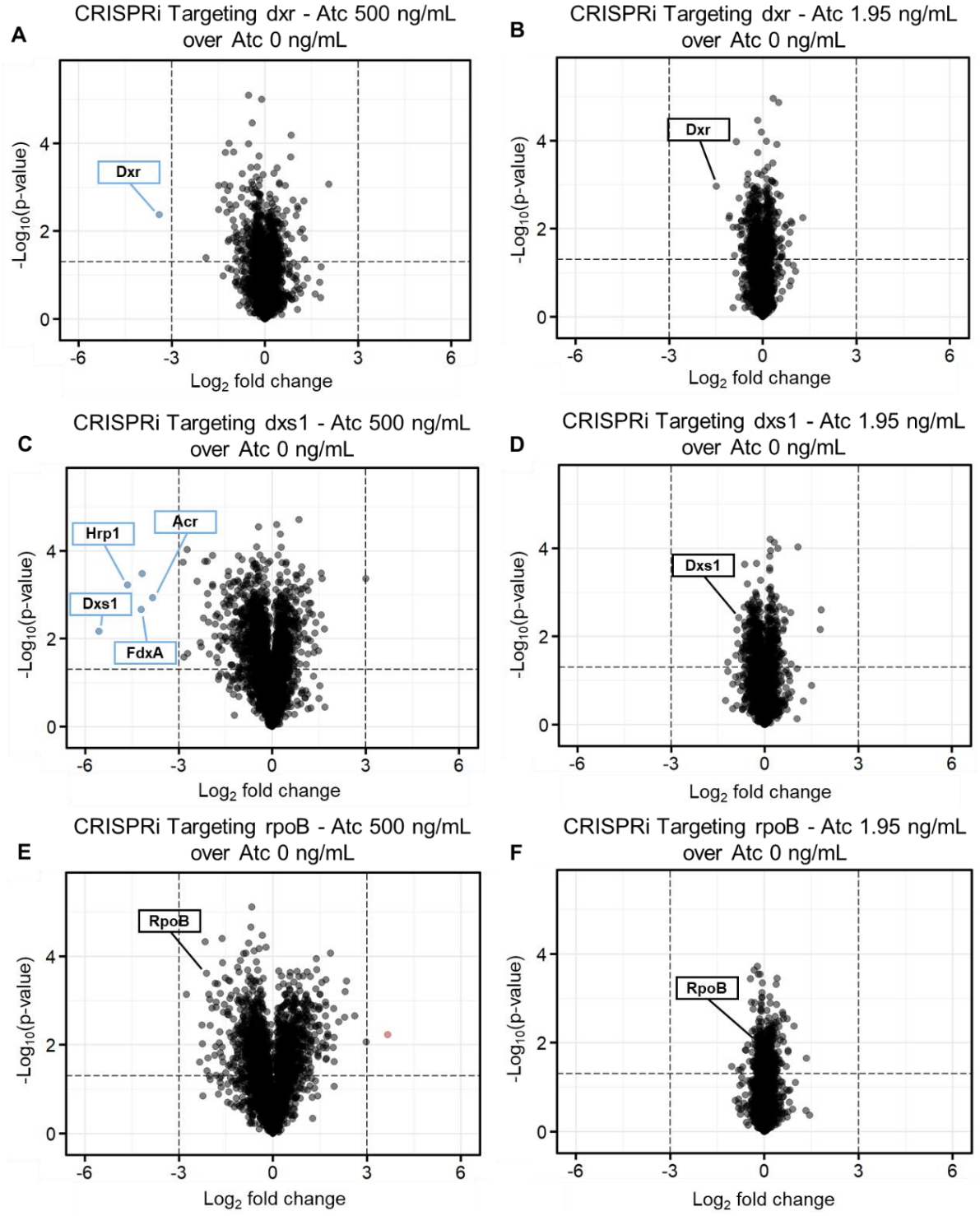


**Figure 3.** Volcano plots displaying the differential abundance of proteins following CRISPRi-mediated gene repression by comparing protein abundance in *Mycobacterium tuberculosis* at anhydrotetracycline (Atc) concentrations of 1.95 ng/mL and 500 ng/mL over 0 ng/mL. The x-axis represents the $\log_2$ fold change (log2FC) and the y-axis the $-\log_{10}$ p-value. Proteins significantly downregulated or upregulated at each Atc concentration are highlighted, using thresholds of a log2FC > |3.0| and a p-value < 0.05 (dashed lines). Red, upregulated proteins with $\log_2$FC > 3.0 and p-value < 0.05; blue, downregulated proteins with $\log_2$FC < -3.0 and p-value < 0.05; gray/black, proteins with -3.0 < $\log_2$FC < 3.0 and p-value < 0.05 and proteins with p-value > 0.05.

These findings underscore the utility of CRISPRi in investigating genes involved in key metabolic pathways. The selective repression of Dxs1 and Dxr, both of which are essential enzymes in the MEP pathway, not only validates CRISPRi as a powerful tool for modulating gene expression in *M. tuberculosis* but also highlights the potential of targeting these enzymes to disrupt isoprenoid precursor biosynthesis. The integration of CRISPRi with global proteomics provides a powerful approach for both functional validation and future target identification in drug discovery.

The proteomics data revealed not only the expected downregulation of the targeted proteins but also broader proteomic shifts, offering valuable insights into compensatory mechanisms and secondary effects triggered by gene repression. These global changes enrich our understanding of the cellular response to gene modulation, providing a more comprehensive view of the biological impact of CRISPRi. Moreover, CRISPRi can be leveraged for validating drug targets by assessing changes in drug susceptibility, serving as a robust method for confirming the mechanism of action of potential drug candidates, particularly in the context of drug-resistant *M. tuberculosis* strains.

In conclusion, the results of our CRISPRi experiments downregulating *rpoB*, *dxs1*, and *dxr* in *M. tuberculosis* demonstrate that CRISPRi is a highly effective tool for precise, dose-dependent gene repression. The combination of CRISPRi and proteomics provides a powerful platform for the validation of drug targets and the exploration of essential metabolic pathways, such as the MEP pathway. The high selectivity observed for Dxs1 and Dxr, along with the broader proteomic changes identified, lays the foundation for future research into the development of novel antimicrobial therapies targeting these enzymes. It should be noted that these experiments were performed in duplicate, and repeating them with multiple biological replicates may yield a more accurate representation of the results. For instance, the observed downregulation of RpoB could be enhanced. Overall, this integrated approach offers a scalable and efficient method for investigating gene function and validating drug targets in *M. tuberculosis* and could prove crucial in addressing the global challenge of antibiotic resistance.

## METHODS

### Bacterial cultures and cell extracts preparation

*Mycobacterium tuberculosis* (strain H37Rv) heat-inactivated cells were obtained from the Research Centre Borstel (Germany). *Escherichia coli* (strain K12), *Klebsiella pneumoniae* (strain ATCC13883), *Pseudomonas aeruginosa* (strain PA01), and *Staphylococcus aureus* (strain Newman) cell lysates were obtained from the Helmholtz Institute for Pharmaceutical Research Saarland (HIPS). *Plasmodium falciparum* (strain NF54) cell lysates were obtained from the Swiss Tropical And Public Health Institute (Swiss TPH).

*E. coli*, *K. pneumoniae*, *P. aeruginosa*, and *S. aureus* were grown aerobically overnight (ON) with agitation at 200 rpm, 37 °C in lysogeny broth. *M. tuberculosis* was prepared according to Brandenburg et al.[42] In brief, the bacteria were grown in 10mL Middlebrook 7H9 broth supplemented with 10% Middlebrook Oleic albumin-dextrose-catalase (OADC) enrichment medium, 0.2% Glycerol, and 0.05% Tween 80, in 490 $cm^2$ Corning roller bottles. The culture was harvested at the mid-log phase (OD600 0.3–0.6) by centrifugation at 3,200 g, for 10 min, at 4 °C, followed by resuspension in 1 mL 1xPBS. The cells were subjected to heat treatment at 90 °C for 20 min followed by centrifugation. The *M. tuberculosis* cultures subjected to CRISPRi experiments were grown with the addition of anhydrotetracycline (Atc) at concentrations of 500 ng/mL, 1.95 ng/mL, or 0 ng/mL. *P. falciparum* asynchronous NF54 wild-type strain parasites were cultured at 3% hematocrit until parasitemia reached 3–5%. The culture medium used was RPMI 1640, supplemented with 25 mM HEPES, 0.36 mM

hypoxanthine, 24 mM sodium bicarbonate (pH 7.3), 0.5% Albumax II, and 100 µg/mL neomycin. Cultures were maintained at 37 °C in an incubator with a gas mixture of 3% $O_2$, 4% $CO_2$, and 93% $N_2$ under atmospheric pressure. Erythrocytes were lysed using saponin. Briefly, cultures were transferred to 50-mL falcon tubes and centrifuged at 1,200 g for 5 min at room temperature (RT). The supernatant was discarded, and 10 volumes of 0.1% (w/v) saponin solution were added. The mixture was incubated on ice for 10 min with shaking every 60 s. The solution was then centrifuged at 4,000 g for 15 min at 4 °C, resulting in a dark red supernatant of lysed erythrocytes and a brown pellet of intact parasites. The pellet was washed with ice-cold PBS and centrifuged at 4,000 g for 5 min at 4 °C. This washing step was repeated until the supernatant became clear. All cell species, except *M. tuberculosis*, were re-suspended in 3x cell pellet volume with ice-cold lysis buffer containing 50 mM Tris/HCl pH 7.5, 5% glycerol, 150 mM NaCl, 1.5 mM $MgCl_2$, 1 mM DTT, 0.8% IGEPAL CA-630, 1X Halt Protease and Phosphatase Inhibitor-Cocktails (Thermo Fisher Scientific). *M. tuberculosis* pellet was resuspended in 3x cell pellet volume with lysis buffer containing 5% SDS, 50 mM Tris-HCl (pH 7.5), 1 tablet per 50 mL EDTA-free Protease Inhibitor Cocktail and 1 tablet per 10 mL PhosSTOP Phosphatase Inhibitor Cocktail. The resuspended cell pellets were vortexed for 30 s, incubated 30 min on ice and further lysed via homogenization (BANDELIN SONOPULS mini20) with 5 cycles at 70% amplitude for 30 s. Each cycle was followed by 90 s pause where the suspension was kept at 4 °C. The lysate was then centrifuged twice for 30 min at 4 °C, 17,000 g and the supernatant collected. The protein lysates were diluted to 0.8 mg/mL (Pierce™ BCA Protein Assay Kit, Thermo Fisher Scientific) using the same lysis buffer and then stored at –80 °C until further use.

### Generation of CRISPRi mutants

CRISPRi conditional mutants of *M. tuberculosis* were generated as described by Rock and colleagues [15] and detailed by Sonawane.[43] Briefly, sgRNAs were designed using the web-based tool PEBBLE: sgRNA Design. The 21 bp sgRNA oligos were ordered from Eurofins Genomics, with 'GGGA' and 'AAAC' overhangs to facilitate cloning using the BsmBI restriction enzyme. For the non-targeting (NT) mutants, used as negative controls, a 'scrambled' sgRNA sequence was employed, which was confirmed to have no significant matches in the *M. tuberculosis* genome via BLASTn analysis (maximum observed complementarity was 11 bp).

The sgRNA oligos were annealed using a thermocycler (BIOER Technology, China) at 95 °C for 2 min and subsequently ligated into the CRISPRi backbone plasmid pLJR965 (Addgene plasmid #115163). Prior to ligation, the plasmid was digested with the BsmBI-HF® restriction enzyme (New England Biolabs #R3136) at 55 °C for 4 h. The digested plasmid DNA was separated via gel electrophoresis, then ligated with the annealed oligos using T4 DNA ligase buffer and T4 DNA ligase enzyme (New England Biolabs). The ligation product was transformed into *E. coli* competent cells, plated on Luria broth (LB) agar with 50 µg/mL kanamycin, and individual colonies were picked for culturing in LB broth. Plasmids were extracted from *E. coli* and verified by Sanger sequencing (Eurofins).

The verified plasmids were electroporated into *M. tuberculosis* using a MicroPulser Electroporator (Bio-Rad, California, United States). After electroporation, the bacteria were grown on 7H10 agar plates containing 50 µg/mL kanamycin. Colonies were picked after 20 days and cultured in 7H9 broth for further experiments, with stocks prepared for future use. To confirm CRISPRi functionality, the mutants were grown in 7H9 broth containing kanamycin for 17 days, and growth was monitored using OD600 measurements and colony-forming unit (CFU) counts. Additionally, mRNA expression levels of the CRISPRi strains were quantified using RT-qPCR.

### Sample preparation for LC-MS/MS analysis

The cell lysates were prepared for global proteomic analysis. To reduce disulfide bonds, 10 mM DTT (Carl Roth) was added, followed by incubation for 30 min at 35 °C, 700 rpm on a ThermoMixer C (Eppendorf). Protein alkylation was performed with 55 mM chloroacetamide (CAA, Merck) and 30 min incubation at room temperature, in the dark. Samples were acidified by adding phosphoric acid to a final concentration of 2.5% and subsequently diluted 7-fold with 90% methanol (Th. Geyer) in 100 mM TEAB pH 7.5. Samples were transferred to an S-trap column (Protifi), washed 4x with the same buffer. Sequencing grade modified trypsin (Promega) in TEAB pH 8.5 was added to the S-trap column at a ratio of 1:10 (trypsin/protein), and the digest reaction was carried out overnight at 37 °C. Peptides were eluted with 50 mM TEAB pH 8.5, followed by 0.1% formic acid (FA, Th. Geyer) and then 50:50 acetonitrile (ACN, Sigma-Aldrich)/water with 0.1% FA. Samples were dried down and peptides resuspended with 0.5% FA. Peptides were desalted on the Bravo Automated Liquid Handling Platform using C18 cartridges (5 µL bed volume, Agilent) and the standard AssayMAP peptide cleanup v2.0 protocol. Samples were dried down and stored at −80 °C until further use.

### Liquid chromatography and mass spectrometry data-acquisition

All samples were solubilized in 0.1% FA before being injected in volumes equivalent to 1 µg on a Dionex UltiMate 3000 nano System (Thermo Fisher Scientific) coupled online to a Q Exactive Plus (Thermo Fisher Scientific) equipped with an Orbitrap mass-analyzer. Peptides were delivered to a trap column (75 µm × 2 cm, packed in-house with ReproSil-Pur 120 ODS-3 resin, Dr. Maisch). Subsequently they were separated on an analytical column (75 µm × 55 cm, packed in-house with Reprosil-Gold 120 C18, 3 µm resin, Dr. Maisch) at a flow rate of 300 nL/min using a 100 min gradient, ranging from 2% to 32% solvent B (0.1% FA, 5% DMSO in HPLC-MS grade acetonitrile) in solvent A (0.1% FA, 5% DMSO in HPLC-MS grade water). The column oven temperature was set at 50 °C. The QE plus instrument was operated in data-independent acquisition (DIA), in positive ionization mode. Full scan spectra (m/z 400−1,000) were acquired in centroid mode at an Orbitrap resolution of 70,000, an AGC target set to 3e6, a maximum injection time of 20 ms. Subsequently, DIA scans were collected utilizing 30 windows, with a 1 Da window overlap. HCD collision was set to 27%, loop count to 30, Orbitrap resolution to 35,000, AGC target to 3e6, and a maximum injection time set to automatic.

### Peptide and protein identification and quantification

Raw LFQ-DIA files were processed with DIA-NN (v1.8.1). They were analyzed by library-free mode, using the UniProt FASTA files for each organism: *M. tuberculosis* (strain ATCC 25618 / H37Rv) taxon identifier: 83332; *E. coli* K12, taxon identifier: 83333; *P. aeruginosa* PAO1, taxon identifier: 208964; *K. pneumoniae* ATCC13883, taxon identifier: 1125630 (ATCC13883 proteome is redundant to the reference HS11286); *S. aureus* Newman, taxon identifier: 93061 (Newman proteome is redundant to the reference NCTC 8325 / PS 47); *P. falciparum* NF54, taxon identifier: 5843; canonical versions, not older than five months prior to MS measurements. The raw files were digested selecting Trypsin/P as enzyme specificity with maximal two missed cleavages. Peptide length was restricted from 7 to 30 peptides, and the pre-cursor m/z range was set from 300 to 1,800. Cysteine carbamidomethylation was selected as a fixed modification, methionine oxidation and N-terminal acetylation as variable modifications. The maximum number of variable modifications was set to three and match between runs (MBR) was enabled. All other parameters were set to default, including the 1% precursor FDR. Cross-run normalization (RT-dependent) was enabled.

### Data analysis

Protein intensity values of biological replicates across all conditions were normalized to their median abundance and $\log_{10}$ transformed using Excel. The box plot was generated in RStudio by ggplot2 package (v. 3.5.0).[44] The volcano plots were generated in RStudio by EnhancedVolcano package (v.

1.20.0),[45] plotting proteins by statistical significance (vertical axis, -$\log_{10}$ p-value) and magnitude of change (horizontal axis, $\log_2$ fold change) of the quantified LFQ-DIA protein intensities for each condition over control.

## ACKNOWLEDGMENTS

We thank Patricia Bravo, Pascal Mäser, and Matthias Rottmann for their contributions to preparing cell cultures and providing lysates for *Plasmodium falciparum*.

## REFERENCES

[1] Mallick P, Kuster B. Proteomics: a pragmatic perspective. Nature Biotechnology 2010 28:7 2010;28:695–709. https://doi.org/10.1038/nbt.1658.

[2] Meissner F, Geddes-McAlister J, Mann M, Bantscheff M. The emerging role of mass spectrometry-based proteomics in drug discovery. Nat Rev Drug Discov 2022;21:637–54. https://doi.org/10.1038/s41573-022-00409-3.

[3] Masini T, Hirsch AKH. Development of inhibitors of the 2C-methyl-D-erythritol 4-phosphate (MEP) pathway enzymes as potential anti-infective agents. J Med Chem 2014;57:9740–63. https://doi.org/10.1021/jm5010978.

[4] Bantscheff M, Schirle M, Sweetman G, Rick J, Kuster B. Quantitative mass spectrometry in proteomics: a critical review. Anal Bioanal Chem 2007;389:1017–31. https://doi.org/10.1007/S00216-007-1486-6.

[5] Zhang G, Ueberheide BM, Waldemarson S, Myung S, Molloy K, Eriksson J, et al. Protein quantitation using mass spectrometry. Methods Mol Biol 2010;673:211–22. https://doi.org/10.1007/978-1-60761-842-3_13.

[6] Shuken SR. An Introduction to Mass Spectrometry-Based Proteomics. J Proteome Res 2023. https://doi.org/10.1021/acs.jproteome.2c00838.

[7] Schirle M, Bantscheff M, Kuster B. Mass spectrometry-based proteomics in preclinical drug discovery. Chem Biol 2012;19:72–84. https://doi.org/10.1016/j.chembiol.2012.01.002.

[8] Gao Y, Ma M, Li W, Lei X. Chemoproteomics, A Broad Avenue to Target Deconvolution. Advanced Science 2024;11. https://doi.org/10.1002/ADVS.202305608.

[9] Qi LS, Larson MH, Gilbert LA, Doudna JA, Weissman JS, Arkin AP, et al. Repurposing CRISPR as an RNA-γuided platform for sequence-specific control of gene expression. Cell 2013;152:1173–83. https://doi.org/10.1016/j.cell.2013.02.022.

[10] Singh V, Braddick D, Dhar PK. Exploring the potential of genome editing CRISPR-Cas9 technology. Gene 2017;599:1–18. https://doi.org/10.1016/J.GENE.2016.11.008.

[11] Jinek M, Chylinski K, Fonfara I, Hauer M, Doudna JA, Charpentier E. A programmable dual-RNA-guided DNA endonuclease in adaptive bacterial immunity. Science (1979) 2012;337:816–21. https://doi.org/10.1126/SCIENCE.1225829/SUPPL_FILE/JINEK.SM.PDF.

[12] Gilbert LA, Horlbeck MA, Adamson B, Villalta JE, Chen Y, Whitehead EH, et al. Genome-Scale CRISPR-Mediated Control of Gene Repression and Activation. Cell 2014;159:647. https://doi.org/10.1016/J.CELL.2014.09.029.

[13] Li S, Poulton NC, Chang JS, Azadian ZA, DeJesus MA, Ruecker N, et al. CRISPRi chemical genetics and comparative genomics identify genes mediating drug potency in Mycobacterium tuberculosis. Nat Microbiol 2022;7:766–79. https://doi.org/10.1038/s41564-022-01130-y.

[14] Bosch B, DeJesus MA, Poulton NC, Zhang W, Engelhart CA, Zaveri A, et al. Genome-wide gene expression tuning reveals diverse vulnerabilities of M. tuberculosis. Cell 2021;184:4579-4592.e24. https://doi.org/10.1016/J.CELL.2021.06.033/ATTACHMENT/765ADB11-DAC0-43E6-9E73-FB6D3B6C1895/MMC3.XLSX.

[15] Rock JM, Hopkins FF, Chavez A, Diallo M, Chase MR, Gerrick ER, et al. Programmable transcriptional repression in mycobacteria using an orthogonal CRISPR interference platform. Nat Microbiol 2017;2:1–9. https://doi.org/10.1038/nmicrobiol.2016.274.

[16] Dominguez AA, Lim WA, Qi LS. Beyond editing: repurposing CRISPR–Cas9 for precision genome regulation and interrogation. Nat Rev Mol Cell Biol 2016;17:5. https://doi.org/10.1038/NRM.2015.2.

[17] Gill SK, Garcia GA. Rifamycin inhibition of WT and Rif-resistant Mycobacterium tuberculosis and Escherichia coli RNA polymerases in vitro. Tuberculosis 2011;91:361–9. https://doi.org/10.1016/j.tube.2011.05.002.

[18] Brown AC, Eberl M, Crick DC, Jomaa H, Parish T. The nonmevalonate pathway of isoprenoid biosynthesis in Mycobacterium tuberculosis is essential and transcriptionally regulated by Dxs. J Bacteriol 2010;192:2424–33. https://doi.org/10.1128/jb.01402-09.

[19] Cane DE, Chow C, Lillo A, Kang I. Molecular cloning, expression and characterization of the first three genes in the mevalonate-independent isoprenoid pathway in Streptomyces coelicolor. Bioorg Med Chem 2001;9:1467–77. https://doi.org/10.1016/S0968-0896(01)00050-5.

[20] Bailey AM, Mahapatra S, Brennan PJ, Crick DC. Identification, cloning, purification, and enzymatic characterization of Mycobacterium tuberculosis 1-deoxy-D-xylulose 5-phosphate synthase. Glycobiology 2002;12:813–20. https://doi.org/10.1093/GLYCOB/CWF100.

[21] Bateman A, Martin MJ, Orchard S, Magrane M, Ahmad S, Alpi E, et al. UniProt: the Universal Protein Knowledgebase in 2023. Nucleic Acids Res 2023;51:D523–31. https://doi.org/10.1093/NAR/GKAC1052.

[22] Yimer SA, Birhanu AG, Kalayou S, Riaz T, Zegeye ED, Beyene GT, et al. Comparative proteomic analysis of Mycobacterium tuberculosis lineage 7 and lineage 4 strains reveals differentially abundant proteins linked to slow growth and virulence. Front Microbiol 2017;8:1–14. https://doi.org/10.3389/fmicb.2017.00795.
[23] Birhanu AG, Gómez-Muñoz M, Kalayou S, Riaz T, Lutter T, Yimer SA, et al. Proteome Profiling of Mycobacterium tuberculosis Cells Exposed to Nitrosative Stress. ACS Omega 2022;7:3470–82. https://doi.org/10.1021/acsomega.1c05923.
[24] Palande A, Patil S, Veeram A, Sahoo SS, Lodhiya T, Maurya P, et al. Proteomic Analysis of the Mycobacterium tuberculosis Outer Membrane for Potential Implications in Uptake of Small Molecules. ACS Infect Dis 2024;10:890–906. https://doi.org/10.1021/ACSINFECDIS.3C00517.
[25] Bespyatykh J, Shitikov E, Butenko I, Altukhov I, Alexeev D, Mokrousov I, et al. Proteome analysis of the Mycobacterium tuberculosis Beijing B0/W148 cluster. Sci Rep 2016;6:1–11. https://doi.org/10.1038/srep28985.
[26] Mateus A, Hevler J, Bobonis J, Kurzawa N, Shah M, Mitosch K, et al. The functional proteome landscape of Escherichia coli. Nature 2020;588:473–8. https://doi.org/10.1038/s41586-020-3002-5.
[27] Chatterjee B, Thakur SS. Single-Run Mass Spectrometry Analysis Provides Deep Insight into E. coli Proteome. J Am Soc Mass Spectrom 2018;29:2394–401. https://doi.org/10.1007/s13361-018-2066-z.
[28] Soufi B, Krug K, Harst A, Macek B. Characterization of the E. coli proteome and its modifications during growth and ethanol stres. Front Microbiol 2015;6:128127. https://doi.org/10.3389/fmicb.2015.00103.
[29] Reales-Calderón JA, Sun Z, Mascaraque V, Pérez-Navarro E, Vialás V, Deutsch EW, et al. A wide-ranging Pseudomonas aeruginosa PeptideAtlas build: A useful proteomic resource for a versatile pathogen. J Proteomics 2021;239:104192. https://doi.org/10.1016/j.jprot.2021.104192.
[30] Goodyear MC, Seidel L, Krieger JR, Geddes-McAlister J, Levesque RC, Khursigara CM. Quantitative proteomics reveals unique responses to antimicrobial treatments in clinical Pseudomonas aeruginosa isolates. MSystems 2023;8. https://doi.org/10.1128/msystems.00491-23.
[31] Wright BW, Kamath KS, Krisp C, Molloy MP. Proteome profiling of Pseudomonas aeruginosa PAO1 identifies novel responders to copper stress. BMC Microbiol 2019;19:1–13. https://doi.org/10.1186/s12866-019-1441-7.
[32] Becher D, Hempel K, Sievers S, Zühlke D, Pané-Farré J, Otto A, et al. A proteomic view of an important human pathogen-Towards the quantification of the entire staphylococcus aureus proteome. PLoS One 2009;4:e8176. https://doi.org/10.1371/journal.pone.0008176.
[33] Pan Z, Fan L, Zhong Y, Guo J, Dong X, Xu X, et al. Quantitative proteomics reveals reduction in central carbon and energy metabolisms contributes to gentamicin resistance in Staphylococcus aureus. J Proteomics 2023;277:104849. https://doi.org/10.1016/j.jprot.2023.104849.
[34] Sukumaran A, Pladwig S, Geddes-McAlister J. Zinc limitation in Klebsiella pneumoniae profiled by quantitative proteomics influences transcriptional regulation and cation transporter-associated capsule production. BMC Microbiol 2021;21:1–15. https://doi.org/10.1186/s12866-021-02091-8.
[35] Hao L, Yang X, Chen H, Mo Z, Li Y, Wei S, et al. Molecular Characteristics and Quantitative Proteomic Analysis of Klebsiella pneumoniae Strains with Carbapenem and Colistin Resistance. Antibiotics 2022;11:1341. https://doi.org/10.3390/antibiotics11101341.
[36] Miller RM, Smith LM. Overview and Considerations in Bottom-Up Proteomics. Analyst 2023;148:475. https://doi.org/10.1039/D2AN01246D.
[37] Dupree EJ, Jayathirtha M, Yorkey H, Mihasan M, Petre BA, Darie CC. A Critical Review of Bottom-Up Proteomics: The Good, the Bad, and the Future of This Field. Proteomes 2020, Vol 8, Page 14 2020;8:14. https://doi.org/10.3390/PROTEOMES8030014.
[38] Eoh H, Brennan PJ, Crick DC. The Mycobacterium tuberculosis MEP (2C-methyl-d-erythritol 4-phosphate) pathway as a new drug target. Tuberculosis 2009;89:1–11. https://doi.org/10.1016/j.tube.2008.07.004.
[39] Yuan Y, Crane DD, Barry CE. Stationary phase-associated protein expression in Mycobacterium tuberculosis: function of the mycobacterial alpha-crystallin homolog. J Bacteriol 1996;178:4484–92. https://doi.org/10.1128/JB.178.15.4484-4492.1996.
[40] Sun C, Yang G, Yuan J, Peng X, Zhang C, Zhai X, et al. Mycobacterium tuberculosis hypoxic response protein 1 (Hrp1) augments the pro-inflammatory response and enhances the survival of Mycobacterium smegmatis in murine macrophages. J Med Microbiol 2017;66:1033–44. https://doi.org/10.1099/JMM.0.000511.
[41] Nzuza N, Padayachee T, Chen W, Gront D, Nelson DR, Syed K. Diversification of ferredoxins across living organisms. Curr Issues Mol Biol 2021;43:1374–90. https://doi.org/10.3390/CIMB43030098/S1.
[42] Brandenburg J, Marwitz S, Tazoll SC, Waldow F, Kalsdorf B, Vierbuchen T, et al. WNT6/ACC2-induced storage of triacylglycerols in macrophages is exploited by Mycobacterium tuberculosis. J Clin Invest 2021;131. https://doi.org/10.1172/JCI141833.
[43] Sonawane VV. Dissertation; Identification and characterisation of novel antimicrobials against Mycobacterium tuberculosis. Lübeck: 2024. https://katalog.ub.uni-kiel.de/DB=4/SET=1/TTL=1/SHW?FRST=2
[44] Wickham H. ggplot2. 2nd ed. Cham: Springer International Publishing; 2016. https://doi.org/10.1007/978-3-319-24277-4.
[45] Blighe K, Rana S, Lewis M. EnhancedVolcano version 1.10.0: Publication-ready volcano plots with enhanced colouring and labeling. R-Package 2021:2–3. https://doi.org/doi:10.18129/B9.bioc.EnhancedVolcano.

## 3.2 Chapter B: Affinity-Based Chemoproteomics for Bacterial Target Identification

Lorenzo Bizzarri, Daan Willocx, Maria Braun Cornejo, Jonas Lohse, Anna K. H. Hirsch, Hannes Hahne

Contributions: Lorenzo Bizzarri, Jonas Lohse, Anna K. H. Hirsch and Hannes Hahne conceived the project; Lorenzo Bizzarri planned and performed all chemoproteomics experiments and analyzed the resulting data from LC-MS/MS measurements; Daan Willocx designed and synthesized the urea-class chemical probe; Maria Braun Cornejo designed and synthesized the pyrazole-amide-class chemical probe; Lorenzo Bizzarri wrote the manuscript with contributions of all authors. Anna K. H. Hirsch and Hannes Hahne coordinated the project.

All authors have given approval to the final version of the manuscript.

This chapter will be submitted to the *ACS Journal of Proteome Research* (American Chemical Society) without or with minor modifications.

# Affinity-Based Chemoproteomics for Bacterial Target Identification

Lorenzo Bizzarri,[a,b] Daan Willocx,[b,c] Maria Braun Cornejo,[b,d] Jonas Lohse,[a] Anna K. H. Hirsch,*[b,c] Hannes Hahne*[a]

[a]OmicScouts GmbH, Lise-Meitner-Straße 30, D-85354 Freising, Germany.
[b]Saarland University, Department of Pharmacy, Campus E8.1, D-66123 Saarbrücken, Germany
[c]Helmholtz Institute for Pharmaceutical Research Saarland (HIPS) – Helmholtz Centre for Infection Research (HZI), Campus Building E8.1, D-66123 Saarbrücken, Germany.
[d]Specs Research Laboratory, Specs Compound Handling, B.V., Bleiswijkseweg 55, 2712 PB Zoetermeer, The Netherlands.

## ABSTRACT

The rise of antimicrobial resistance (AMR) represents a global health threat. The 2-*C*-methyl-D-erythritol-4-phosphate (MEP) pathway, which includes enzymes such as IspD and IspE, is crucial for the biosynthesis of essential isoprenoid precursors, making it a promising target for drug discovery in pathogens such as *Plasmodium falciparum* and *Escherichia coli*. Chemoproteomics techniques, specifically affinity-based pull-down assays, play a crucial role in drug discovery by identifying protein targets of small molecules. This study employed chemical probes that were designed and functionalized for immobilization, with the objective of enriching the enzymes IspD and IspE while also profiling additional target proteins. Challenges such as low proteome abundance of the target protein, poor target affinity, and the high protein amount required for pull-down assays, particularly problematic in organisms with low protein yields like *P. falciparum*, considerably affected target enrichment.

## INTRODUCTION

Drug resistance represents a growing global health threat, severely complicating the development of new therapeutic agents.[1] This issue is particularly critical in the context of antimicrobial resistance (AMR), where the rapid emergence of resistant pathogens has resulted in some infections being nearly untreatable.[2] Although the crisis is most prominent in antibiotic discovery, the impact of AMR extends across a wide range of diseases, including malaria, which is caused by the parasite *Plasmodium falciparum*.[3,4] If current trends continue, it is projected that deaths attributable to AMR could surpass those caused by cancer by 2050.[5] Therefore, the urgent design and discovery of novel antimicrobial agents is imperative to combat this escalating challenge.

The 2-*C*-methyl-D-erythritol-4-phosphate (MEP) pathway plays a crucial role in the biosynthesis of the isoprenoid precursors isopentenyl diphosphate (IDP) and dimethylallyl diphosphate (DMADP) in several key pathogens, including *P. falciparum*, *Haemophilus infuenzae*, *Mycobacterium tuberculosis* and *Escherichia coli*.[6] Notably, the MEP pathway is absent in humans, who utilize the classical mevalonate pathway, making it an attractive target for the development of novel anti-infective drugs.[7,8]

The discovery of new therapeutic agents necessitates not only the elucidation of their precise mechanisms of action but also a thorough understanding of their potential off-target effects, which could lead to unwanted biological consequences.[9] In this context, chemoproteomics has emerged as a pivotal discipline within chemical biology, offering techniques that enhance the drug discovery process.[10] Chemical biology integrates principles from synthetic chemistry, cellular biology, biochemistry, and mass spectrometry to systematically identify and characterize the protein targets of bioactive small molecules within complex biological systems under close-to-physiological

conditions.[11] One of the cornerstone techniques in chemoproteomics is affinity-based proteomics, commonly referred to as pull-down assay. This method is essential for isolating and identifying the protein targets of a given small molecule, thereby revealing both its on- and off-target interactions. The technique comprises two critical steps: (i) the design and synthesis of a chemical probe, and (ii) the enrichment and identification of target proteins from a cellular extract, typically through the use of an affinity matrix.[12]

(i) The first step involves the strategic functionalization of the small molecule of interest to create a chemical probe. This probe is engineered to contain a specific chemical handle, often a reactive group or linker, which facilitates its subsequent immobilization onto a solid support, such as sepharose or agarose beads. The result is the formation of an affinity matrix, which serves as a bait for capturing the target proteins from cell lysates or other complex biological mixtures.

(ii) Second, the affinity matrix is incubated with the cellular extract, allowing the probe to bind selectively to its target proteins. Non-specifically bound proteins are washed away, and the enriched protein complexes are then eluted from the matrix. These proteins can be identified and quantified through quantitative mass spectrometry (LC-MS/MS),[13,14] enabling a comprehensive identification of the interaction landscape of the small molecule.

Such methodologies are indispensable in modern drug discovery, offering a powerful means to deconvolute the molecular targets of lead compounds and to optimize their specificity and efficacy.

As illustrated in Figure 1, pull-down experiments are commonly conducted as competition assays.[15] In these assays, the cell lysate is first incubated with a competitor compound or a vehicle control, (DMSO or $ddH_2O$). The competition assay is performed in a dose-dependent format, using increasing concentrations of the competitor.[16] This approach enables the evaluation of the competitor's capacity to displace the probe from its target proteins, thereby providing insights into the relative binding affinities and specificity of the competitor. The competitor is often the unmodified parent compound of the probe, chosen for its high affinity toward the anticipated protein targets. To confirm that both the probe and its parent compound engage the same primary target, a comparison of their activities in a relevant functional assay is essential. The complexity of cell extracts can lead to non-specific binding of the probe, complicating the differentiation between background interactions and true target binding. This challenge can be mitigated by optimizing the linker length and the coupling density of the compound on the beads.[16] Therefore, competitive pull-down experiments can reliably identify true targets, helping to differentiate specific interactions from background binding.

Following this pre-incubation step, the lysate is incubated with the affinity matrix. Proteins that specifically bind to the probe, upon competition with the competitor for the binding site, are captured by the affinity matrix, while non-binding or weakly binding proteins are removed through multiple washing steps.[15] The enriched proteins are then subjected to proteolytic digestion using a sequence-specific protease such as trypsin. This step cleaves the proteins into peptides, generating a complex peptide mixture suitable for bottom-up proteomic analysis. The resulting peptides are subsequently analyzed by liquid chromatography coupled with tandem mass spectrometry (LC-MS/MS). Data-acquisition and analysis are performed using specialized software tools like MaxQuant or DIA-NN.[17,18]

To ensure the specificity of the captured targets, a parallel control experiment is conducted using an affinity matrix without the immobilized probe (uncoupled beads). This control serves to identify proteins that non-specifically bind to the solid support, thereby generating a background reference. Comparative analysis between the experimental and control conditions allows for the identification of

true hits—proteins that are significantly enriched in the probe-bound samples relative to the background. This approach is critical for distinguishing specific interactions from non-specific binding events, thereby enhancing the reliability of target identification in chemoproteomics studies.[19,20]

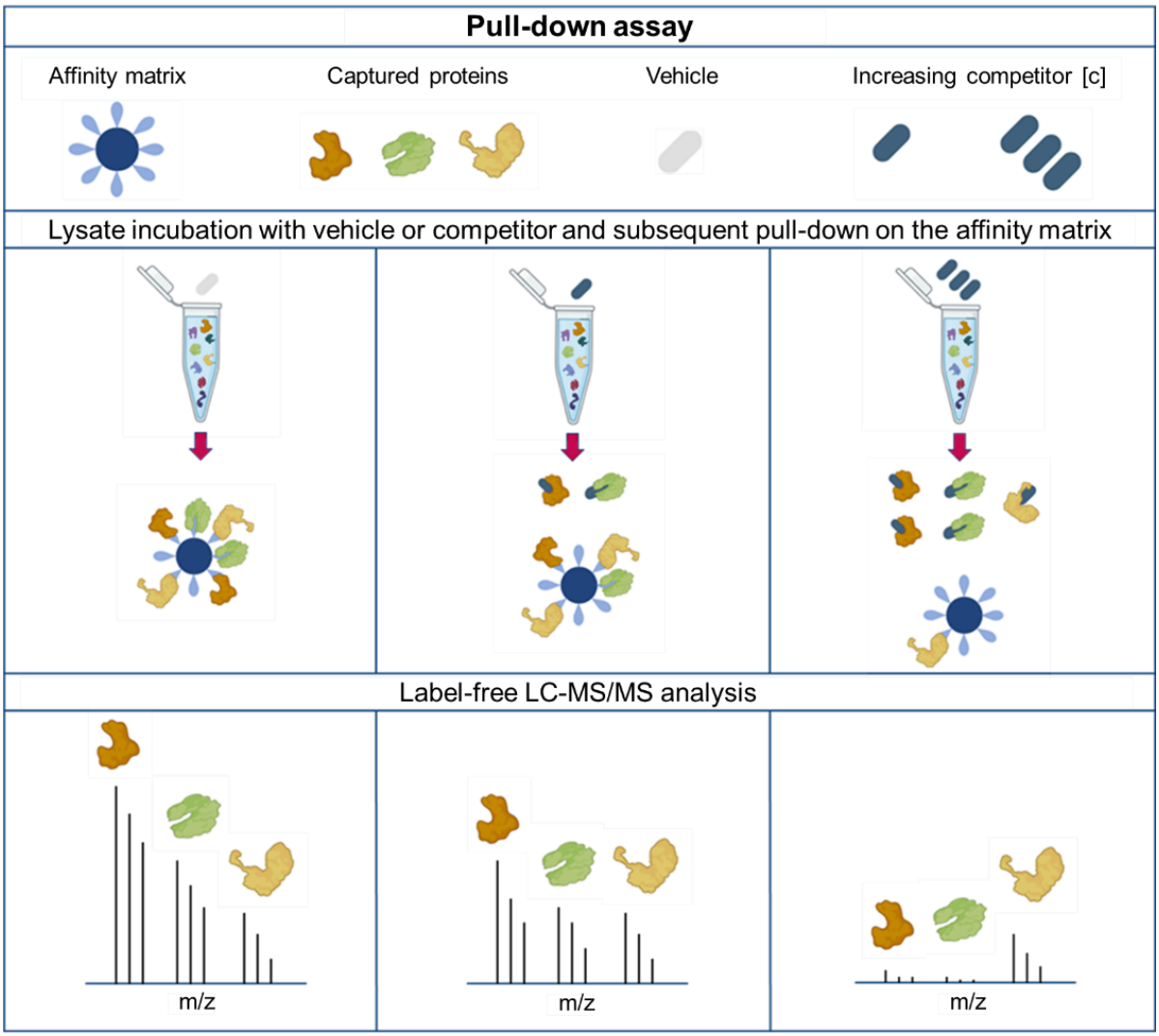


**Figure 1.** Workflow of the pull-down competition assay. Cell lysates are pre-incubated with either a competitor compound in a dose-dependent manner or vehicle control. The lysate is then incubated with an affinity matrix containing the probe linked to sepharose or agarose beads. Proteins specifically bound to the probe are retained, while non-binding proteins are washed away. The retained proteins are prepared and analyzed by LC-MS/MS. Image created with BioRender.com.

In our study, we conducted pull-down experiments to profile inhibitors from two distinct chemical classes. The first class, referred to as the urea class, emerged from a high-throughput screening (HTS) campaign targeting *P. falciparum* 2-*C*-methyl-D-erythritol 4-phosphate cytidylyltransferase (IspD), an essential enzyme in the 2-*C*-methyl-D-erythritol 4-phosphate (MEP) pathway. This class, recently published by Willocx and colleagues,[21] demonstrated potent activity in the low nanomolar range. They were subjected to comprehensive investigations, including whole-cell activity assays, mode-of-inhibition studies, metabolic and plasma stability assessments, and in vivo pharmacokinetic profiling of selected compounds. IspD is a cytidylyltransferase that catalyzes the conversion of 2-*C*-methyl-D-erythritol 4-phosphate (MEP) into 4-diphosphocytidyl-2-*C*-methyl-D-erythritol (CDP-ME).[22] The urea class is represented by compound **1** (Scheme 1A), a functionalized probe with an $IC_{50}$ value of 0.45 µM against *P. falciparum* IspD. During the functionalization process, the probe exhibited approximately a 10-fold reduction in potency compared to the parent compound. This probe contains

a small alkyne handle, enabling immobilization through Copper-catalyzed Azide-Alkyne Cycloaddition (CuAAC) click chemistry[23] onto azide agarose beads, achieving coupling densities of 2 µmol/mL.

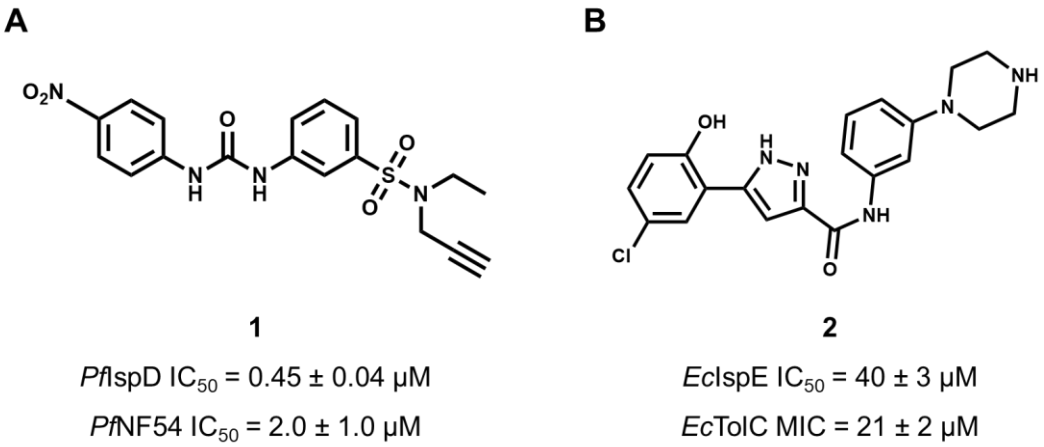


**Scheme 1.** Chemical structures and enzymatic inhibition of (A) urea class chemical probe **1** and (B) pyrazole-amide class chemical probe **2**. *Pf*, *Plasmodium falciparum*; *Ec*, *Escherichia coli*.

The second class was identified by Braun-Cornejo et al.[24] through phenotypic screenings, leading to the discovery of a new pyrazole-amide chemical class with broad-spectrum anti-infective activity. Braun-Cornejo and colleagues synthesized a library of eNTRy-rule-complying compounds by introducing ionizable nitrogens to an antimalarial compound. The eNTRy rules (N = ionizable nitrogen, T = low three-dimensionality, R = rigidity) can be a useful structural guideline for enhancing the permeability of compounds into Gram-negative bacteria. To achieve this, they introduced amines and (cyclic) N-alkyl guanidines into the pyrazole-amide scaffold—already characterized by its planar and rigid structure—successfully extending the compound's activity beyond *P. falciparum* to include Gram-negative and Gram-positive bacteria, as well as *Mycobacterium tuberculosis*. These inhibitors demonstrated strong bioactivity against a range of critical bacterial species, including *E. coli*, *A. baumannii*, *S. aureus*, and *M. tuberculosis*, making them a promising scaffold for further development against multidrug-resistant pathogens. This class of inhibitors exhibited limited potency against 4-diphosphocytidyl-2-*C*-methyl-D-erythritol kinase (IspE), the fourth enzyme in the MEP pathway, in *E. coli*. IspE, a kinase, catalyzes the ATP-dependent phosphorylation of CDP-ME to produce 4-diphosphocytidyl-2-*C*-methyl-D-erythritol 2-phosphate (CDP-MEP).[22] The inhibitors showed some level of inhibition with $IC_{50}$ values in the micromolar range, indicating that while they inhibit IspE, their activity is not high and they may have additional targets. The functionalized probe, compound **2**, has an $IC_{50}$ value of 40 µM against *E. coli* IspE as determined by in vitro activity assays (Scheme 1B), representing a 2.5-fold reduction in activity relative to the parent compound. This probe features a secondary amine handle, which facilitates rapid and spontaneous coupling to the N-hydroxysuccinimide (NHS) esters of NHS-activated sepharose beads through nucleophilic attack, resulting in the formation of a stable amide bond. The probe was immobilized producing two distinct coupling densities of 1 µmol/mL and 2 µmol/mL.

Both affinity matrices failed to enrich the expected protein targets under the tested conditions. Multiple factors could explain these results, including the low proteomic abundance of IspD in *P. falciparum* and the low affinity of compound **2** for IspE ($IC_{50}$ = 40 µM). Nevertheless, several proteins were significantly enriched, potentially representing additional targets or interacting partners of the probes. Additionally, the outcome was further complicated by the large amounts of protein required for the

pull-down assay, which is particularly problematic for pathogens with slow growth rates and low protein yields, such as *P. falciparum*.

Given that IspE is a kinase, we decided to apply the concept of Kinobeads, which was introduced by Bantscheff et al.[20] in 2007 to profile ATP-competitive small-molecule kinase inhibitors. The original Kinobeads affinity matrix was designed using seven immobilized broad-spectrum human ATP-competitive kinase inhibitors on sepharose beads, which successfully enriched 183 protein kinases from K-562 cell lysates. Over time, the approach has been refined, increasing the kinome coverage to about 300 kinases in human cell lysates.[25–27] This method allows for selectivity profiling of kinase inhibitors through competitive pull-down assays, which we attempted with compound **2** as the inhibitor of interest. Despite the promising results in human kinase profiling, we had some concerns about the potential efficacy of this approach for bacterial kinases, particularly IspE. Bacterial kinases have structural and functional features distinct from their human counterparts.[28–30] IspE phosphorylates small molecules within the MEP biosynthetic pathway, whereas human kinases primarily phosphorylate proteins, specifically targeting amino-acid residues like serine, threonine, or tyrosine to regulate cellular processes. The catalytic site of IspE is optimized for its small, organic substrate (CDP-ME), rather than the larger protein substrates typical of human kinases.

Despite these uncertainties, we proceeded with the competitive pull-down assay. The results revealed that IspE was not captured by any of the affinity matrices. However, the Kinobead experiment on *E. coli* lysate successfully enriched 46 distinct proteins having kinase activity out of the 165 annotated in the UniProt Database,[31] demonstrating substantial coverage of the bacterial kinase repertoire. This outcome suggests that the Kinobeads approach can be a valuable tool for enriching bacterial kinases other than IspE, providing a platform for profiling and identifying potential inhibitors. Inhibitors identified through this approach could serve as valuable lead compounds for antibiotic development, given the importance of kinase regulation in bacterial physiology.

## RESULTS AND DISCUSSION

### Urea Class Profiling

To validate the engagement between the urea-based inhibitors and their intended target, IspD, an affinity pull-down experiment was conducted using the affinity matrix based on the immobilized compound **1** on *P. falciparum* 3D7 cell extract. Despite the strategic design of the experiment, IspD was not detected in the pull-down assay: neither in the sample treated with compound **1** nor in the background control (Figure 2).

There are several potential explanations for this observation. One possibility is that compound **1** has insufficient affinity for IspD, which may be due to structural modifications required for immobilization that could compromise its binding efficacy. However, this explanation seems less likely, as the probe exhibits an $IC_{50}$ value of 0.45 μM, indicating relatively strong activity in the nanomolar range. Therefore, it is more plausible that the lack of detection is due to the inherently low abundance of IspD in the *P. falciparum* proteome, which might fall below the detection threshold in the enrichment of the pull-down assay. This hypothesis is supported by our recent study,[32] where global proteomic analysis via LC-MS/MS identified IspD in *P. falciparum* with limited peptide coverage and low abundance, indicating its low expression levels. The violin plot presented in Figure 2B, shows all identified proteins ranked by their $Log_{10}$ LFQ-DIA median intensities (n=3). IspD fell within the lowest 10% of proteins in terms of abundance, reflecting its low presence in the proteome. The low proteomic abundance of IspD not only complicates its detection but also poses significant challenges for its effective targeting in drug-discovery efforts. Nevertheless, our pull-down experiments successfully

identified multiple proteins that were significantly enriched over the background, demonstrating the efficacy of the affinity matrix in capturing protein targets.

The protein with the greatest $\log_2$ fold enrichment was Actin-1 (Act1), a highly conserved cytoskeletal protein that polymerizes to form filaments essential for various cellular processes. In *P. falciparum*, Act1 is critical for gliding motility and host cell invasion, processes vital to the parasite's life cycle.[33] Another significantly enriched protein was glyceraldehyde-3-phosphate dehydrogenase (GAPDH), a key enzyme in glycolysis that plays a central role in energy production and redox balance, both of which are crucial for the survival and proliferation of *P. falciparum*.[34]

Ornithine aminotransferase (OAT) also showed substantial enrichment. OAT catalyzes the transamination of alpha-ketoglutarate and glutamate-5-semialdehyde, reactions that are vital for maintaining amino-acid homeostasis and providing precursors for the synthesis of proline and polyamines.[35] These metabolites are essential for the parasite's growth and survival. Additionally, S-adenosylmethionine synthase (MAT), which was highly enriched in our study, catalyzes the synthesis of S-adenosylmethionine (SAM) from methionine and ATP. SAM is a key molecule in cellular metabolism, acting as the primary methyl donor in numerous methylation reactions, which are critical for regulating gene expression and other cellular functions in *P. falciparum*.[36]

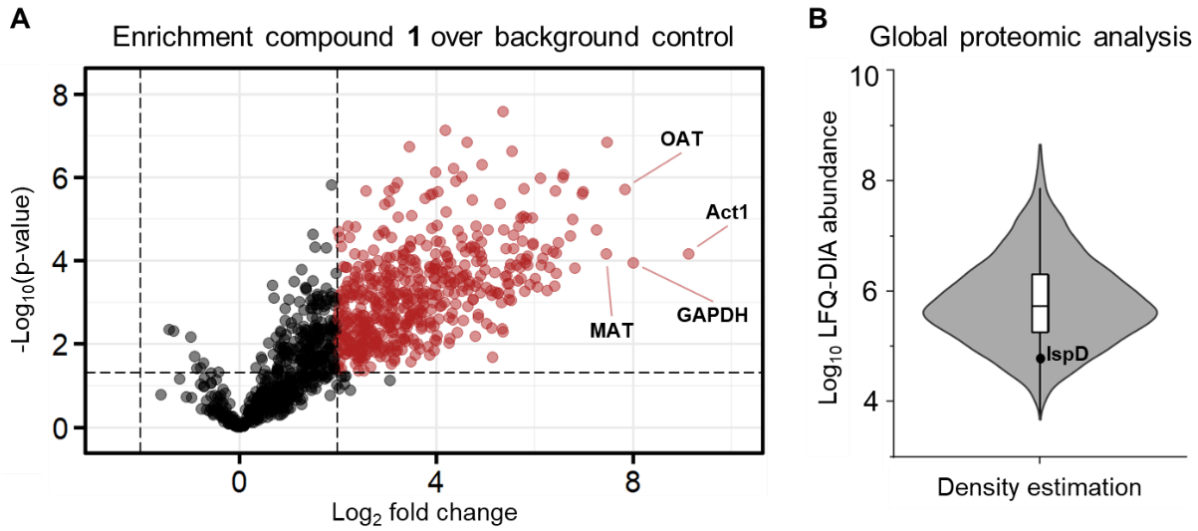


**Figure 2.** (A) Volcano plot showing the results of the affinity pull-down experiment on *Plasmodium falciparum* for the affinity matrix based on the immobilized compound **1** (2 µmol/mL). The plot shows the $\log_2$ fold change (x-axis) of compound **1** over background control versus the significance (y-axis) for proteins enriched in the pull-down assay. The horizontal dashed line represents the threshold for statistical significance ($p < 0.05$), and the vertical dashed lines indicate a 2-fold enrichment threshold. The plot visually demonstrates the relative abundance of proteins, with highly enriched proteins appearing further to the right, and their statistical significance indicated by the height of the data points. (B) Violin plot showing the global proteomic analysis via LC-MS/MS of *P. falciparum*. The plot displays the distribution of 3,450 proteins. The width corresponds to the frequency of data points while the box plot contained within shows the median and the first and third quartiles. IspD is highlighted as black filled circle.

These enriched proteins represent potential targets of the probe, and their identification adds valuable insights into the probe's broader protein interaction profile, possibly responsible for its low micromolar $IC_{50}$ in *P. falciparum*. In conclusion, the target–engagement study with *P. falciparum* proved inconclusive regarding IspD, largely due to the enzyme's low abundance in the proteome, which hampered its detection in the affinity pull-down assay. This highlights a critical challenge in chemical biology: the difficulty of targeting low-abundance proteins, particularly when modifications to the inhibitor are necessary for probe design. Additionally, the pull-down methodology itself presents a critical limitation in this context. These experiments typically require around 2 mg of total protein per

sample, posing a major challenge for organisms like *P. falciparum*, which are characterized by slow growth rates and low protein yields. The need for such large protein amounts can be prohibitive, further complicating target enrichment and limiting the feasibility of these assays with low-yield pathogens.

## Pyrazole-Amide Class Profiling

Pull-down experiments for the pyrazole-amide class were performed on *E. coli* K12 using the affinity matrix based on immobilized compound **2**. Two different coupling densities of the probe were prepared, specifically 1 µmol/mL and 2 µmol/mL. The enrichment results are illustrated in Figures 3A and 3B. Similar to the findings with IspD in the urea class profiling, IspE was not detected in the pull-down assay by LC-MS/MS under the tested conditions. This lack of detection is likely attributed to the low affinity of the probe for *Ec*IspE ($IC_{50}$ = 40 µM). Due to the functionalization of the parent molecule for immobilization, retaining the activity and selectivity of the probe can be challenging. Functionalization can alter the compound's interaction profile, potentially affecting both its binding affinity and specificity. Consequently, the probe may not fully replicate the original binding characteristics of the parent molecule, which can influence the outcome of the assay. Despite the absence of IspE, several proteins were significantly enriched across both coupling densities. Notable among these is FMN-dependent NADH-quinone reductase (AzoR), which confers resistance to thiol-specific stress induced by electrophilic quinones. This enzyme is essential for protecting cells from oxidative stress.[37,38]

Another enriched protein is glutamine synthetase (GS), a key enzyme involved in ammonia assimilation and the synthesis of glutamine from glutamate and ammonia. Given its central role in nitrogen metabolism, GS is crucial for cellular growth and survival under conditions of nitrogen limitation.[39] Transcriptional activator protein NhaR was also identified. NhaR regulates the nhaA gene, which encodes a sodium-proton antiporter. This antiporter is critical for maintaining intracellular pH and sodium homeostasis, playing a vital role in bacterial adaptation to osmotic and ionic stresses.[40] Additionally, the EIIBC component of the phosphoenolpyruvate-dependent sugar phosphotransferase system (EII-Tre) was highly enriched. This system is a major carbohydrate transport mechanism in *E. coli*, responsible for the phosphorylation of incoming sugar substrates during their translocation across the cell membrane. The EII-Tre protein is integral to carbohydrate metabolism and energy production, making it a promising target for interventions aimed at disrupting sugar uptake and metabolism.[41]

Figure 3C is a scatter plot showing the enrichment comparison of the two coupling densities. It enables quick visual identification of proteins similarly enriched by both coupling densities, those next to the fitted curve, and proteins with higher enrichment for one coupling density, those above or below the fitted curve. The proteins are also colored by significance ($-Log_{10}$ p-value). As expected, there are several proteins plotted above the fitted curve due to the higher coupling density and therefore proteins capture ability of 2 µmol/mL compared to 1 µmol/mL. Some of the enriched proteins show a similar behavior between the two coupling densities, sharing comparable $Log_2$ fold change.

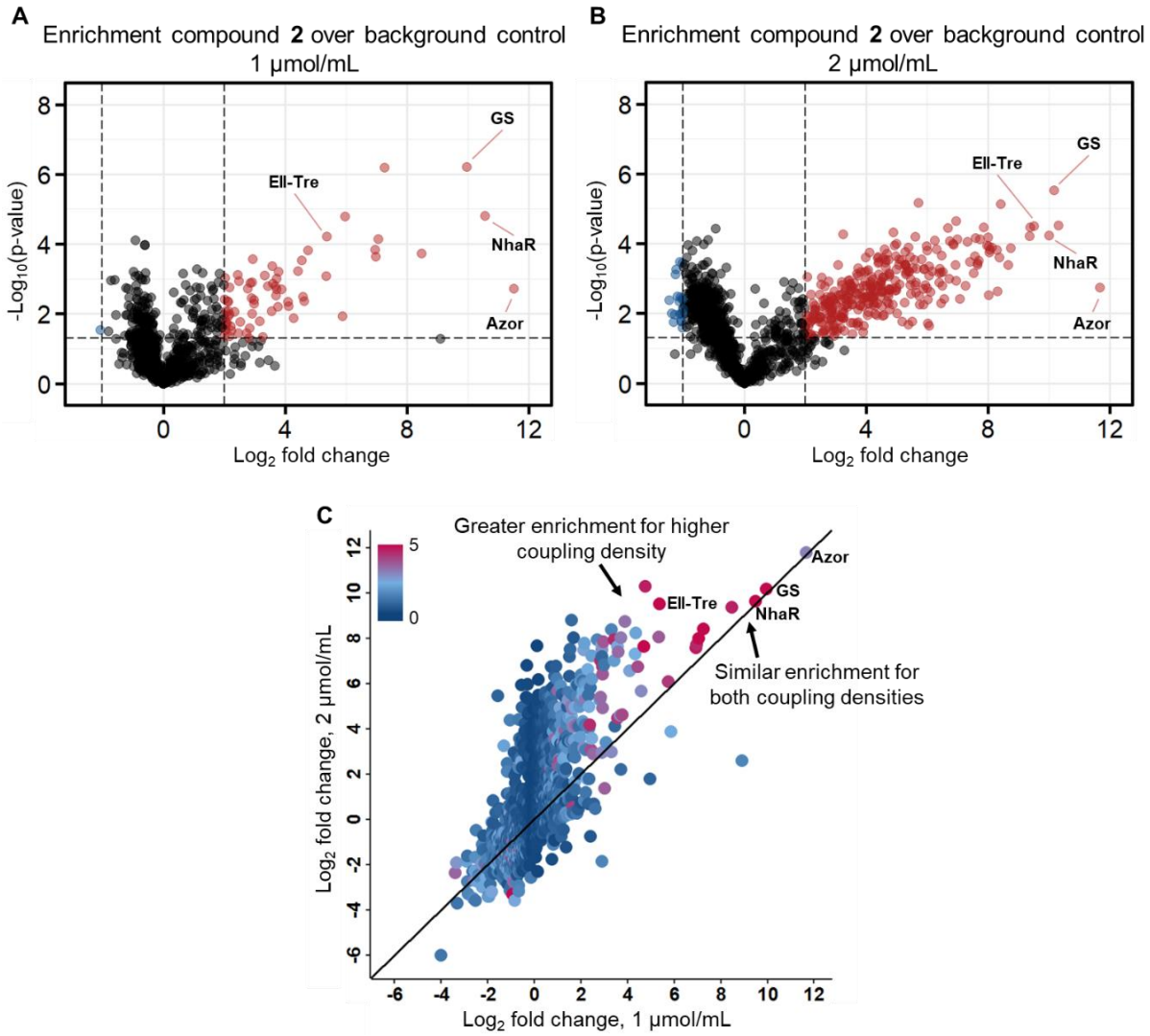


**Figure 3.** Volcano plots showing the results of the affinity pull-down experiment on *Escherichia coli* for the affinity matrix based on the immobilized compound **2**, using the coupling density (A) 1 µmol/mL and (B) 2 µmol/mL. The plot shows the $\log_2$ fold change (x-axis) of compound **2** over background control versus the significance (y-axis) for proteins enriched in the pull-down assay. The horizontal dashed line represents the threshold for statistical significance ($p < 0.05$), and the vertical dashed lines indicate a 2-fold enrichment threshold. The plots visually demonstrates the relative abundance of proteins, with highly enriched proteins appearing further to the right, and their statistical significance indicated by the height of the data points. (C) Scatter plot showing enrichment levels of the two coupling densities tested, 1 µmol/mL (x-axis) over 2 µmol/mL (y-axis). Proteins are colored based on the significance ($-\text{Log}_{10}$(p-value)).

## Kinase Inhibitor Profiling by Kinobeads on *E. coli* Lysate

In an effort to enrich *E. coli* IspE, we applied the Kinobeads approach, originally developed for human kinases, using three different probes—cpd15,[25] cpd19,[25] and cpd3[42]—as affinity matrices, as well as an affinity matrix containing a mixture of the three probes. Additionally, we performed a competition assay using compound **2** as competitor at a concentration of 10 µM. Figure 4 shows the results of the experiment. IspE was not successfully captured by any of the affinity matrices. This outcome is likely attributed to the structural differences between bacterial and human kinases, particularly in substrate specificity. The results of the competition assay using compound **2** did not reveal any significantly competed proteins. Moreover, these results are not conclusive, as the expected target, IspE, was not enriched in the assay. Without IspE's successful enrichment, its binding competition with compound **2** could not be effectively evaluated.

Nevertheless, the selected matrices were able to enrich 46 proteins classified as having kinase activity, according to the UniProt Database, which lists 165 of them in the *E. coli* K12 proteome. This outcome demonstrates that despite the absence of IspE, the experiment captured a decent number of kinases. Among the affinity matrices tested, the one based on the immobilized cpd19 exhibited the highest performance, enriching 33 distinct kinases (Figure 4A). The cpd15 matrix also showed strong performance, capturing 25 kinases, with an overlap of 15 kinases shared between cpd19 and cpd15 (Figure 4B). In contrast, the matrix based on cpd3 was the least effective, with only 5 kinases enriched.

Several of the kinases enriched in this experiment play critical roles in *E. coli*. Ribose-phosphate pyrophosphokinase (Prs) and phosphoglycerate kinase (Pgk) were strongly captured by both cpd15 and cpd19. Prs catalyzes the synthesis of phospho-alpha-D-ribosyl-1-pyrophosphate (PRPP), a central metabolite involved in the biosynthesis of nucleotides, amino-acids, and histidine. This enzyme is crucial for maintaining cellular metabolism and viability, making it an appealing target for inhibitors designed to disrupt bacterial growth.[43] Pgk is a key enzyme in the glycolytic pathway, catalyzing the reversible transfer of a phosphate group from 1,3-bisphosphoglycerate to ADP, generating ATP and 3-phosphoglycerate. Pgk plays an essential role in energy production and the central metabolic pathway of glycolysis.[44]

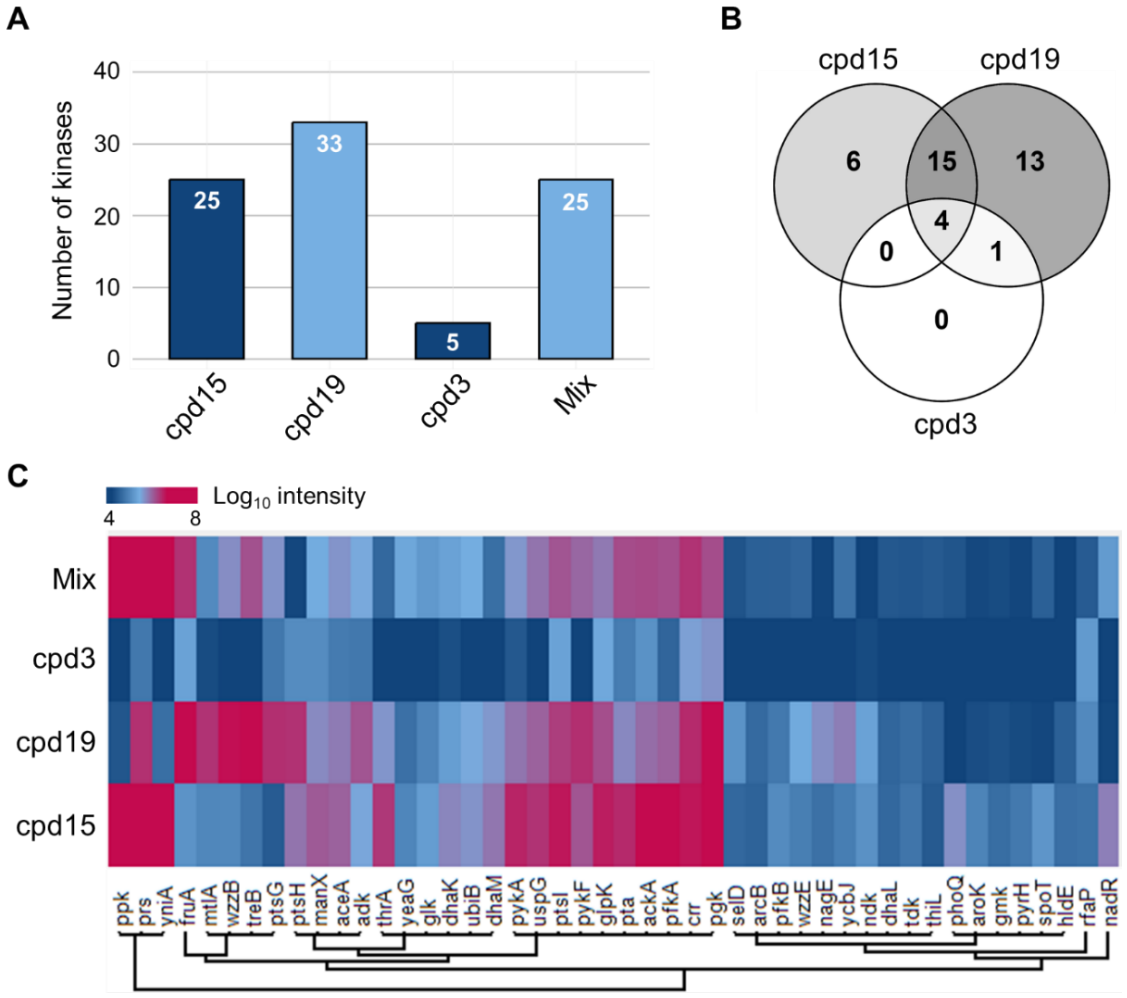


**Figure 4.** *Escherichia coli* kinome enrichment by Kinobeads using the affinity matrices cpd15, cpd19, cpd3 and their mixture. (A) The bar chart shows the number of kinases captured by each condition. (B) The Venn diagram illustrates the overlap of kinases enriched by cpd15, cpd19, and cpd3. The shared sections represent kinases that were captured by more than one compound, highlighting common targets between the different probes. Unique areas show kinases selectively enriched by each specific compound. (C) Heatmap showing the $Log_{10}$ intensity of the enriched kinases for each condition. Proteins are based on the $Log_{10}$ intensity. Gene names of the proteins are shown in the clustering tree.

Additionally, polyphosphate kinase (Ppk) and ATP-dependent 6-phosphofructokinase isozyme 1 (PfkA) were enriched predominantly by cpd15. Ppk catalyzes the reversible transfer of the terminal phosphate from ATP to form polyphosphate (polyP). PolyP is involved in various cellular functions, including energy storage, stress response, and regulation of gene expression. Targeting Ppk could therefore disrupt multiple metabolic processes in *E. coli*, weakening the bacterial cell's ability to manage stress and regulate key survival mechanisms.[45] Pfka plays a central role in glycolysis by catalyzing the phosphorylation of fructose-6-phosphate to fructose-1,6-bisphosphate. As this reaction represents one of the major regulatory steps of glycolysis, PfkA is crucial for controlling the flux of glucose through this pathway.[46]

In conclusion, these findings underscore the potential of affinity-based enrichment strategies, particularly the Kinobeads approach, for capturing kinases that play essential roles in bacteria. Future studies will build on these initial results by including a broader range of ATP-competitive small-molecule kinase inhibitors, specifically designed to target bacterial kinases involved in the phosphorylation of metabolites. This would likely enhance the coverage of enriched kinases. The failure to enrich IspE underscores the limitations of adapting a method originally designed for human kinases to bacterial systems. The differences between human and bacterial kinases, particularly in terms of substrate specificity and catalytic site architecture, likely contributed to this result. In human cells, kinases typically phosphorylate large, diverse protein substrates, while bacterial kinases like IspE act on small metabolites in specific biosynthetic pathways. This fundamental difference in substrate size and chemistry may explain why the affinity matrices, optimized for human kinases, were unable to capture IspE. Nevertheless, the ability of Kinobeads to enrich a decent number of *E. coli* kinases offers valuable insight into the bacterial kinome and its potential for inhibitor profiling. The enrichment of 46 kinases highlights the method's applicability in bacterial systems, even if modifications are necessary to target specific kinases like IspE. Future iterations of this approach could benefit from bacterial kinase-specific probes or further optimization of the affinity matrices to better account for the distinct structural and functional features of bacterial kinases.

## METHODS

### Bacterial cultures and cell extracts preparation

*P. falciparum* strain 3D7 (chloroquine-sensitive, provided by BEI resources, MRA-102) cell lysates were obtained from the Institute of Tropical Medicine, University of Tübingen. Parasites were cultivated in complete culture medium consisting of RPMI-1640 supplemented with 1 M HEPES solution (2.4% v/v), 200 mM L-glutamine (Gibco), 50 µg/mL gentamicin (Gibco), and 10% of AlbuMax II solution containing RPMI, HEPES, $NaHCO_3$, D-Glucose, hypoxanthine and 50 g/L of AlbuMax II (0.5% wt/vol in culture medium) at 2.5% hematocrit. The cultures were maintained at 5% $CO_2$, 5% $O_2$, at 37 °C, with a change of medium every two days. Multistage parasite cultures (2.5% and 8% parasitemia) were centrifuged for 5 min at 1,800 rpm. The pellets were washed with TBS (1:10) and centrifuged for 10 min, at 1,800 rpm, and 4 °C. Then, the samples were resuspended in TBS (1:10) containing 0.1% saponin and kept on ice for 8 min, with mixing in between. Then, the parasites were centrifuged for 5 min, at 5,000 rpm, and 4 °C and washed with ice-cold TBS (10 mL) until the supernatant was clear. The final pellets were resuspended in 600 µL TBS. After that, the samples were sonicated (4x 30 s, 75% intensity, with breaks of 30 min in between) while keeping the sample on ice. Finally, the lysate was centrifuged for 15 min, at 5,000 rpm, and 4 °C and the supernatant was filtered using a 0.22 µM non-binding filter. The samples were stored at –80 °C until further use.
*E. coli* (strain K12) was grown aerobically overnight (ON) with agitation at 200 rpm, 37 °C in lysogeny broth. Cell pellet was re-suspended in 3x cell pellet volume with ice-cold lysis buffer containing 50

mM Tris/HCl pH 7.5, 5% glycerol, 150 mM NaCl, 1.5 mM $MgCl_2$, 1 mM DTT, 0.8% IGEPAL CA-630, 1X Halt Protease and Phosphatase Inhibitor-Cocktails (Thermo Fisher Scientific). The resuspended cell pellets were vortexed for 30 s, incubated for 30 min on ice and further lysed via homogenization (BANDELIN SONOPULS mini20) with 5 cycles at 70% amplitude for 30 s. Each cycle was followed by 90 s pause where the suspension was kept at 4 °C. The lysate was then centrifuged twice for 30 min at 4 °C, 17,000 g and the supernatant collected and stored at –80 °C until use.

**Affinity matrices preparation**

Compound **1** was immobilized on azide agarose beads, while compound **2** on N-hydroxy-succinimide (NHS) activated sepharose beads. 2 mL of both beads/solvent mixture (ratio 1:1) was washed 3X with 10 mL ethanol and DMSO, respectively. To the washed azide beads, 200 µL of compound **1** 10 µM were added in order to obtain the selected coupling density of 2 µmol compound/mL. The washed NHS beads were separated into two 1 mL aliquots, to which 100 µL and 50 µL of compound **2** (10 µM) were added, respectively, in order to obtain the selected coupling density of 2 µmol compound/mL and 1 µmol compound/mL. For compound **1**, 100 mM copper(II) sulfate $CuSO_4$ (Sigma-Aldrich) with 100 mM BTTAA (Jena Bioscience) in a ratio 1:2 were mixed and incubated for 30 min at room temperature (RT). The preformed copper-ligand-complex was then added to the mixture, obtaining 1 mM/2 mM as final concentration (fc) of $CuSO_4$/BTTAA. The mixture was spun at 300 g for 2 min, followed by the collection of 10 µL of the supernatant. The coupling reaction was started by the addition of 100 mM sodium ascorbate, 4 mM fc. The mixture reaction was vortexed and incubated ON on an end-over-end shaker at RT in the dark. The following day, the reaction mixture was spun at 300 g for 2 min. A 10 µL aliquot of the supernatant was collected to verify the successful coupling by LC/MS analysis. After that, the mixture was washed 2X with 10 mL ethanol, 2X with 10 mL EDTA (Sigma-Aldrich), 1X with $ddH_2O$, 3X with ethanol and then stored in ethanol (1 mL/mL beads) at 4°C. For compound **2**, the mixture was spun at 300 g for 2 min, followed by the collection of 10 µL of the supernatant. The coupling reaction was started by the addition of 15 µL triethylamine, and the reaction was vortexed and then incubated ON on an end-over-end shaker at RT in the dark. The following day, the reaction mixture was spun at 300 g for 2 min. A 10 µL aliquot of the supernatant was collected to verify the successful coupling by LC/MS analysis. 50 µL Aminoethanol was then added, and the mixture was vortexed and incubated for 4 h at RT in the dark. The mixture was then washed 1X with 10 mL DMSO and 3X with 10 mL ethanol and stored in ethanol (1 mL/mL beads) at 4 °C.

**Affinity chromatography and sample preparation for LC-MS/MS analysis**

The *P. falciparum* 3D7 cell extract was diluted to a final protein concentration of 2.5 mg/mL (Pierce™ BCA Protein Assay Kit, Thermo Fisher Scientific) using the same lysis buffer. For each affinity enrichment condition, 1 mL of cell extract (2.5 mg total protein/well) was added to a combinatorial microlute plate (Dunn Labortechnik) and then incubated at 4 °C for 30 min on an end-over-end shaker with 40 µL of the corresponding affinity matrix which were washed with 1 mL of lysis buffer. Upon incubation, each sample was washed 1X with 1 mL of lysis buffer with 0.4% IGEPAL CA-630, 2X with 1 mL of lysis buffer with 0.2% IGEPAL CA-630 and 3X with 1mL of lysis buffer without addition of detergent. Protein denaturation and reduction was achieved by addition of 40 µL of urea buffer (8 M Urea, 10 mM DTT in 50 mM Tris/HCl pH 8.0) to each sample and incubation for 30 min at 30 °C, 700 rpm. 5 µL of 550 mM 2-Chloroacetamide (CAA) was added to each sample, incubating 30 min at RT, 700 rpm in the dark to obtain protein's cysteine alkylation. The urea concentration was then diluted to 1.5 M by adding 250 µL of 50 mM Tris/HCl pH 8.0 to each well. On-bead digestion was performed by incubation ON at 35 °C, at 700 rpm with 200 ng of sequencing grade modified trypsin (Promega) in each sample. The following day, the trypsinized peptides were eluted from the

combinatorial microlute plate into a 96-well plate and then acidified by addition of formic acid (FA) to reach 0.5% in the well. Peptides were desalted on the Bravo Automated Liquid Handling Platform using C18 cartridges (5 µL bed volume, Agilent) and the standard AssayMAP peptide cleanup v2.0 protocol. Samples were dried down and stored at −80 °C until further use.

**Liquid chromatography and mass spectrometry data-acquisition**

All samples were solubilized in 0.1% FA before being injected in volumes equivalent to 1 µg on a Dionex UltiMate 3000 nano System (Thermo Fisher Scientific) coupled online to a Q Exactive Plus (Thermo Fisher Scientific) equipped with an Orbitrap mass-analyzer. Peptides were delivered to a trap column (75 µm × 2 cm, packed in-house with ReproSil-Pur 120 ODS-3 resin, Dr. Maisch). Subsequently, they were separated on an analytical column (75 µm × 55 cm, packed in-house with Reprosil-Gold 120 C18, 3 µm resin, Dr. Maisch) at a flow rate of 300 nL/min using a 70 min gradient, ranging from 2% to 32% solvent B (0.1% FA, 5% DMSO in HPLC-MS grade acetonitrile) in solvent A (0.1% FA, 5% DMSO in HPLC-MS grade water). The column oven temperature was set at 50 °C. The QE plus instrument was operated in data-dependent acquisition (DDA), in positive ionization mode, automatically switching between MS and MS2. Full scan MS spectra (m/z 360−1300) were acquired in the Orbitrap at 70,000 resolution using an automatic gain control (AGC) target value of 3e6 charges. Precursor ion isolation width was set to 2.0 Th, the maximum injection time for MS/MS was 100 ms, and dynamic exclusion was set to 20 s. Tandem mass spectra of up to 20 precursors were generated in the multipole collision cell by using higher-energy collisional dissociation (HCD) (AGC target value 1e5) and analyzed in the Orbitrap at a resolution of 17,500. Precursor ion isolation width was set to 1.7 m/z, the maximum injection time for MS/MS was 50 ms, and dynamic exclusion was set to 35 s.

**Peptide and protein identification and quantification**

Raw LFQ-DDA files were processed with MaxQuant (v. 1.6.17.0). The complete UniProt *P. falciparum* 3D7 proteome reference database (UP000001450) was applied for matching MS/MS spectra. Intensity based label-free quantification was defined as MS quantification technique. Cysteine carbamidomethylation was used as a fixed modification; methionine oxidation and N-term acetylation were used as variable modifications. Trypsin/P was selected as enzyme specificity with maximum of two missed cleavages allowed. For peptide and protein identification 1% FDR were used. To maximize the number of proteins identified, match-between-runs (MBR) functionality was applied.

**Data analysis**

Protein intensity values of biological replicates across all conditions were normalized to their median abundance using Excel. Data were then uploaded on Perseus (v. 1.6.15.0) where proteins were filtered for reverse identifications (false positives) and contaminants. LFQ intensity values were $\log_2$ transformed and then missing values were imputed from a normal distribution (width 0.3, down shift 1.5, only for the background control). p-Values were obtained by a two-sample t test over replicates with a permutation-based false discovery rate correction (FDR 0.05). The scatter plot and heatmap were both generated on Perseus. The volcano plots were generated in RStudio by EnhancedVolcano package (v. 1.20.0),[47] plotting proteins by statistical significance (vertical axis, -$\log_{10}$ p-value) and magnitude of change (horizontal axis, $\log_2$ fold change) of the quantified LFQ-DIA protein intensities for each compound condition over vehicle control. The bar chart was generated in RStudio by ggplot2 package (v. 3.5.0).[48] The venn diagram was generated in Venny (v. 2.1.0).[49]

# REFERENCES


[1] Smith WPJ, Wucher BR, Nadell CD, Foster KR. Bacterial defences: mechanisms, evolution and antimicrobial resistance. Nat Rev Microbiol 2023;21:519–34. https://doi.org/10.1038/s41579-023-00877-3.

[2] Grundmann H, Glasner C, Albiger B, Aanensen DM, Tomlinson CT, Andrasević AT, et al. Occurrence of carbapenemase-producing Klebsiella pneumoniae and Escherichia coli in the European survey of carbapenemase-producing Enterobacteriaceae (EuSCAPE): a prospective, multinational study. Lancet Infect Dis 2017;17:153–63. https://doi.org/10.1016/S1473-3099(16)30257-2.

[3] WHO World Health Organization. World malaria report. 2023.

[4] Björkman A, Gil P, Alifrangis M. Alarming Plasmodium falciparum resistance to artemisinin-based combination therapy in Africa: the critical role of the partner drug. Lancet Infect Dis 2024;24:e540–1. https://doi.org/10.1016/S1473-3099(24)00427-4.

[5] O'Neill J. Antimicrobial Resistance : Tackling a crisis for the health and wealth of nations. Review on Antimicrobial Resistance 2016:1–16.

[6] Zhu D, Johannsen S, Masini T, Simonin C, Haupenthal J, Illarionov B, et al. Discovery of novel drug-like antitubercular hits targeting the MEP pathway enzyme DXPS by strategic application of ligand-based virtual screening. Chem Sci 2022;13:10686–98. https://doi.org/10.1039/d2sc02371g.

[7] Diamanti E, Hamed MM, Lacour A, Bravo P, Illarionov B, Fischer M, et al. Targeting the IspD Enzyme in the MEP Pathway: Identification of a Novel Fragment Class. ChemMedChem 2022;17. https://doi.org/10.1002/cmdc.202100679.

[8] Obiol-Pardo C, Rubio-Martinez J, Imperial S. The Methylerythritol Phosphate (MEP) Pathway for Isoprenoid Biosynthesis as a Target for the Development of New Drugs Against Tuberculosis. Curr Med Chem 2011;18:1325–38. https://doi.org/10.2174/092986711795029582.

[9] Sun D, Gao W, Hu H, Zhou S. Why 90% of clinical drug development fails and how to improve it? Acta Pharm Sin B 2022;12:3049–62. https://doi.org/10.1016/j.apsb.2022.02.002.

[10] Gao Y, Ma M, Li W, Lei X. Chemoproteomics, A Broad Avenue to Target Deconvolution. Advanced Science 2024;11. https://doi.org/10.1002/ADVS.202305608.

[11] Bantscheff M, Drewes G. Chemoproteomic approaches to drug target identification and drug profiling. Bioorg Med Chem 2012;20:1973–8. https://doi.org/10.1016/J.BMC.2011.11.003.

[12] Chen X, Wang Y, Ma N, Tian J, Shao Y, Zhu B, et al. Target identification of natural medicine with chemical proteomics approach: probe synthesis, target fishing and protein identification. Signal Transduct Target Ther 2020;5. https://doi.org/10.1038/s41392-020-0186-y.

[13] Schirle M, Bantscheff M, Kuster B. Mass spectrometry-based proteomics in preclinical drug discovery. Chem Biol 2012;19:72–84. https://doi.org/10.1016/j.chembiol.2012.01.002.

[14] Meissner F, Geddes-McAlister J, Mann M, Bantscheff M. The emerging role of mass spectrometry-based proteomics in drug discovery. Nat Rev Drug Discov 2022. https://doi.org/10.1038/s41573-022-00409-3.

[15] Wright MH, Sieber SA. Chemical proteomics approaches for identifying the cellular targets of natural products. Nat Prod Rep 2016;33:681–708. https://doi.org/10.1039/c6np00001k.

[16] Rix U, Superti-Furga G. Target profiling of small molecules by chemical proteomics. Nat Chem Biol 2008;5:616–24. https://doi.org/10.1038/nchembio.216.

[17] Tyanova S, Temu T, Cox J. The MaxQuant computational platform for mass spectrometry-based shotgun proteomics. Nat Protoc 2016;11:2301–19. https://doi.org/10.1038/nprot.2016.136.

[18] Demichev V, Messner CB, Vernardis SI, Lilley KS, Ralser M. DIA-NN: neural networks and interference correction enable deep proteome coverage in high throughput. Nat Methods 2020;17:41–4. https://doi.org/10.1038/s41592-019-0638-x.

[19] Daub H. Quantitative proteomics of kinase inhibitor targets and mechanisms. ACS Chem Biol 2015;10:201–12. https://doi.org/10.1021/cb5008794.

[20] Bantscheff M, Eberhard D, Abraham Y, Bastuck S, Boesche M, Hobson S, et al. Quantitative chemical proteomics reveals mechanisms of action of clinical ABL kinase inhibitors. Nat Biotechnol 2007;25:1035–44. https://doi.org/10.1038/nbt1328.

[21] Willocx D, Bizzarri L, Alhayek A, Kannan D, Bravo P, Illarionov B, et al. Targeting Plasmodium falciparum IspD in the Methyl-d-erythritol Phosphate Pathway: Urea-Based Compounds with Nanomolar Potency on Target and Low-Micromolar Whole-Cell Activity. J Med Chem 2024. https://doi.org/10.1021/ACS.JMEDCHEM.4C00212.

[22] Masini T, Hirsch AKH. Development of inhibitors of the 2C-methyl-D-erythritol 4-phosphate (MEP) pathway enzymes as potential anti-infective agents. J Med Chem 2014;57:9740–63. https://doi.org/10.1021/jm5010978.

[23] Neumann S, Biewend M, Rana S, Binder WH. The CuAAC: Principles, Homogeneous and Heterogeneous Catalysts, and Novel Developments and Applications. Macromol Rapid Commun 2020;41. https://doi.org/10.1002/marc.201900359.

[24] Braun-Cornejo M, Platteschorre M, Vries V de, Bravo P, Sonawane V, Hamed MM, et al. A Positive Charge in an Antimalarial Compound Unlocks Broad-spectrum Antibacterial Activity. ChemRxiv 2024. https://doi.org/10.26434/CHEMRXIV-2024-RS2V8-V2.

[25] Médard G, Pachl F, Ruprecht B, Klaeger S, Heinzlmeir S, Helm D, et al. Optimized chemical proteomics assay for kinase inhibitor profiling. J Proteome Res 2015;14:1574–86. https://doi.org/10.1021/pr5012608.

[26] Reinecke M, Ruprecht B, Poser S, Wiechmann S, Wilhelm M, Heinzlmeir S, et al. Chemoproteomic Selectivity Profiling of PIKK and PI3K Kinase Inhibitors. ACS Chem Biol 2019;14:655–64. https://doi.org/10.1021/acschembio.8b01020.

[27] Pachl F, Plattner P, Ruprecht B, Médard G, Sewald N, Kuster B. Characterization of a chemical affinity probe targeting Akt kinases. J Proteome Res 2013;12:3792–800. https://doi.org/10.1021/pr400455j.

[28] Kannan N, Taylor SS, Zhai Y, Venter JC, Manning G. Oceanic Metagenomics: Structural and Functional Diversity of the Microbial Kinome. PLoS Biol 2007;5:0467–78. https://doi.org/10.1371/JOURNAL.PBIO.0050017.
[29] Manuse S, Fleurie A, Zucchini L, Lesterlin C, Grangeasse C. Role of eukaryotic-like serine/threonine kinases in bacterial cell division and morphogenesis. FEMS Microbiol Rev 2016;40:41–56. https://doi.org/10.1093/FEMSRE/FUV041.
[30] Grangeasse C, Nessler S, Mijakovic I. Bacterial tyrosine kinases: Evolution, biological function and structural insights. Philosophical Transactions of the Royal Society B: Biological Sciences 2012;367:2640–55. https://doi.org/10.1098/rstb.2011.0424.
[31] Bateman A, Martin MJ, Orchard S, Magrane M, Ahmad S, Alpi E, et al. UniProt: the Universal Protein Knowledgebase in 2023. Nucleic Acids Res 2023;51:D523–31. https://doi.org/10.1093/NAR/GKAC1052.
[32] Bizzarri L, Sonawane V, Bravo P, Haupenthal J, Lohse J, Mäser P, Rottmann M, Reiling N, Hirsch A K H, Hahne H. Comprehensive Proteomic Profiling of Human Pathogens and CRISPRi-Driven Gene Modulation in Mycobacterium tuberculosis. Manuscript in Preparation
[33] Kumpula EP, Lopez AJ, Tajedin L, Han H, Kursula I. Atomic view into Plasmodium actin polymerization, ATP hydrolysis, and fragmentation. PLoS Biol 2019;17. https://doi.org/10.1371/JOURNAL.PBIO.3000315.
[34] Satchell JF, Malby RL, Luo CS, Adisa A, Alpyurek AE, Klonis N, et al. Structure of glyceraldehyde-3-phosphate dehydrogenase from Plasmodium falciparum. Acta Crystallogr D Biol Crystallogr 2005;61:1213–21. https://doi.org/10.1107/S0907444905018317.
[35] Gafan C, Wilson J, Berger LC, Berger BJ. Characterization of the ornithine aminotransferase from Plasmodium falciparum. Mol Biochem Parasitol 2001;118:1–10. https://doi.org/10.1016/S0166-6851(01)00357-7.
[36] Musabyimana JP, Distler U, Sassmannshausen J, Berks C, Manti J, Bennink S, et al. Plasmodium falciparum S-Adenosylmethionine Synthetase Is Essential for Parasite Survival through a Complex Interaction Network with Cytoplasmic and Nuclear Proteins. Microorganisms 2022;10. https://doi.org/10.3390/MICROORGANISMS10071419/S1.
[37] Liu G, Zhou J, Fu QS, Wang J. The Escherichia coli azoreductase AzoR Is involved in resistance to thiol-specific stress caused by electrophilic quinones. J Bacteriol 2009;191:6394–400. https://doi.org/10.1128/JB.00552-09.
[38] Mercier C, Chalansonnet V, Orenga S, Gilbert C. Characteristics of major Escherichia coli reductases involved in aerobic nitro and azo reduction. J Appl Microbiol 2013;115:1012–22. https://doi.org/10.1111/JAM.12294.
[39] Liaw SH, Jun G, Eisenberg D. Interactions of nucleotides with fully unadenylylated glutamine synthetase from Salmonella typhimurium. Biochemistry 1994;33:11184–8. https://doi.org/10.1021/BI00203A014.
[40] Karpel R, Taglicht D, Glaserz G, Schuldiner S, Padan E. NhaR, a Protein Homologous to a Family of Bacterial Regulatory Proteins (LysR), Regulates nhaA, the Sodium Proton Antiporter Gene in Escherichia coli*. J Biol Chem 1992;267:10433–8. https://doi.org/10.1016/S0021-9258(19)50037-0.
[41] Boos W, Ehmann U, Forkl H, Klein W, Rimmele M, Postma P. Trehalose transport and metabolism in Escherichia coli. J Bacteriol 1990;172:3450–61. https://doi.org/10.1128/JB.172.6.3450-3461.1990.
[42] Gower CM, Thomas JR, Harrington E, Murphy J, Chang MEK, Cornella-Taracido I, et al. Conversion of a Single Polypharmacological Agent into Selective Bivalent Inhibitors of Intracellular Kinase Activity. ACS Chem Biol 2016;11:121–31. https://doi.org/10.1021/acschembio.5b00847.
[43] Willemoës M, Hove-Jensen B, Larsen S. Steady state kinetic model for the binding of substrates and allosteric effectors to Escherichia coli phosphoribosyl-diphosphate synthase. J Biol Chem 2000;275:35408–12. https://doi.org/10.1074/JBC.M006346200.
[44] Nellemann LJ, Holm F, Atlung T, Hansen FG. Cloning and characterization of the Escherichia coli phosphoglycerate kinase (pgk) gene. Gene 1989;77:185–91. https://doi.org/10.1016/0378-1119(89)90373-9.
[45] Tzeng CM, Kornberg A. The multiple activities of polyphosphate kinase of Escherichia coli and their subunit structure determined by radiation target analysis. J Biol Chem 2000;275:3977–83. https://doi.org/10.1074/JBC.275.6.3977.
[46] Nakahigashi K, Toya Y, Ishii N, Soga T, Hasegawa M, Watanabe H, et al. Systematic phenome analysis of Escherichia coli multiple-knockout mutants reveals hidden reactions in central carbon metabolism. Mol Syst Biol 2009;5. https://doi.org/10.1038/MSB.2009.65.
[47] Blighe K, Rana S, Lewis M. EnhancedVolcano version 1.10.0: Publication-ready volcano plots with enhanced colouring and labeling. R-Package 2021:2–3. https://doi.org/doi:10.18129/B9.bioc.EnhancedVolcano.
[48] Wickham H. ggplot2. 2nd ed. Cham: Springer International Publishing; 2016. https://doi.org/10.1007/978-3-319-24277-4.
[49] Oliveros JC. Venny. An interactive tool for comparing lists with Venn's diagrams. https://bioinfogp.cnb.csic.es/tools/venny/index.html n.d.:2007–15.

## 3.3 Chapter C: Studying Target–Engagement of Anti-Infectives by Solvent-Induced Protein Precipitation and Quantitative Mass Spectrometry

Lorenzo Bizzarri, Dominik Steinbrunn, Thibaut Quennesson, Antoine Lacour, Gabriella Ines Bianchino, Patricia Bravo, Philippe Chaignon, Jonas Lohse, Pascal Mäser, Myriam Seemann, Serge Van Calenbergh, Anna K. H. Hirsch, and Hannes Hahne

Contributions: Lorenzo Bizzarri and Hannes Hahne conceived the project. Lorenzo Bizzarri planned and performed all iSPP experiments on bacterial lysates and analyzed the resulting data from LC-MS/MS measurements; Dominik Steinbrunn conceived and conducted the experiments for the semi-automatization of the iSPP workflow; Thibaut Quennesson and Serge Van Calenbergh designed and synthesized the reverse β-aza fosmidomycin analogues; Antoine Lacour performed the iSPP validation experiments on *Klebsiella pneumoniae* and *Pseudomonas aeruginosa*, under the supervision of Lorenzo Bizzarri and Anna K. H. Hirsch; Gabriella Ines Bianchino, Philippe Chaignon, and Myriam Seemann designed and synthesized the diphosphate derivatives; Jonas Lohse contributed to the selection of model drugs for validation experiments; Patricia Bravo and Pascal Mäser contributed to the generation of plots and figures; Lorenzo Bizzarri wrote the manuscript with contributions from all authors; Hannes Hahne coordinated the project.

All authors have given approval to the final version of the manuscript.

This chapter was published in the *ACS Infectious Diseases* Journal (American Chemical Society) on November 20, 2024. Reprinted with permission https://pubs.acs.org/doi/10.1021/acsinfecdis.4c00417.

ACS Infectious Diseases



pubs.acs.org/journal/aidcbc
Article

# Studying Target–Engagement of Anti-Infectives by Solvent-Induced Protein Precipitation and Quantitative Mass Spectrometry

Lorenzo Bizzarri, Dominik Steinbrunn, Thibaut Quennesson, Antoine Lacour, Gabriella Ines Bianchino, Patricia Bravo, Philippe Chaignon, Jonas Lohse, Pascal Mäser, Myriam Seemann, Serge Van Calenbergh, Anna K. H. Hirsch, and Hannes Hahne*

Cite This: https://doi.org/10.1021/acsinfecdis.4c00417



**ABSTRACT:** Antimicrobial resistance (AMR) poses a serious threat to global health. The rapid emergence of resistance contrasts with the slow pace of antimicrobial development, emphasizing the urgent need for innovative drug discovery approaches. This study addresses a critical bottleneck in early drug development by introducing integral solvent-induced protein precipitation (iSPP) to rapidly assess the target−engagement of lead compounds in extracts of pathogenic microorganisms under close-to-physiological conditions. iSPP measures the change in protein stability against solvent-induced precipitation in the presence of ligands. The iSPP method for bacteria builds upon established SPP procedures and features optimized denaturation gradients and minimized sample input amounts. The effectiveness of the iSPP workflow was initially demonstrated through a multidrug target−engagement study. Using quantitative mass spectrometry (LC-MS/MS), we successfully identified known drug targets of seven different antibiotics in cell extracts of four AMR-related pathogens: the three Gram-negative bacteria *Escherichia coli*, *Klebsiella pneumoniae*, *Pseudomonas aeruginosa* and the Gram-positive bacterium *Staphylococcus aureus*. The iSPP method was ultimately applied to demonstrate target−engagement of compounds derived from target-based drug discovery. We employed five small molecules targeting three enzymes in the 2-C-methyl-D-erythritol 4-phosphate (MEP) pathway—a promising focus for anti-infective drug development. The study showcases iSPP adaptability and efficiency in identifying anti-infective drug targets, advancing early-stage drug discovery against AMR.

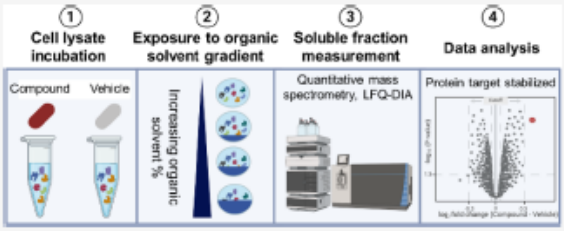


**KEYWORDS:** *mass spectrometry, proteomics, solvent-induced precipitation, antibiotics, MEP pathway, target identification*

Antibiotic therapy for bacterial infections is among the most significant medical advancements in human history. Although being a cornerstone of contemporary medicine, antibiotic efficacy is increasingly in jeopardy due to the emergence of antimicrobial resistance (AMR). The World Health Organization (WHO) asserts that AMR is a rapidly expanding global issue and it represents one of the primary healthcare concerns.[1,2] According to a 2022 study,[3] the six primary pathogens responsible for deaths linked to AMR are *Escherichia coli*, *Staphylococcus aureus*, *Klebsiella pneumoniae*, *Streptococcus pneumoniae*, *Acinetobacter baumannii*, and *Pseudomonas aeruginosa*. In 2019, they accounted for 3.57 million deaths globally associated with AMR. The main issue is that resistance emerges rapidly, while the development of antimicrobials requires a substantial amount of time,[2] primarily due to insufficient validation of discoveries. One way to tackle AMR is through the identification of new protein target candidates for anti-infective drug discovery. Enzymes involved in the 2-C-methyl-D-erythritol 4-phosphate (MEP) pathway represent promising and underexploited targets.[4] The MEP pathway is absent in humans but essential in green algae and numerous pathogenic bacteria and apicomplexan protozoa, including important human pathogens. Composed of seven enzymes, it leads to the production of isopentenyl diphosphate (IDP) and its isomer, dimethylallyl diphosphate (DMADP), which are the five-carbon (C5) building units essential for the biosynthesis of all isoprenoids (Scheme 1).

In addition to the urgent need for new target candidates, a key obstacle throughout the early drug discovery stages to be addressed is the lack of techniques for determining the mode of action (MoA) of antibiotics.[5] Proteomics and chemical proteomics approaches are emerging as important tools for overcoming this challenge. By quantitatively measuring protein activity and function in response to, e.g., compound treatment,

Received: May 20, 2024
Revised: October 10, 2024
Accepted: October 18, 2024

**Scheme 1. MEP Pathway and Its Associated Enzyme Idi**[a]

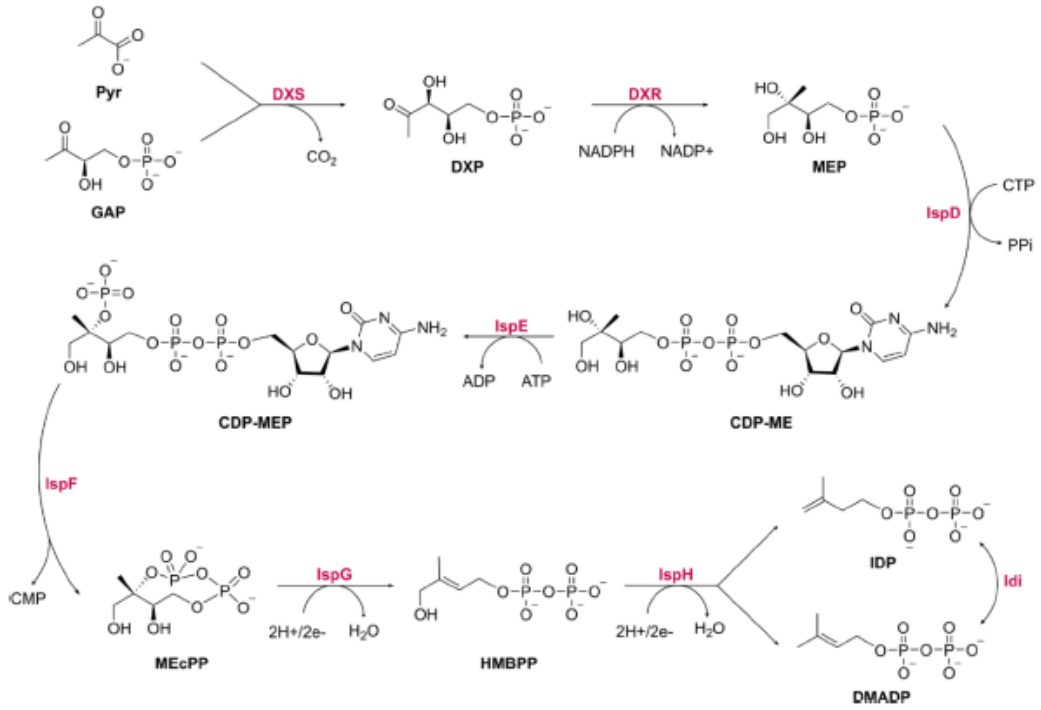


[a]Pyr, pyruvate; GAP, glyceraldehyde 3-phosphate; DXS, 1-deoxy-D-xylulose-5-phosphate synthase; DXP, 1-deoxy-D-xylulose 5-phosphate; DXR, 1-deoxy-D-xylulose 5-phosphate reductoisomerase; MEP, 2-C-methylerythritol 4-phosphate; IspD, 2-C-methyl-D-erythritol 4-phosphate cytidylyltransferase; CTP, cytidine triphosphate; PPi, inorganic diphosphate; CDP-ME, 4-diphosphocytidyl-2-C-methylerythritol; IspE, 4-diphosphocytidyl-2-C-methyl-D-erythritol kinase; CDP-MEP, 4-diphosphocytidyl-2-C-methyl-D-erythritol 2-phosphate; IspF, 2-C-methyl-D-erythritol 2,4-cyclodiphosphate synthase; CMP, cytidine monophosphate; MEcPP, 2-C-methyl-D-erythritol 2,4-cyclodiphosphate; IspG, 4-hydroxy-3-methyl-but-2-en-1-yl diphosphate synthase; HMBPP, (*E*)-4-hydroxy-3-methyl-but-2-enyl pyrophosphate; IspH, 4-hydroxy-3-methylbut-2-enyl diphosphate reductase; IDP, isopentenyl diphosphate; DMADP, dimethylallyl diphosphate; Idi, Isopentenyl-diphosphate delta-isomerase

they provide critical insights into target deconvolution, target–engagement, selectivity, and MoA studies, among others. Ultimately, they can provide a comprehensive picture of protein–ligand interactions and subsequent cellular events.[6,7]

Numerous mass spectrometry (MS)-based chemical proteomics methods have been developed to screen the proteome for evidence of protein–ligand interactions. One of the most recent additions to that toolbox is the solvent-induced protein precipitation (SPP), which represents a quantitative MS-based proteomics (LC-MS/MS) assay for evaluating proteome-wide target–engagement.[8−10] SPP is based on the detection of ligand-induced changes in protein stability upon incubation of a cell lysate with a compound of interest and exposure to increasing concentrations of organic solvents. The denaturation of proteins, and consequently their precipitation, induced by organic solvents is mainly caused by a reduction of the dielectric constant of the solution and destruction of the hydration shell of proteins.[11] The compound–protein complex has a lower energy state than the unbound protein and therefore requires more energy to be unfolded, resulting in an increased tolerance to solvent-induced precipitation. The approach, originally demonstrated by Zhang and coworkers[8] in human cell extracts, is modification-free, thereby omitting the necessity for any label on the tested compound or target proteins. Akin to other label-free proteome-wide stability assays, such as Thermal Proteome Profiling (TPP),[12,13] SPP can be conducted in multiple formats and with different readouts. Most of these formats rely on resolving denaturation curves, which are typically generated by measuring the response of the system at each data point—each representing a single sample across the gradient of the denaturant that contributes to the overall curve, capturing how the system responds at that particular denaturant concentration or condition. Therefore, these techniques are challenging because they typically consume high amounts of sample material, have considerable instrument measurement time, and require intricate data analysis for fitting denaturation curves. Fortunately, these assays can be simplified and streamlined by determining the integral of the denaturation curve. This can be achieved by pooling the soluble fractions of the samples exposed to the selected denaturant gradient after denaturation and precipitation. This compressed approach was initially introduced by Gaetani et al.[14] in a TPP study, termed Proteome Integral Solubility Alteration (PISA), and more recently also applied to SPP by Van Vranken et al.[9] These studies reported that the approach can result in a compression of the observable effect size, thereby presenting a challenge in the detection of stabilized proteins. To prevent this compression, it is necessary to use an appropriate gradient tailored to the region of the most substantial solubility changes of the known target proteins, as it substantially affects the observed stabilization.[9,14]

To that end, we developed integral SPP (iSPP) as a procedure that (i) requires only 20 $\mu$g of total protein experimental input


https://doi.org/10.1021/acsinfecdis.4c00417
ACS Infect. Dis. XXXX, XXX, XXX−XXX

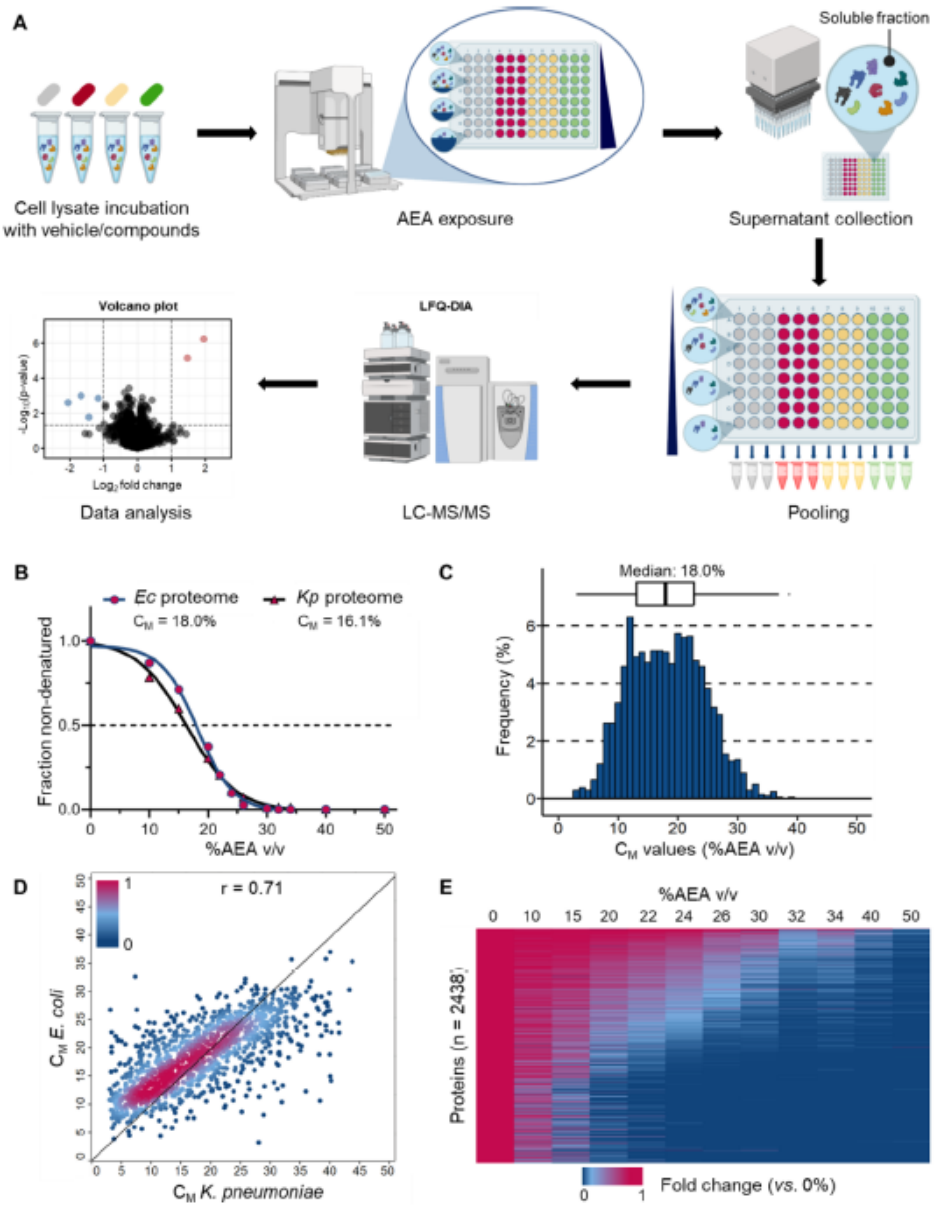


**Figure 1.** Solvent profiling of the *Escherichia coli* and *Klebsiella pneumoniae* proteomes. (A) Schematic representation of the iSPP approach for target–engagement studies (both compound incubation and soluble fractions pooling were omitted during the solvent profiling experiments). Workflow graphic created with BioRender.com. (B) Denaturation curve of the *E. coli* and *K. pneumoniae* proteomes. For each data point, the median value of all quantified proteins is shown. (C) Distribution of $C_M$ values for *E. coli* proteins with high-quality denaturation curves (1984 proteins, $R^2 \geq 0.8$, and plateau $\leq 0.3$). (D) Pearson correlation of $C_M$ values for 1249 predicted orthologs identified in our experiments between *E. coli* and *K. pneumoniae*, showing a strong positive correlation ($r = 0.71$). Proteins are colored based on the density of the points. (E) Heatmap representation of all *E. coli* proteins quantified in the performed experiment (2438 proteins). For each protein, its relative abundance (fold change) at the indicated %AEA (v/v) compared to the lowest concentration (0%) is shown. Proteins are sorted by intensity (in descending order).

material per data point, (ii) utilizes a target-specific, empirically selected solvent concentration range for denaturation to maximize the observable effect size of the area-under-the-denaturation-curve readout, and (iii) employs data-independent acquisition (DIA) quantitative MS as sensitive and versatile alternative to antibody-based readouts, especially useful given that the antibodies for bacterial target proteins are frequently not available.

Initially, we explored the iSPP assay to demonstrate target–engagement of seven well-known antibiotics. We established the approach in cell extracts of four key pathogens for deaths associated with AMR: the three Gram-negative bacteria *Escherichia coli*, *Klebsiella pneumoniae*, and *Pseudomonas aeruginosa* and the Gram-positive bacterium *Staphylococcus aureus*. The designated protein targets of the model drugs were significantly and selectively stabilized and thus identified as the


https://doi.org/10.1021/acsinfecdis.4c00417
ACS Infect. Dis. XXXX, XXX, XXX−XXX

main interactors (hereafter also referred to as top hits). The entire workflow is highly reproducible with a median coefficient of variation (CV) of 6.1% across all quantified proteins in all performed measurements.

We then confirmed the target−engagement of compounds derived from a target-based drug discovery approach. To this end, we employed two classes targeting enzymes of the MEP pathway: (i) diphosphate derivatives as IspG−IspH inhibitors and (ii) recently discovered reverse $\beta$-aza fosmidomycin analogues as DXR inhibitors. The iSPP approach successfully identified the respective MEP enzymes as main targets, together with some potential additional interactors, demonstrating its adaptability and utility in early-stage drug discovery of novel potential anti-infective small molecules.

## RESULTS

**iSPP Workflow.** The workflow of the iSPP assay presented in this study is shown in Figure 1A. First, the bacterial proteins are extracted from cell pellets by means of a native lysis buffer containing the non-denaturing detergent IGEPAL CA-630. Aliquots of cell lysates are then incubated with either compound or vehicle, representing distinct conditions. Then, the aliquots are evenly distributed into a 96-well plate, followed by exposure to an increasing acetone/ethanol/acetic acid mixture (50:50:0.1 v/v, abbreviated as AEA), to initiate denaturation and precipitation of proteins. After precipitation, centrifugation is employed to separate soluble proteins from denatured and aggregated ones. Subsequently, equal supernatant volumes are collected. At this stage, the soluble fractions across the AEA gradient are combined (separately for each condition). The pooled samples are then prepared using a standard bottom-up proteomics workflow for quantitative MS readout.[15] The integral values of the denaturation curves are determined based on the measured protein intensities in the pooled samples. These values are used to identify stabilized proteins by comparing compound and vehicle-treated groups, serving as an indicator for target−engagement. Stabilized proteins exhibit an increase in soluble protein abundance relative to the vehicle, leading to a positive $\log_2$ fold change ($\log_2$FC). Conversely, destabilized proteins show a reduction in soluble protein abundance relative to the vehicle, resulting in a negative $\log_2$FC. Biological replicates of the same condition allow for reproducibility testing and evaluation of the statistical significance of the observed results.

In this study, we present a protocol that utilizes a low protein input amount, making it applicable to hard-to-culture pathogens. A typical experimental design—such as four distinct conditions, one vehicle control, and three distinct compounds, each in triplicate, distributed across eight solvent concentrations—requires about 2.0 mg of total protein extract, representing 20 $\mu$g per data point. Detailed results from the corresponding validation experiments, essential to the minimal input material of the protocol, are provided in Figure S1. We sought to further facilitate the protocol by omitting dimethyl or TMT peptide labeling, deviating from approaches employed in previous SPP publications.[8−10] Consequently, we decided to employ DIA[16,17] as an LC-MS/MS identification and quantification strategy, which enabled recording a bacterial proteome within a single LC-MS/MS measurement.

**Solvent Profiling of *E. coli* and *K. pneumoniae* Proteomes.** To establish a robust assay for assessing proteome-wide target−engagement in bacterial lysates, we initially focused on examining the effect of increasing concentrations of AEA on bacterial proteome stability. We evaluated the denaturation behavior of the *E. coli* K12 proteome, the most widely studied model organism in microbiology, as well as that of *K. pneumoniae* ATCC13883. We adapted the SPP protocols (Zhang et al.,[8] 2020; Van Vranken et al.,[9] 2021; Yu et al.,[10] 2023), which were applied to human cell lysates, by optimizing the AEA range to be compatible with bacterial lysate. This adjustment resulted in a considerably broader solvent gradient compared with that used for human lysates. The physicochemical properties of proteins vary, as proteomes can exhibit considerable diversity in denaturation patterns.[18] Therefore, the adjustment of the AEA range is crucial as it ensures compatibility by establishing optimal conditions for different species.

As a result, *E. coli* and *K. pneumoniae* lysates were exposed to a wide range of AEA concentrations, from 0% to 50% (v/v) for the purpose of generating complete protein denaturation curves for the entire proteomes. After supernatant collection, soluble fractions were initially resolved and visualized using SDS-PAGE (Figure S2A,C), and in a subsequent experiment, they were analyzed by LC-MS/MS in biological triplicates. The majority of both proteomes appeared to effectively undergo denaturation and precipitation, reaching a bottom plateau at around 35% (v/v) AEA (Figure 1B). In total, we quantified 2438 proteins in *E. coli* and 2584 in *K. pneumoniae* by LC-MS/MS readout, achieving proteome coverage of 89% and 81%, respectively, relative to a global proteomic analysis. Subsequently, we used the measured protein intensities across different AEA concentrations (% v/v) to generate protein denaturation curves and calculate the melting concentrations ($C_M$). $C_M$ represents the concentration of AEA (% v/v) at which a protein is equally distributed between the folded and unfolded states, based on the assumption that an unfolded protein precipitates. We successfully fitted high-quality denaturation curves ($R^2 \geq 0.8$ and plateau $\leq 0.3$) for 1984 proteins in *E. coli* and 2033 in *K. pneumoniae*, corresponding to 81% and 79% of all quantified proteins, respectively, thus generating $C_M$ values for each of them. The calculated median $C_M$ of the *E. coli* proteome in the experiment was 18.0% (v/v) AEA, compared to 16.1% (v/v) AEA for *K. pneumoniae*. As illustrated in Figure 1B, the denaturation curves for these two bacterial proteomes exhibit similar profiles and a nearly complete overlap. Furthermore, we assessed the Pearson correlation of $C_M$ values for 1249 predicted orthologs[19] identified in our experiments between *E. coli* and *K. pneumoniae*, finding a strong positive correlation ($r = 0.71$, Figure 1D). This result underscores the high degree of similarity in the solvent-induced precipitation profiles of proteins extracted in the same native lysis buffer across these bacterial species. The $C_M$ values of the *E. coli* and *K. pneumoniae* proteins are provided in Tables S1 and S2, respectively. Subsequently, we further analyzed the data from the model organism *E. coli*, examining the correlation between $C_M$ values and protein abundance. This analysis revealed a weak correlation ($r = 0.20$), demonstrating that the biophysical stability of a protein is (largely) independent of its abundance (Figure S3A). Furthermore, to evaluate the reproducibility of our findings, we compared the determined $C_M$ values across three independent replicates. The results revealed a strong correlation with $r \geq 0.87$ in each comparison (Figure S3B−D). Additionally, we also computed the CV of $C_M$ values, obtaining a median CV of 5.8%, underscoring the high precision and reliability of the assay (Figure S3E).



https://doi.org/10.1021/acsinfecdis.4c00417
ACS Infect. Dis. XXXX, XXX, XXX−XXX

We then categorized proteins into three groups based on the distribution of their $C_M$ values: (i) the upper quartile (most stable proteins, $C_M$ > 22.64% v/v), (ii) the interquartile range (12.99% v/v ≤ $C_M$ ≤ 22.64% v/v), and (iii) the lower quartile (least stable proteins, $C_M$ < 12.99% v/v). Subsequently, we conducted a functional annotation analysis using the Database for Annotation, Visualization and Integrated Discovery (DAVID)[20,21] to investigate the potential overrepresentation of specific protein classes within each group. The analysis of group (i) revealed enrichment in hydrolases ($n$ = 79), chaperones ($n$ = 18), isomerases ($n$ = 31), and rotamases ($n$ = 9). This group is representative of *E. coli* proteins which showed high tolerance to organic solvent-induced precipitation and did not completely denature (up to 40% v/v AEA, Figure 1E). These proteins are mainly involved in the biological processes related to stress response ($n$ = 30), glycolysis ($n$ = 7), translation regulation ($n$ = 7), and lipid metabolism ($n$ = 13). Specifically, among this group, we find the superoxide-radical degradation proteins (SodA, SodB, and SodC), DNA binding proteins involved in bacterial chromosome organization and compaction under extreme environmental conditions (H-NS, HU-alpha, and HU-beta), chaperones (DnaK, Skp, SurA, GroEL, and GroES), Tat translocation system proteins (TatA and TatE), and outer membrane proteins (e.g., BamA, BamC, BamD, and BamE). Notably, as reported by Mateus et al.[5] in a TPP study in *E. coli*, the chaperones, superoxide-radical degradation proteins, Tat translocation system, and outer membrane proteins were also highly resistant against heat denaturation, indicating extraordinarily stable protein structures. In contrast, group (ii) exhibited enrichment in oxidoreductases ($n$ = 124), ligases ($n$ = 39), ribonucleoproteins ($n$ = 32), ribosomal proteins ($n$ = 32), and RNA-binding proteins ($n$ = 65). The proteins in this group are responsible for amino acid ($n$ = 35) and protein biosynthesis ($n$ = 25), tRNA processing ($n$ = 26), the tricarboxylic acid cycle ($n$ = 17), isoprene biosynthesis ($n$ = 7), cell-wall biogenesis/degradation ($n$ = 23), and carbohydrate metabolism ($n$ = 33), among others. Group (iii) displayed an overrepresentation of kinases ($n$ = 40), exonucleases ($n$ = 9), and transferases ($n$ = 131), such as methyltransferases and aminotransferases. This group is primarily involved in rRNA processing ($n$ = 13), folate biosynthesis ($n$ = 5), amino-acid biosynthesis ($n$ = 35), cell cycle, and cell division ($n$ = 19). Mateus et al.[5] in their TPP study highlighted low thermal stability in multiple essential proteins, a finding consistent with our observations. Specifically, proteins exhibiting low stability to heat and organic solvents include topoisomerases (GyrB, TopB, and ParC), proteins involved in DNA replication (DnaA, DnaB, and DnaC), and those associated with cell shape (FtsA, FtsZ, FtsI, ZapA, ZapD, and ZapE). Conversely, multiple components of the small ribosomal subunit and the RNA polymerase sigma D factor RpoD, which exhibited low thermal stability in Mateus et al.'s study, clustered within the interquartile range in our solvent profiling.

**Application of iSPP to Bacterial Cell Lysates.** The iSPP assay was initially validated through a target−engagement study, employing several drugs in proof-of-principle experiments. The anti-infectives rifampicin, ampicillin, piperacillin, imipenem, cefazolin, nafcillin, and fosmidomycin were systematically investigated in pathogen cell lysates (Table 1).

Rifampicin is an ansamycin antibiotic used to treat several types of bacterial infections caused by Gram-negative and Gram-positive bacteria. It interferes with transcription by binding to the $\beta$-subunit of the bacterial DNA-dependent RNA polymerase (RNAP), known as RpoB.[22] Ampicillin, piperacillin, imipenem, cefazolin, and nafcillin belong to the class of $\beta$-lactam antibiotics, exhibiting a spectrum ranging from narrow to broad antibacterial activity.[23−26] These antibiotics exert their therapeutic effects by irreversibly binding to membrane-bound penicillin-binding proteins (PBPs). Their inhibition disrupts the integrity of the cell-wall peptidoglycan, leading to bacterial cell lysis and subsequent elimination.[27] Fosmidomycin is a natural product having antiparasitic and antibacterial activities.[28] Its known target is DXR, which is the most studied enzyme in the MEP pathway. It is responsible for the catalysis of the second and rate-limiting step of the MEP pathway, involving an intramolecular isomerization and reduction to convert the substrate DXP to MEP (Scheme 1). To date, fosmidomycin is the only clinically investigated MEP inhibitor.[28] However, its clinical use is limited by unfavorable pharmacokinetic properties, mainly insufficient membrane permeability and rapid clearance.[29,30] Additionally, methotrexate (MTX), which is widely used to treat autoimmune and neoplastic diseases, was also included in the study.[31] As a chemotherapeutic agent, MTX competitively inhibits human dihydrofolate reductase (DHFR), an enzyme that participates in tetrahydrofolate synthesis. We decided to investigate its target−engagement because of its impact on the growth and diversity of gut bacteria.[32,33] Moreover, it has been reported that MTX displays potent activity with low inhibition constant ($K_i$) values for various bacterial DHFR enzymes.[34]

We initially evaluated the detectability and abundance of the corresponding known target proteins within the selected bacterial cell lysates through a comprehensive global proteomic characterization using LC-MS/MS. Our analysis led to the identification of 2752 proteins in *E. coli* (strain K12), 3196 in *K. pneumoniae* (strain ATCC13883), 4139 in *P. aeruginosa* (strain PA01), and 1849 in *S. aureus* (strain Newman). These numbers correspond to UniProt predicted full proteome coverage of 62%, 56%, 74%, and 64%, respectively, for each organism. Notably, this coverage ranks among the highest reported in the literature based on LC-MS/MS analysis, indicating close-to the entirety of

**Table 1. Summary of the Tested Drugs (Each at a Concentration of 10 $\mu$M) in Bacterial Lysates with the Corresponding Target Proteins/Protein Groups Shown**[a]

| Model drug | AEA range (v/v) | Target protein(s) ($C_M$ %AEA) |
|---|---|---|
| ***Escherichia coli*** | | |
| Ampicillin | 14−28% | PBPs: PBP1a (13.0), PBP1b (16.9), PBP 4 (23.3), PBP5 (15.6), PBP6 (21.0) |
| Rifampicin | 20−34% | RNAP: RpoA (19.9), RpoB (19.3), RpoC (19.3), RpoZ (22.4) |
| Fosmidomycin | 14−28% | DXR: (14.7) |
| Methotrexate | 20−34% | DHFR: (20.5) |
| ***Klebsiella pneumoniae and Pseudomonas aeruginosa*** | | |
| Piperacillin, Imipenem | 12−29.5 % | PBPs: PBP1a (6.9), PBP1b (16.5), PBP 4 (19.7), PBP5 (14.7), PBP6 (16.6) |
| Fosmidomycin | 12−29.5 % | DXR: ND[b] |
| Methotrexate | 12−29.5 % | DHFR: (18.3) |
| ***Staphylococcus aureus*** | | |
| Cefazolin, Nafcillin | 14−28% | PBPs |
| Rifampicin | 20−34% | RNAP |

[a]Selected AEA range windows for iSPP target−engagement studies in *Escherichia coli*, *Klebsiella pneumoniae*, *Pseudomonas aeruginosa*, and *Staphylococcus aureus* are displayed. Determined $C_M$ values for known *E. coli* and *Klebsiella pneumoniae* target proteins of model drugs are shown in brackets. [b]ND: Not Determined.



https://doi.org/10.1021/acsinfecdis.4c00417
ACS Infect. Dis. XXXX, XXX, XXX−XXX

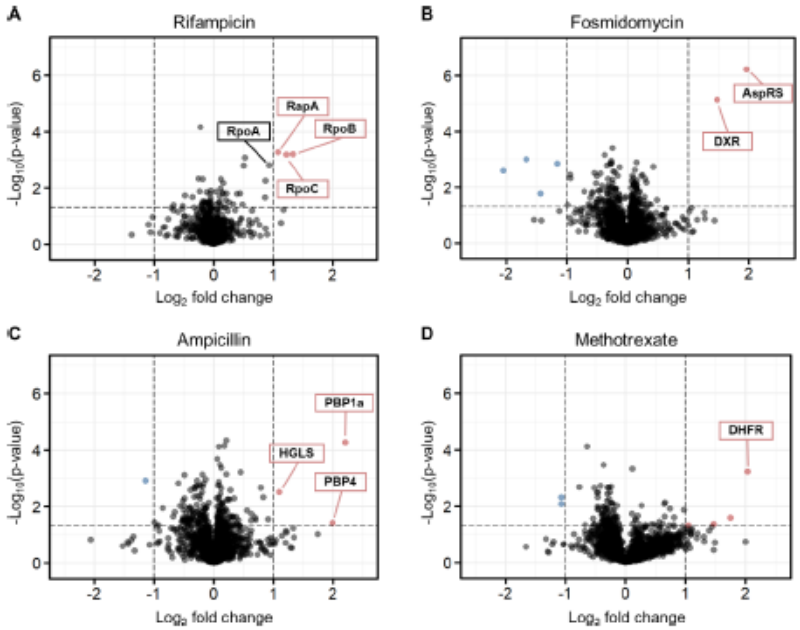


**Figure 2.** iSPP approach in *Escherichia coli* cell lysates to identify the protein targets of model drugs. *E. coli* lysates were incubated with vehicle, rifampicin (A), or methotrexate (D) and then exposed to the AEA gradient 20−34% v/v. Fosmidomycin (B), ampicillin (C), or the corresponding vehicle control-incubated cell lysates were exposed to the AEA gradient 14−28% v/v. All drugs were tested at a concentration of 10 $\mu$M. Data are presented as a volcano plot to highlight changes in protein abundance of each drug over vehicle sample vs statistical significance. We implemented criteria to ensure robust identification and selection of proteins exhibiting statistically significant changes in response to the experimental conditions by setting thresholds of a $\log_2$ fold change ($\log_2$FC) > |1.0| and a $p$-value < 0.05 (dashed lines). Red, stabilized proteins with $\log_2$FC > 1.0 and $p$-value < 0.05; blue, destabilized proteins with $\log_2$FC < −1.0 and $p$-value < 0.05; gray/black, proteins with −1.0 < $\log_2$FC < 1.0 and $p$-value < 0.05 and proteins with $p$-value > 0.05.

the estimated expressed proteome for each bacterium.[35−44] All expected target proteins of model drugs were identified and quantified with more than two unique peptides across the bacterial species proving their detectability by LC-MS/MS (Figure S4).

Subsequently, following the methodology applied to *E. coli* and *K. pneumoniae*, we assessed the denaturation behavior of *P. aeruginosa* and *S. aureus* proteomes upon organic solvent exposure. This involved exposing cell lysates to a wide AEA gradient (v/v, 0−50%) and subsequently resolving the soluble fractions using SDS-PAGE (Figure S2B−D). The resulting denaturation profiles guided the selection of the AEA range windows for subsequent iSPP target−engagement experiments. Additionally, we considered the denaturation behavior obtained by LC-MS/MS readout of the *E. coli* and *K. pneumoniae* proteins as a proxy for their homologs in the other pathogens (Figures S5−S7). Therefore, based on the determined denaturation curves and $C_M$ values for the well-known targets of the model drugs, we narrowed the AEA gradient to the region of the most substantial solubility changes, maximizing the effect size in stability for the known interactors. As a result, for some bacteria, we employed multiple AEA windows given the variations in denaturation behaviors observed for the target proteins of the employed drugs (Table 1). We utilized a more generalized gradient to confirm the engagement of proteins with $C_M$ values closely aligned with the median proteome denaturation behavior, thereby representing the optimal AEA concentration range for most proteins. Conversely, we adopted a targeted approach, selecting a higher range of AEA concentrations for confirming the engagement of proteins exhibiting a high tolerance to solvent-induced precipitation. The model drugs tested in the corresponding bacterial lysates and the selected AEA gradients are summarized in Table 1.

All bacterial cell lysates were incubated with 10 $\mu$M of the respective drug ($n = 3$) or vehicle (DMSO or $ddH_2O$, $n = 3$), to ensure the binding equilibrium. The samples were then exposed to eight different concentrations of AEA, and the resulting soluble fractions were pooled together. The iSPP approach demonstrated high reproducibility of protein intensity measurements, as evidenced by low CV values (Figure S8).

**Validation of iSPP in *E. coli* by Model Drugs.** To demonstrate iSPP suitability for the detection of target−engagement in *E. coli* cell lysate, we employed the assay to confirm targets of four well-characterized drugs (Table 1). The iSPP experiments resulted in an average identification of 2163 proteins under all conditions.

The iSPP experiments confirmed stabilization for all target proteins (DXR, DHFR, and RpoB) and target protein groups (PBPs). Interestingly, for rifampicin, we observed (Figure 2A) the stabilization of other subunits within the RNAP complex in addition to the primary target RpoB, specifically the subunits alpha (RpoA, close-to the predefined threshold) and beta (RpoC). Moreover, the protein RapA, a transcription regulator forming a stable complex with the RNAP core enzyme,[45,46] was also identified among the top hits.

Our study also unveiled the Aspartate-tRNA Synthetase (AspRS) as a putative target of fosmidomycin. AspRS is an aminoacyl-tRNA synthetase, catalyzing the attachment of aspartate to tRNA(Asp).[47] As depicted in Figure 2B, AspRS emerged as one of the two prominently stabilized proteins,


https://doi.org/10.1021/acsinfecdis.4c00417
ACS Infect. Dis. XXXX, XXX, XXX−XXX

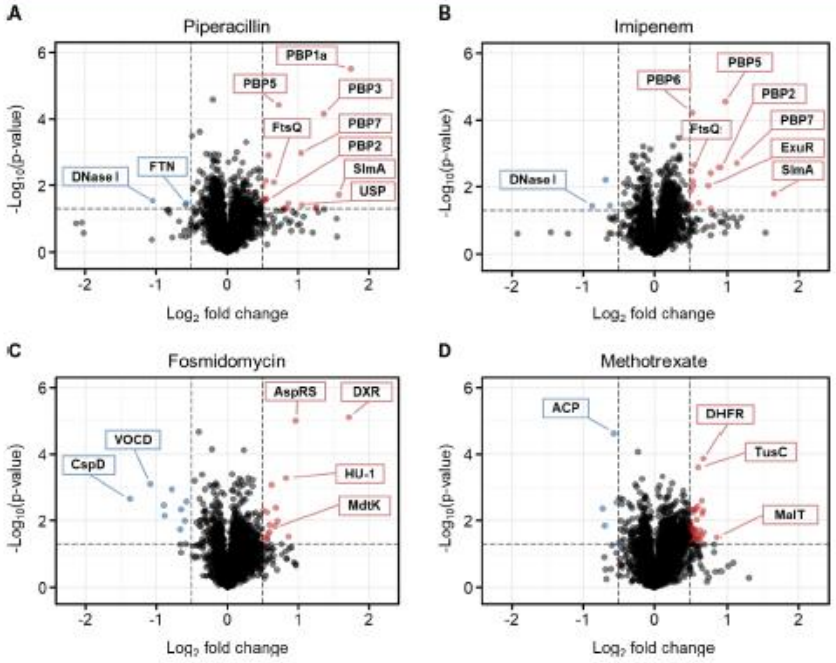


**Figure 3.** iSPP approach in *Klebsiella pneumoniae* cell lysates. *K. pneumoniae* cell lysates were incubated with vehicle, piperacillin (A), imipenem (B), fosmidomycin (C), or methotrexate (D) and then exposed to the AEA gradient 12−29.5% v/v (10 $\mu$M for all drugs). Data are presented as a volcano plot to highlight changes in abundance of each drug over vehicle sample vs statistical significance. The thresholds were set to a $\log_2$ fold change ($\log_2$FC) > |0.5| and a $p$-value < 0.05 (dashed lines). Red, stabilized proteins with $\log_2$FC > 0.5 and $p$-value < 0.05; blue, destabilized proteins with $\log_2$FC < −0.5 and $p$-value < 0.05; gray/black, proteins with −0.5 < $\log_2$FC < 0.5 and $p$-value < 0.05 and proteins with $p$-value > 0.05.

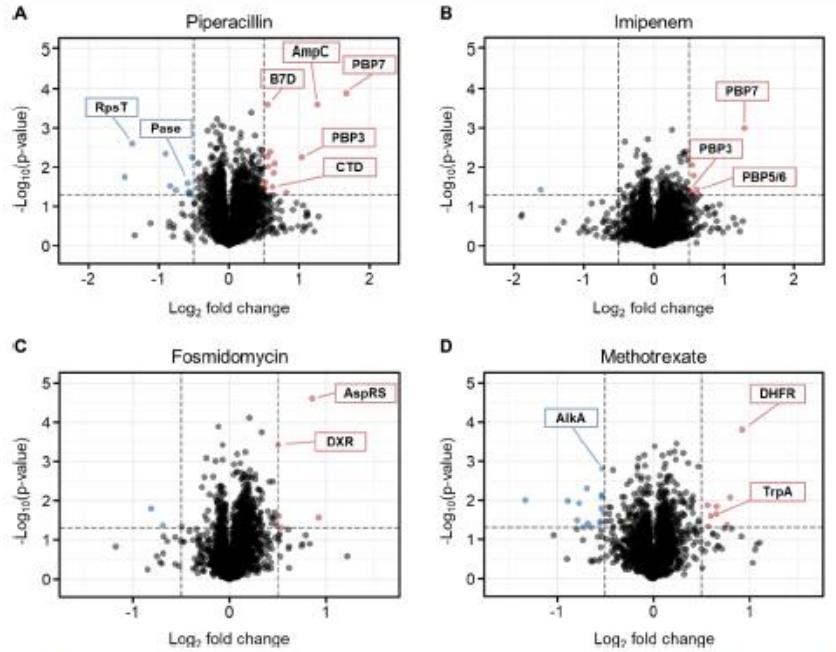


**Figure 4.** iSPP approach in *Pseudomonas aeruginosa* cell lysates. *P. aeruginosa* cell lysates were incubated with vehicle, piperacillin (A), imipenem (B), fosmidomycin (C), or methotrexate (D) and then exposed to the AEA gradient 12−29.5% v/v (10 $\mu$M for all drugs). Data are presented as a volcano plot to highlight changes in abundance of each drug over vehicle vs statistical significance. The thresholds were set to a log2 fold change ($\log_2$FC) > |0.5| and a $p$-value < 0.05 (dashed lines). Red, stabilized proteins with $\log_2$FC > 0.5 and $p$-value < 0.05; blue, destabilized proteins with $\log_2$FC < −0.5 and $p$-value < 0.05; gray/black, proteins with −0.5 < $\log_2$FC < 0.5 and $p$-value < 0.05 and proteins with $p$-value > 0.05.



https://doi.org/10.1021/acsinfecdis.4c00417
ACS Infect. Dis. XXXX, XXX, XXX−XXX

alongside the known target DXR. Notably, AspRS was consistently identified as a top hit in both experimental repetitions ($n$ = 2) with the selected gradient (14−28% v/v AEA, Figure S9A). To further assess the stabilization of AspRS by fosmidomycin, we employed an additional AEA range. Specifically, we shifted the gradient to higher solvent concentrations (20−34% v/v AEA). Within this range, only AspRS emerged as the main stabilized protein, while DXR was not identified in the quantitative proteomics data due to its lower $C_M$ value (Figure S9B). These findings suggest that *Ec*AspRS could be an additional target of fosmidomycin.

Ampicillin led to a significant stabilization of PBP1a (MrcA) and PBP4 (DacB), the two top hits showing the largest magnitude of change, as well as 2-hydroxyglutarate synthase (HGLS), which is involved in D-lysine metabolism (Figure 2C).[48] These results are in accordance with the study performed by Mateus et al.,[5] who employed two-dimensional (2D)-TPP to identify targets of ampicillin in *E. coli* living cells and cell lysates. Their target−engagement study in cell lysates showed significant stabilization of only three proteins: MrcA, DacB, and AmpC, the latter being a $\beta$-lactamase.[5]

**Validation of iSPP in *K. pneumoniae* and *P. aeruginosa* by Model Drugs.** We applied the iSPP workflow to two additional Gram-negative bacteria, *K. pneumoniae* and *P. aeruginosa*, using the drugs listed in Table 1. We identified over all conditions an average of 2674 proteins in *K. pneumoniae* and 3409 in *P. aeruginosa*, corresponding to 84% and 82% proteome coverage compared to the global proteomic analysis, respectively. Again, the iSPP results clearly identified among the top hits the known target proteins, indicating that the selected drugs bound and stabilized their targets against solvent-induced denaturation (Figures 3,4).

In *K. pneumoniae*, piperacillin and imipenem showed stabilization of a broad-spectrum of PBPs, with five and four PBPs being stabilized, respectively (Figure 3A,B). The same $\beta$-lactams in *P. aeruginosa* also led to the stabilization of PBPs, with two of them being stabilized by piperacillin and three by imipenem (Figure 4A,B). Notably, PBP7 (PbpG) stood out as the only PBP shared between the two bacterial species and $\beta$-lactams. In addition to the expected protein targets, our analysis identified several other proteins exhibiting significant (de)-stabilization. In *K. pneumoniae*, piperacillin was found to stabilize a universal stress protein (USP), necessary for resistance to DNA-damaging agents, and to destabilize ferritin (FTN), an iron-storage protein. Imipenem stabilized the DNA-binding transcriptional repressor ExuR. Additionally, both $\beta$-lactams led to the stabilization of the nucleoid occlusion factor SlmA, which prevents Z-ring formation and cell division over the nucleoid, and the cell division protein FtsQ. Conversely, both $\beta$-lactams resulted in the destabilization of DNA-specific endonuclease I (DNase I). In *P. aeruginosa*, as shown in Figure 4A, the $\beta$-lactamase AmpC, which confers resistance to penicillins and cephalosporins,[49] was stabilized by piperacillin. Moreover, a carboxyltransferase domain-containing protein (CTD) and a band 7 domain-containing protein (B7D) of unknown function were also stabilized. Conversely, phosphoesterase (Pase) and the small ribosomal subunit protein bS20 (RpsT) were destabilized.

The incubation of fosmidomycin with the two Gram-negative lysates resulted in the identification of the expected target DXR and the putative target AspRS, which is consistent with our previous observations in *E. coli* (Figures 3C, 4C). Noteworthy, DXR exhibited a larger stabilization effect in *K. pneumoniae* ($\log_2$FC = 1.7) than in *P. aeruginosa* ($\log_2$FC = 0.5). As a reference, the half-maximal inhibitory concentration ($IC_{50}$) values of fosmidomycin reported in the literature indicate stronger inhibition for *Kp*DXR, $IC_{50}$ = 20 nM, compared to *Pa*DXR, $IC_{50}$ = 150 nM.[28] Moreover, in *K. pneumoniae*, we observed the stabilization of the DNA-binding protein HU-beta (HU-1), responsible for wrapping DNA to prevent its denaturation under extreme environmental conditions. We also identified the stabilization of multidrug resistance protein MdtK, a multidrug efflux pump likely functioning as a $Na^+$/drug antiporter. Major proteins that found to be destabilized include the cold shock-like protein CspD and a VOC domain-containing protein (VOCD). The latter is part of the fosfomycin resistance enzyme family, which confers resistance to the antibiotic.

Finally, MTX led to the stabilization of the expected target, DHFR, in both Gram-negative lysates (Figures 3D, 4D). Additionally, in *K. pneumoniae*, we observed the stabilization of transcriptional regulator MalT and the tRNA 2-thiouridine synthesizing protein C (TusC), which is part of a complex pathway that catalyzes the conversion of uridine into 2-thiouridine. This modification is important for the structure and function of tRNA molecules. Conversely, we saw the destabilization of the acyl carrier protein (ACP), which functions as a carrier of the growing fatty acid chain in fatty acid biosynthesis. In *P. aeruginosa*, stabilization of the tryptophan synthase alpha chain (TrpA), involved in amino acid biosynthesis, was observed. As for destabilized proteins, we identified the DNA-3-methyladenine glycosylase II (AlkA), which is involved in the hydrolysis of alkylated DNA.

**Validation of iSPP in *S. aureus* by Model Drugs.** After establishing the iSPP approach in Gram-negative bacteria, we assessed its applicability to the Gram-positive bacterium *S. aureus*. As one of the most pathogenic Gram-positives, *S. aureus* is responsible for a wide range of infections, from mild skin infections to life-threatening conditions such as septicemia, pneumonia, endocarditis, and osteomyelitis.[50]

For *S. aureus*, we identified over all conditions 1752 proteins in the iSPP assay (95% coverage of the total detected proteome in the global analysis) and identified the designated targets of the tested antibiotics (Figure S10).

Cefazolin and nafcillin induced the stabilization of two PBPs. PBP3 (FtsI) emerged as the top hit for both $\beta$-lactams, as illustrated in Figure S10A,B. Notably, an efflux transporter of the Bcr/CflA family was found to be destabilized by both $\beta$-lactams. Members of this family with known activity include Bcr (bicyclomycin resistance protein) in *E. coli*,[51] Flor (chloramphenicol and florfenicol resistance) in *Salmonella typhimurium*,[52] and CmlA (chloramphenicol resistance) found in the *Pseudomonas* plasmid R1033.[53]

Incubation of *S. aureus* lysate with rifampicin resulted in the highly significant stabilization of the two RNAP subunits RpoB and RpoC (Figure S10C). Additionally, RpoA exhibited stabilization, close-to the predefined threshold.

**Target−engagement of MEP Pathway Inhibitors in *E. coli*.** One of the primary objectives of our study was to leverage the iSPP platform for target−engagement studies of small molecules in early drug discovery stages. To that end, we employed compounds targeting enzymes within the MEP pathway, which is a valuable focus for the development of new antimicrobial agents. Due to the unfavorable pharmacokinetic properties of fosmidomycin, intensive efforts for optimizations based on its lead structure have resulted in DXR inhibitors.[28] Recently, a series of $\beta$-aza-reversed fosmidomycin analogues


https://doi.org/10.1021/acsinfecdis.4c00417
ACS Infect. Dis. XXXX, XXX, XXX−XXX

**Scheme 2. Chemical Structures and Enzymatic Inhibition of Reverse $\beta$-Aza Fosmidomycin Analogues 1−3, AMBPP 4, and Propargyl Diphosphate 5**[a]

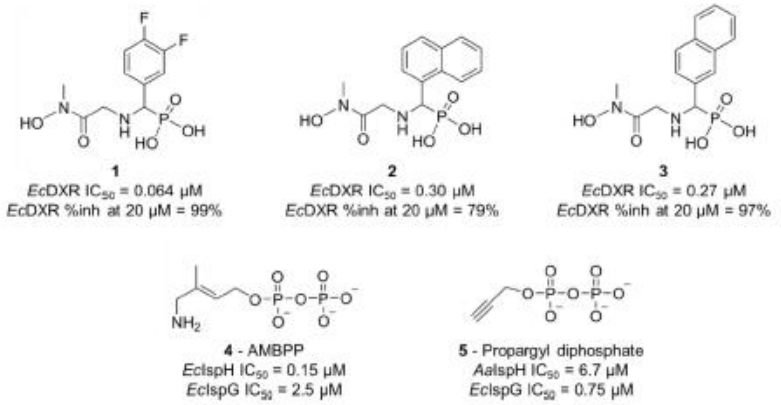


[a]Ec, *Escherichia coli* ; Aa, *Aquifex aeolicus*

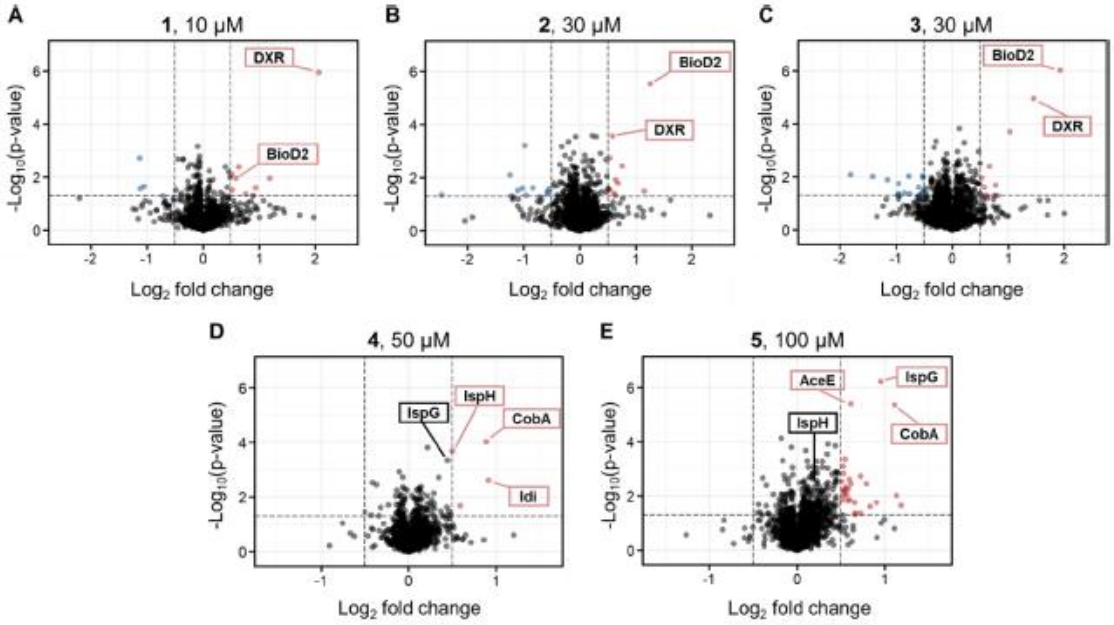


**Figure 5.** iSPP approach in *Escherichia coli* cell lysates to identify (A−C) the putative targets of fosmidomycin analogues (**1**−**3**, 10, 30, and 30 $\mu$M, respectively) and (D, E) diphosphate derivatives (**4** and **5**, 50 and 100 $\mu$M, respectively). *E. coli* cell lysates were incubated with vehicle or the above-mentioned compounds and then exposed to the AEA gradient 14−28% v/v. Data are presented as a volcano plot to highlight changes in abundance of each compound over vehicle vs statistical significance. The thresholds were set to a $\log_2$ fold change ($\log_2$FC) > |0.5| and a $p$-value < 0.05. Red, stabilized proteins with $\log_2$FC > 0.5 and $p$-value < 0.05; blue, destabilized proteins with $\log_2$FC < −0.5 and $p$-value < 0.05; gray/black, proteins with −0.5 < $\log_2$FC < 0.5 and $p$-value < 0.05 and proteins with $p$-value > 0.05.

were discovered by the Van Calenbergh group. In our study, we investigated the target−engagement of compounds **1**−**3** (Schemes 2, S1) in *E. coli* cell lysates. The analogues showed potent *in vitro* enzyme inhibitory activity against *Ec*DXR with nanomolar $IC_{50}$ values.

Additionally, we included small molecules targeting the final two enzymes in the MEP pathway: (*E*)-4-amino-3-methylbut-2-en-1-yl diphosphate (AMBPP, **4**) and propargyl diphosphate **5** (Schemes 2, S2). The penultimate enzyme in the pathway, IspG, catalyzes the reductive dehydroxylation of MEcPP to form HMBPP (Scheme 1), while IspH, the final enzyme, converts HMBPP into a mixture of the two isoprenoid precursors IDP and DMADP. Both proteins are oxygen-sensitive [4Fe-4S] cluster-containing metalloenzymes, oxidoreductases that catalyze a 2e$^-$ reduction and the elimination of a water molecule.[54]

AMBPP was originally designed as an analogue of HMBPP, the substrate of IspH.[55,56] Noteworthy, AMBPP is the most potent IspH inhibitor published to date.[57] It is a slow-binding competitive inhibitor displaying a $K_i$ value in the nanomolar range ($K_i$ = 54 nM, *E. coli* IspH; $IC_{50}$ = 0.15 $\mu$M) that binds to the fourth unique iron of the $[4Fe\text{-}4S]^{2+}$ cluster with its amino functional group.[55,56] In contrast, propargyl diphosphate was


https://doi.org/10.1021/acsinfecdis.4c00417
ACS Infect. Dis. XXXX, XXX, XXX−XXX

rationally designed as a mechanism-based fragment. As reported in the literature, its interaction with the reduced [4Fe-4S] cluster was elucidated through electron paramagnetic resonance (EPR), revealing the formation of a $\pi$-complex between its alkyne group and the apical iron (*Aquifex aeolicus* IspH; $IC_{50}$ = 6.7 $\mu$M).[58,59] Additionally, these two compounds inhibit *Ec*IspG by interacting with its [4Fe-4S] cluster. AMBPP demonstrates moderate *Ec*IspG inhibition *in vitro* ($IC_{50}$ = 2.5 $\mu$M),[54] while the propargyl diphosphate shows good potency with an $IC_{50}$ of 0.75 $\mu$M from which a $K_i$ value of 0.33 $\mu$M was estimated.[60]

In our study, these five MEP pathway inhibitors were tested in *E. coli* using the previously chosen generalized gradient (14−28% v/v AEA) because the $C_M$ values of the MEP enzymes predominantly clustered within the interquartile range in the functional annotation analysis of *E. coli* solvent profiling. Our iSPP approach revealed the stabilization of the expected MEP enzymes DXR, IspG, and IspH, aligning with their respective *in vitro* enzymatic activities, along with the identification of some additional targets (Figure 5). Fosmidomycin analogues **1**−**3** were incubated with *E. coli* cell lysate at a concentration approximately 100 times their respective $IC_{50}$ values. The statistical analysis revealed stabilization of the expected target DXR for all analogues (Figure 5A−C). The most potent inhibitor **1** exhibited selective DXR stabilization, representing the top hit with a $\log_2$FC of 2.05 (Figure 5A). Additionally, BioD2 emerged as a second target, particularly for **2** and **3** (Figure 5B,C). BioD2 is an ATP-dependent dethiobiotin synthetase involved in biotin synthesis. The biotin synthesis pathway is crucial for the pathogenesis of several important human pathogens, and it is absent in mammals. Therefore, BioD2 and the other enzymes in this pathway are attractive targets for novel therapeutic agents.[61] Interestingly, BioD2 is a metalloenzyme, suggesting a role for the hydroxamate moiety present in **1**−**3** in its $Mg^{2+}$ chelation.[62]

The incubation of *E. coli* lysate with AMBPP **4** and propargyl diphosphate **5** was conducted at high concentrations (50 and 100 $\mu$M, respectively), considering the dual inhibition of IspG and IspH and their distinct potencies. Incubation with AMBPP **4** resulted in the stabilization of IspH, with this enzyme identified among the top hits (Figure 5D). IspG did not surpass the set fold change threshold for being identified as a hit candidate. Conversely, propargyl diphosphate **5** induced a marked stabilization of IspG, while IspH did not exhibit stabilization ($\log_2$FC = 0.16, Figure 5E). Furthermore, this analysis revealed significantly stabilized additional targets. Specifically, both inhibitors exhibited stabilization of the corrinoid adenosyltransferase (CobA), the enzyme responsible for transferring an adenosyl moiety from MgATP to a broad range of corrinoid substrates.[63] The observed stabilization suggests a possible binding of the diphosphate groups in **4** and **5** to the ATP binding site of CobA. Additionally, **4** stabilized the isopentenyl-diphosphate delta-isomerase (Idi), an enzyme associated with the MEP pathway, responsible for the isomerization of IDP to its electrophilic isomer DMADP (Scheme 1).[64] IspH and Idi share a high degree of structural similarity in substrates, which provides a plausible explanation for association.

## ■ DISCUSSION

In the current era marked by soaring AMR and an imperative need for novel anti-infectives, MS-based proteomics can play a decisive role in identifying and validating protein−ligand interactions. The SPP approach was established by Zhang et al.[8] in human cell extracts as an LC-MS/MS-based method to assess target−engagement by measuring a protein's resistance to solvent-induced denaturation and aggregation. Subsequently, Van Vranken and coworkers[9] applied the compressed format to SPP, which relies on pooling multiple aliquots of the lysate upon exposure to an increasing concentration of AEA (in our study referred to as iSPP). As a result, the SPP assay has emerged as a valuable alternative to TPP.[9,65] Both approaches are modification-free and analogous in their ability to induce protein unfolding and aggregation, yet they differ in their denaturation principles.[8,65]

In our study, we have established a comprehensive workflow for iSPP target−engagement in the three Gram-negative bacteria *E. coli*, *K. pneumoniae*, and *P. aeruginosa* and the Gram-positive bacterium *S. aureus*. We utilized DIA quantitative mass spectrometry, which offers advantages over other acquisition methods, including accurate label-free proteome quantification, a low number of missing values, and cost-effectiveness.[16,66,67] A key aspect of this study involved adapting the protocol to utilize minimal protein input amounts, specifically 20 $\mu$g of total protein per data point. This adaptation makes the workflow particularly well-suited for hard-to-culture pathogens and, more broadly, for biological systems characterized by slow growth rates and limited protein yields.

Our ultimate goal was to exploit the assay for the target−engagement study of small molecules derived from target-based drug discovery. To that end, we first assessed the *E. coli* and *K. pneumoniae* proteomes' response to organic solvents by performing a solvent proteome profiling. We identified 2438 *E. coli* and 2584 *K. pneumoniae* proteins and generated high-quality denaturation curves and $C_M$ values for 1984 and 2033 of them, respectively. We then conducted a functional annotation analysis on *E. coli* proteins categorized into three groups based on their $C_M$ values: the upper quartile (most stable proteins), the interquartile range, and the lower quartile (least stable proteins). We identified overrepresented protein classes and related biological processes within each group. Notably, the MEP enzymes responsible for isoprene biosynthesis fell into the interquartile range.

Subsequently, we utilized the model drugs rifampicin, ampicillin, piperacillin, imipenem, cefazolin, nafcillin, fosmidomycin, and methotrexate to demonstrate the iSPP target−engagement approach employing a rational selection of target-specific AEA gradient ranges based on the denaturation behavior of the corresponding target proteins and their respective $C_M$ values (Table 1). All of the established targets were stabilized and identified as top hits. Our findings, following *E. coli* incubation with ampicillin, exhibited an overlap in the stabilization of PBP1a (MrcA) and PBP4 (DacB) with the results obtained by Mateus et al.[5] in a 2D-TPP study. The consistency between 2D-TPP and iSPP results underscores the validity of iSPP as target−engagement assay for bacteria. Furthermore, certain proteins that may not exhibit drug-binding stabilization during thermal denaturation could be responsive to organic solvent-induced denaturation and vice versa.[65] We also observed a phenomenon reminiscent of thermal proximity coaggregation (TPCA), initially reported by Tan and colleagues[68] in Cellular Thermal Shift Assay (CETSA) experiments. TPCA involves the comelting of proteins within the same complex, where the denaturation of one component can destabilize others, resulting in similar melting curves. In our solvent proteome profiling study of *E. coli*, we observed multiple subunits (RpoA, RpoB, and RpoC) of the RNAP core enzyme


https://doi.org/10.1021/acsinfecdis.4c00417
ACS Infect. Dis. XXXX, XXX, XXX−XXX

displaying nearly identical denaturation curves and comparable $C_M$ values (Figure S5). Furthermore, these subunits, along with the RNAP-associated protein RapA,[45,46] exhibited similar stabilization by rifampicin in our iSPP experiments (Figure 2A). This result shows the potential for detecting the costabilization of protein−protein interactors as a consequence of ligand binding.

Additionally, we demonstrated the importance of AEA gradient selection for successful target−engagement studies in an iSPP format. To that end, we explored suboptimal AEA range windows beyond those listed in Table 1. We applied the targeted AEA range of 20−34% v/v in *E. coli* cell lysate for fosmidomycin and the generalized AEA range of 14−28% v/v in both *E. coli* and *S. aureus* cell lysates for rifampicin. These windows were not tailored to the regions exhibiting the most substantial solubility changes for the corresponding target proteins, thereby diminishing the observed effect size in stability and precluding their identification among the top hits (Figure S9).

Finally, we assessed the target−engagement for inhibitors of the MEP enzymes. Our experiments led to the identification of the putative targets *Ec*DXR, *Ec*IspG, and *Ec*IspH as main stabilized proteins, along with some potential additional targets, such as BioD2, CobA, and Idi. Some of these additional targets can confer a positive attribute to anti-infective agents, potentially resulting in a decreased development of resistance. Consequently, the $\beta$-aza-reversed fosmidomycin analogues **1**−**3** represent promising *Ec*DXR inhibitors, providing an interesting step forward for this class. The HMBPP analogue **4** and the propargyl diphosphate **5** are potent *in vitro* inhibitors of the enzymes IspH and IspG, respectively, and represent a starting point for the development of novel inhibitors with improved drug-like properties.

The results of our iSPP experiments also highlighted some limitations related to the compressed format. Specifically, achieving robust stabilization of target protein(s) upon certain compound−protein interactions can be difficult, as observed specifically for DXR in *P. aeruginosa* lysate following incubation with fosmidomycin. Denaturation curve experiments using the standard SPP assay have the potential to overcome this limitation. However, they would require additional time for MS measurements and data analysis. In our study, we also observed the presence of multiple (de)stabilized proteins alongside the designated targets for some conditions, e.g., imipenem and fosmidomycin in *K. pneumoniae*. For proteins such as the multidrug efflux pump MdtK and the fosfomycin resistance enzyme VOCD, the observed (de)stabilization may be linked to binding events. However, in other cases, the (de)stabilization does not necessarily indicate engagement but rather arises from an artifact associated with the low signal-to-noise ratio, potentially leading to false-positive hits. Destabilization may also occur when ligands bind to a (partially) unfolded state of a protein, thereby reducing its stability—a phenomenon previously observed in thermal shift assays (TSAs), as reported, for instance, by Cimmperman and colleagues.[69] Alternatively, destabilization might result from downstream effects on proteins caused by upstream target inhibition.[10,70] However, since the experiments performed in our study were conducted in cell lysates, the downstream effects are less relevant due to lower metabolic activity compared to live cells, indicating that the observed destabilized proteins need to be interpreted with great care. Whether conducting iSPP analysis in living bacterial cells is feasible remains unexplored, and this will be tested in the future. Such an analysis holds great potential and would provide valuable insights into the effects of compounds in living bacteria as well as the concentration dependency of changes in solvent stability.

During our target−engagement studies of model drugs, we also encountered potential additional targets, such as the aminoacyl-tRNA synthetase AspRS, which exhibited stabilization by fosmidomycin in various experimental iterations in *E. coli* (across multiple gradients), *K. pneumoniae*, and *P. aeruginosa* extracts. Table S3 contains a list of (de)stabilized proteins of all the model anti-infectives used in our iSPP experiments that could be useful for potential exploration of off-targets or cytotoxicity studies. Although not the primary focus of our investigation, the iSPP assay serves as a valuable tool for target deconvolution, e.g., following phenotypic screenings. Nonetheless, conducting these studies and obtaining a comprehensive target profile via iSPP may require the use of multiple solvent range windows or various compound concentrations.

## ■ CONCLUSIONS

In this study, we demonstrated the potential of the chemical proteomics iSPP assay for supporting drug discovery and development of novel anti-infectives. The solvent profiling of *E. coli* and *K. pneumoniae* proteomes revealed a strong positive correlation, indicating a high degree of similarity in the solvent-induced precipitation profiles of proteins across these bacterial species. Our iSPP method builds upon established SPP procedures and implements optimized denaturation gradients and minimized sample input amounts required for target−engagement studies. The solvent concentration range was specifically tailored to the region where the known target proteins exhibited the most substantial solubility changes, ensuring that the observable effect size was maximized. Through DIA-based quantitative mass spectrometry, we successfully identified established drug targets for seven antibiotics in cell extracts of four AMR-related pathogens, underscoring the assay's adaptability and applicability across multiple infectious disease models. Additionally, the iSPP approach confirmed target−engagement of compounds developed through target-based drug discovery for MEP pathway enzyme inhibitors. We hope the assay will serve as a valuable tool to tackle the global AMR emergence and will enable faster and more affordable discovery and development of lead compounds against primary human pathogens.

## ■ METHODS

***Ec*DXR Activity Assay.** The *Ec*DXR activity was measured through a DXS−DXR coupled assay previously described, using *M. tuberculosis* DXS (*Mt*DXS) as the coupling enzyme.[71] *Ec*DXR and *Mt*DXS were expressed and purified as previously described.[72,73] First, a *Mt*DXS reaction was prepared with a final concentration of 250 $\mu$M D-L-glyceraldehyde 3-phosphate, 500 $\mu$M pyruvate, 300 $\mu$M thiamine diphosphate, and 1.5 $\mu$M of *Mt*DXS, in an assay buffer composed of 200 mM HEPES pH 8, 2 mM $MgCl_2$. The *Mt*DXS reaction mixture was incubated at 25 °C for 90 min. The DXR reaction was then started with the addition of *Ec*DXR and NADPH to final concentrations of 75 nM and 150 $\mu$M, respectively. The activity was monitored through the decrease in fluorescence of NADPH oxidation using a plate reader SYNERGY H1 (BioTEK) with wavelengths 340/450 nm (excitation/emission) for 15 min at 30 °C. Initial velocity was calculated through the slope of the linear region in the first 10 min of reaction using OriginPro8. For dose−



https://doi.org/10.1021/acsinfecdis.4c00417
ACS Infect. Dis. XXXX, XXX, XXX−XXX

response assays, *Ec*DXR was previously incubated for 15 min with a serial dilution of the desired compound starting at 50 $\mu$M. 1% DMSO was used as a negative control whereas 50 $\mu$M of fosmidomycin was used as a positive control. The inhibition percentage was measured using the following equation:

$$\text{Inhibition}(\%) = 100 \times \left[1 - \frac{\text{Slope Reaction} - \text{Slope Positive Control}}{\text{Slope Negative Control} - \text{Slope Positive Control}}\right]$$

The percentage of inhibition was calculated for each compound concentration, and the dose−response curve was fitted using the Hill1 model with OriginPro8. Half-maximal inhibitory concentration ($IC_{50}$) values were then calculated using the interpolation method. All experiments were conducted in triplicates.

**Bacterial Culture and Cell Extract Preparation.** *Escherichia coli* (strain K12), *Klebsiella pneumoniae* (strain ATCC13883), *Pseudomonas aeruginosa* (strain PA01), and *Staphylococcus aureus* (strain Newman) cell lysates were obtained from the Helmholtz Institute for Pharmaceutical Research Saarland (HIPS). All bacteria were grown aerobically overnight (ON) with agitation at 200 rpm and 37 °C in lysogeny broth. Cells were washed and resuspended in 3× cell pellet volume with ice-cold lysis buffer containing 50 mM Tris/HCl pH 7.5, 5% glycerol, 150 mM NaCl, 1.5 mM $MgCl_2$, 1 mM DTT, 0.8% IGEPAL CA-630, and 1× Halt Protease and Phosphatase Inhibitor Cocktails (Thermo Fisher Scientific). The resuspended cell pellet was vortexed for 30 s, incubated for 30 min on ice, and further lysed via homogenization (BANDELIN SONOPULS mini20) with 5 cycles at 70% amplitude for 30 s. Each cycle was followed by 90 s pause where the suspension was kept at 4 °C. The lysate was then centrifuged twice for 30 min at 4 °C 17 000× g, and the supernatant was collected (centrifuge MIKRO 220R, Hettich). The protein lysates were diluted to 0.8 mg/mL (Pierce BCA Protein Assay Kit, Thermo Fisher Scientific) using lysis buffer without IGEPAL CA-630, resulting in a reduced percentage of 0.4% IGEPAL CA-630, and then stored at −80 °C until further use.

**Solvent Proteome Profiling for LC-MS/MS Readout.** *E. coli* and *K. pneumoniae* cell lysates were thawed on ice. The lysates were distributed into a 96-well plate, 20 $\mu$g total protein per each data point, and then exposed to 12 increasing concentrations of acetone/ethanol/acetic acid mixture (AEA, v/v) from 0% to 50% (0, 10, 15, 20, 22, 24, 26, 30, 32, 34, 40, and 50%, performed on the Bravo Automated Liquid Handling Platform, Agilent) in a final reaction volume of 50 $\mu$L. Samples were incubated at 37 °C at 750 rpm for 20 min (ThermoMixer C, Eppendorf). Precipitated proteins were removed by centrifugation at 4402× g for 35 min (centrifuge 5920R, Eppendorf). An equal volume of each soluble fraction was collected (Bravo Automated Liquid Handling Platform) and prepared for LC-MS/MS analysis. All experimental conditions were conducted in triplicates.

**Solvent Proteome Profiling for SDS-PAGE Readout.** *E. coli*, *K. pneumoniae*, *P. aeruginosa*, and *S. aureus* cell lysates were thawed on ice and then exposed to an increasing concentration of AEA from 0% to 50% (v/v). For *E. coli* cell lysate, 14 aliquots were prepared (0, 7, 10, 13, 16, 19, 22, 25, 28, 31, 34, 37, 40, and 50%). For *K. pneumoniae*, *P. aeruginosa*, and *S. aureus* cell lysates, 13 aliquots were prepared (0, 8, 11, 14, 17, 20, 23, 26, 29, 32, 35, 40, and 50%). The samples were then processed as described above. Upon supernatant collection, the soluble fractions were dried down in a concentrator plus (Eppendorf) and then resuspended to a final protein concentration of 1.0 mg/mL with 2× NuPAGE LDS Sample Buffer (Thermo Fisher Scientific) containing 25 mM DTT. Proteins were resolved on NuPAGE 4−12% Bis-Tris Protein Gels (Thermo Fisher Scientific). Gels were stained ON with Coomassie-staining solution (ROTI Blue, Carl Roth). Images were acquired on a ChemiDoc MP Imaging System (BIO-RAD).

**iSPP Assay.** All bacterial cell lysates were thawed on ice and then distributed in aliquots. Each aliquot was then incubated with the corresponding compound (solubilized in DMSO or $ddH_2O$) or vehicle control (DMSO or $ddH_2O$, respectively), at the desired concentration (Table 1). The samples were incubated at room temperature (RT) for 30 min on an end-over-end shaker. Rifampin, ampicillin (trihydrate), and methotrexate were purchased from Selleckchem. Piperacillin and imipenem were purchased from Sigma-Aldrich. Fosmidomycin (sodium), nafcillin (sodium monohydrate), and cefazolin (sodium) were purchased from MedChemExpress. Each aliquot was then distributed into eight wells, treated with an increasing concentration of AEA (v/v) from 14% to 28% (14, 16, 18, 20, 22, 24, 26, and 28%), 20% to 34% (20, 22, 24, 26, 28, 30, 32, and 34%), or 12% to 29.5% (12, 14.5, 17, 19.5, 22, 24.5, 27, and 29.5%). Samples were incubated at 37 °C and 750 rpm for 20 min. Precipitated proteins were removed by centrifugation at 4400× g for 35 min. An equal volume of each resulting soluble fraction was pooled into a single sample (Bravo Automated Liquid Handling Platform) and prepared for LC-MS/MS analysis. All experimental conditions were conducted in triplicates.

**Sample Preparation for LC-MS/MS Analysis.** The soluble fractions were dried and then resuspended to a final protein concentration of 1.0 mg/mL with 5% SDS buffer containing 50 mM TEAB at pH 7.5. The bacterial cell lysates for global proteomic analysis were diluted 1:1 to a final protein concentration of 0.4 mg/mL with 10% SDS buffer. To reduce disulfide bonds, 10 mM DTT was added to all samples, followed by incubation for 30 min at 35 °C and 700 rpm on the ThermoMixer C. Protein alkylation was performed with 55 mM chloroacetamide and 30 min incubation at RT. Samples were acidified by adding phosphoric acid to a final concentration of 2.5% and subsequently diluted 7-fold with 90% methanol in 100 mM TEAB pH 7.5. The samples were transferred to an S-trap column (Protifi) and washed 4× with the same buffer. Sequencing Grade Modified Trypsin (Promega) in TEAB pH 8.5 was added to the S-trap column at a ratio of 1:10 (trypsin/protein), and the digestion reaction was carried out ON at 37 °C. Peptides were eluted with 50 mM TEAB pH 8.5, followed by 0.1% formic acid and then 50/50/0.1 v/v acetonitrile (ACN)/water/FA. Samples were dried down, and peptides were resuspended with 0.5% FA. Peptides were desalted on the Bravo Automated Liquid Handling Platform using C18 cartridges (5 $\mu$L bed volume, Agilent) and the standard AssayMAP peptide cleanup v2.0 protocol. Briefly, C18 cartridges were primed with 100 $\mu$L of 50/50/0.1 (v/v) acetonitrile (ACN)/water/FA and equilibrated with 50 $\mu$L of 0.1% FA at a flow rate of 10 $\mu$L/min. The samples were loaded at 5 $\mu$L/min, followed by an internal cartridge wash with 0.1% FA at a flow rate of 10 $\mu$L/min. Peptides were eluted with 50 $\mu$L of 60/40/0.1 (v/v) acetonitrile (ACN)/water/FA at a flow rate of 5 $\mu$L/min. Samples were dried and stored at −80 °C until further use.



https://doi.org/10.1021/acsinfecdis.4c00417
ACS Infect. Dis. XXXX, XXX, XXX−XXX

**Liquid Chromatography and Mass Spectrometry Data Acquisition.** All samples were solubilized in 0.1% FA before being injected in volumes equivalent to 1 $\mu$g on a Dionex UltiMate 3000 nano System (Thermo Fisher Scientific) coupled online to a Q Exactive Plus (Thermo Fisher Scientific) equipped with an Orbitrap mass analyzer. Peptides were delivered to a trap column (75 $\mu$m × 2 cm, packed in-house with ReproSil-Pur 120 ODS-3 resin, Dr. Maisch). Subsequently, they were separated on an analytical column (75 $\mu$m × 55 cm, packed in-house with Reprosil-Gold 120 C18, 3 $\mu$m resin, Dr. Maisch) at a flow rate of 300 nL/min using a 100 min gradient, ranging from 2% to 32% solvent B (0.1% FA, 5% DMSO in HPLC-MS-grade acetonitrile) in solvent A (0.1% FA, 5% DMSO in HPLC-MS-grade water). The column oven temperature was set at 50 °C. The QE plus instrument was operated in data-independent acquisition (DIA), in positive ionization mode. Full scan spectra (m/z 400−1000) were acquired in centroid mode at an Orbitrap resolution of 70 000, an AGC target set to 3e6, and a maximum injection time of 20 ms. Subsequently, DIA scans were collected by utilizing 30 windows, with a 1 Da window overlap. HCD collision was set to 27%, loop count to 30, Orbitrap resolution to 35 000, AGC target to 3e6, and a maximum injection time set to automatic.

**Peptide and Protein Identification and Quantification.** Raw LFQ-DIA files were processed with DIA-NN (v. 1.8.1). They were analyzed in library-free mode using the UniProt FASTA files for each organism: *Escherichia coli* K12, taxon identifier: 83333; *Pseudomonas aeruginosa* PAO1, taxon identifier: 208964; *Klebsiella pneumoniae* ATCC13883, taxon identifier: 1125630 (ATCC13883 proteome is redundant to the reference HS11286); *Staphylococcus aureus* Newman, taxon identifier: 93061 (Newman proteome is redundant to the reference NCTC 8325/PS 47); and canonical versions, not older than 5 months prior to MS measurements. The raw files were digested selecting Trypsin/P as enzyme specificity with two maximal missed cleavages. Peptide length was restricted from 7 to 30 peptides, and the precursor m/z range was set from 300 to 1800. Cysteine carbamidomethylation was selected as a fixed modification, and methionine oxidation and N-terminal acetylation were selected as variable modifications. The maximum number of variable modifications was set to three, and a match between runs (MBR) was enabled. All other parameters were set to default, including the 1% precursor FDR. Cross-run normalization (RT-dependent) was enabled for raw files of the iSPP experiments.

**Solvent Profiling Data Analysis.** Protein intensity values of each replicate were normalized to their median abundance and expressed as a ratio to the lowest AEA concentration sample using Excel software. Statistical analyses of data and plot generation were then performed in GraphPad Prism (v. 8.3.0) and RStudio (v. 4.3.2) using dplyr package (v. 1.1.4) and ggplot2 package (v. 3.5.0).[74,75] The sigmoidal denaturation curves were generated using a nonlinear regression model and then filtered according to the following criteria: denaturation curves must reach a plateau of $\leq$0.3, the coefficient of determination ($R^2$) must be $\geq$0.8, and a valid slope must be obtained. The functional annotation analysis was performed on the Database for Annotation, Visualization and Integrated Discovery (DAVID).[20,21]

**iSPP Data Analysis.** Protein intensity values of biological replicates across all conditions were normalized to their median abundance and $\log_2$-transformed. Missing values were imputed from a normal distribution (width of 0.3, downshift of 1.5) for vehicle controls only. Moreover, *p*-values were obtained by a two-sample t test over replicates with a permutation-based false discovery rate correction (FDR 0.05) on Perseus (v. 2.0.10.0). The volcano plots were generated in RStudio by EnhancedVolcano package (v. 1.20.0), plotting proteins by statistical significance (vertical axis, $-\log_{10}$ *p*-value) and magnitude of change (horizontal axis, $\log_2$ fold change) of the quantified LFQ-DIA protein intensities for each compound condition over vehicle control.[76]

## ■ ASSOCIATED CONTENT

### Supporting Information

The Supporting Information is available free of charge at https://pubs.acs.org/doi/10.1021/acsinfecdis.4c00417.

Additional information on the iSPP protocol adaptation and related data (Figures S1, S8−S10); solvent proteome profiling (Figures S2 and S3); denaturation curves for the expected target proteins of the model drugs and compounds tested (Figures S4−S7); synthetic procedure for compounds **1**−**5** (Schemes S1 and S2); and purity assessments (Figures S11−S14) (PDF)

Melting concentration ($C_M$) values for *Escherichia coli* (Table S1) and *Klebsiella pneumoniae* (Table S2) proteomes; proteins destabilized/stabilized in the iSPP confirmation experiments by model drugs (Table S3) (XLSX)

## ■ AUTHOR INFORMATION


### Corresponding Author

**Hannes Hahne** − *OmicScouts GmbH, Freising D-85354, Germany*; Email: hannes.hahne@omicscouts.com

### Authors

**Lorenzo Bizzarri** − *OmicScouts GmbH, Freising D-85354, Germany; Department of Pharmacy, Saarland University, Saarbrücken D-66123, Germany;* orcid.org/0009-0003-7017-5770

**Dominik Steinbrunn** − *OmicScouts GmbH, Freising D-85354, Germany; TUM School of Natural Sciences, Department of Bioscience, Technical University of Munich, Center for Functional Protein Assemblies (CPA), Garching bei München D-85748, Germany*

**Thibaut Quennesson** − *Laboratory for Medicinal Chemistry (Campus Heymans), Ghent University, Gent B-9000, Belgium*

**Antoine Lacour** − *Department of Pharmacy, Saarland University, Saarbrücken D-66123, Germany; Helmholtz Institute for Pharmaceutical Research (HIPS), Helmholtz Centre for Infection Research (HZI), Saarland University, Saarbrücken D-66123, Germany*

**Gabriella Ines Bianchino** − *Equipe Chimie Biologique et Applications Thérapeutiques, Institut de Chimie de Strasbourg, Strasbourg F-67070, France*

**Patricia Bravo** − *Swiss Tropical and Public Health Institute (Swiss TPH), Allschwil CH-4123, Switzerland; University of Basel, Basel CH-4001, Switzerland;* orcid.org/0000-0001-5454-3826

**Philippe Chaignon** − *Equipe Chimie Biologique et Applications Thérapeutiques, Institut de Chimie de Strasbourg, Strasbourg F-67070, France*

**Jonas Lohse** − *OmicScouts GmbH, Freising D-85354, Germany*

**Pascal Mäser** − *Swiss Tropical and Public Health Institute (Swiss TPH), Allschwil CH-4123, Switzerland; University of*

*Basel, Basel CH-4001, Switzerland;* orcid.org/0000-0003-3122-1941

**Myriam Seemann** – *Equipe Chimie Biologique et Applications Thérapeutiques, Institut de Chimie de Strasbourg, Strasbourg F-67070, France;* orcid.org/0000-0002-2615-1574

**Serge Van Calenbergh** – *Laboratory for Medicinal Chemistry (Campus Heymans), Ghent University, Gent B-9000, Belgium;* orcid.org/0000-0002-4201-1264

**Anna K. H. Hirsch** – *Department of Pharmacy, Saarland University, Saarbrücken D-66123, Germany; Helmholtz Institute for Pharmaceutical Research (HIPS), Helmholtz Centre for Infection Research (HZI), Saarland University, Saarbrücken D-66123, Germany;* orcid.org/0000-0001-8734-4663

Complete contact information is available at: https://pubs.acs.org/10.1021/acsinfecdis.4c00417

### Notes

The authors declare the following competing financial interest(s): Hannes Hahne is co-founder and shareholder of OmicScouts GmbH, a proteomics and chemical proteomics-focused contract research organization.

## ■ ACKNOWLEDGMENTS

This work was funded by the European Union's Horizon 2020 research and innovation program under the Marie Skłodowska-Curie grant agreement no. 860816. We thank Victor Gawriljuk and Prof. Dr. Matthew Groves at the University of Groningen for the activity data on the enzyme *Ec*DXR. We also thank Simone Amann and Dr. Jörg Haupenthal at the Helmholtz Institute for Pharmaceutical Research (HIPS) for providing bacterial cell lysates. TOC graphic and Figure 1A were created with BioRender.com.

## ■ REFERENCES

(1) Gauba, A.; Rahman, K. M. Evaluation of Antibiotic Resistance Mechanisms in Gram-Negative Bacteria. *Antibiotics* **2023**, *12* (11), 1590.

(2) Cook, M. A.; Wright, G. D. The Past, Present, and Future of Antibiotics. *Sci. Transl. Med.* **2022**, *14* (657), No. eabo7793.

(3) Murray, C. J.; Ikuta, K. S.; Sharara, F.; Swetschinski, L.; Robles Aguilar, G.; Gray, A.; Han, C.; Bisignano, C.; Rao, P.; Wool, E.; et al. Global Burden Of Bacterial Antimicrobial Resistance In 2019: a Systematic Analysis. *The Lancet* **2022**, *399* (10325), 629–655.

(4) Masini, T.; Hirsch, A. K. H. Development of Inhibitors of the 2C-Methyl-D-Erythritol 4-Phosphate (MEP) Pathway Enzymes as Potential Anti-Infective Agents. *J. Med. Chem.* **2014**, *57*, 9740–9763.

(5) Mateus, A.; Bobonis, J.; Kurzawa, N.; Stein, F.; Helm, D.; Hevler, J.; Typas, A.; Savitski, M. M. Thermal Proteome Profiling in Bacteria: Probing Protein State in Vivo. *Mol. Syst. Biol.* **2018**, *14* (7), No. e8242.

(6) Meissner, F.; Geddes-McAlister, J.; Mann, M.; Bantscheff, M. The Emerging Role of Mass Spectrometry-Based Proteomics in Drug Discovery. *Nat. Rev. Drug Discovery* **2022**, *21*, 637–654.

(7) Schirle, M.; Bantscheff, M.; Kuster, B. Mass Spectrometry-Based Proteomics in Preclinical Drug Discovery. *Chem. Biol.* **2012**, *19*, 72–84.

(8) Zhang, X.; Wang, Q.; Li, Y.; Ruan, C.; Wang, S.; Hu, L.; Ye, M. Solvent-Induced Protein Precipitation for Drug Target Discovery on the Proteomic Scale. *Anal. Chem.* **2020**, *92* (1), 1363–1371.

(9) Van Vranken, J. G.; Li, J.; Mitchell, D. C.; Navarrete-Perea, J.; Gygi, S. P. Assessing Target Engagement Using Proteome-Wide Solvent Shift Assays. *Elife* **2021**, *10*, 1–21.

(10) Yu, C.; Chen, X.; Xu, W.; Li, S.; Chai, Q.; Zhang, Y. Solvent-Induced Proteome Profiling for Proteomic Quantitation and Target Discovery of Small Molecular Drugs. *Proteomics* **2023**, *23*, 1–10.

(11) Cowan, D. A. Thermophilic Proteins: Stability and Function in Aqueous and Organic Solvents. *Comp. Biochem. Physiol., Part A: mol. Integr. Physiol.* **1997**, *118* (3), 429–438.

(12) Becher, I.; Werner, T.; Doce, C.; Zaal, E. A.; Tögel, I.; Khan, C. A.; Rueger, A.; Muelbaier, M.; Salzer, E.; Berkers, C. R.; Fitzpatrick, P. F.; Bantscheff, M.; Savitski, M. M. Thermal Profiling Reveals Phenylalanine Hydroxylase As An Off-Target Of Panobinostat. *Nat. Chem. Biol.* **2016**, *12* (11), 908–910.

(13) Mateus, A.; Kurzawa, N.; Becher, I.; Sridharan, S.; Helm, D.; Stein, F.; Typas, A.; Savitski, M. M. Thermal Proteome Profiling for Interrogating Protein Interactions. *Mol. Syst. Biol.* **2020**, *16* (3), No. e9232.

(14) Gaetani, M.; Sabatier, P.; Saei, A. A.; Beusch, C. M.; Yang, Z.; Lundström, S. L.; Zubarev, R. A. Proteome Integral Solubility Alteration: A High-Throughput Proteomics Assay for Target Deconvolution. *J. Proteome Res.* **2019**, *18* (11), 4027–4037.

(15) Hailemariam, M.; Eguez, R. V.; Singh, H.; Bekele, S.; Ameni, G.; Pieper, R.; Yu, Y. S-Trap, an Ultrafast Sample-Preparation Approach for Shotgun Proteomics. *J. Proteome Res.* **2018**, *17* (9), 2917–2924.

(16) Chapman, J. D.; Goodlett, D. R.; Masselon, C. D. Multiplexed and Data-Independent Tandem Mass Spectrometry for Global Proteome Profiling. *Mass Spectrom. Rev.* **2014**, *33* (6), 452–470.

(17) George, A. L.; Sidgwick, F. R.; Watt, J. E.; Martin, M. P.; Trost, M.; Marín-Rubio, J. L.; Dueñas, M. E. Comparison of Quantitative Mass Spectrometric Methods for Drug Target Identification by Thermal Proteome Profiling. *J. Proteome Res.* **2023**, *22* (8), 2629–2640.

(18) Jarzab, A.; Kurzawa, N.; Hopf, T.; Moerch, M.; Zecha, J.; Leijten, N.; Bian, Y.; Musiol, E.; Maschberger, M.; Stoehr, G.; Becher, I.; Daly, C.; Samaras, P.; Mergner, J.; Spanier, B.; Angelov, A.; Werner, T.; Bantscheff, M.; Wilhelm, M.; Klingenspor, M.; Lemeer, S.; Liebl, W.; Hahne, H.; Savitski, M. M.; Kuster, B. Meltome Atlas—Thermal Proteome Stability across the Tree of Life. *Nat. Methods* **2020**, *17* (5), 495–503.

(19) Altenhoff, A. M.; Vesztrocy, A. W.; Bernard, C.; Train, C. M.; Nicheperovich, A.; Bãnos, S. P.; Julca, I.; Moi, D.; Nevers, Y.; Majidian, S.; Dessimoz, C.; Glover, N. M. OMA Orthology in 2024: Improved Prokaryote Coverage, Ancestral and Extant GO Enrichment, a Revamped Synteny Viewer and More in the OMA Ecosystem. *Nucleic Acids Res.* **2024**, *52* (D1), D513–D521.

(20) Huang, D. W.; Sherman, B. T.; Lempicki, R. A. Systematic and Integrative Analysis of Large Gene Lists Using DAVID Bioinformatics Resources. *Nat. Protoc.* **2009**, *4* (1), 44–57.

(21) Sherman, B. T.; Hao, M.; Qiu, J.; Jiao, X.; Baseler, M. W.; Lane, H. C.; Imamichi, T.; Chang, W. DAVID: A Web Server for Functional Enrichment Analysis and Functional Annotation of Gene Lists (2021 Update). *Nucleic Acids Res.* **2022**, *50* (W1), W216–W221.

(22) Wehrli, W. Mechanisms of Action and Resistance. *Rev. Infect. Dis.* **1983**, *5* (Supplement_3), S407–S411.

(23) Halawa, E. M.; Fadel, M.; Al-Rabia, M. W.; Behairy, A.; Nouh, N. A.; Abdo, M.; Olga, R.; Fericean, L.; Atwa, A. M.; El-Nablaway, M.; Abdeen, A. Antibiotic Action and Resistance: Updated Review of Mechanisms, Spread, Influencing Factors, and Alternative Approaches for Combating Resistance. *Front. Pharmacol.* **2024**, *14*, 14.

(24) Wade, K. C.; Benjamin, D. K. Clinical pharmacology of anti-infective drugs, infectious diseases of the fetus and newborn. *Clin. Pharmacol. Anti-Infect. Drugs* **2011**, *37*, 1160–1211.

(25) Chen, P.; Seth, A. K.; Abercrombie, J. J.; Mustoe, T. A.; Leung, K. P. Activity of Imipenem against Klebsiella Pneumoniae Biofilms in Vitro and in Vivo. *Antimicrob. Agents Chemother.* **2014**, *58* (2), 1208–1213.

(26) Karruli, A.; Catalini, C.; D'Amore, C.; Foglia, F.; Mari, F.; Harxhi, A.; Galdiero, M.; Durante-Mangoni, E. Evidence-Based Treatment of Pseudomonas Aeruginosa Infections: A Critical Reappraisal. *Antibiotics* **2023**, *12*, 399.

(27) Lima, L. M.; Silva, B. N. M. D.; Barbosa, G.; Barreiro, E. J. β-Lactam Antibiotics: An Overview from a Medicinal Chemistry Perspective. *Eur. J. Med. Chem.* **2020**, *208*, 112829.

(28) Knak, T.; Abdullaziz, M. A.; Höfmann, S.; Alves Avelar, L. A.; Klein, S.; Martin, M.; Fischer, M.; Tanaka, N.; Kurz, T. Over 40 Years of

Fosmidomycin Drug Research: A Comprehensive Review and Future Opportunities. *Pharmaceuticals MDPI* **2022**, *15*, 1553.
(29) Chofor, R.; Risseeuw, M. D. P.; Pouyez, J.; Johny, C.; Wouters, J.; Dowd, C. S.; Couch, R. D.; Van Calenbergh, S. Synthetic Fosmidomycin Analogues with Altered Chelating Moieties Do Not Inhibit 1-Deoxy-d-Xylulose 5-Phosphate Reductoisomerase or Plasmodium Falciparum Growth in Vitro. *Molecules* **2014**, *19* (2), 2571−2587.
(30) Baumeister, S.; Wiesner, J.; Reichenberg, A.; Hintz, M.; Bietz, S.; Harb, O. S.; Roos, D. S.; Kordes, M.; Friesen, J.; Matuschewski, K.; Lingelbach, K.; Jomaa, H.; Seeber, F. Fosmidomycin Uptake into Plasmodium and Babesia-Infected Erythrocytes Is Facilitated by Parasite-Induced New Permeability Pathways. *PLoS One* **2011**, *6*, No. e19334.
(31) Cronstein, B. N. The Mechanism of Action of Methotrexate. *Rheum. Dis. Clin. North. Am.* **1997**, *23* (4), 739−755.
(32) Letertre, M. P. M.; Munjoma, N.; Wolfer, K.; Pechlivanis, A.; McDonald, J. A. K.; Hardwick, R. N.; Cherrington, N. J.; Coen, M.; Nicholson, J. K.; Hoyles, L.; Swann, J. R.; Wilson, I. D. A Two-Way Interaction between Methotrexate and the Gut Microbiota of Male Sprague-Dawley Rats. *J. Proteome Res.* **2020**, *19* (8), 3326−3339.
(33) Nayak, R. R.; Alexander, M.; Deshpande, I.; Stapleton-Gray, K.; Rimal, B.; Patterson, A. D.; Ubeda, C.; Scher, J. U.; Turnbaugh, P. J. Methotrexate Impacts Conserved Pathways in Diverse Human Gut Bacteria Leading to Decreased Host Immune Activation. *Cell Host Microbe* **2021**, *29* (3), 362−377.e11.
(34) Kopytek, S. J.; Dyer, J. C. D.; Knapp, G. S.; Hu, J. C. Resistance to Methotrexate Due to AcrAB-Dependent Export from *Escherichia Coli*. *Antimicrob. Agents Chemother.* **2000**, *44* (11), 3210−3212.
(35) Mateus, A.; Hevler, J.; Bobonis, J.; Kurzawa, N.; Shah, M.; Mitosch, K.; Goemans, C. V.; Helm, D.; Stein, F.; Typas, A.; Savitski, M. M. The Functional Proteome Landscape of *Escherichia Coli*. *Nature* **2020**, *588* (7838), 473−478.
(36) Chatterjee, B.; Thakur, S. S. Single-Run Mass Spectrometry Analysis Provides Deep Insight into E. *Coli Proteome*. *J. Am. Soc. Mass. Spectrom.* **2018**, *29* (12), 2394−2401.
(37) Soufi, B.; Krug, K.; Harst, A.; Macek, B. Characterization of the *E. Coli* Proteome and Its Modifications during Growth and Ethanol Stress. *Front. Microbiol.* **2015**, *6*, 128127.
(38) Reales-Calderón, J. A.; Sun, Z.; Mascaraque, V.; Pérez-Navarro, E.; Vialás, V.; Deutsch, E. W.; Moritz, R. L.; Gil, C.; Martínez, J. L.; Molero, G. A Wide-Ranging Pseudomonas Aeruginosa PeptideAtlas Build: A Useful Proteomic Resource for a Versatile Pathogen. *J. Proteomics* **2021**, *239*, 104192.
(39) Goodyear, M. C.; Seidel, L.; Krieger, J. R.; Geddes-McAlister, J.; Levesque, R. C.; Khursigara, C. M. Quantitative Proteomics Reveals Unique Responses to Antimicrobial Treatments in Clinical Pseudomonas Aeruginosa Isolates. *mSystems* **2023**, *8* (5), No. e00491−23.
(40) Wright, B. W.; Kamath, K. S.; Krisp, C.; Molloy, M. P. Proteome Profiling of Pseudomonas Aeruginosa PAO1 Identifies Novel Responders to Copper Stress. *BMC Microbiol.* **2019**, *19* (1), 1−13.
(41) Becher, D.; Hempel, K.; Sievers, S.; Zühlke, D.; Pané-Farré, J.; Otto, A.; Fuchs, S.; Albrecht, D.; Bernhardt, J.; Engelmann, S.; Völker, U.; van Dijl, J. M.; Hecker, M. A Proteomic View of an Important Human Pathogen-Towards the Quantification of the Entire Staphylococcus Aureus Proteome. *PLoS One* **2009**, *4* (12), No. e8176.
(42) Pan, Z.; Fan, L.; Zhong, Y.; Guo, J.; Dong, X.; Xu, X.; Wang, C.; Su, Y. Quantitative Proteomics Reveals Reduction in Central Carbon and Energy Metabolisms Contributes to Gentamicin Resistance in Staphylococcus Aureus. *J. Proteomics* **2023**, *277*, 104849.
(43) Sukumaran, A.; Pladwig, S.; Geddes-McAlister, J. Zinc Limitation in Klebsiella Pneumoniae Profiled by Quantitative Proteomics Influences Transcriptional Regulation and Cation Transporter-Associated Capsule Production. *BMC Microbiol.* **2021**, *21* (1), 1−15.
(44) Hao, L.; Yang, X.; Chen, H.; Mo, Z.; Li, Y.; Wei, S.; Zhao, Z. Molecular Characteristics and Quantitative Proteomic Analysis of Klebsiella Pneumoniae Strains with Carbapenem and Colistin Resistance. *Antibiotics* **2022**, *11* (10), 1341.
(45) Sukhodolets, M. V.; Jin, D. J. Interaction between RNA Polymerase and RapA, a Bacterial Homolog of the SWI/SNF Protein Family. *J. Biol. Chem.* **2000**, *275* (29), 22090−22097.
(46) Liu, B.; Zuo, Y.; Steitz, T. A.; Yang, W. Structural Basis for Transcription Reactivation by RapA. *Proc. Natl. Acad. Sci. U. S. A.* **2015**, *112* (7), 2006−2010.
(47) Soutourina, J.; Plateau, P.; Blanquet, S. Metabolism of D-Aminoacyl-TRNAs in *Escherichia Coli* and Saccharomyces Cerevisiae Cells. *J. Biol. Chem.* **2000**, *275* (42), 32535−32542.
(48) Thompson, M. G.; Blake-Hedges, J. M.; Pereira, J. H.; Hangasky, J. A.; Belcher, M. S.; Moore, W. M.; Barajas, J. F.; Cruz-Morales, P.; Washington, L. J.; Haushalter, R. W.; Eiben, C. B.; Liu, Y.; Skyrud, W.; Benites, V. T.; Barnum, T. P.; Baidoo, E. E. K.; Scheller, H. V.; Marletta, M. A.; Shih, P. M.; Adams, P. D.; Keasling, J. D. An Iron (II) Dependent Oxygenase Performs the Last Missing Step of Plant Lysine Catabolism. *Nat. Commun.* **2020**, *11* (1), 2931.
(49) Jacoby, G. A. AmpC $\beta$-Lactamases. Clin. *Microbiol Rev.* **2009**, *22* (1), 161.
(50) Cheung, G. Y. C.; Bae, J. S.; Otto, M. Pathogenicity and Virulencef Staphylococcus Aureus. *Virulence* **2021**, *12*, 547−569.
(51) Bentley, J.; Hyatt, L. S.; Ainley, K.; Parish, J. H.; Herbert, R. B.; White, G. R. Cloning and Sequence Analysis of an *Escherichia Coli* Gene Conferring Bicyclomycin Resistance. *Gene* **1993**, *127* (1), 117−120.
(52) Braibant, M.; Chevalier, J.; Chaslus-Dancla, E.; Pagès, J. M.; Cloeckaert, A. Structural and Functional Study of the Phenicol-Specific Efflux Pump FloR Belonging to the Major Facilitator Superfamily. *Antimicrob. Agents Chemother.* **2005**, *49* (7), 2965−2971.
(53) Bissonnette, L.; Champetier, S.; Buisson, J. P.; Roy, P. H. Characterization of the Nonenzymatic Chloramphenicol Resistance (CmlA) Gene of the In4 Integron of Tn1696: Similarity of the Product to Transmembrane Transport Proteins. *J. Bacteriol.* **1991**, *173* (14), 4493−4502.
(54) Guerra, F.; Wang, K.; Li, J.; Wang, W.; Liu, Y. L.; Amin, S.; Oldfield, E. Inhibition of the 4Fe-4S Proteins IspG and IspH: An EPR, ENDOR and HYSCORE Investigation. *Chem. Sci.* **2014**, *5* (4), 1642−1649.
(55) Ahrens-Botzong, A.; Janthawornpong, K.; Wolny, J. A.; Tambou, E. N.; Rohmer, M.; Krasutsky, S.; Poulter, C. D.; Schünemann, V.; Seemann, M. Biosynthesis of Isoprene Units: Mössbauer Spectroscopy of Substrate and Inhibitor Binding to the [4Fe-4S] Cluster of the LytB/IspH Enzyme. *Angew. Chem.* **2011**, *123* (50), 12182−12185.
(56) Janthawornpong, K.; Krasutsky, S.; Chaignon, P.; Rohmer, M.; Poulter, C. D.; Seemann, M. Inhibition of IspH, a [4Fe-4S]2+ Enzyme Involved in the Biosynthesis of Isoprenoids via the Methylerythritol Phosphate Pathway. *J. Am. Chem. Soc.* **2013**, *135* (5), 1816−1822.
(57) Jobelius, H.; Bianchino, G. I.; Borel, F.; Chaignon, P.; Seemann, M. The Reductive Dehydroxylation Catalyzed by IspH, a Source of Inspiration for the Development of Novel Anti-Infectives. *Molecules* **2022**, *27*, 708.
(58) Wang, K.; Wang, W.; No, J. H.; Zhang, Y.; Zhang, Y.; Oldfield, E. Inhibition of the Fe4S4-Cluster-Containing Protein IspH (LytB): Electron Paramagnetic Resonance, Metallacycles, and Mechanisms. *J. Am. Chem. Soc.* **2010**, *132* (19), 6719−6727.
(59) Wang, W.; Wang, K.; Liu, Y. L.; No, J. H.; Li, J.; Nilges, M. J.; Oldfield, E. Bioorganometallic Mechanism of Action, and Inhibition, of IspH. *Proc. Natl. Acad. Sci. U. S. A.* **2010**, *107* (10), 4522−4527.
(60) Wang, W.; Li, J.; Wang, K.; Huang, C.; Zhang, Y.; Oldfield, E. Organometallic Mechanism of Action and Inhibition of the 4Fe-4S Isoprenoid Biosynthesis Protein GcpE (IspG). *Proc. Natl. Acad. Sci. U. S. A.* **2010**, *107* (25), 11189−11193.
(61) Sirithanakorn, C.; Cronan, J. E. Biotin, a Universal and Essential Cofactor: Synthesis, Ligation and Regulation. *FEMS Microbiol. Rev.* **2021**, *45* (4), 1−18.
(62) Bertrand, S.; Hélesbeux, J.-J.; Larcher, G.; Duval, O. Hydroxamate, a Key Pharmacophore Exhibiting a Wide Range of Biological Activities. *Mini-Rev. Med. Chem.* **2013**, *13* (9), 1311−1326.
(63) Bauer, C. B.; Fonseca, M. V.; Holden, H. M.; Thoden, J. B.; Thompson, T. B.; Escalante-Semerena, J. C.; Rayment, I. Three-Dimensional Structure of ATP: Corrinoid Adenosyltransferase from


https://doi.org/10.1021/acsinfecdis.4c00417
*ACS Infect. Dis.* XXXX, XXX, XXX−XXX

*Salmonella* Typhimurium in Its Free State, Complexed with MgATP, or Complexed with Hydroxycobalamin and MgATP. *Biochemistry* **2001**, *40* (2), 361−374.
(64) Hahn, F. M.; Hurlburt, A. P.; Poulter, C. D. *Escherichia Coli* Open Reading Frame 696 Is Idi, a Nonessential Gene Encoding Isopentenyl Diphosphate Isomerase. *J. Bacteriol.* **1999**, *181* (15), 4499−4504.
(65) Savitski, M. M.; Reinhard, F. B. M.; Franken, H.; Werner, T.; Savitski, M. F.; Eberhard, D.; Molina, D. M.; Jafari, R.; Dovega, R. B.; Klaeger, S.; Kuster, B.; Nordlund, P.; Bantscheff, M.; Drewes, G. Tracking Cancer Drugs in Living Cells by Thermal Profiling of the Proteome. *Science* **2014**, *346* (6205), 1255784.
(66) Figueroa-Navedo, A. M.; Ivanov, A. R. Experimental and Data Analysis Advances in Thermal Proteome Profiling. *Cells Rep. Methods* **2024**, *4* (2), 100717.
(67) Li, J.; Smith, L. S.; Zhu, H. J. Data-Independent Acquisition (DIA): An Emerging Proteomics Technology for Analysis of Drug-Metabolizing Enzymes and Transporters. *Drug Discovery Today: Technol.* **2021**, *39*, 49−56.
(68) Tan, C. S. H.; Go, K. D.; Bisteau, X.; Dai, L.; Yong, C. H.; Prabhu, N.; Ozturk, M. B.; Lim, Y. T.; Sreekumar, L.; Lengqvist, J.; Tergaonkar, V.; Kaldis, P.; Sobota, R. M.; Nordlund, P. Thermal Proximity Coaggregation for System-Wide Profiling of Protein Complex Dynamics in Cells. *Science* **2018**, *359* (6380), 1170−1177.
(69) Cimmperman, P.; Baranauskiene, L.; Jachimovičiute, S.; Jachno, J.; Torresan, J.; Michailoviene, V.; Matuliene, J.; Sereikaite, J.; Bumelis, V.; Matulis, D. A Quantitative Model of Thermal Stabilization and Destabilization of Proteins by Ligands. *Biophys. J.* **2008**, *95* (7), 3222−3231.
(70) Van Vranken, J. G.; Li, J.; Mintseris, J.; Gadzuk-Shea, M.; Gygi, S. P.; Schweppe, D. K. Large-Scale Characterization of Drug Mechanism of Action Using Proteome-Wide Thermal Shift Assays. *eLife* **2024**, *13*, RP95595.
(71) Humnabadkar, V.; Jha, R. K.; Ghatnekar, N.; De Sousa, S. M. A High-Throughput Screening Assay for Simultaneous Selection of Inhibitors of Mycobacterium Tuberculosis 1-Deoxy-D-Xylulose-5-Phosphate Synthase (Dxs) or 1-Deoxy-D-Xylulose 5-Phosphate Reductoisomerase (Dxr). *J. Biomol. Screen* **2011**, *16* (3), 303−312.
(72) Brammer, L. A.; Smith, J. M.; Wades, H.; Meyers, C. F. 1-Deoxy-D-Xylulose 5-Phosphate Synthase Catalyzes a Novel Random Sequential Mechanism. *J. Biol. Chem.* **2011**, *286* (42), 36522−36531.
(73) Gierse, R. M.; Oerlemans, R.; Reddem, E. R.; Gawriljuk, V. O.; Alhayek, A.; Baitinger, D.; Jakobi, H.; Laber, B.; Lange, G.; Hirsch, A. K. H.; Groves, M. R. First Crystal Structures of 1-Deoxy-D-Xylulose 5-Phosphate Synthase (DXPS) from Mycobacterium Tuberculosis Indicate a Distinct Mechanism of Intermediate Stabilization. *Sci. Rep.* **2022**, *12* (1), 7221.
(74) Wickham, H. *ggplot2: Elegant Graphics for Data Analysis*; Springer Cham, 2016. .
(75) Wickham, H.; François, R.; Henry, L.; Müller, K.; Vaughan, D. *Dplyr: A Grammar of Data Manipulation*. R package version 1.1.4. 2023, https://github.com/tidyverse/dplyr, https://dplyr.tidyverse.org.
(76) Blighe, K.; Rana, S.; Lewis, M.. *EnhancedVolcano Version 1.10.0: Publication-Ready Volcano Plots with Enhanced Colouring and Labeling*; R-Package, 2021. .


https://doi.org/10.1021/acsinfecdis.4c00417
*ACS Infect. Dis.* XXXX, XXX, XXX−XXX

SUPPORTING INFORMATION

# Studying target–engagement of anti-infectives by solvent-induced protein precipitation and quantitative mass spectrometry

Lorenzo Bizzarri,[†,¶] Dominik Steinbrunn,[†,#] Thibaut Quennesson,[§] Antoine Lacour,[¶,∥] Gabriella Ines Bianchino,[⊥] Patricia Bravo,[∂,∫] Philippe Chaignon,[⊥] Jonas Lohse,[†] Pascal Mäser,[∂,∫] Myriam Seemann,[⊥] Serge Van Calenbergh,[§] Anna K. H. Hirsch,[¶,∥] and Hannes Hahne[*,†]

[†]OmicScouts GmbH, Lise-Meitner-Straße 30, D-85354 Freising, Germany.
[¶]Saarland University, Department of Pharmacy, Campus E8.1, D-66123 Saarbrücken, Germany.
[#]TUM School of Natural Sciences, Department of Bioscience, Technical University of Munich, Center for Functional Protein Assemblies (CPA), D-85748 Garching bei München, Germany
[§]Laboratory for Medicinal Chemistry (Campus Heymans), Ghent University, Ottergemsesteenweg 460, B-9000 Gent, Belgium
[∥]Helmholtz Institute for Pharmaceutical Research (HIPS), Helmholtz Centre for Infection Research (HZI), Saarland University, Campus E8.1, D-66123 Saarbrücken, Germany.
[⊥]Equipe Chimie Biologique et Applications Thérapeutiques, Institut de Chimie de Strasbourg, UMR 7177, Université de Strasbourg/CNRS, 4, Rue Blaise Pascal, F-67070 Strasbourg, France
[∂]Swiss Tropical and Public Health Institute (Swiss TPH), Kreuzstrasse 2, CH-4123 Allschwil, Switzerland.
[∫]University of Basel, Petersgraben 1, CH-4001 Basel, Switzerland

* *Corresponding author* (hannes.hahne@omicscouts.com)

## Contents

## Synthetic Procedure for Compound 1–3.

Synthesis of compounds **1–3** was achieved by the following synthetic route.

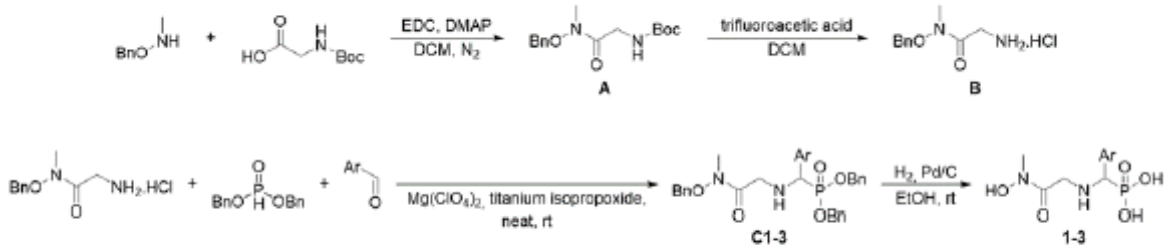


**Scheme S1**. Synthetic route for compounds **1–3.**

**General.** All reactions using oxygen- and/or moisture-sensitive materials were carried out in dry solvents (*vide infra*) under a nitrogen atmosphere using oven-dried glassware. The reaction progress was monitored on thin layer chromatography (TLC) on Machery Nagel ALUGRAM Xtra SIL G UV254 sheets or by liquid chromatography-mass spectrometry (LC-MS). LC-MS analysis for reaction monitoring and purity analyses were carried out on a Waters Autopurification system equipped with a Waters CORTECS column (4.6x100 mm, C18, 2.7 µm) and using a water/acetonitrile/formic acid linear gradient. Peak detection was achieved using mass spectrometry (ESI-MD) and a photo-diode-array detector (PDA). Purification by column chromatography was performed on a Reveleris X2 automated flash chromatography system (Grace/Büchi) using disposable silica gel cartridges (Agela). Nuclear magnetic resonance analyses including $^{1}H$- and $^{13}C$- spectra were carried out on a Bruker Avance Neo 400MHz spectrometer equipped with an autosampler and using TOPSPIN/ICON-NMR. Chemical shifts are given in ppm ($\delta$) relative to the solvent peak. NMR solvents included $CDCl_3$ (7.26 ppm in $^{1}H$ NMR, 77.16 ppm in $^{13}C$ NMR) or DMSO-$d_6$ (2.50 ppm in $^{1}H$ NMR and 39.52 ppm in $^{13}C$ NMR) and were all purchased from Euriso-Top (Saint Aubin, France). Systematic nomenclature was used to name the synthesized compounds. High-resolution mass spectrometry was performed on a Waters Premier XE HRMS system that is calibrated using a solution of Le-enkephalin. Infusion of the analyte into the HRMS system was done as a solution (0.5 ngmL-1) in UPLC grade water and acetonitrile. All solvents utilized (HPLC grade or equivalent or superior purity) were purchased from ChemLab (Zedelgem, Belgium) and used as received. All building blocks and reagents were purchased from common chemical suppliers including but not limited to: Fluorochem (Glossop, Derbyshire UK), Apollo Scientific (Bredbury/Stockport Cheshire UK), Sigma-Aldrich (Diegem, Belgium), and Fisher Scientific (Merelbeke, Belgium). All tested compounds had purity > 95%, as assayed by analytical HPLC (UV) using a linear gradient water/acetonitrile 0 -> 98 % + 0.1% formic acid in 10 minutes on a Waters CORTECS column (4.6x100 mm, C18, 2.7µm).

*tert-butyl (2-((benzyloxy)(methyl)amino)-2-oxoethyl)carbamate* (**A**)

A solution O-benzyl-*N*-methylhydroxylamine (5 g, 36.5 mmol) and 4-dimethylaminopyridine (DMAP) (4.457 g, 36.5 mmol) in dichloromethane (DCM) (160 mL) was stirred for 15 minutes under $N_2$ atmosphere, then added to a solution of *N*-Boc glycine (5.345 g, 30.5 mmol) and 1-ethyl-3-(3-dimethylaminopropyl)carbodiimide (EDC) (6.997 g, 36.5 mmol) in DCM (240 mL) under $N_2$ atmosphere and stirred until completion (5 h, followed by TLC). The suspension was washed with an aqueous solution of 0.5 M citric acid (200 mL). The aqueous phase was extracted with DCM (2 x 100 mL). The organic phases were combined, washed with brine, dried over $Na_2SO_4$ and concentrated *in vacuo*. The crude product was purified using automated flash column chromatography with a gradient from 0 to 2.5% methanol in DCM to give tert-butyl (2-((benzyloxy)(methyl)amino)-2-oxoethyl)carbamate (**A**) as a colourless oil (7.299 g, 81% yield).

$^{1}H$ NMR (400 MHz, $CDCl_3$): $\delta$ = 7.27-7.40 (m, 5H), 5.25 (s, 1H), 4.85 (s, 2H), 4.07 (s, 2H), 3.21 (s, 3H), 1.45 (s, 9H). $^{13}C$ NMR (101 MHz, $CDCl_3$): $\delta$ = 171.0, 155.9, 134.0, 129.3, 129.1, 128.8, 79.6, 76.6, 42.0, 33.9, 28.4. LCMS (ESI): rt:5.58 min; *m/z* calcd for $C_{15}H_{22}N_2O_4 + H^+$ $[M + H]^+$: 295,16; Found: 294.98.

*2-amino-N-(benzyloxy)-N-methylacetamide hydrochloride* (**B**)

**A** (7.299 g, 24.81 mmol) was dissolved in a solution of 5% trifluoroacetic acid in DCM (250 mL) and stirred until completion (followed by TLC, 3 h). Volatiles were removed *in vacuo*, the solid residue was suspended in DCM (100 mL), washed two times with saturated $Na_2CO_3$ in water, dried over $Na_2SO_4$ and filtered. 4 N HCl in dioxane (6.25 mL, 25 mmol) was added at 0 °C, the white solid was filtered, washed with cold DCM, dissolved in water and lyophilised to obtain 2-amino-*N*-(benzyloxy)-*N*-methylacetamide hydrochloride (**B**) as a white solid (5.709 g, 100% yield).

$^1$H NMR (400 MHz, DMSO-d6): δ = 8.35 (s, 3H), 7.38-7.51 (m, 5H), 4.99 (s, 2H), 3.83 (s, 2H), 3.22 (s, 3H). $^{13}$C NMR (101 MHz, DMSO-d6): δ = 167.8, 134.8, 130.1, 129.4, 129.1, 76.0, 39.6, 33.5. LCMS (ESI): rt: 3.78 min; *m/z* calcd for $C_{10}H_{14}N_2O_2 + H^+$ $[M + H]^+$: 195,11; Found: 195.13.

General procedure for the Kabashnik-Fields reaction (compounds **C1–C3**):

2-amino-*N*-(benzyloxy)-*N*-methylacetamide hydrochloride (**B**), the appropriate aldehyde and magnesium perchlorate (0.05 equiv.) were suspended in dibenzyl phosphite under an $N_2$ atmosphere and stirred until a homogeneous semi solid was obtained. Titanium isopropoxide was added portion-wise and stirred until completion. The reaction was diluted in DCM, poured in water and vigorously stirred for 1 h. The resulting mixture was filtered through a pad of celite. The aqueous phase was extracted three times with DCM, the organic phases were combined, washed with brine, dried over $Na_2SO_4$, filtered and concentrated. The crude product was purified using automated flash column chromatography to give the desired product.

*Dibenzyl (((2-((benzyloxy)(methyl)amino)-2-oxoethyl)amino)(3,4-difluorophenyl)methyl)*phosphonate (**C1**)

General procedure using 2-amino-*N*-(benzyloxy)-*N*-methylacetamide (800 mg, 3.48 mmol, 1 equiv.), 3,4-difluorobenzaldehyde (378 µL, 3.48 mmol, 1 equiv.), dibenzyl phosphite (935 µL, 3.83 mmol, 1.1 equiv.), titanium isopropoxide (600 µL, 2.25 mmol, 0.65 equiv.) and magnesium perchlorate (39 mg, 0.17 mmol, 0.05 equiv.)

Purified by automated flash chromatography column with 40 g of silica and a gradient petroleum ether/EtOAc (100:0 to 20:80 (v:v) over 20 CV), to afford dibenzyl (((2-((benzyloxy)(methyl)amino)-2-oxoethyl)amino)(3,4-difluorophenyl)methyl)phosphonate (250 mg, 0.43 mmol, 13% yield) as a colourless oil.

$^1$H NMR (400 MHz, $CDCl_3$): δ = 7.14-7.33 (m, 16H), 7.00-7.08 (m, 2H), 4.88-5.0 (m, 4H), 4.66 (d, *J* = 10.7 Hz, 1H), 4.59 (d, *J* = 10.7 Hz, 1H), 4.10 (d, $J_{H\text{-}P}$ = 17.8 Hz, 1H), 3.36 (d, *J* = 17.3 Hz, 1H), 3.22 (d, *J* = 17.2 Hz, 1H), 3.16 (s, 3H), 2.67 (br s, 1H). $^{13}$C NMR (101 MHz, $CDCl_3$): δ = 172.7,151.4, 148.9, 136.2, 134.0, 132.2, 129.3, 129.1, 128.7, 128.5, 128.4, 128.0, 128.0, 124.9, 117.8 ($J_{C\text{-}F}$ = 5.8 Hz), 117.6 ($J_{C\text{-}F}$ = 5.7 Hz), 117.2, 117.0, 76.3, 68.3, 59.7 ($J_{C\text{-}P}$ = 154.5 Hz), 47.6 ($J_{C\text{-}P}$ = 16.6 Hz), 33.6

Note: N–C(O) –$CH_2$ at 172.7ppm only visible by HMBC. $^{31}$P NMR (162 MHz, $CDCl_3$): δ = 22.8. $^{19}$F NMR (376 MHz, DMSO-*d6*): δ = -137.13, -138.60. LCMS (ESI): rt: 7.05 min; *m/z* calcd for $C_{31}H_{31}F_2N_2O_5P + H^+$ $[M + H]^+$: 581,20; Found: 580.83.

*dibenzyl (((2-((benzyloxy)(methyl)amino)-2-oxoethyl)amino)(naphthalen-1-yl)methyl)phosphonate* (**C2**):

General procedure using 2-amino-*N*-(benzyloxy)-*N*-methylacetamide (62 mg, 3.0 mmol, 1 equiv.), 2-naphtaldehyde (468 mg, 3.0 mmol, 1 equiv.), dibenzyl phosphite (2.94 mL, 12 mmol, 4 equiv.), titanium isopropoxide (0.91 mL, 3.0 mmol, 1 equiv.) and magnesium perchlorate (35 mg, 0.15 mmol, 0.05 equiv.).

Purified by automated flash chromatography column with 40g of silica and a gradient petroleum ether/EtOAc (100:0 to 0:80 (v:v) over 20 CV), then with 20 g of silica and a gradient DCM/MeOH (100:0 to 99:1 (v:v) over 15 CV) to afford dibenzyl (((2-((benzyloxy)(methyl)amino)-2-oxoethyl)amino)(naphthalen-1-yl)methyl)phosphonate (614 mg, 1.03 mmol, 34% yield) as a colorless oil.

$^1$H NMR (400 MHz, $CDCl_3$): δ = 8.14 (br s, 1H) 7.84-7.88 (m, 2H), 7.81 (d, $J$ = 8.4 Hz, 1H), 7.44-7.51 (m, 3H), 7.21-7.28 (m, 5H), 7.11-7.20 (m, 6H), 6.90-7.00 (m, 4H), 5.15 (d, $J_{H\text{-}P}$ = 18.9 Hz, 1H), 4.93-5.04 (m, 2H), 4.83 (dd, $J$ = 11.8 Hz, $J$ = 7.3 Hz, 1H), 4.58 (dd, $J$ = 11.9 Hz, $J$ = 8.0 Hz, 1H), 4.39-4.48 (m, 1H), 4.26-4.37 (m, 1H), 3.36 (s, 2H), 3.09 (s, 3H), 2.92 (s, 1H). $^{13}$C NMR (101 MHz, $CDCl_3$): δ = 136.4, 136.1, 133.9, 132.4, 131.0, 129.1, 128.9, 128.7, 128.6, 128.5, 128.4, 128.2, 128.1, 128.0, 127.9, 126.2, 125.6, 125.5, 123.6, 76.1, 68.2, 55.4 ($J_{C\text{-}P}$ = 163.7 Hz), 47.6, 33.6. Note: P–CH at 55.4ppm was only visible by HSQC. $^{31}$P NMR (162 MHz, $CDCl_3$): δ = 23.9. LCMS (ESI): rt: 6.43 min; *m/z* calcd for $C_{35}H_{35}N_2O_5P + H^+$ $[M + H]^+$: 595,23; Found: 595.29.

*dibenzyl (((2-((benzyloxy)(methyl)amino)-2-oxoethyl)amino)(naphthalen-2-yl)methyl)phosphonate* (**C3**)

General procedure using 2-amino-*N*-(benzyloxy)-*N*-methylacetamide (508 mg, 2.21 mmol, 1 equiv.), 2-naphthaldehyde (345 mg, 2.21 mmol, 1 equiv.), dibenzyl phosphite (1.08 mL, 4.42 mmol, 2 equiv.), titanium isopropoxide (668 µL, 2.2 mmol, 1equiv.) and magnesium perchlorate (25 mg, 0.11 mmol, 0.05 equiv.)

Purified by automated flash chromatography column with 40 g of silica and a gradient petroleum ether/EtOAc (100:0 to 0:100 (v:v) over 20 CV), then with 20 g of silica and a gradient DCM/MeOH (100:0 to 99:1 (v:v) over 15 CV) to afford dibenzyl (((2-((benzyloxy)(methyl)amino)-2-oxoethyl)amino)(naphthalen-2-yl)methyl)phosphonate (331 mg, 0.51 mmol, 25% yield) as a colorless oil.

$^1$H NMR (400 MHz, $CDCl_3$): δ = 7.72-7.85 (m, 5H), 7.57 (td, $J$ = 8.5 Hz, $J$ = 1.5 Hz, 1H), 7.45-7.51 (m, 2H), 7.06-7.28 (m, 13H), 6.96 (d, $J$ = 7.2Hz, 2H), 4.81-5.02 (m, 4H), 4.56 (d, $J$ = 10.4 Hz, 1H), 4.44 (d, $J$ = 10.5 Hz, 1H), 4.37 (d, $J_{H\text{-}P}$ = 17.9 Hz, 1H), 3.39 (dd, $J$ = 27.4 Hz, $J$ = 17.2 Hz, 2H), 3.13 (s, 3H), 2.83 (br s, 1H). $^{13}$C NMR (101 MHz, $CDCl_3$): δ = 172.8, 136.4, 136.3, 133.9, 133.3, 129.2, 128.9, 128.5, 128.4, 128.4, 128.3, 128.2, 128.1, 128.0, 127.9, 127.7, 126.5, 126.1, 76.3, 68.2, 60.7 ($J_{C\text{-}P}$ = 154.8 Hz), 47.7, 47.6, 33.6. $^{31}$P NMR (162 MHz, $CDCl_3$): δ = 23.6. LCMS (ESI): rt: 6.45 min; *m/z* calcd for $C_{35}H_{35}N_2O_5P + H^+$ $[M + H]^+$: 595,23; Found: 595.31.

General procedure for debenzylation (compounds **1–3**):

The benzylated intermediate was dissolved in EtOH (10 mL) and AcOH (1 mL) under $N_2$ atmosphere. 10% Pd/C (0.05 equiv.) was added, the mixture was stirred under a flow of $N_2$ for 10 minutes, then hydrogenated until completion. The reaction was filtered and evaporated to dryness. The resulting solid was solubilised in water, filtered and lyophilized to obtain the desired product.

*((3,4-difluorophenyl)((2-(hydroxy(methyl)amino)-2-oxoethyl)amino)methyl)phosphonic acid* (**1**)

General procedure using dibenzyl (((2-((benzyloxy)(methyl)amino)-2-oxoethyl)amino)(3,4-difluorophenyl)methyl)phosphonate (230 mg, 0.40 mmol), hydrogenated for 1h. Solid suspended in water, filtered and lyophilized to obtain ((3,4-difluorophenyl)((2-(hydroxy(methyl)amino)-2-oxoethyl)amino)methyl)phosphonic acid (99 mg, 0.32 mmol, 80% yield) as a white powder

$^{1}$H NMR (400 MHz, DMSO-*d6*): δ = 7.64 (dd, *J* = 9.3 Hz, *J* = 12.0, 1H), 7.41 (dd, *J* = 9.0 Hz, *J* = 18.6 Hz, 1H), 7.33 (br s, 1H), 4.37 (d, $J_{H\text{-}P}$ = 16.0 Hz, 1H), 3.95 (d, *J* = 16.8 Hz, 1H), 3.74 (d, *J* = 16.8 Hz, 1H), 3.09 (s, 3H). $^{13}$C NMR (101 MHz, DMSO-*d6*): δ = 165.1, 149.6 (dd, $J_{C\text{-}F}$ = 12.4 Hz, $J_{C\text{-}F}$ = 7.7 Hz), 147.2 (dd, $J_{C\text{-}F}$ = 12.5 Hz, $J_{C\text{-}F}$ = 6.1 Hz), 131.4, 125.9, 117.6 (d, $J_{C\text{-}F}$ = 19.1 Hz), 116.4 (d, $J_{C\text{-}F}$ = 17.0 Hz), 58.9 (d, $J_{C\text{-}P}$ = 133.3 Hz), 45.1, 35.1. $^{31}$P NMR (162 MHz, DMSO-*d6*): δ = 7.99 (d, $J_{P\text{-}H}$ = 14.8 Hz). $^{19}$F NMR (376 MHz, DMSO-*d6*): δ = -138.8, -140.0. HRMS (ESI-TOF): *m/z* calcd for $C_{10}H_{13}F_2N_2O_5P$ + $H^+$ $[M + H]^+$: 311,0603; Found: 311,0603. *m/z* calcd for $C_{10}H_{13}F_2N_2O_5P$ + $Na^+$ $[M + Na]^+$: 333,0422. Found: 333,0413.

*(((2-(hydroxy(methyl)amino)-2-oxoethyl)amino)(naphthalen-1-yl)methyl)phosphonic* (**2**):

General procedure using dibenzyl (((2-((benzyloxy)(methyl)amino)-2-oxoethyl)amino)(naphthalen-1-yl)methyl)phosphonate (300 mg, 0.505 mmol), hydrogenated for 5 h to obtain (((2-(hydroxy(methyl)amino)-2-oxoethyl)amino)(naphthalen-1-yl)methyl)phosphonic acid (115 mg, 0.35 mmol, 70% yield) as a white powder.

$^{1}$H NMR (400 MHz, DMSO-*d6*): δ = 8.18 (d, *J* = 6.5 Hz, 1H), 7.88-8.04 (m, 3H), 7.50-7.60 (m, 3H), 5.42 (d, $J_{H\text{-}P}$ = 16.8 Hz, 1H), 4.18 (d, *J* = 16.8 Hz, 1H), 3.82 (d, *J* = 16.8 Hz, 1H), 3.06 (s, 3H). $^{13}$C NMR (101 MHz, DMSO-$d_6$): δ = 165.1, 132.7, 131.0, 130.0, 127.9, 127.5, 125.9, 125.7, 125.0, 124.7, 123.3, 55.6 (d, $J_{C\text{-}P}$ = 138.6 Hz), 45.3, 35.1. $^{31}$P NMR (162 MHz, DMSO-$d_6$): δ = 9.13 (d, $J_{P\text{-}H}$ = 11.0 Hz). HRMS (ESI-TOF): *m/z* calcd for $C_{14}H_{17}N_2O_5P$ + $H^+$ $[M + H]^+$: 325,0948; Found: 325,0948. *m/z* calcd for $C_{14}H_{17}N_2O_5P$ + $Na^+$ $[M + Na]^+$: 347,0767; Found: 347,0774.

*(((2-(hydroxy(methyl)amino)-2-oxoethyl)amino)(naphthalen-2-yl)methyl)phosphonic acid* (**3**):

General procedure using dibenzyl (((2-((benzyloxy)(methyl)amino)-2-oxoethyl)amino)(naphthalen-2-yl)methyl)phosphonate (300 mg, 0.50 mmol), hydrogenated for 8 h. Solid suspended in water, filtered and lyophilized to obtain (((2-(hydroxy(methyl)amino)-2-oxoethyl)amino)(naphthalen-2-yl)methyl)phosphonic acid (103 mg, 0.32 mmol, 63% yield) as a white powder.

$^{1}$H NMR (400 MHz, DMSO-*d6*): δ = 7.99 (s, 1H), 7.82-7.93 (m, 3H), 7.73 (d, *J* = 8.6 Hz, 1H), 7.48-7.56 (m, 2H), 4.56 (d, $J_{H\text{-}P}$ = 17.2 Hz, 1H), 4.04 (d, *J* = 17.2 Hz, 1H), 3.79 (d, *J* = 17.2 Hz, 1H), 3.08 (s, 3H). $^{13}$C NMR (101 MHz, DMSO-*d6*): δ = 166.2, 133.1, 132.9, 132.3, 128.8, 128.8, 128.3, 128.0, 128.0, 127.5, 126.6, 61.4 (d, $J_{C\text{-}P}$ = 133.5 Hz), 46.3, 36.2. $^{31}$P NMR (162 MHz, DMSO-*d6*): δ = 8.48 (d, $J_{P\text{-}H}$ = 14.1 Hz). HRMS (ESI-TOF): *m/z* calcd for $C_{14}H_{17}N_2O_5P$ + $H^+$ $[M + H]^+$: 325.0948; Found: 325.0948. *m/z* calcd for $C_{14}H_{17}N_2O_5P$ + $Na^+$ $[M + Na]^+$: 347,0767; Found: 347,0768.

## Synthetic Procedure for Compound **4**.

Compound **4** was synthesized according to a previously reported protocol.[1]

## Synthetic Procedure for Compound **5**.

Compound **5** was synthesized following a previously reported protocol,[2] with modifications to the cation exchange column procedure, utilizing Amberchrome 50WX8 (100 – 200 mesh, ammonium form).

**4** - AMBPP  **5** - Propargyl diphosphate

**Scheme S2.** Chemical structures of compounds **4**–**5**.

## Compound **5**.

$^{1}$H NMR (500 MHz, $D_2O$): δ = 4.44 (dt, $J_{P\text{-}H}$ = 9.0 Hz, $J_{H\text{-}H}$ = 2.5 Hz, 2H), 2.74 (t, $J$ = 2.5 Hz, 1H). $^{13}$C NMR (126 MHz, $D_2O$): δ = 79.5 (d), 75.3, 53.6 (d). $^{31}$P NMR (121 MHz, $D_2O$): δ = -8.19 (d, $J_{P\text{-}P}$ = 21.5 Hz, 1P), -11.03 (d, $J_{P\text{-}P}$ = 21.5 Hz, 1P). HRMS *m/z* calcd for $C_3H_5O_7P_2$ [M - H]$^-$: 214.9516; Found: 214.9526.

## REFERENCES


(1) Janthawornpong, K.; Krasutsky, S.; Chaignon, P.; Rohmer, M.; Poulter, C. D.; Seemann, M. Inhibition of IspH, a [4Fe-4S]2+ Enzyme Involved in the Biosynthesis of Isoprenoids via the Methylerythritol Phosphate Pathway. *J. Am. Chem. Soc.* **2013**, *135* (5), 1816–1822. https://doi.org/10.1021/ja309557s.

(2) Wang, K.; Wang, W.; No, J. H.; Zhang, Y.; Zhang, Y.; Oldfield, E. Inhibition of the Fe4S4-Cluster-Containing Protein IspH (LytB): Electron Paramagnetic Resonance, Metallacycles, and Mechanisms. *J. Am. Chem. Soc.* **2010**, *132* (19), 6719–6727. https://doi.org/10.1021/ja909664j.

Supplemental Information - Figure S1

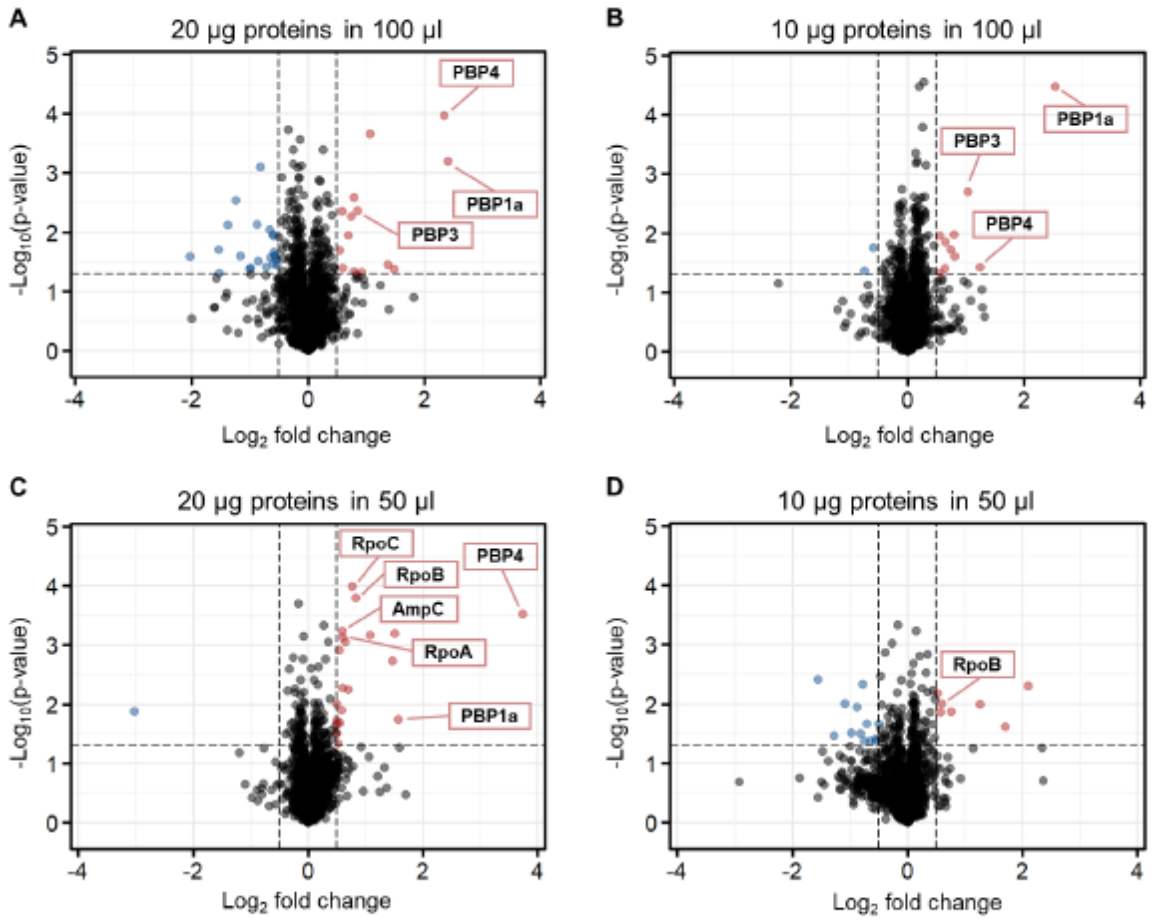


**SI Figure S1.** iSPP protocol adaptation for minimal input protein amount. A mixture of rifampicin and ampicillin (10 µM each one) or the corresponding vehicle control were incubated with *Escherichia coli* cell lysate, followed by 20–34% AEA gradient exposure (v/v). Data are presented as a volcano plot to highlight changes in abundance of drugs over vehicle *vs.* statistical significance. The thresholds were set to a $\log_2 fc > |0.5|$ and a p-value $< 0.05$. (A) 20 µg of total proteins were added to each data point in a final reaction volume of 100 µL. Three proteins of the penicillin-binding protein (PBP) class were stabilized. (B) 10 µg of total proteins were added to each data point in a final reaction volume of 100 µL. Three proteins of the PBP class were stabilized. (C) 20 µg of total proteins were added to each data point in a final reaction volume of 50 µL. Two proteins of the PBP class, a β-lactamase (AmpC), and three subunits of the DNA-dependent RNA polymerase (RNAP) complex were stabilized. (D) 10 µg of total proteins were added to each data point in a final reaction volume of 50 µL. One subunit of the RNAP complex was stabilized. The protocol employed in (C) successfully identified the target protein groups of rifampicin and ampicillin. As a result, it was deemed the optimal condition for further target–engagement experiments.

Supplemental Information - Figure S2

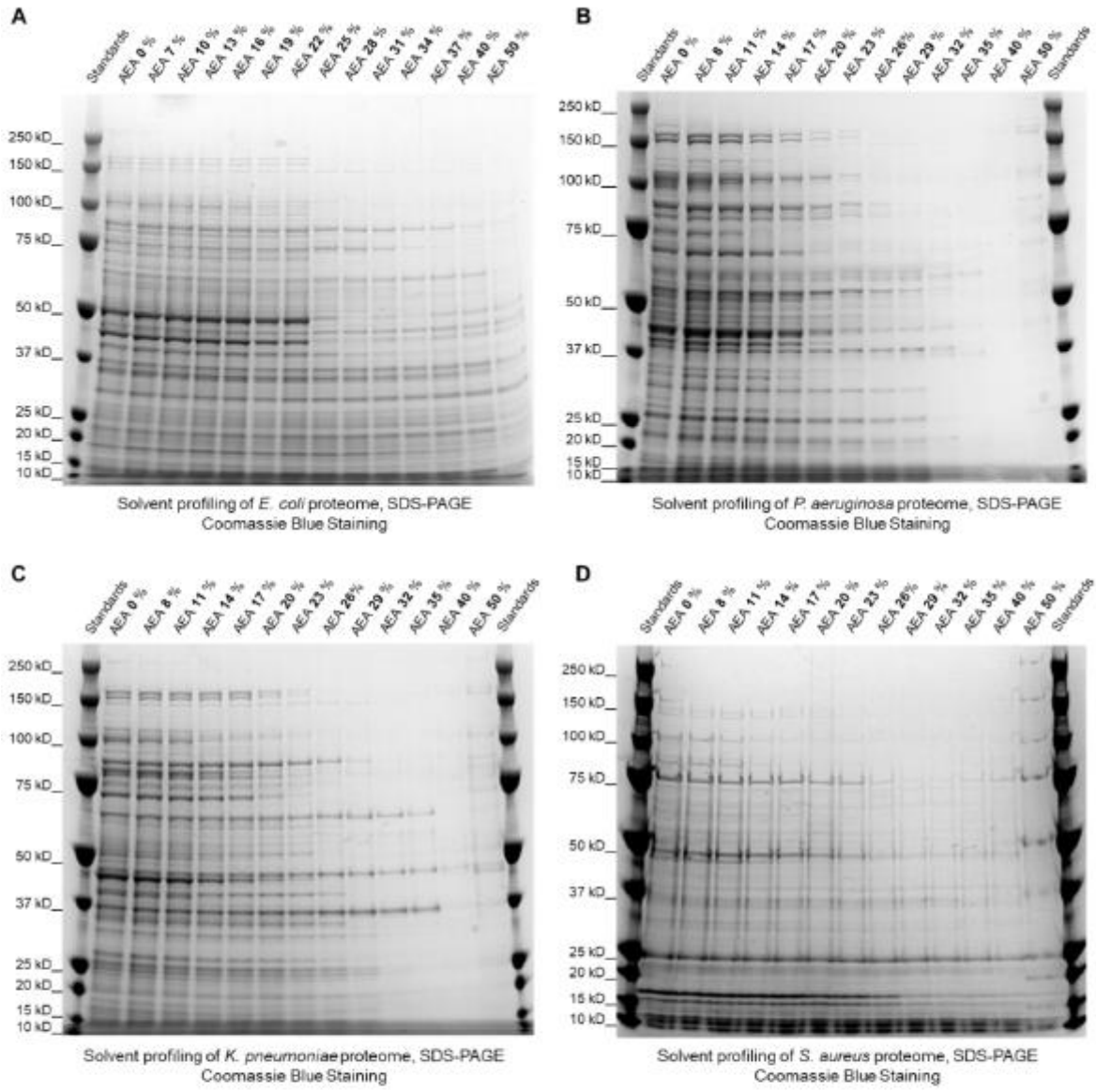


**SI Figure S2.** Solvent profiling of the *Escherichia coli* (A), *Pseudomonas aeruginosa* (B), *Klebsiella pneumoniae* (C), and *Staphylococcus aureus* (D) proteomes by gel electrophoresis readout. Cell lysates were exposed to a wide AEA gradient (0–50%) and the soluble fractions were resolved using SDS-PAGE.

Supplemental Information - Figure S3

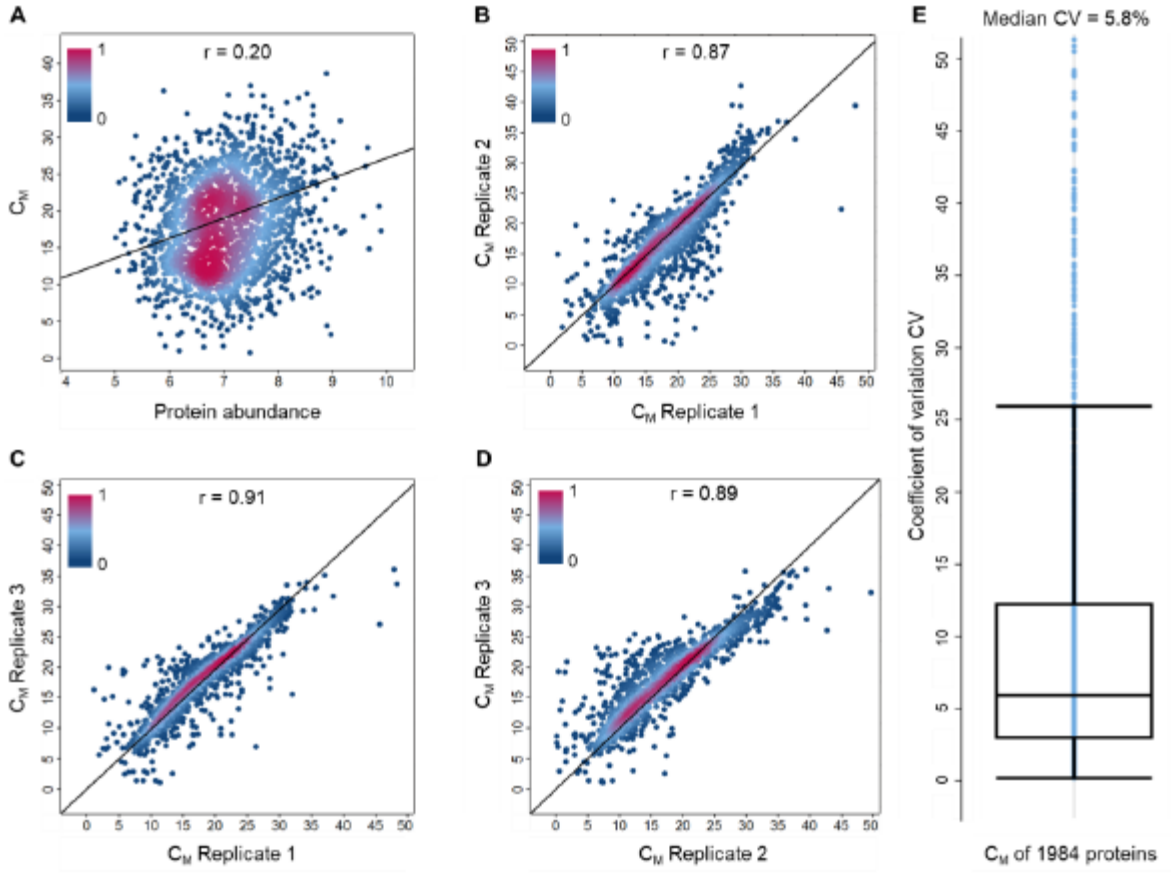


**SI Figure S3.** Quality controls on the solvent profiling study by LC-MS/MS readout of the *Escherichia coli* proteome. We fitted high-quality denaturation curves for 1984 proteins ($n$=3, $R^2 \geq 0.8$ and plateau $\leq 0.3$), generating $C_M$ values for each of them. (A) The obtained $C_M$ values were compared to the respective protein abundance ($\log_{10}$ LFQ-DIA abundance), revealing a very weak Pearson correlation coefficient (r) = 0.20. (B–D) Reproducibility of protein's $C_M$ measures between individual replicates. A high correlation was achieved in all comparisons; (B) replicate 1 *vs*. replicate 2 (r = 0.87), (C) replicate 1 *vs*. replicate 3 (r = 0.91), (D) replicate 2 *vs*. replicate 3 (r = 0.89). Data points in the scatter plots are colored based on the density of the points. (E) Coefficient of variation (CV) of $C_M$ values for the three independent replicates, showing a median CV of 5.8%.

Supplemental Information - Figure S4

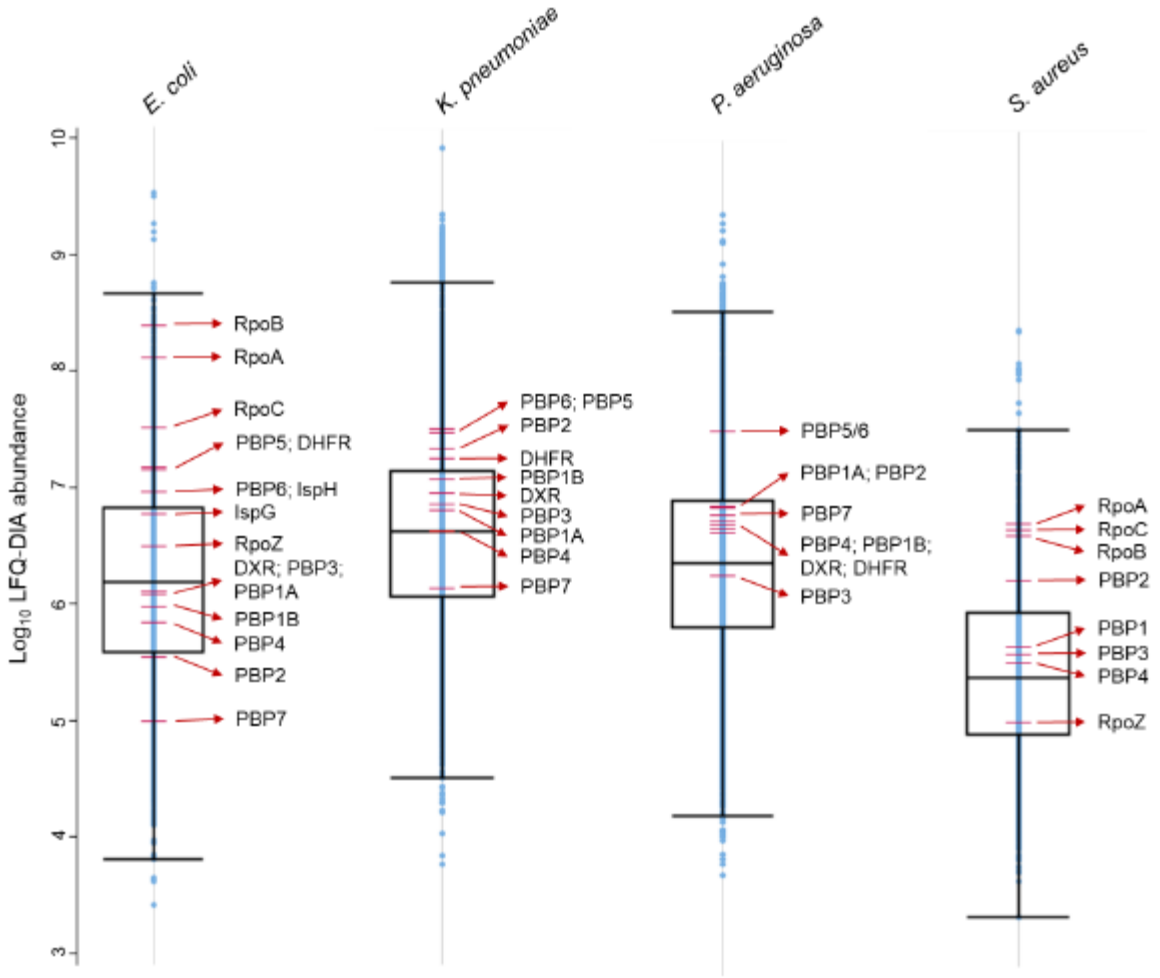


**SI Figure S4.** Global proteomic characterization by LC-MS/MS of the *Escherichia coli*, *Klebsiella pneumoniae*, *Pseudomonas aeruginosa*, and *Staphylococcus aureus* proteomes. All quantified proteins are sorted by $\log_{10}$ LFQ-DIA abundance. Known target proteins and protein groups of drugs employed in iSPP experiments are highlighted for each bacterial species; *E. coli*, targets of ampicillin, rifampicin, fosmidomycin, methotrexate, and **1-5**; *K. pneumonia* and *P. aeruginosa*, targets of piperacillin, imipenem, fosmidomycin, and methotrexate; *S. aureus*, targets of cefazolin, nafcillin, and rifampicin.

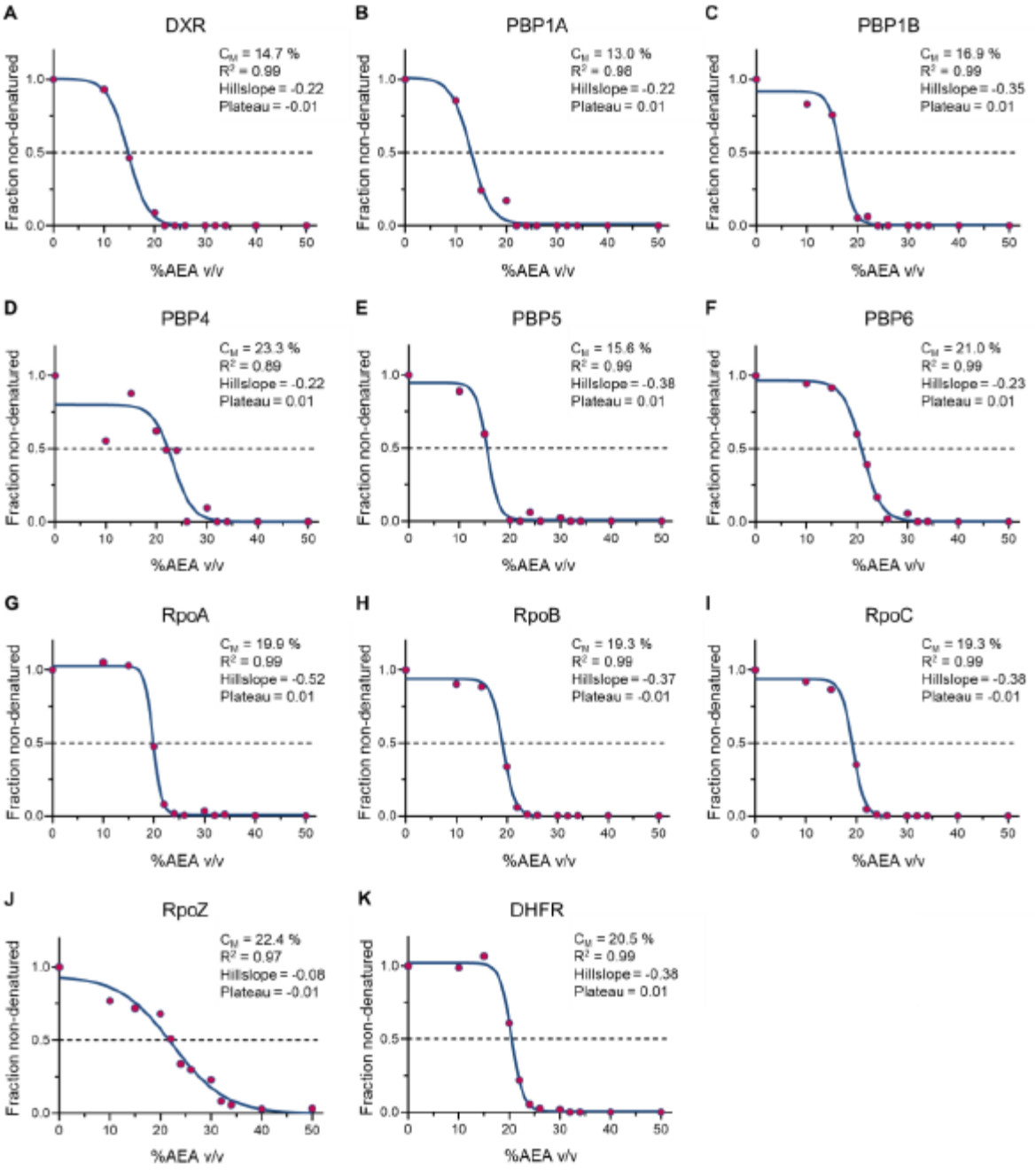


**SI Figure S5.** Denaturation curves of *Escherichia coli* proteins and protein groups targeted by the employed model drugs. (A) DXR, target of fosmidomycin. (B–F) PBPs, target protein class of β-lactam antibiotics. (G–J) RpoB, target of rifampicin and other RNAP core enzyme subunits. (K) DHFR, target of methotrexate.

Supplemental Information - Figure S6

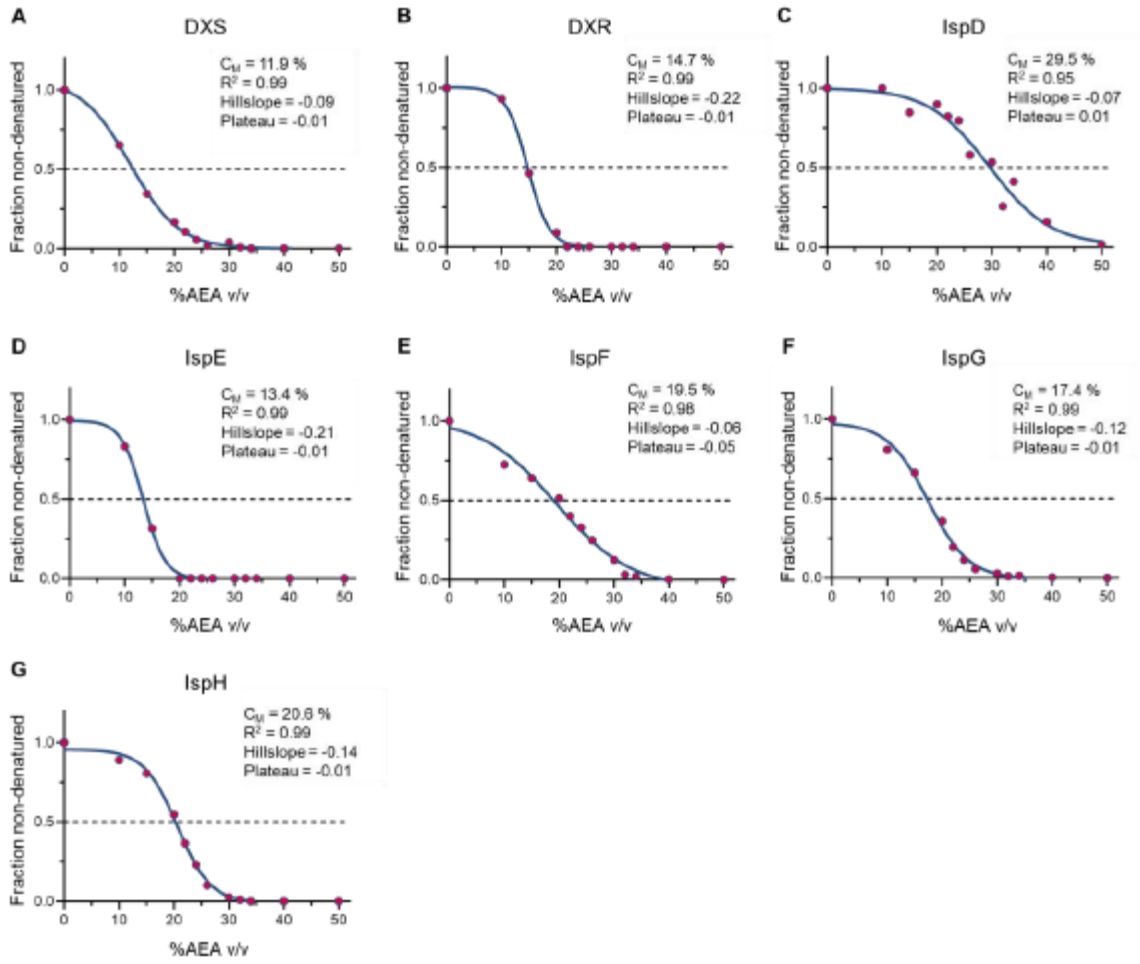


**SI Figure S6.** Denaturation curves of *Escherichia coli* MEP pathway enzymes. (B) DXR, target of reverse β-aza fosmidomycin analogues **1**–**3**. (F–G) IspG and IspH, targets of diphosphate derivatives **4**, **5**.

Supplemental Information - Figure S7

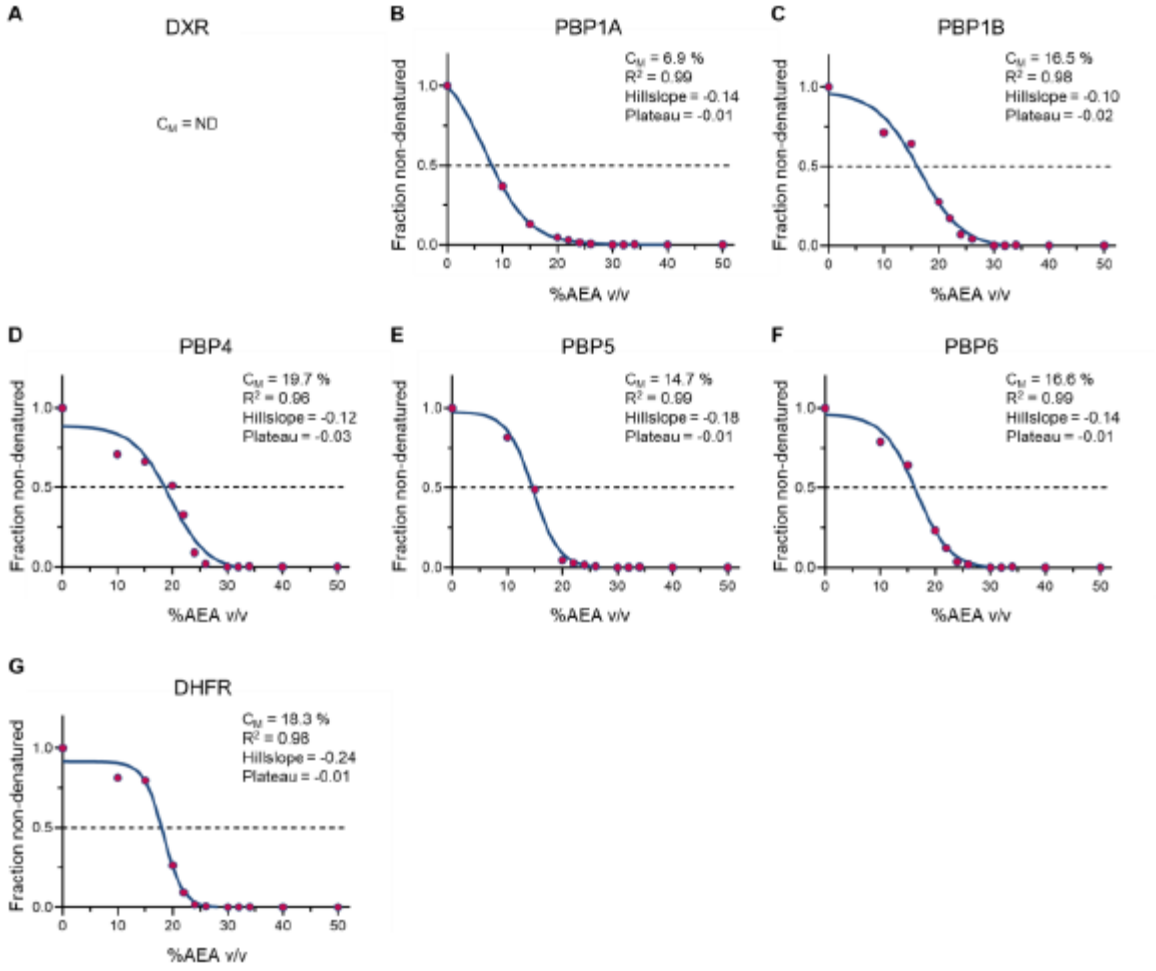


**SI Figure S7.** Denaturation curves of *Klebsiella pneumoniae* proteins and protein groups targeted by the employed model drugs. (A) DXR, target of fosmidomycin, $C_M$ not determined (too low to quantify). (B–F) PBPs, target protein class of β-lactam antibiotics. (G) DHFR, target of methotrexate.

Supplemental Information - Figure S8

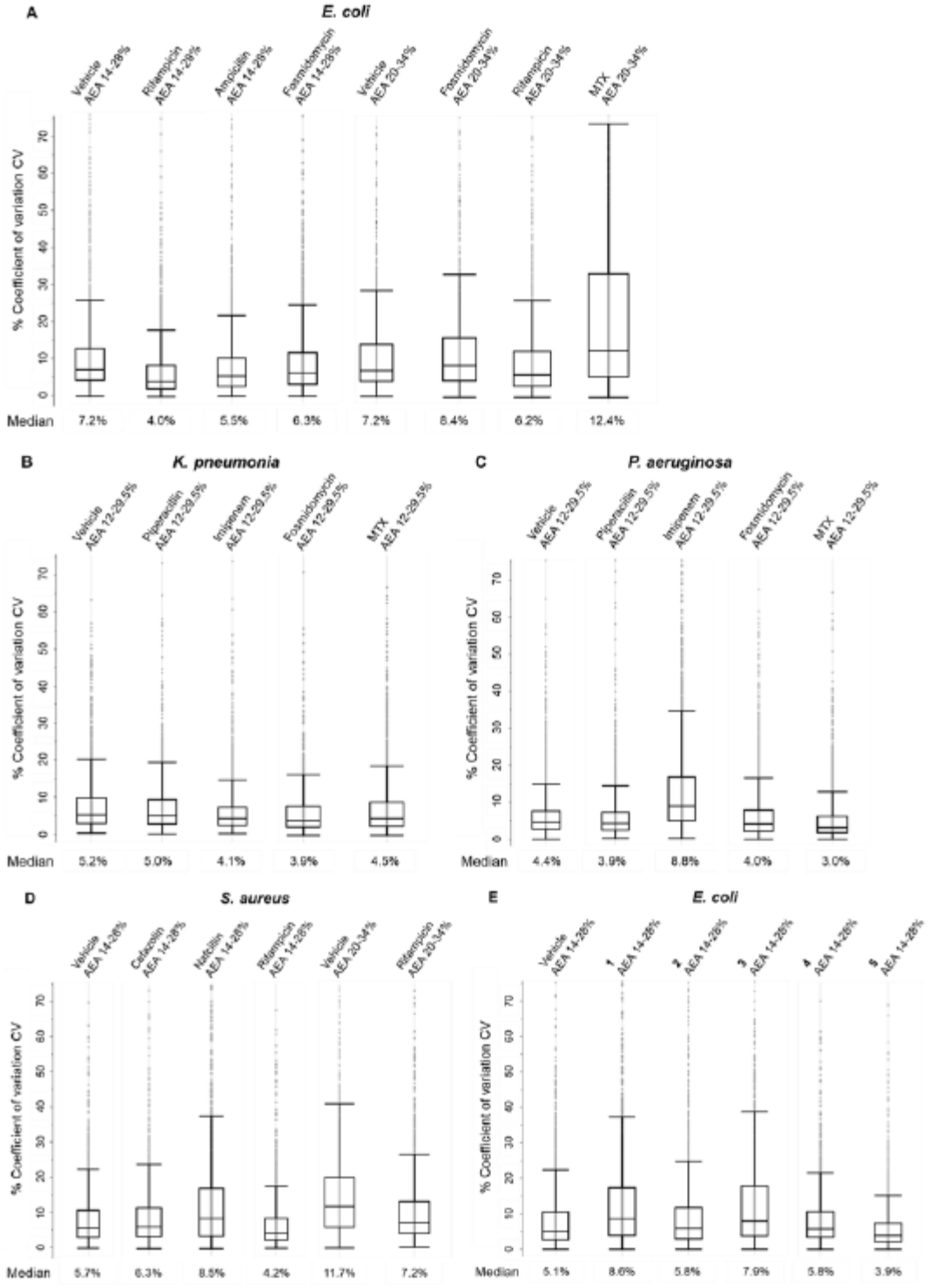


**SI Figure S8.** Box plots showing coefficient of variation (CV) values across biological replicates ($n$=3) of all quantified proteins for iSPP target validation studies with model drugs on *Escherichia coli* (A), *Klebsiella pneumoniae* (B), *Pseudomonas aeruginosa* (C), and *Staphylococcus aureus* (D). (E) CV values for target engagement of MEP pathway inhibitors on *E. coli*.

Supplemental Information - Figure S9

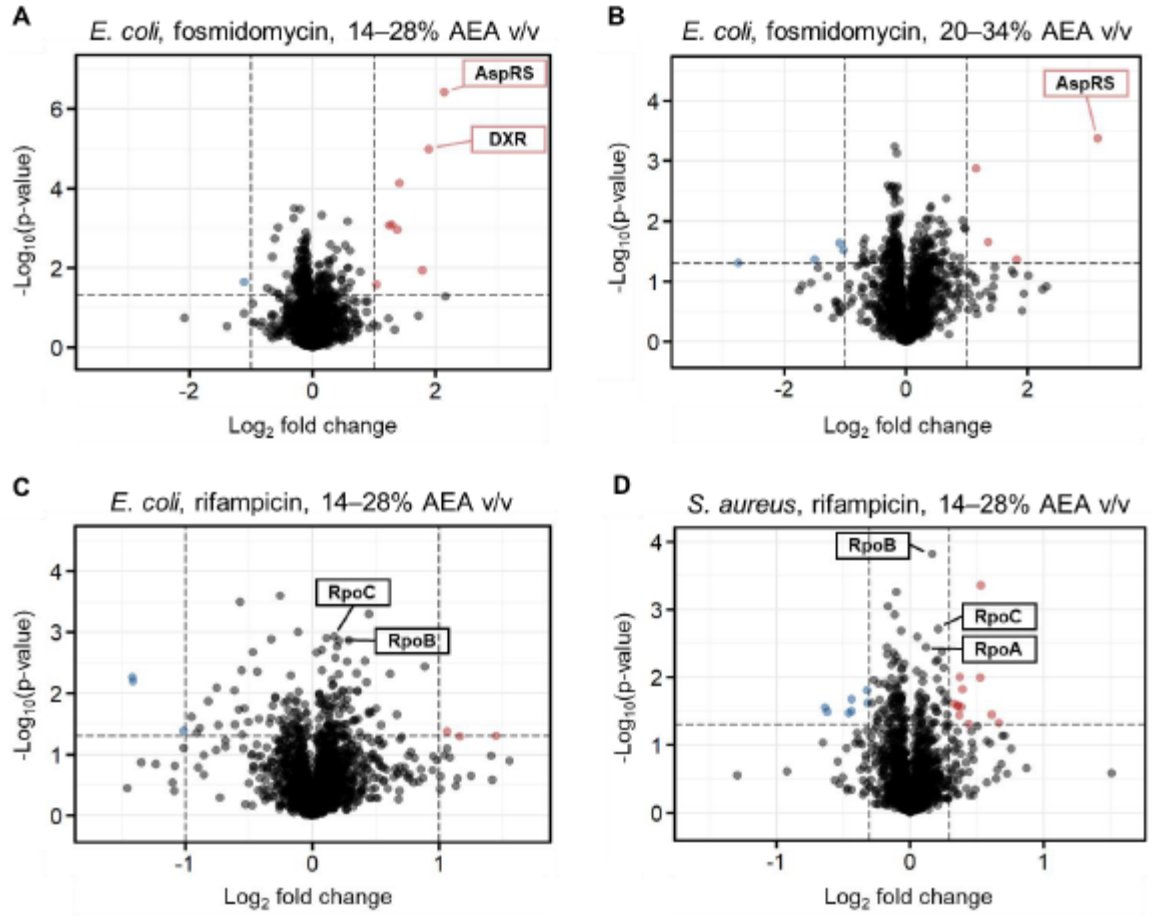


**SI Figure S9.** iSPP target validation experiments employing multiple AEA range windows. *Escherichia coli* cell lysate was incubated with fosmidomycin (A–B), rifampicin (C) or vehicle. *Staphylococcus aureus* cell lysate was incubated with rifampicin (D), or vehicle. (A) Experimental repetition employing the rationally selected gradient 14–28% (v/v). The known target DXR and the putative target AspRS were stabilized. (B) Suboptimal AEA range (20–34%, v/v) exhibiting stabilization exclusively of AspRS. (C–D) Suboptimal AEA range (14–28% v/v) demonstrating a notable reduction in the stabilization of RpoB and other RNAP core enzyme subunits. Data are presented as a volcano plot to highlight changes in abundance of each drug over vehicle *vs.* statistical significance. The thresholds were set to a $\log_2$fc > |1.0| and a p-value < 0.05 for *E. coli* data and $\log_2$fc > |0.3| and a p-value < 0.05 for *S. aureus* data (due to the compressed magnitude of change obtained by iSPP in this bacterium).

Supplemental Information - Figure S10

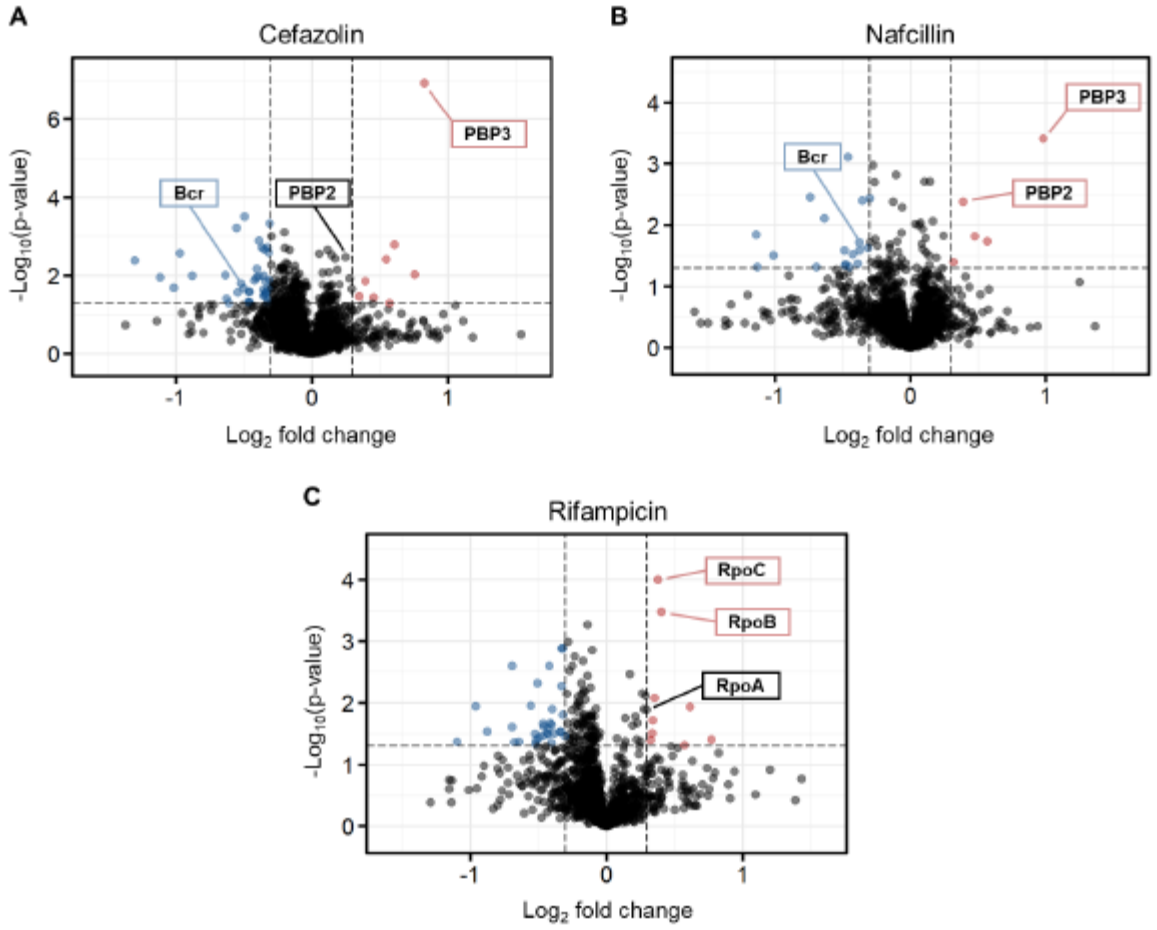


**SI Figure S10.** iSPP approach on *Staphylococcus aureus* cell lysates. *S. aureus* was incubated with vehicle, cefazolin (A), or nafcillin (B), and then exposed to the AEA gradient 14–28% v/v. Rifampicin (C) and the corresponding vehicle control incubated cell lysates were exposed to the AEA gradient 20–34% v/v. All drugs were tested at 10 µM. Data are presented as a volcano plot to highlight changes in abundance of each drug over vehicle *vs*. statistical significance. The threshold levels of significance necessary to identify proteins as potential hits were set to log2fc > |0.3| and p-value < 0.05.

Supplemental Information - Figure S11

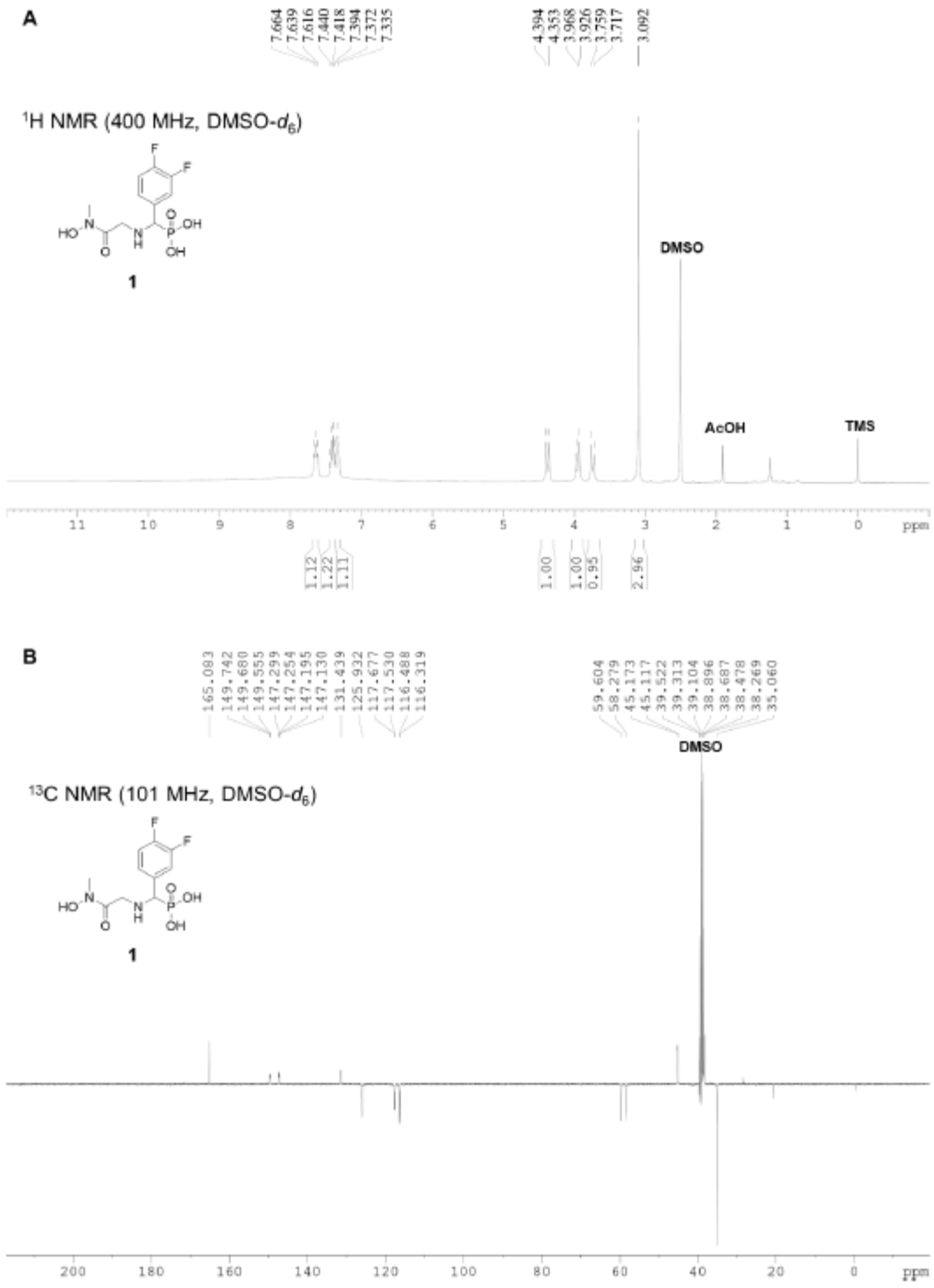

C

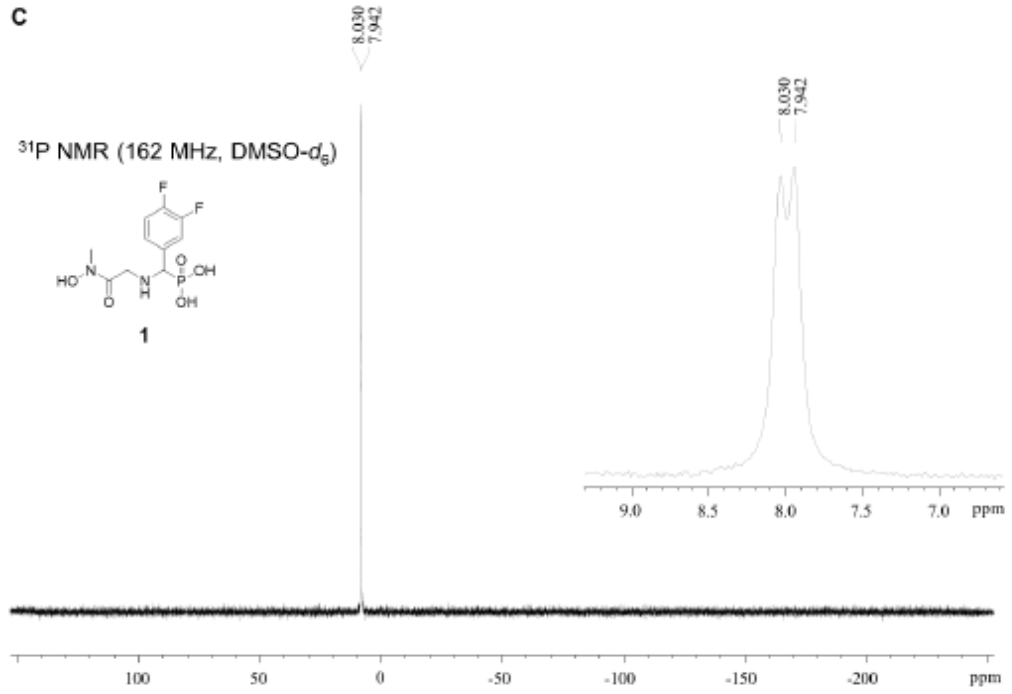
8.030
7.942
$^{31}$P NMR (162 MHz, DMSO-$d_6$)
1
9.0
8.5
8.0
7.5
7.0
ppm
100
50
0
-50
-100
-150
-200
ppm

D

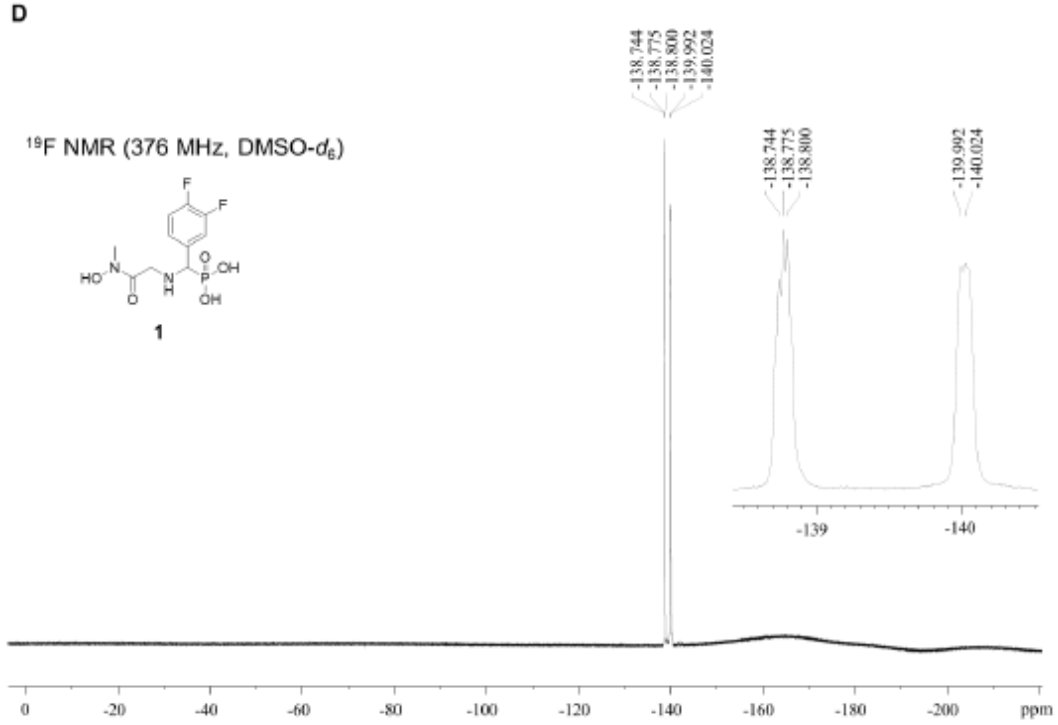
-138.744
-138.775
-138.800
-139.992
-140.024
$^{19}$F NMR (376 MHz, DMSO-$d_6$)
1
-139
-140
0
-20
-40
-60
-80
-100
-120
-140
-160
-180
-200
ppm

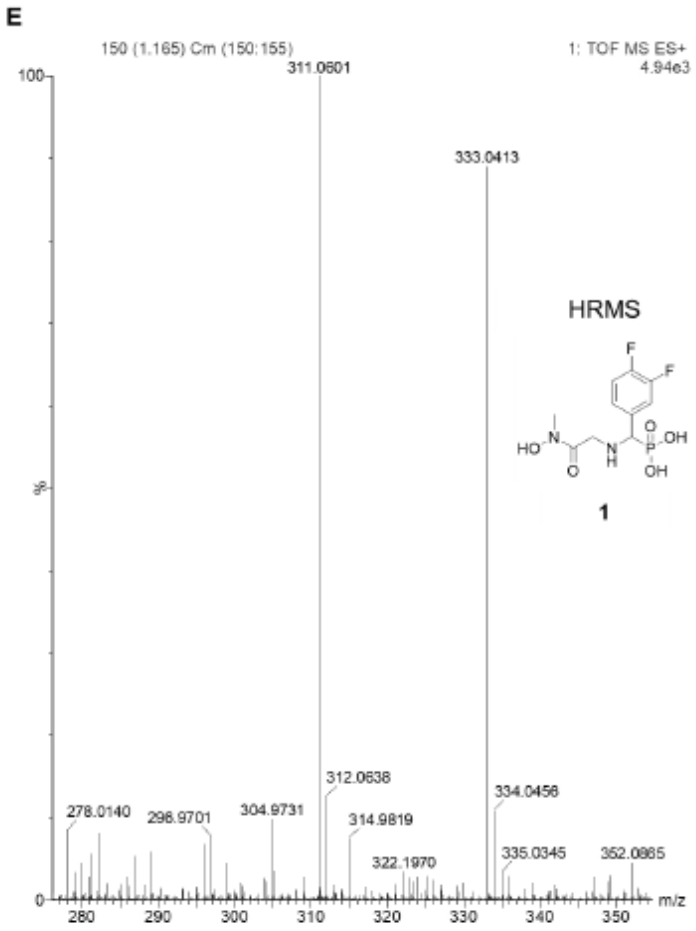


**SI Figure S11.** (A) $^{1}$H NMR spectrum of compound **1**. (B) $^{13}$C NMR spectrum of compound **1**. (C) $^{31}$P NMR spectrum of compound **1**. (D) $^{19}$F NMR spectrum of compound **1**. (E) HRMS spectrum of compound **1**.

Supplemental Information - Figure S12

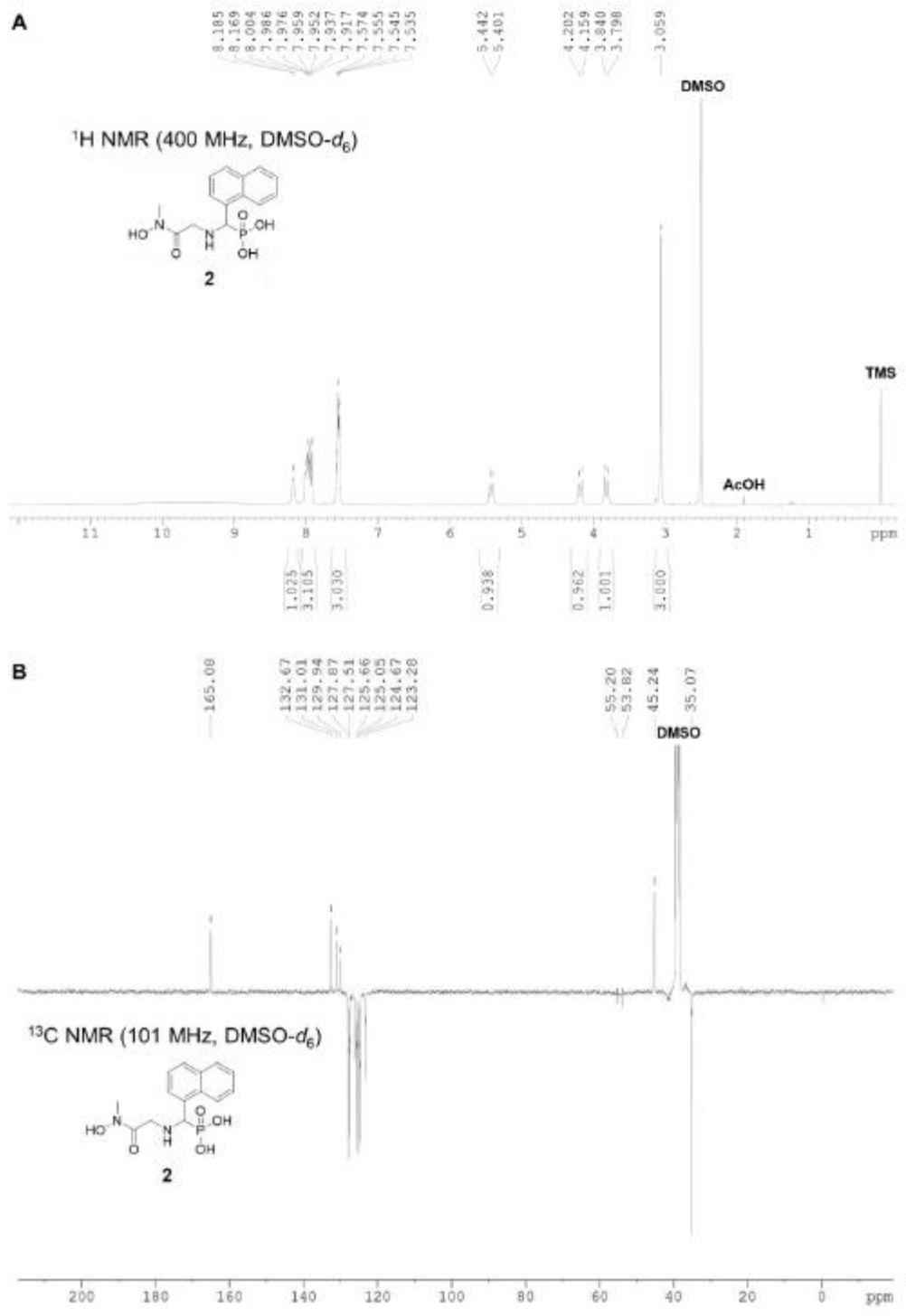

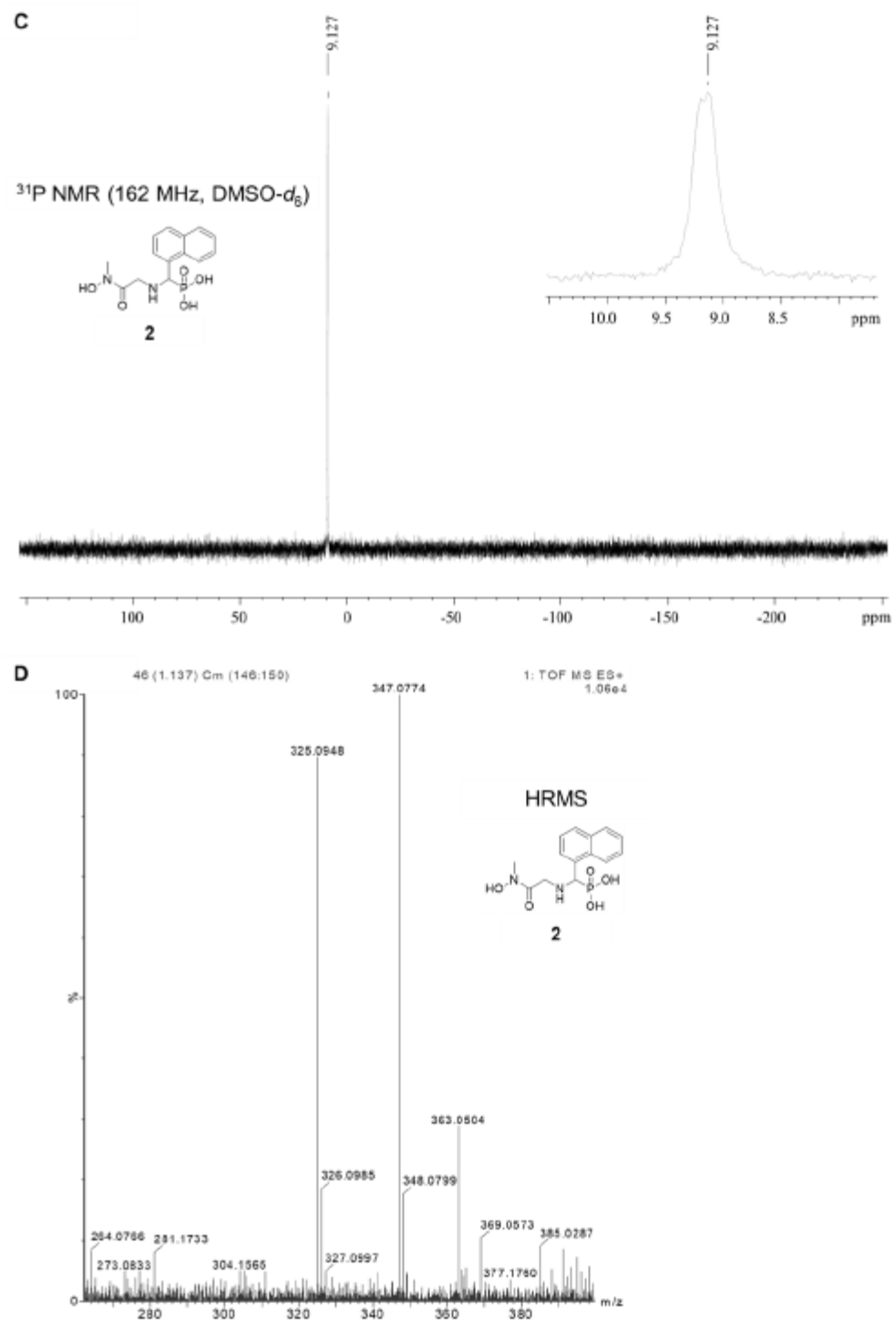


**SI Figure S12.** (A) $^{1}$H NMR spectrum of compound **2**. (B) $^{13}$C NMR spectrum of compound **2.** (C) $^{31}$P NMR spectrum of compound **2.** (D) HRMS spectrum of compound **2**.

Supplemental Information - Figure S13

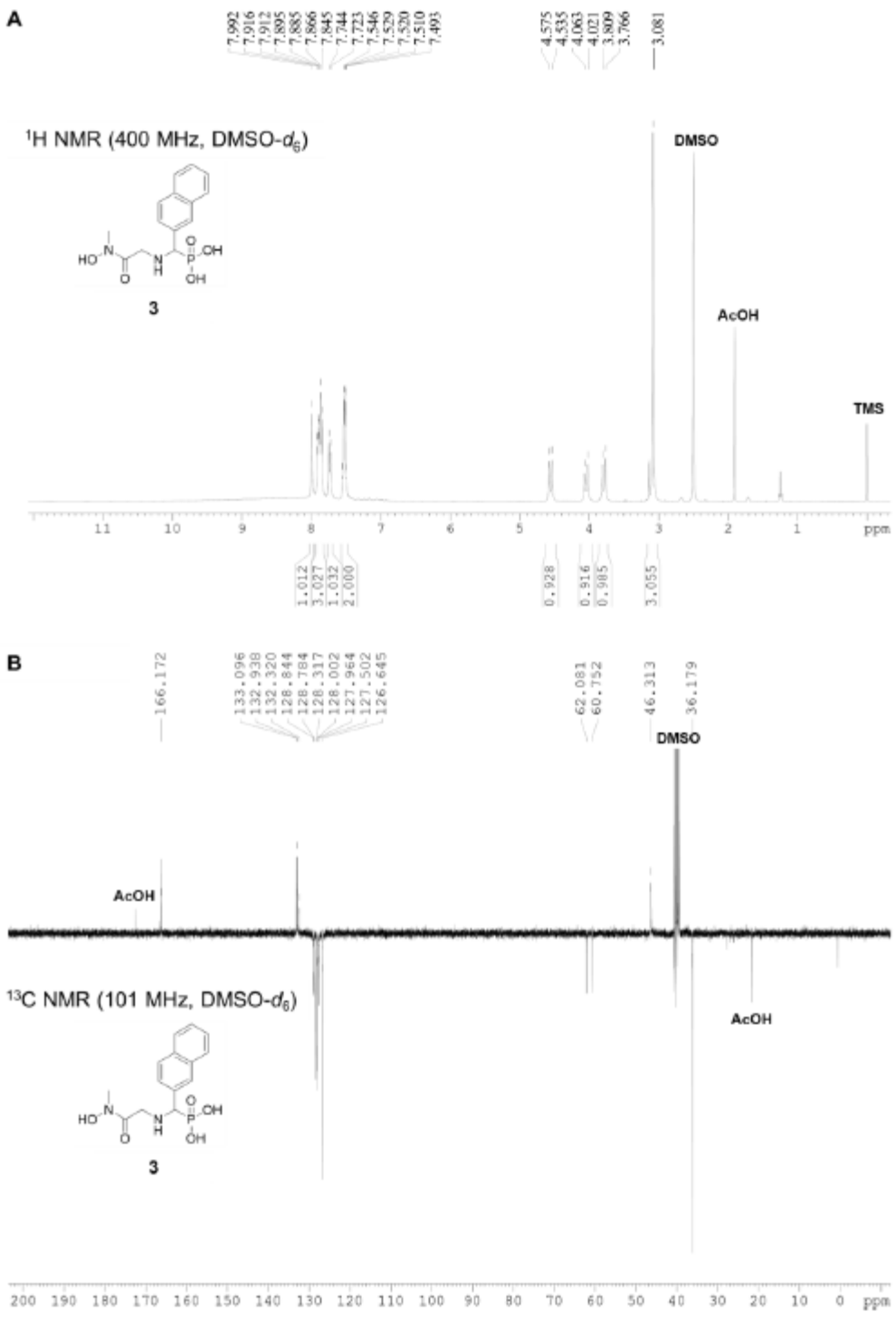

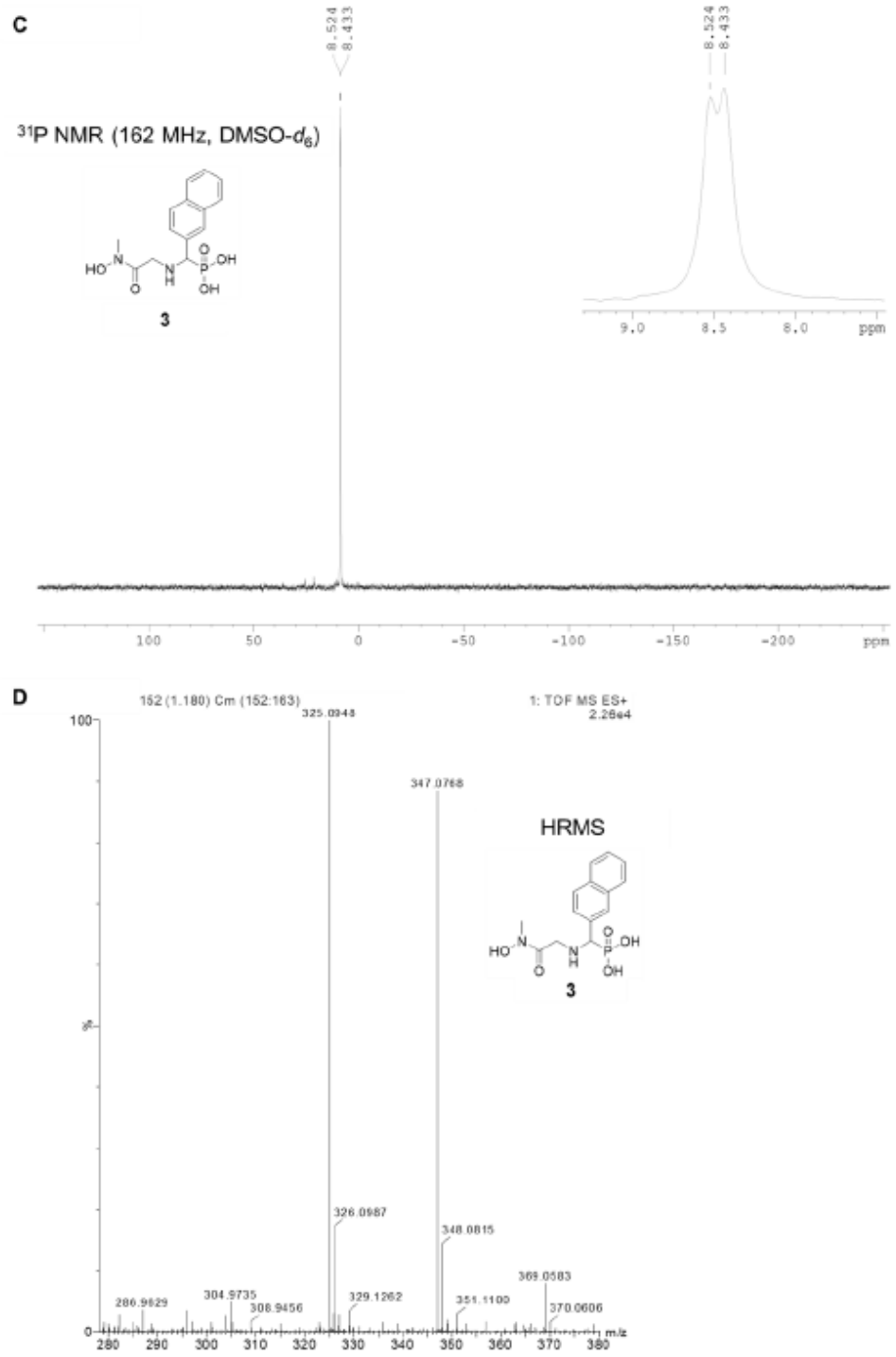


**SI Figure S13.** (A) $^{1}$H NMR spectrum of compound **3**. (B) $^{13}$C NMR spectrum of compound **3.** (C) $^{31}$P NMR spectrum of compound **3**. (D) HRMS spectrum of compound **3**.

Supplemental Information - Figure S14

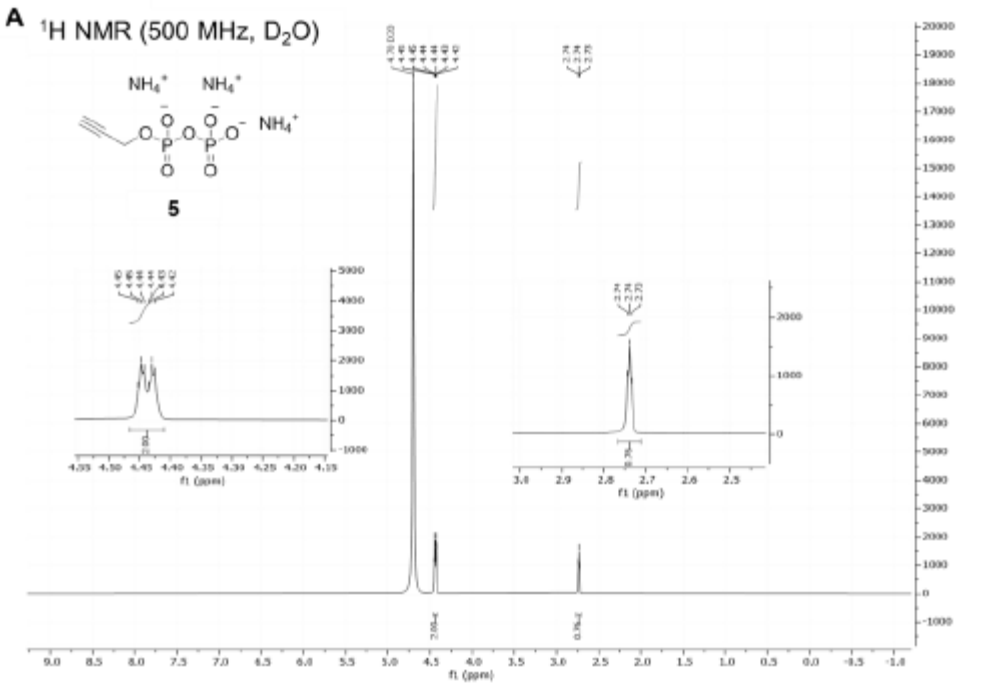


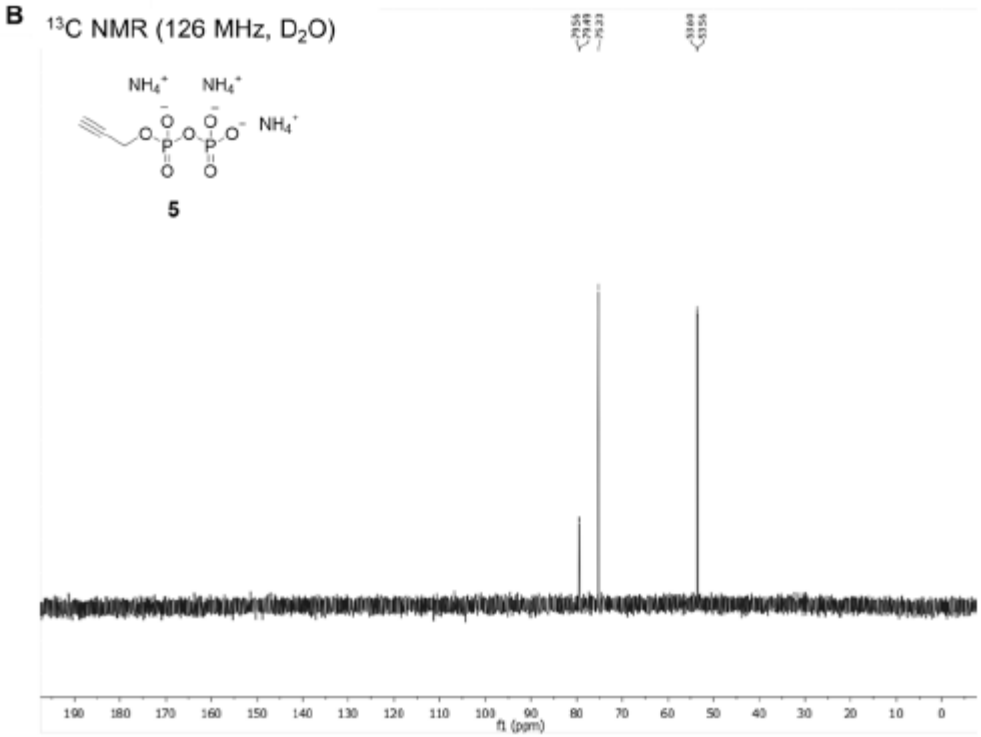

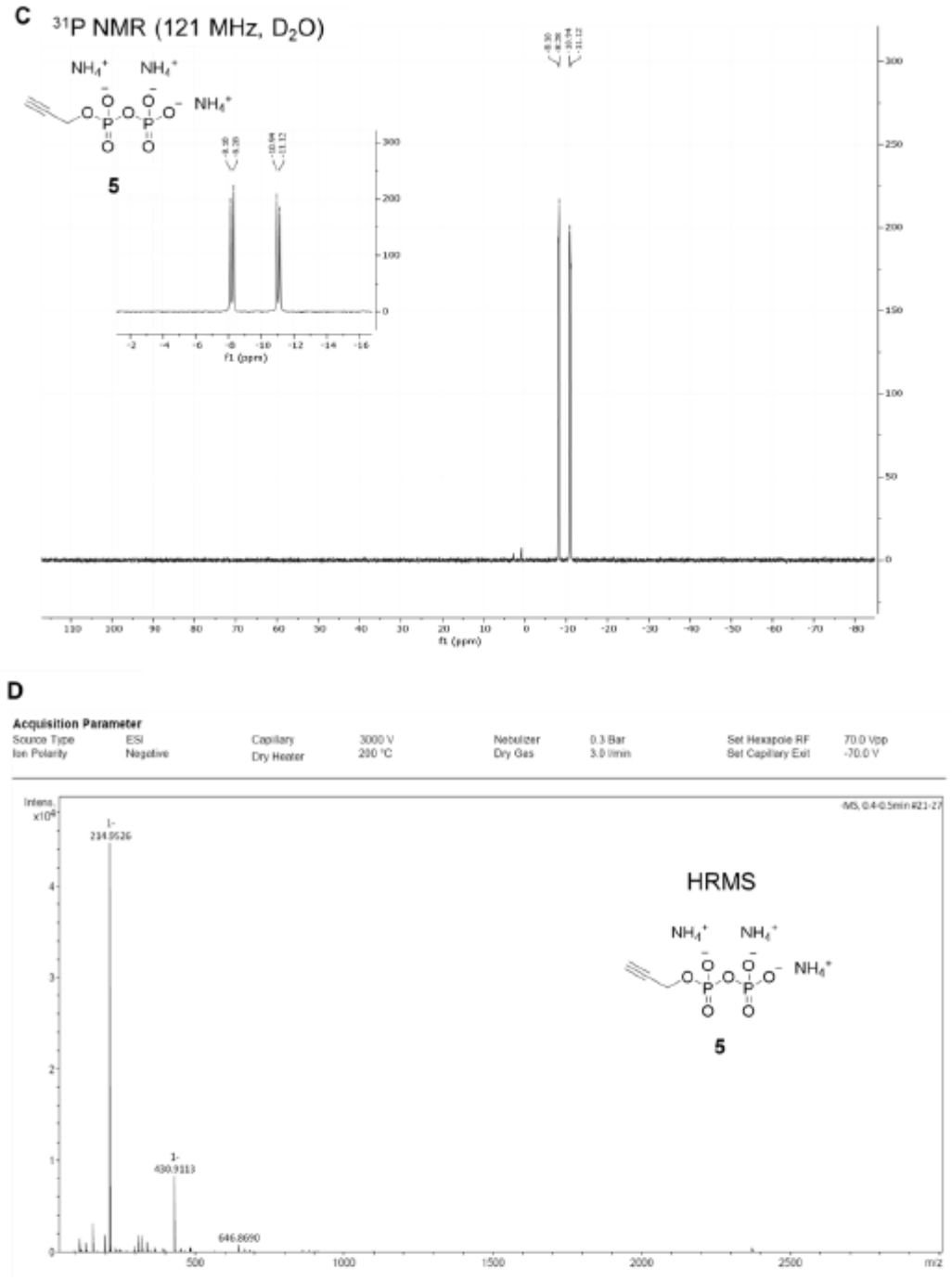


**SI Figure S14.** (A) $^{1}$H NMR spectrum of compound **5**. (B) $^{13}$C NMR spectrum of compound **5**. (C) $^{31}$P NMR spectrum of compound **5**. (D) HRMS spectrum of compound **5**.

## 3.4 Chapter D: Integral Solvent-Induced Protein Precipitation for Target-Engagement Studies in *Plasmodium falciparum*

Patricia Bravo,⊥ Lorenzo Bizzarri,⊥ Dominik Steinbrunn, Jonas Lohse, Anna K. H. Hirsch, Pascal Mäser, Matthias Rottmann, Hannes Hahne

⊥ these authors contributed equally

Contributions: Lorenzo Bizzarri and Hannes Hahne conceived the project; Lorenzo Bizzarri supervised the iSPP experiments, which were planned, executed and analyzed in collaboration with Patricia Bravo; Dominik Steinbrunn conceived and conducted the experiments for the semi-automatization of the iSPP workflow; Patricia Bravo, Pascal Mäser and Matthias Rottmann prepared the *Plasmodium falciparum* culture and cell lysate; Jonas Lohse contributed to the selection of model drugs for validation experiments; Patricia Bravo and Lorenzo Bizzarri wrote the manuscript with contributions from all authors; Hannes Hahne coordinated the project.

All authors have given approval to the final version of the manuscript.

This chapter was published in the *ACS Infectious Diseases* Journal (American Chemical Society) on December 4, 2024. Reprinted with permission https://pubs.acs.org/doi/10.1021/acsinfecdis.4c00418.

ACS Infectious Diseases



pubs.acs.org/journal/aidcbc
Article

# Integral Solvent-Induced Protein Precipitation for Target-Engagement Studies in *Plasmodium Falciparum*

Patricia Bravo,[‡] Lorenzo Bizzarri,[‡] Dominik Steinbrunn, Jonas Lohse, Anna K. H. Hirsch, Pascal Mäser, Matthias Rottmann, and Hannes Hahne*

Cite This: https://doi.org/10.1021/acsinfecdis.4c00418

Read Online

ACCESS | Metrics & More | Article Recommendations | Supporting Information

**ABSTRACT:** The limited understanding of the mechanism of action (MoA) of several antimalarials and the rise of drug resistance toward existing malaria therapies emphasizes the need for new strategies to uncover the molecular target of compounds in *Plasmodium falciparum*. Integral solvent-induced protein precipitation (iSPP) is a quantitative mass spectrometry-based (LC−MS/MS) proteomics technique. The iSPP leverages the change in solvent-induced denaturation of the drug-bound protein relative to its unbound state, allowing identification of the direct drug−protein target without the need to modify the drug. Here, we demonstrate proof-of-concept of iSPP in *P. falciparum* (Pf) lysate. At first, we profiled the solvent-induced denaturation behavior of the Pf proteome, generating denaturation curves and determining the melting concentration ($C_M$) of 2712 proteins. We then assessed the extent of stabilization of three antimalarial target proteins in multiple organic solvent gradients, allowing for a rational selection of an optimal solvent gradient. Subsequently, we validated iSPP by successfully showing target-engagement of several standard antimalarials. The iSPP assay allows the testing of multiple conditions within reasonable LC−MS/MS measurement time. Furthermore, it requires a minimal amount of protein input, reducing culturing time and simplifying protein extraction. We envision that iSPP will be useful as a complementary tool for MoA studies for next-generation antimalarials.

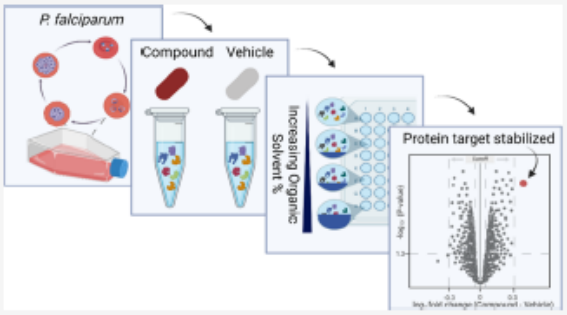


**KEYWORDS:** *target-engagement, antimalarial, solvents, iSPP, proteomics, drug discovery*

## INTRODUCTION

Malaria is a global health challenge with an estimated incidence of 249 million cases in 2022 and a mortality of 608,000.[1] Over 95% of malaria deaths occur in Africa, and 78% of these in children under 5 years.[1] Malaria is caused by parasites of the genus *Plasmodium*, with the highest incidence and mortality attributed to *Plasmodium falciparum*.[1] The asexual blood stage form of the parasite is responsible for the disease and a possible fatal outcome if left untreated.[2] Therefore, this stage represents the primary target of first-line antimalarials.[2] An active drug against all lifecycle stages would provide a more effective treatment and interruption of transmission.[3] Artemisinin-based combination therapies remain the first-line treatment in most malaria-endemic regions.[1] However, the emergence of resistance to artemisinins, along with the growing resistance to its partner drugs, underscores the need for new antimalarials with new modes of action.[4−6] Identifying the mechanism of action (MoA) of antimalarial molecules is crucial for the rational design of new inhibitors and their optimization by medicinal chemistry. Moreover, understanding the MoA guides drug combinations and supports the management of drug resistance.

Various strategies are employed to elucidate the MoA of antimalarials. These include in vitro resistance evolution and whole-genome sequencing (IVIEWGA),[7] metabolic profiling,[8,9] chemogenomic profiling,[10] chemical screens,[11] and transcriptomic analysis.[12] In IVIEWGA, parasites are exposed to sublethal drug pressure until resistant mutants emerge. Whole-genome sequencing of the parent and resistant strains is then conducted to identify the genetic variants associated with the resistance phenotype.[13,14] These variants often manifest as single point mutations or copy number variations in the target protein.[13,14] Notable compounds whose targets were identified or validated with this method include fosmidomycin,[15] DSM265,[16] MMV390048,[17] and NITD609.[18] IVIEWGA has been one of the most successful methods for identifying drug targets. However, resistance selection can also result in genetic

Received: May 20, 2024
Revised: July 25, 2024
Accepted: October 14, 2024

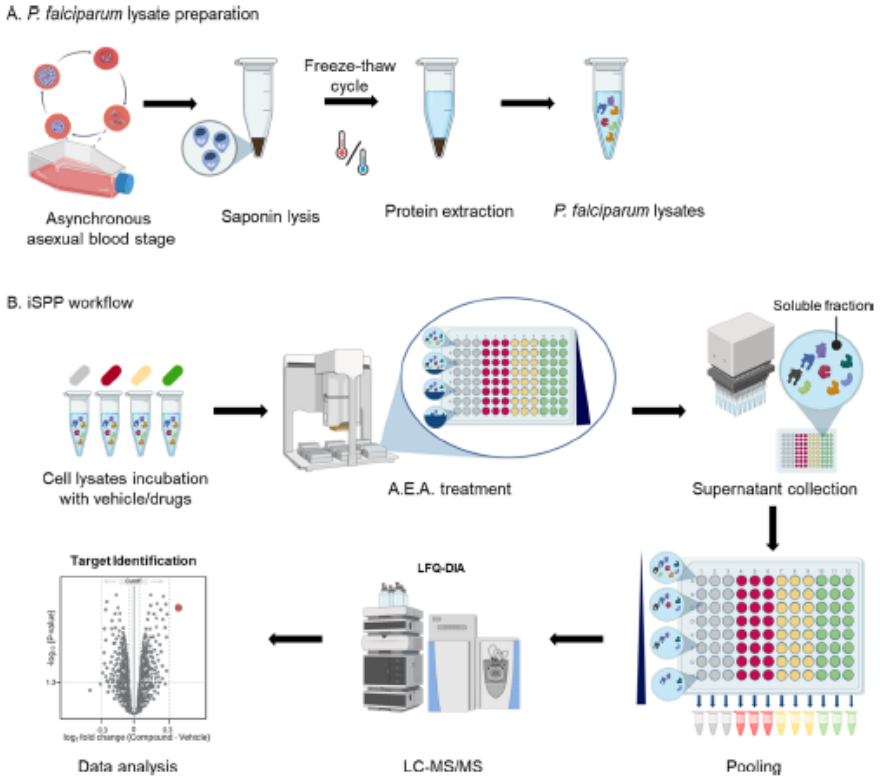


**Figure 1.** Schematic workflow of iSPP in *Plasmodium falciparum* (created with BioRender.com).

changes not directly related to the drug target, such as mutations in drug efflux transporters (e.g., *pfcrt* gene, *pfcarl* gene).[19,20] This makes it challenging to discern the direct MoA of the compound.[13,14] Additionally, the generation of resistant parasites is frequently a time-consuming process and not always successful.[13,14]

Proteomics and chemical proteomics have emerged as alternative or complementary approaches to IVIEWGA, mainly through quantitative mass spectrometry (LC−MS/MS) readout.[21] Conventional chemical proteomics utilize a compound analogue that can be linked to a resin or matrix through, e.g., click chemistry for subsequent chemical pulldown.[22] This often requires the addition of functional groups to the small molecule.[23] For instance, the target of MMV390048, phosphatidylinositol 4-kinase (PI4k), was identified with this method.[17] However, chemically modifying the small molecule can alter its efficacy and specificity to the target.[22]

Proteome-wide target−engagement approaches have emerged which do not involve modification of the drug or the target protein. Instead, they exploit the physical or chemical stabilization of proteins upon binding to their ligands.[24−30] An example is the drug affinity responsive target stability method, which utilizes the change in protease degradation of drug-bound proteins relative to their unbound form.[31] For instance, the target of Torin 2, a compound displaying low nanomolar activity on the sexual stages of *P. falciparum*, was identified with this method.[31] The cellular thermal shift assay (CETSA) and thermal proteome profiling (TPP) have been at the forefront of modification-free approaches.[28,29,32] They rely on detecting changes in the melting temperature ($T_M$) of the protein−drug complexes compared to the unbound, free state of the same proteins. CETSA and TPP have recently been established in both cell lysates and intact cells of *P. falciparum*, facilitating the identification of protein targets for quinine, mefloquine, and antimalarials with previously unknown MoA.[24,25,33]

Solvent-induced protein precipitation (SPP) is a recent addition to this field. It leverages the principle of denaturing proteins through organic solvents.[27,34] Zhang et al. demonstrated in human cell lysates that drug-binding proteins can be identified upon exposure to organic solvents by comparing the denaturation curves of a drug-treated versus a non-treated cell lysate.[27] The throughput of the standard SPP approach was then improved by Van Vranken and co-workers[34] by pooling the soluble fractions after denaturation across the organic solvent gradient.[34,35] The soluble proteins in each pool are then quantified by quantitative MS-based proteomics. This compressed approach yields an estimation of the area under the solvent denaturation curve, and the fold change measured in vehicle-treated lysates vs. drug-treated lysates is then calculated to determine protein stability.[34,35] Recently, Bizzarri et al. extended the technique to Gram-negative and Gram-positive bacteria.[36] We refer to the compressed format of SPP as integral solvent-induced protein precipitation (iSPP).

Here, we apply the iSPP assay to *P. falciparum*. First, we characterized the solvent-induced denaturation behavior of the Pf proteome, followed by iSPP experiments in which multiple organic solvent gradients were employed on three antimalarials. This enabled the selection of the optimal solvent gradient for iSPP target validation. To demonstrate the


https://doi.org/10.1021/acsinfecdis.4c00418
ACS Infect. Dis. XXXX, XXX, XXX−XXX

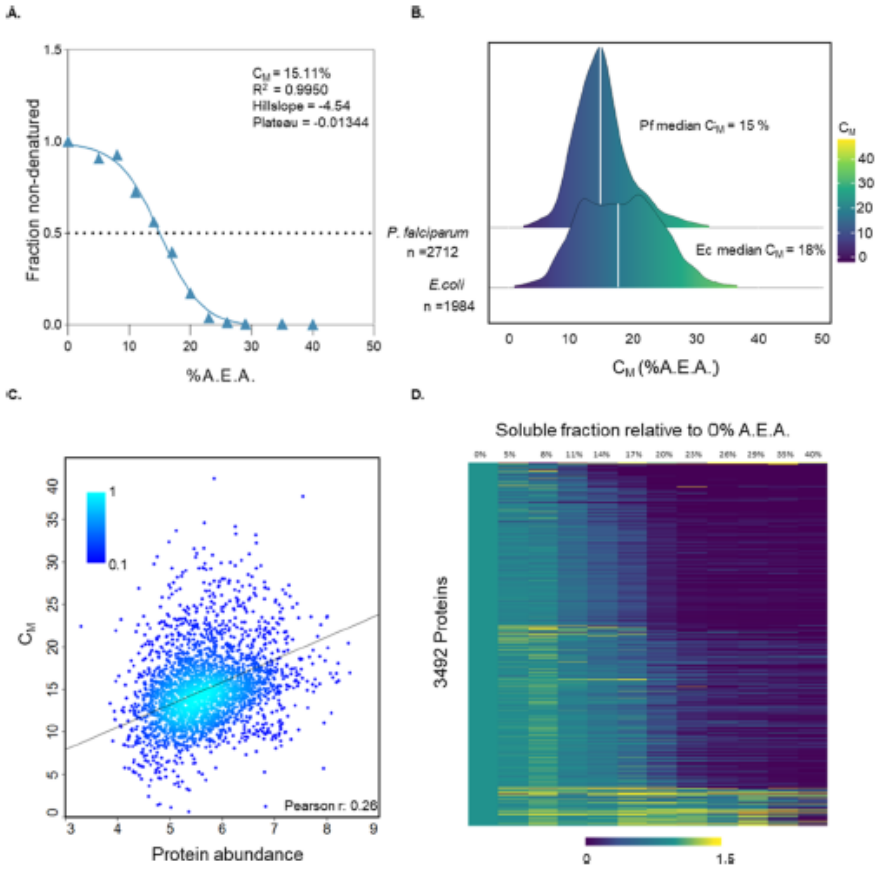


**Figure 2.** Solvent profiling of the *Plasmodium falciparum* proteome. (A) Denaturation curve of the *P. falciparum* proteome. For each data point, the median value among all quantified proteins is shown. The fold change of the relative abundance was calculated relative to 0% A.E.A. The curve was obtained for proteins with high-quality fitting curves (2712; $R^2 \geq 0.8$, Plateau < 0.3, $C_M \geq 4$). The inset shows the calculated $C_M$, $R^2$, Hillslope and bottom plateau; (B) distribution profiles of high confidence $C_M$ values calculated in *P. falciparum* and *Escherichia coli* proteomes. (C) Correlation between $C_M$ values (*y*-axis) vs protein abundance (*x*-axis, $\log_{10}$ intensity), displaying a weak relationship between the two variables ($r = 0.26$); (D) heatmap representation of all proteins quantified ($n = 3492$). For each protein, the relative abundance (fold-change) was calculated relative to 0% A.E.A. Protein fold-changes were then clustered.

potential of iSPP as target deconvolution tool for Pf, we validated the approach with six antimalarials and successfully observed target-engagement of the designated target for four of them as well as identified potential secondary targets for fosmidomycin and MMV390048.

## ■ RESULTS

**iSPP Workflow in *P. falciparum*.** The iSPP approach was conducted on cell lysates of Pf (NF54 strain) derived from asynchronous culture. Because some antimalarial compounds are stage-specific,[37] asynchronous cultures were necessary to ensure the presence of the presumed target proteins. First, the cells were treated with saponin, resulting in erythrocyte lysis, followed by several wash steps to get rid of excess hemoglobin. The parasite pellet was then resuspended in lysis buffer and subjected to freeze−thaw cycles to extract proteins. The lysates were incubated with drug or vehicle, and then exposed to eight increasing concentrations of acetone/ethanol/acetic acid (50:50:0.1 v/v, abbreviated as A.E.A.). These chemical reagents are common, cost-effective, and readily available in most laboratories. Organic solvents such as acetone, ethanol, methanol, and acetonitrile are frequently used to precipitate proteins and remove contaminants. Zhang and colleagues demonstrated that increasing concentrations of the A.E.A. mixture effectively induce protein precipitation, a property that can be exploited to identify ligand-binding events.[27] This approach has consistently proven effective for various ligand−target pairs in human cell lysates.[26,34]

The iSPP protocol used in this study requires only 20 $\mu$g total protein input material per data point (each sample across the gradient), representing 0.5 mg total protein per condition (drug or vehicle, in triplicates). This renders the process more applicable to compound screening campaigns in Pf considering the relatively low protein yield after saponin lysis. After centrifugation, the soluble fractions were collected and pooled for iSPP. The resulting proteins underwent bottom-up proteomics sample preparation for LC−MS/MS with label-free quantification in data-independent acquisition mode (LFQ-DIA) (Figure 1). The readout of an iSPP assay was the calculated fold change of drug-treated samples over control samples. These data were used to generate volcano plots,


https://doi.org/10.1021/acsinfecdis.4c00418
ACS Infect. Dis. XXXX, XXX, XXX−XXX

plotting fold change versus *p*-value, which had been derived from statistical testing of the biological replicates.

**Solvent Profile of the *P. falciparum* Proteome.** Before employing the iSPP workflow for target-engagement studies, we investigated the solvent-induced denaturation of the complete Pf proteome. Thus, we first assessed the effect of increasing A.E.A. concentrations (0 to 50% v/v) on Pf proteins. The soluble fractions were first resolved by SDS-PAGE. The SDS-PAGE readout showed that most of the proteins responded in a gradient-dependent manner with a substantial fraction of proteins precipitating after exposure to 20% of A.E.A. (v/v) (Figure S1). Subsequently, the denaturation behavior was assessed by quantitative mass spectrometry.

We quantified approximately 3400 proteins in each biological replicate ($n = 2$), achieving more than 50% coverage of the theoretical *P. falciparum* NF54 proteome (UniProt ID: UP000030673). This represents a substantial improvement over the reported proteome coverage achieved by previous MS-based TPP and CETSA in Pf, which had reported approximately 2600 proteins.[24,25,38]

Each protein has a denaturation profile, which can be modeled similarly to thermal denaturation.[39] This profile is essentially described by the melting point, the slope, and top and bottom plateaus of the curve.[34] The melting concentration, $C_M$, represents the solvent concentration at which there is an equal distribution between the folded and the unfolded state of the protein. It provides a measure for a protein's susceptibility toward organic solvents.[34] As described by Van Vranken et al.,[34] the assigned curves for each protein were evaluated for quality of the fitting according to two parameters: the coefficient of determination ($R^2$) which is the measure of goodness of fit, and the bottom plateau of the curve. We then selected the curves having a high-quality fit using the following criteria: $R^2 \geq 0.8$ and Plateau < 0.3, which allowed us to confidently assign $C_M$ values for 2712 proteins. The $C_M$ value of each protein is provided in Supporting Information file Table S1. This will be useful in determining appropriate gradients for further iSPP approaches with *P. falciparum*.

Consistent with the SDS-PAGE readout, we observed a decreasing protein abundance with increasing A.E.A. % (v/v), reaching a bottom plateau at approximately 30% (v/v) (Figure 2A). The calculated median $C_M$ of the Pf proteome in the experiment was 15% (v/v) A.E.A. ($R^2 = 0.99$). This median value was marginally lower than the median $C_M$ measured by SPP for *Escherichia coli* K12 cell using the same protocol by Bizzarri et al. ($C_M$ = 18% (v/v) A.E.A, Figure 2B).[36] These findings suggest that the Pf proteome overall exhibits a similar tolerance to organic solvent-induced denaturation as to the *E. coli* proteome. In contrast, the distribution profiles of $C_M$ values for Pf and *E. coli* exhibited a notably different pattern. The distribution in Pf displays a narrow peak, suggesting a high degree of uniformity among $C_M$ values (Figure 2B). This indicates that a large portion of Pf proteins share a similar denaturation profile, resulting in a concentrated peak in the distribution. Notably, this distribution pattern closely resembles the one obtained by Van Vranken et al.[34] in their solvent profiling of the Human HCT116 proteome, as well as the $T_M$ distribution profile of human proteome obtained by Jarzab et al.[40] in a TPP meltome atlas study. This similarity in denaturation profiles may be attributed to the fact that the parasite lives intracellularly within the human host at this particular stage. Consequently, the parasite proteins are shielded against external stressors akin to human proteins. In contrast, the distribution of $C_M$ values of *E. coli* proteins is broader with a less pronounced peak, implying greater variability among proteins in terms of their solvent stability.

We found a low correlation between $C_M$ value and protein abundance (Pearson $r = 0.26$, Figure 2C), demonstrating that we can confidently assign $C_M$ values to proteins regardless of their relative abundance. To confirm this, we calculated the percentage of low-abundant proteins for which we assigned high-quality $C_M$ values. Proteins classified as low-abundance fell in the lowest 30th percentile based on their intensity. Out of the 1045 low-abundant proteins, we fit high-confidence curves and determined $C_M$ values for 707 of them (68%, Figure S2).

To analyze the solvent denaturation of the Pf proteome, we performed a hierarchal clustering based on the relative abundance of proteins across the gradient. The gene ontology (GO) terms on the upper and bottom clusters were then analyzed using DAVID.[41,42] Hierarchal clustering and GO analysis revealed a group of proteins that displayed a high resistance to solvent-based precipitation (Figures 2D and S3). This cluster consists of proteins involved in proteasomal protein degradation such as the proteasome complex subunits (median $C_M$ = 32.8%), as well as proteins involved in protein folding such as Hsp70/Hsp90 organizing protein, peptidyl-prolyl cis−trans isomerase, and prefoldin subunits. The cluster also contained a group of proteins functioning as surface-exposed antigens. For instance, the 6-cysteine protein family, which is the most abundant surface antigen present throughout all stages of *Plasmodium*,[43] has 6 proteins in this group (median $C_M$ = 24.79%). In addition, proteins involved in the invasion of host cells are found in this cluster, such as the ring-infected surface antigen (RESA) *N*-terminal domain-containing protein family, which is exported to the host erythrocyte.[44] Moreover, the merozoite surface proteins MSP3 and MSP6, a potential vaccine development candidate[45] and chaperones such as heat shock proteins (Hsp110) and histone chaperones were also identified within this group.

GO analysis of protein clusters displaying low tolerance toward A.E.A. revealed 58 proteins belonging to ribosomal protein subunits (median $C_M$ = 9.99%). Moreover, they contained proteins involved in ribosome biogenesis such as the nucleolar GTP-binding protein 1 ($C_M$ = 9.7%), RNA cytidine acetyltransferase ($C_M$ = 8.3%), the ribosome biogenesis proteins TSR1 ($C_M$ = 9.39%), BOP1 homologue ($C_M$ = 10.24%), and the ATP-dependent RNA helicase family (median $C_M$ = 8.98%).

**Selection of Gradients for iSPP Experiments in *P. falciparum*.** After assessing the behavior of the Pf proteome when exposed to organic solvents, we examined the capability of iSPP to validate the known protein targets of the standard antimalarials pyrimethamine, DSM265, and fosmidomycin. To determine the optimal gradient for target-engagement studies, we evaluated the stabilization extent of the known targets by employing five different A.E.A. range windows. Previous studies in iSPP[34] and the compressed TPP format[46] have highlighted the importance of selecting the suitable solvent/thermal gradient and its impact on the observed stabilization ($\log_2$ fold-change, $\log_2$FC) for drug-target proteins.

Pf cell lysate was incubated with either the vehicle control (DMSO or $ddH_2O$, $n = 3$) or 50 $\mu$M of the drugs ($n = 3$). To save Pf input material, we performed a mixed drug approach by


https://doi.org/10.1021/acsinfecdis.4c00418
ACS Infect. Dis. XXXX, XXX, XXX−XXX

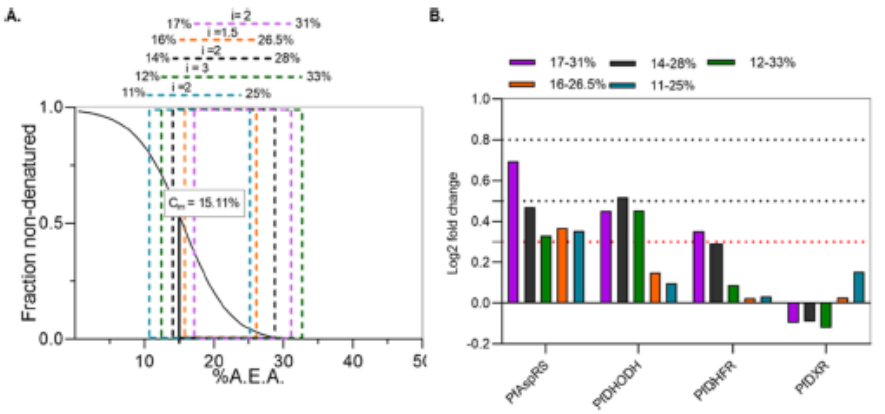


**Figure 3.** Solvent gradient has an impact on the extent of stabilization for each expected target (A) schematic figure of the iSPP solvent gradients used and the different increments (i) 1.5% A.E.A, 2% A.E.A, and 3% A.E.A. (v/v) (B) $\log_2$FC for the expected targets across solvent gradient used. Red inline displays the threshold $\log_2$FC = 0.3.

incubating the lysate with the three selected standard antimalarials as single condition.

Pyrimethamine is a well-known antimalarial and inhibitor of the bifunctional dihydrofolate reductase-thymidylate synthase (PfDHFR).[25,47,48] Multiple in vitro studies, including CETSA assay, and clinical studies support that PfDHFR inhibition is the cause of death of the parasite during pyrimethamine treatment.[25,47,48] DSM265 is a compound derived from a target-based high throughput screening of novel dihydroorotate dehydrogenase (PfDHODH) inhibitors,[49,50] which exhibits a low nanomolar activity against PfDHODH.[51] Lastly, fosmidomycin is an inhibitor of the 1-deoxy-D-xylulose 5-phosphate reductoisomerase (PfDXR),[52] which had been further validated through IVIEWGA[15] and metabolic profiling.[53]

After drug or vehicle incubation, the samples were exposed to the A.E.A. gradient with eight increasing concentrations, and the resulting soluble fractions were pooled. We selected gradients encompassing proteins with low $C_M$ values relative to the median $C_M$ (11−25%) and moderate-to-high $C_M$ values (14−28%, 16−26.5% and 17−31%), also accounting for narrow and wide increments ($i$ = 1.5%, $i$ = 2%, $i$ = 3%) within the gradient. Figure 3A illustrates the schematic diagram of the solvent gradients employed, and Table 1 shows the calculated $C_M$ for each expected target. In the following iSPP data analysis, we applied a $\log_2$FC > 0.3 and a $p$-value < 0.05 as inclusion criteria.

The iSPP approach was able to quantify approximately 3000 proteins ($n$ = 3) for all the conditions tested with a coefficient of variation < 8% between replicates (Figure S4A). We observed an inverse correlation between the %A.E.A. gradient and the number of proteins detected. Higher %A.E.A. gradients corresponded to lower numbers of identified proteins, as expected by a more pronounced precipitation. For instance, we detected 353 proteins using the gradient 11−25% A.E.A (n = 3414) which were not detected in the gradient 17−31% A.E.A. ($n$ = 3061) (Figure S5).

**Table 1. Calculated $C_M$ of the Expected Drug Targets**

| compound | designated target | $C_M$ (%A.E.A.) |
|---|---|---|
| fosmidomycin | PfDXR[a] | 20.1 |
| pyrimethamine | PfDHFR[b] | 20.1 |
| DSM265 | PfDHODH[c] | 21.4 |

[a]1-deoxy-D-xylulose5-phosphate reductoisomerase. [b]Bifunctional dihydrofolate reductase-thymidylate synthase. [c]Dihydroorotate dehydrogenase.

The iSPP approach revealed the stabilization of PfDHFR and PfDHODH in at least one of the A.E.A. gradients (Figure 3B). PfDXR did not result in a significant stabilization or destabilization in any of the gradients employed. Notably, aspartate tRNA ligase (PfAspRS) was identified among the top hits, as already observed in the iSPP study by Bizzarri et al. in *E. coli*, *Klebsiella pneumonia* (Kp), and *Pseudomonas aeruginosa* (Pa) cell lysates upon fosmidomycin incubation.[36] Therefore, AspRS was also considered as a secondary target of fosmidomycin in the current iSPP approach in Pf. We observed a more pronounced stabilization for most of the designated target proteins when using the higher A.E.A. (v/v) concentration gradients 14−28% and 17−31% (Figure 3B). This is consistent with their denaturation profiles, as they demonstrated high tolerance to chemical denaturation, with $C_M$ values greater than the median $C_M$ of the Pf proteome.

There was a larger number of stabilized proteins when utilizing the broadest concentration increment (12−33%, $i$ = 3%, Figure 3B). In this scenario, a substantial number of proteins unrelated to the employed drugs were stabilized ($n$ = 154, Figure 4B). Conversely, the narrowest concentration increment (16−26.5%, $i$ = 1.5%) resulted in a compressed magnitude of change in protein stability, with only a few proteins exhibiting stabilization ($n$ = 15, Figure 4D).

This result guided the rational selection of the solvent gradient for target validation studies in the succeeding experiments. The 14−28% A.E.A. (v/v) gradient successfully identified two out of three designated protein targets as stabilized proteins in addition to the secondary target of fosmidomycin, AspRS. This gradient maintained a relatively low number of nonspecific targets (de)stabilized (Figure 4C). Thus, it was selected as the optimal gradient for subsequent experiments. Moreover, this gradient encompasses the median $C_M$ value of the Pf proteome, making it the most suitable choice for target validation studies of the majority of Pf proteins.

**iSPP Validation for Target-Engagement Studies in *P. falciparum*.** We proceeded to verify the target validation of


https://doi.org/10.1021/acsinfecdis.4c00418
ACS Infect. Dis. XXXX, XXX, XXX−XXX

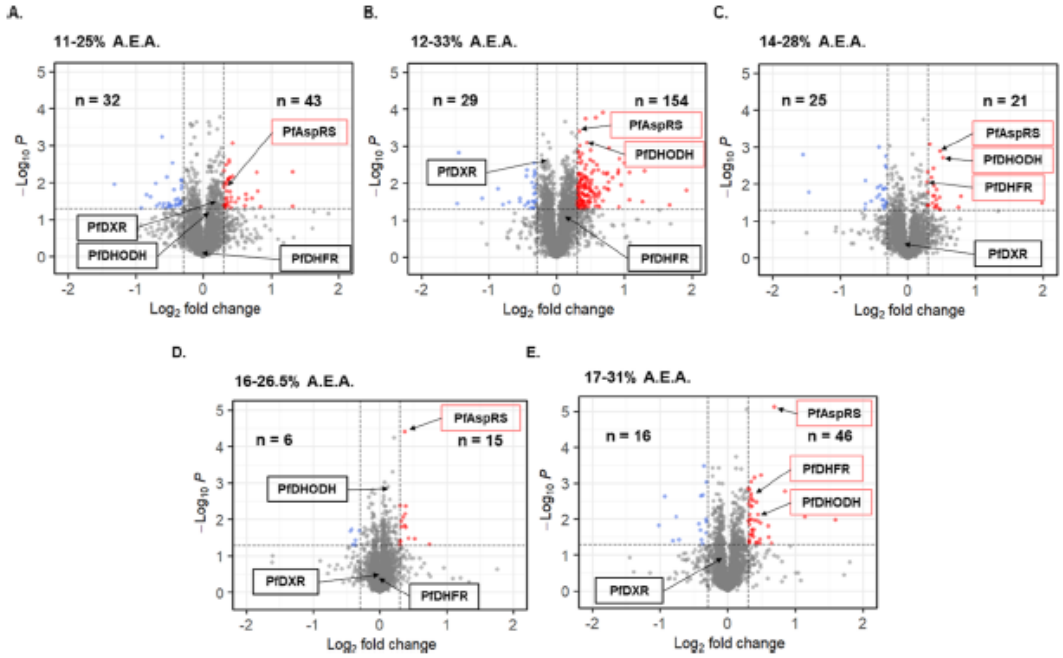


**Figure 4.** The solvent gradient 14−28% stabilized the majority of the expected protein targets with the least nonspecific proteins (de)stabilized. *P. falciparum* lysates were incubated with vehicle control or 50 $\mu$M of pyrimethamine, DSM265, and fosmidomycin (mixed drug approach). Lysates were then exposed to either of the five % A.E.A. gradient v/v: (A) 11−25%, (B) 12−33%, the broadest gradient which resulted in the most (de)stabilization of unexpected proteins, (C) 14−28%, (D) 16−26.5%, the narrowest increment and (E) 17−31%. Data is shown as volcano plots where the threshold criteria for identification of proteins exhibiting statistically significant changes in response to the compound treatment was set to a $\log_2$ fold change ($\log_2$FC) > |0.3| and $p$-value < 0.05. Red shows stabilized proteins with $\log_2$FC > 0.3 and $p$-value < 0.05; Blue shows destabilized proteins with $\log_2$FC < −0.3 and $p$-value < 0.05; gray shows proteins with −0.3 < $\log_2$FC < 0.3 and $p$-value < 0.05 and proteins with $p$-value > 0.05.

fosmidomycin, pyrimethamine, and DSM265 using iSPP by individually incubating each drug with Pf lysate. We also included the three structurally diverse antimalarials MMV390048 (inhibiting PI4k[17]), sulfadoxine (targeting dihydropteroate synthase[54]), and mefloquine (likely targeting the cytoplasmic ribosomes[25,55]). The drugs were tested at 100 $\mu$M, to ensure maximum target occupancy.

Consistent with our previous data, we detected approximately 3200 proteins for each condition. Pyrimethamine stabilized its known target, PfDHFR (Figure 5A; $\log_2$FC = 0.56). The compound DSM265 stabilized PfDHODH ($\log_2$FC = 0.31; Figure 5B). Interestingly, we also detected a similar level of stabilization of transcription elements such as RNA polymerase Rpb4/RPC9 core domain-containing protein ($\log_2$FC = 0.62; Table S2) and transcription initiation factor subunit 10 ($\log_2$FC = 0.37; Table S2). Fosmidomycin did not lead to the stabilization of PfDXR but resulted in the identification of PfAspRS among the top hits (Figure 5C). For MMV390048, we observed a significant stabilization for its protein target PfPI4k[17] ($p$-value <0.05, $\log_2$FC = 0.86, Figure 5D). Interestingly, we also observed a stabilization of CDP-diacylglycerol-inositol 3-phosphatidyltransferase (PfPIS), an enzyme also implicated in inositol phosphate metabolism ($p$-value < 0.05, $\log_2$FC = 0.54) (KEGG pfa00562, 2.7.8.11). Moreover, we detected significant stabilization for proteins involved in protein trafficking and signal transduction such as the signal peptidase complex subunit SPC1 ($\log_2$FC = 0.53), protein phosphatase inhibitor 2 ($\log_2$FC = 0.53), osmiophilic body protein ($\log_2$FC = 1.2), and EMP1-trafficking protein ($\log_2$FC = 0.37). As for sulfadoxine, its validated target, dihydropteroate synthase[54] (PfDHPS), was significantly stabilized ($p$-value < 0.05, $\log_2$FC = 0.31, Figure 5E). However, it is notable that several other proteins were stabilized similarly ($n$ = 43). Of note are several ribosomal protein subunits: 60 ribosomal protein L7 ($\log_2$FC = 0.58), 60S ribosomal protein L22 ($\log_2$FC = 0.39), 40S ribosomal protein S2 ($\log_2$FC = 0.37), 60S ribosomal protein L34 ($\log_2$FC = 0.34) and 60S ribosomal protein L7a ($\log_2$FC = 0.33). For mefloquine, it was previously suggested that the compound inhibits protein translation by interacting with the 80S ribosome.[55] In our iSPP experiments, we detected a destabilization of two ribosomal subunits: 60S ribosomal protein L18a (Pf60RPL18a, $p$-value <0.05 and $\log_2$FC = −0.44) and ribosomal protein L28 (PfRPL28, $p$-value <0.05, $\log_2$FC = −0.66) (Figure 5F). However, it should be noted that additional proteins were stabilized and destabilized ($n$ = 40 and $n$ = 49, respectively).

## ■ DISCUSSION

Elucidating the MoA is an important aspect in antimalarial drug discovery and development. The iSPP assay represents a modification-free approach that can be used as a complementary tool for existing target validation studies. The iSPP principle relies on detecting changes in the solvent denaturation behavior of protein targets upon binding with the compound of interest. In this work, we have adapted iSPP to *P. falciparum* lysate and validated its potential for target-


https://doi.org/10.1021/acsinfecdis.4c00418
ACS Infect. Dis. XXXX, XXX, XXX−XXX

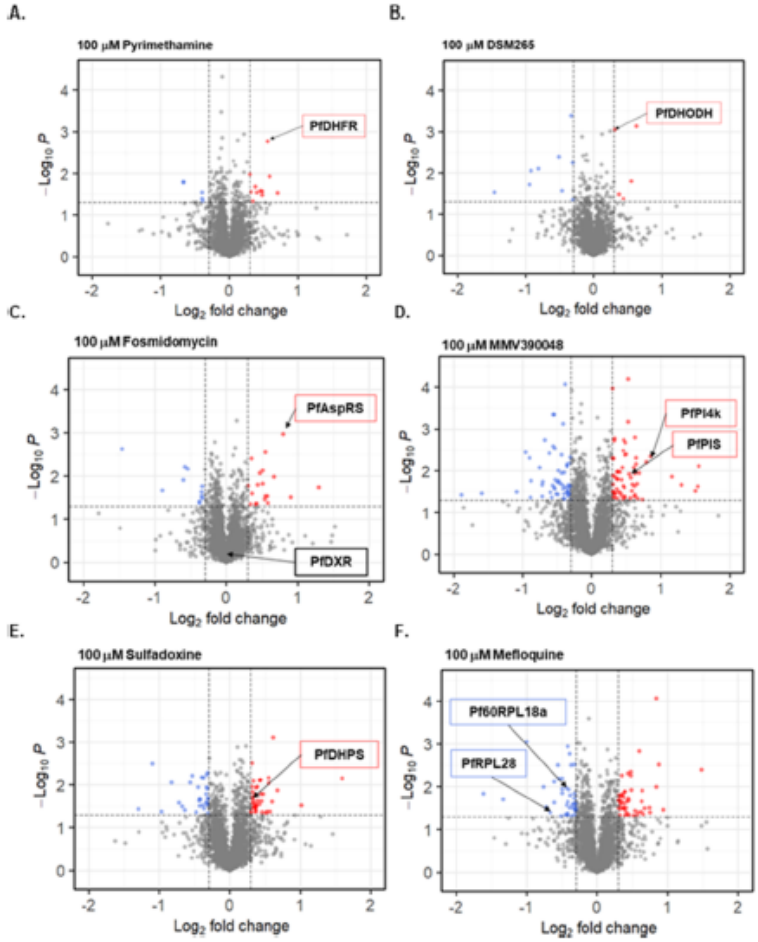


**Figure 5.** The iSPP assay in *Plasmodium falciparum*was able to identify the majority of the expected targets of the standard antimalarials. *P. falciparum* lysates were incubated with vehicle control or 100 $\mu$M of the compounds. The lysates were then exposed to 14−28% A.E.A. gradient (v/v). The threshold criteria for identification of proteins exhibiting statistically significant changes in response to the compound treatment was set to a $\log_2$ fold change ($\log_2$FC) > |0.3| and *p*-value < 0.05. Data is shown as volcano plots that highlights changes in abundance vs statistical significance for treatment with compounds (A) pyrimethamine (B) DSM265 (C) fosmidomycin (D) MMV390048, (E) sulfadoxine, and (F) Mefloquine. Red shows stabilized proteins with $\log_2$FC > 0.3 and *p*-value <0.05; Blue shows destabilized proteins with $\log_2$FC < −0.3 and *p*-value < 0.05; gray shows proteins with −0.3 < $\log_2$FC < 0.3 and *p*-value < 0.05 and proteins with *p*-value > 0.05.

engagement. We used six chemically diverse antimalarials with validated protein targets. These proteins have demonstrated druggability and their inhibitors often exhibited activity against multiple *Plasmodium* life-cycle stages. Furthermore, there has been a rise of novel chemotypes with inhibitory effects on these targets. For instance, several PfDHODH and PfDHFR inhibitors have progressed into the drug development pipeline.[56] Our iSPP assay identified PfDHODH and PfDHFR as main stabilized proteins by DSM265 and pyrimethamine, respectively (Figures 4−5). DHFR has previously been identified as main target of methotrexate in Gram-negative bacteria through the iSPP approach.[36] With isothermal dose response (ITDR)-CETSA approach, PfDHFR was also identified as the main target in pyrimethamine-treated Pf lysates, demonstrating a dose-dependent stabilization.[25]

The list of proteins (de)stabilized by each compound treatment provides insights into potential off-targets or cytotoxicity associated with these antimalarials (Supporting Information file Table S2). For instance, the consistent stabilization of AspRS observed in iSPP experiments in lysates across multiple organisms could be an indication of an additional target for fosmidomycin. The AspRS belongs to the amino-acyl-tRNA synthetases (AaRS) family, with proven druggability and relevant protein targets across organisms.[57] Moreover, inhibitors of AaRS in *Plasmodium* are also active in other pathogens.[58] The AaRS family catalyzes the attachment of amino acids to their cognate tRNAs to produce the aminoacyl tRNAs with the corresponding amino acid code thereby playing a vital role in preventing translational errors.[59] The enzymes have also multiple binding sites for small inhibitors.[57] However, additional experiments are needed to validate the binding of fosmidomycin to aspartate tRNA ligase in vitro. Similarly, iSPP showed stabilization of PfPIS in MMV390048-treated lysates, besides the main target PfPI4k.[17] Both enzymes are involved in signal transduction and synthesis of phosphatidylinositol. PfPI4k is involved in the synthesis of


https://doi.org/10.1021/acsinfecdis.4c00418
ACS Infect. Dis. XXXX, XXX, XXX−XXX

phosphatidylinositol 4-phosphate[60] whereas PfPIS catalyzes the reaction of CDP-diacylglycerol and myo-inositol.[61] PfPIS stabilization can be a result of MMV390048 direct binding, considering the shared similarity of its catalytic site with PfPI4k, given that 1,2-diacyl-*sn*-glycero-3-phospho-(1D-*myo*-inositol) is a substrate of PfPI4k and a product of PfPIS (KEGG pfa00562, 2.7.8.11).

As for mefloquine, we detected the destabilization of two ribosomal protein subunits out of the 40 proteins destabilized. For years, the target of mefloquine has been debated. However, it has been suggested that mefloquine is a putative inhibitor of the cytoplasmic ribosome.[55] Furthermore, ITDR-CETSA in lysate showed the stabilization of four ribosomal subunits upon mefloquine treatment in Pf lysates. However, stronger stabilization was observed for other proteins.[25] It was not the first time that a destabilization occurred for inhibitors of protein−protein interactions. Zhang et al. report a destabilization of proteins interacting with Hsp90 as a result of geldanamycin treatment in human cell lysates.[27] Therefore, the destabilization of the ribosomal subunits in our iSPP experiments could be explained by mefloquine inhibition of ribosomal protein−protein interactions.

The $C_M$ values obtained from the solvent denaturation profile could be valuable for conducting a targeted iSPP profiling of a potential target especially in accommodating for proteins e.g., with extremely high or low $C_M$ values by selecting an appropriate gradient. The extent of drug-induced protein stabilization in iSPP is influenced by the solvent gradient as demonstrated by the extent of stabilization observed for each target protein (Figure 3B). The proteasome complex, which is very stable against solvent-induced denaturation, represents an extreme case (median $C_M$ = 32.8%). Proteasomes are large protein complexes that play a role intracellular protein turnover.[62] Proteasomes have proven druggability and several inhibitors are active not only in *Plasmodium* but also in *Trypanosomes*,[63] Leishmania[63] and cancer cells.[64] In the case of a proteasome inhibitor profiled by iSPP, a higher solvent gradient is recommended due to their high resistance to solvent-induced precipitation.

Similar to other methods for measuring target-engagement, the iSPP approach has limitations. For instance, along with the designated drug targets, multiple proteins are displayed as (de)stabilized. This effect can be attributed to their low signal-to-noise ratio, which results in false-positives. Moreover, since the iSPP approach does not generate full protein denaturation curves, it inevitably leads to false-negatives when proteins have extreme $C_M$ values, and are thus not represented within the selected profiling window of solvent concentrations. Finally, there might be protein-specific reasons why target−engagement might not be detectable. For PfDXR, for instance, we did not observe notable stabilization in the presence of fosmidomycin, although PfDXR was detected and abundant in all replicates and had a calculated $C_M$ that fell within the tested gradients. One explanation could be that it might have been partially unfolded during protein extraction given that it resides within the four membrane-bound organelle−the apicoplast.[52]

In this work, we used an asynchronous culture of Pf. However, iSPP can be extended to synchronized cultures to accommodate for compounds with stage-specific activities and stage-specific target expression. For instance, the antifolates pyrimethamine and sulfadoxine have a higher activity against late trophozoites and early schizonts.[65,66] Moreover, synchronized *P. falciparum* at the midtrophozoite stage are the most metabolically active and might be optimal for target deconvolution studies.[67] The iSPP in Pf was designed to use a low input protein amount, adapting to the protein yield in Pf. This adaptation simplifies the protein extraction workflow as enough lysates are produced without the need for magnetic enrichment or separation of infected erythrocytes. This can be beneficial, especially in extending iSPP for profiling compounds targeting the gametocytes (the transmission stages), or the liver stages which are more challenging to culture.[68,69] We highlighted the potential of iSPP for target-engagement for compounds with known protein targets. However, iSPP could also be extended for target deconvolution studies of compounds with unknown MoA, e.g., from target-based discovery projects and phenotypic-based drug screening attempts. In that case, we would recommend measures to increase the likelihood of success and the specificity of the approach: (i) Structurally related negative control compounds to filter out artifacts. (ii) The use of multiple solvent gradients to enhance the likelihood of success by broadening the accessible $C_M$ range. (iii) Concentration-dependent iSPP profiling to allow differentiating targets based on the concentration-dependent saturation of drug binding. These control measures are also recommended in validating a possible off-target for the standard antimalarials.

## ■ CONCLUSION

In our study, the iSPP assay was adapted and extended to *P. falciparum*. The minimal protein input amount required from our protocol accounts for the low protein yield streamlining the protein extraction process. Thus, permitting iSPP to be extended to stages that are more labor-intensive to cultivate.

We validated iSPP in *P. falciparum* through the identification of the expected drug targets and potential secondary targets of six standard antimalarials. The compounds used in this study and their corresponding expected targets are pyrimethamine (PfDHFR), DSM265 (PfDHODH), fosmidomycin (PfDXR and PfAspRS), MMV390048 (PfPI4k), sulfadoxine (PfDHPS), and mefloquine (cytoplasmic ribosomal subunits). We provide a list of stabilized and destabilized proteins from our iSPP workflow that could be useful for potential exploration of off-targets or cytotoxicity studies of these compounds or their chemical analogues. Moreover, the high-confidence $C_M$ value list for 2712 proteins that we provide will be useful for profiling potential drug targets by iSPP. The $\log_2$FC observed for protein targets are influenced by the solvent gradient used, and we recommend the gradient 14−28% A.E.A. v/v as an initial iSPP profiling because it accommodates for the $C_M$ of the majority of the Pf proteome. However, the $C_M$ values of each protein provided in the Supporting Information Table S1 will be useful in determining an appropriate gradient for targeted iSPP profiling.

We envision that the iSPP would play an important role as a complementary and/or alternative tool for MoA studies in the development of potential antimalarials.

## ■ METHODS

The compounds used in this study were purchased from the following: Pyrimethamine (MedChemExpress, HY-18062), Fosmidomycin sodium salt (MedChemExpress, HY-112853), DSM265 (MedChemExpress, HY-100184), MMV390048


https://doi.org/10.1021/acsinfecdis.4c00418
ACS Infect. Dis. XXXX, XXX, XXX−XXX

(MedChemExpress, HY-106005), Sulfadoxine (Sigma, S7821), and Mefloquine (Sigma, PHR1705).

***P. falciparum* Culture.** *P. falciparum* asynchronous NF54 wild-type strain parasites were cultured at 3% hematocrit until 3−5% parasitemia was reached. RPMI 1640 was used as a culture media supplemented with 25 mM HEPES, 0.36 mM hypoxanthine, 24 mM sodium bicarbonate (pH 7.3), 0.5% Albumax II and 100 μg/mL neomycin as described in ref 70. The cultures were maintained at 37 °C with the mixed gas containing 3% $O_2$, 4% $CO_2$, and 93% $N_2$ and were kept in an incubator under atmospheric pressure.

***P. falciparum* Saponin Lysis.** Saponin lysis was performed to lyse the erythrocytes. Briefly, the cultures were transferred to 50 mL falcon tubes and centrifuged at 1200 g for 5 min at room temperature (RT). The supernatant was then discarded. Then, 10 volumes of 0.1% (w/v) saponin (Calbiochem 558,255, dissolved in PBS, and filtered with 0,22 μM) were added and incubated on ice for 10 min. During the incubation step, the falcon tubes were shaken every 60 s. A centrifugation step was done at 4000 g for 15 min at 4 °C, which resulted in a dark red supernatant corresponding to the lysed erythrocytes and a brown pellet corresponding to the intact parasite. A washing step was done with ice-cold PBS and centrifuged at 4000*g* for 5 min at 4 °C. This was repeated until the supernatant was transparent. The parasite pellet was redissolved in 1 mL ice-cold PBS and transferred to a 1.5 mL Eppendorf tube which was stored at −80 °C or proceeded for protein extraction.

***P. falciparum* Protein Extraction.** The parasite pellet was centrifuged at 4 °C for 20,000*g* for 10 min. Once the supernatant was aspirated, 2.5 volumes of the ice-cold lysis buffer was added to the parasite pellet. The lysis buffer contained 50 mM Tris/HCl pH 7.5 (Avantor), 5% glycerol (Sigma-Aldrich), 150 mM NaCl (Carl Roth), 1.5 mM MgCl2 (Sigma-Aldrich), 1 mM DTT (Carl Roth), 0.8% IGEPAL CA-630 (Sigma-Aldrich), 1X Halt Protease and Phosphatase Inhibitor-Cocktails EDTA-free (Thermo Fisher Scientific). The lysate was then subjected to three cycles of flash freeze−thawing using liquid nitrogen and $ddH_2O$ at RT. The lysate was centrifuged at 20,000*g* for 20 min at 4 °C. The supernatant, which contains the soluble protein fraction, was collected and transferred to a new 1.5 mL Eppendorf tube. The protein content was quantified using the BCA assay (Pierce BCA Protein Assay Kit, Thermo Fisher Scientific). The lysate was stored at −80 °C until further use.

**Solvent Proteome Profiling for SDS-PAGE Readout.** The *P. falciparum* lysate was thawed on ice and diluted to 0.8 mg/mL. The solvent proteome profiling workflow was performed as described.[36] Briefly, the lysate was transferred to a 96-well plate distributing 20 μg protein per well. Then, the samples were exposed to increasing acetone/ethanol/acetic acid (A.E.A.) concentration from 0 to 50% (v/v) using 12 aliquots (0, 8, 11, 14, 17, 20, 23, 26, 32, 35, 40, and 50%). This step was performed on the Bravo Automated Liquid Handling Platform (Agilent) in a final reaction volume of 50 μL. The samples were incubated at 37 °C and mixed at 750 rpm for 20 min (ThermoMixer C, Eppendorf). Centrifugation was then performed at 4402 g for 35 min (centrifuge 5920R, Eppendorf) to remove precipitated proteins. Upon supernatant collection, the soluble fractions were dried using a concentrator plus (Eppendorf). The samples were resuspended to 1.0 mg/mL final protein concentration with 2x NuPAGE LDS Sample Buffer (Thermo Fischer Scientific) which contained 25 mM DTT. Proteins were then resolved on NuPAGE 4−12% Bis-Tris Protein Gels (Thermo Fischer Scientific). The gels were stained using Coomassie-staining solution (ROTI Blue, Carl Roth) and the image was acquired with ChemiDoc MP Imaging System (BIO-RAD).

**Solvent Proteome Profiling for LC−MS/MS Readout.** The *P. falciparum* cell lysate was thawed on ice and distributed in a 96-well plate (Greiner Microplate, 96-well plate, V-Bottom) with 20 μg total protein per well as described.[36] The lysates were exposed to increasing A.E.A. concentrations from 0 to 40% (v/v) in 12 solvent concentrations: 0, 5, 8, 11, 14, 17, 20, 23, 26, 29, 35, and 40% in a final reaction volume of 50 μL using the Bravo Automated Liquid Handling Platform. The samples were incubated at 37 °C and mixed at 750 rpm for 20 min (ThermoMixer, Eppendorf). Centrifugation was then performed at 4402 g for 35 min. The soluble fractions were collected (Bravo Automated Liquid Handling Platform) and prepared for LC−MS/MS analysis.

**iSPP Assay.** *P. falciparum* cell lysate was thawed on ice and distributed in aliquots. Each aliquot was incubated with either vehicle control (DMSO or $ddH_2O$) or compound (dissolved in DMSO or $ddH_2O$) (50 μM or 100 μM). Next, the samples were incubated at RT for 30 min with a rotating mixer. Once the samples were distributed into eight wells, the samples were treated with an increasing A.E.A. (v/v) concentration depending on the gradient used: from 11 to 25% (11, 13, 15, 17, 19, 21, 23, and 25%), 12 to 33% (12, 15, 18, 21, 24, 27, 30, and 33%), 14 to 28% (14, 16, 18, 20, 22, 24, 26, and 28%), 16 to 26.5% (16, 17.5, 19, 20.5, 22, 23.5, 25, and 26.5%), or 17 to 31% (17, 19, 21, 23, 25, 27, 29, and 31%). After an incubation time (37 °C at 750 rpm for 20 min), centrifugation was done (4400*g* for 35 min) and precipitated proteins were removed. The soluble fractions were pooled in equal volumes into a single sample (Bravo Automated Liquid Handling Platform). Pooled samples were then prepared for LC−MS/MS analysis.

**Sample Preparation for LC−MS/MS Analysis.** The soluble fractions were dried down and then resuspended to a final protein concentration of 1.0 mg/mL with 5% SDS which contains 50 mM TEAB pH 7.5. The samples were then diluted to a final protein concentration of 0.4 mg/mL with 10% SDS buffer (1:1). Then, 10 mM DTT was added to all samples to reduce disulfide bonds and incubated at 35 °C for 30 min at 700 rpm (ThermoMixer). Chloroacetamide (55 mM, CAA, Merck) was added for protein alkylation and incubated for 30 min at RT in the dark. Samples were acidified with phosphoric acid to a final concentration of 2.5% and then diluted 7-fold with 90% methanol in 100 mM TEAB pH 7.5. The samples were transferred onto an *S*-trap column (ProtiFi) and subjected to five wash cycles using the same buffer. The Sequencing grade Modified Trypsin (Promega) in TEAB pH 8.5 was added to the *S*-trap column at a ratio of 1:10 (trypsin/protein), and the digestion reaction was carried out overnight at 37 °C. Peptides were eluted with 50 mM TEAB pH 8.5, 0.1% formic acid (FA, Th. Geyer), then 50/50 acetonitrile (ACN, Sigma-Aldrich)/water with 0.1% FA. Once the samples were dried down, peptides were resuspended with 0.5% FA. The peptides underwent desalting on the Bravo Automated Liquid Handling Platform using C18 cartridges (5 μL bed volume, Agilent) by using the standard AssayMAP peptide cleanup v2.0 protocol. First, the C18 cartridges were primed with 100 μL of 50/50 ACN/water with 0.1% FA and then equilibrated with 50 μL of 0.1% FA at a flow rate of 10 μL/min. Next, the samples were loaded at 5 μL/min, followed by


https://doi.org/10.1021/acsinfecdis.4c00418
ACS Infect. Dis. XXXX, XXX, XXX−XXX

an internal cartridge wash with 0.1% FA at a flow rate of 10 μL/min. The peptides were eluted using 50 μL of 60/40 ACN/water with 0.1% FA at a flow rate of 5 μL/min. The eluted samples were then dried and stored at −80 °C until further use.

**Liquid Chromatography and Mass Spectrometry Data Acquisition.** The samples were solubilized in 0.1% FA and injected in a volume equating to 1 μg to an Dionex UltiMate 3000 nano System (Thermo Fisher Scientific) coupled online to a Q Exactive Plus (Thermo Fisher Scientific) equipped with an Orbitrap mass analyzer. The peptides were delivered to a trap column (75 μm × 2 cm, packed in-house with ReproSil-Pur 120 ODS-3 resin, Dr. Maisch). The samples were separated on an analytical column (75 μm × 55 cm) packed in-house with Reprosil-Gold 120C18, 3 μm resin, Dr. Maisch. The flow rate was set at 300 nL/min using a 100 min gradient, ranging from 2−32% solvent B (0.1% FA, 5% DMSO in acetonitrile) in solvent A (0.1% FA, 5% DMSO in HPLC grade water) wherein the column oven temperature was set at 50 °C. The QE plus instrument was operated in DIA, in positive ionization mode. Full scan spectra ($m/z$ 400−1000) were acquired in centroid mode at an Orbitrap resolution of 70,000, an AGC target set to $3 \times 10^6$, a maximum injection time of 20 ms. Subsequently, DIA scans were collected utilizing 30 windows, with a 1 Da window overlap. HCD collision was set to 27%, loop count of 30, Orbitrap resolution of 35,000, AGC target set to $3 \times 10^6$, and a maximum injection time was set to automatic.

**Peptide and Protein Identification and Quantification.** The raw LFQ-DIA files were processed with DIA-NN (v. 18.1). Analysis was conducted in library-free mode, utilizing the UniProt FASTA file for *P. falciparum* NF54 (taxon identifier: 5843); canonical version, not older than five months prior to MS measurements. Raw files were digested with Trypsin/P enzyme specificity, allowing for a maximum of two missed cleavages. Peptide length was constrained within 7 to 30 peptides, and the precursor $m/z$ range was set from 300 to 1800. Cysteine carbamidomethylation was set as a fixed modification, while variable modifications included methionine oxidation and *N*-terminal acetylation. The maximum number of variable modifications was set to three, and 'match between runs' functionality was enabled. All other parameters remained at default settings, including the precursor FDR set at 1%. Cross-run normalization (RT-dependent) was enabled for raw files of iSPP experiments.

**Curve Fitting and $C_M$ Value Calculation for Solvent Proteome Profiling.** The raw LFQ-DIA values of each replicate were normalized to the median abundance and expressed as a ratio to the lowest A.E.A. concentration sample (0%) with Excel. The sigmoidal denaturation curves were generated using a nonlinear regression model with GraphPad prism (v. 8.3.0) which calculated the $C_M$ value for all unique protein IDs. High-quality denaturation curves were filtered based on the following criteria in RStudio (v. 4.3.2) with the dplyr package (v. 1.1.4):[71] (i) curves must reach a bottom plateau of ≤0.3; (ii) coefficient of determination ($R^2$) must be ≥ 0.8; (iii) a valid slope. The distribution profile of *P. falciparum* NF54 $C_M$ values and *E. coli* K12 $C_M$ values were plotted in RStudio using the ggplot2 package (v. 3.5.0).[72]

**Heatmap Generation and GO Analysis.** The previously normalized LFQ-DIA values were used to cluster the quantified proteins. This was performed in Perseus (v2.0.10.0) by using complete linkage with Euclidean distance and number of clusters set to 3 without any constraints. The web tool Database for Annotation, Visualization and Integrated Discovery (DAVID) (https://davidbioinformatics.nih.gov/) was used to analyze the GO terms in each cluster.[42]

**iSPP Data Analysis.** The raw LFQ-DIA intensity values of biological replicates in all conditions were normalized to the median abundance (Excel). Then, the normalized values were $\log_2$ transformed in Perseus (v2.0.10.0). Missing values were imputed from a normal distribution (width 0.3, down shift 1.5) and p-values obtained after a two-sample *t*-test over replicates with a permutation-based false discovery rate correction (FDR 0.05). The volcano plots were generated in RStudio using the EnhancedVolcano package (v. 1.20.0)[73] plotting the proteins by statistical significance where *y*-axis is presented as $-\log_{10}$ *p*-value vs magnitude of change where *x*-axis is presented as $\log_2$ fold change of the protein intensities for each compound condition over vehicle control.

## ■ ASSOCIATED CONTENT

### Supporting Information

The Supporting Information is available free of charge at https://pubs.acs.org/doi/10.1021/acsinfecdis.4c00418.

The Supporting Information contains the solvent proteome profiling of the *P. falciparum* (1−3); quality control of the iSPP experiments (4−5); Denaturation curves for the expected target proteins of the antimalarials tested (6) (PDF)

This contains the list of all the stabilized and destabilized proteins in the iSPP experiments (1); The high-confidence $C_M$ values for the *P. falciparum* proteome (2) (XLSX)

## ■ AUTHOR INFORMATION


### Corresponding Author

**Hannes Hahne** − *OmicScouts GmbH, D-85354 Freising, Germany*; Email: hannes.hahne@omicscouts.com

### Authors

**Patricia Bravo** − *Swiss Tropical and Public Health Institute, 4123 Allschwil, Switzerland; Universität Basel, 4003 Basel, Switzerland*; orcid.org/0000-0001-5454-3826

**Lorenzo Bizzarri** − *OmicScouts GmbH, D-85354 Freising, Germany; Department of Pharmacy, Saarland University, D-66123 Saarbrücken, Germany*; orcid.org/0009-0003-7017-5770

**Dominik Steinbrunn** − *OmicScouts GmbH, D-85354 Freising, Germany; TUM School of Natural Sciences, Department of Bioscience, Technical University of Munich, Center for Functional Protein Assemblies (CPA), D-85748 Garching bei München, Germany*

**Jonas Lohse** − *OmicScouts GmbH, D-85354 Freising, Germany*

**Anna K. H. Hirsch** − *Department of Pharmacy, Saarland University, D-66123 Saarbrücken, Germany; Helmholtz Institute for Pharmaceutical Research (HIPS), Helmholtz Centre for Infection Research (HZI), Saarland University, D-66123 Saarbrücken, Germany*; orcid.org/0000-0001-8734-4663

**Pascal Mäser** − *Swiss Tropical and Public Health Institute, 4123 Allschwil, Switzerland; Universität Basel, 4003 Basel, Switzerland*; orcid.org/0000-0003-3122-1941




https://doi.org/10.1021/acsinfecdis.4c00418
ACS Infect. Dis. XXXX, XXX, XXX−XXX

**Matthias Rottmann** – *Swiss Tropical and Public Health Institute, 4123 Allschwil, Switzerland; Universität Basel, 4003 Basel, Switzerland*

Complete contact information is available at: https://pubs.acs.org/10.1021/acsinfecdis.4c00418

### Author Contributions

‡P.B. and L.B. contributed equally.

### Funding

This project received funding from the European Union's Horizon 2020 Research and Innovation Program under Marie Skłodowska-Curie Grant Agreement 860816. P.B. was also funded by the Emilia-Guggenheim-Schnurr Foundation of the NGiB.

### Notes

The authors declare the following competing financial interest(s): H.H. is a co-founder and shareholder of OmicScouts GmbH, a proteomics and chemical company.

## ■ ACKNOWLEDGMENTS

The Table of Contents figure and Figure 1, were created with BioRender.

## ■ ABBREVIATIONS

MoA, mechanism of action
iSPP, integral solvent-induced protein precipitation
SPP, solvent-induced protein precipitation
LC-MS/MS, liquid chromatography−mass spectrometry/mass spectrometry
ACTs, artemisinin-based combination therapies
IVIEWGA, in vitro resistance evolution and whole-genome sequencing
pfmdr1, *plasmodium falciparum* multidrug resistance 1
pfcarl, *plasmodium falciparum* cyclic amine resistance locus
PI4k, phosphatidylinositol 4-kinase
DARTS, drug affinity responsive target stability
TPP, thermal proteome profiling
CETSA, cellular thermal shift assay
A.E.A., acetone/ethanol/acetic acid
LFQ-DIA, label-free quantification in data-independent acquisition
SDS-PAGE, sodium dodecyl sulfate−polyacrylamide gel electrophoresis
Pf, *plasmodium falciparum*
$C_M$, melting concentration
$T_M$, melting temperature
$R^2$, coefficient of determination
*E. coli*, *escherichia coli*
DAVID, the database for annotation, visualization and integrated discovery
GO, gene ontology
Hsp, heat shock protein
RESA, ring-infected surface antigen
MSP, merozoite surface protein
GTP, guanosine triphosphate
RNA, ribonucleic acid
ATP, adenosine triphosphate
PfDHFR, bifunctional dihydrofolate reductase-thymidylate synthase
PfDHODH, dihydroorotate dehydrogenase
PfDXR, 1-deoxy-D-xylulose 5-phosphate reductoisomerase
PfAspRS, Aspartate tRNA ligase
CV, coefficient of variation
$log_2FC$, $log_2$ fold change
Kp, *Klebsiella pneumonia*
Pa, *Pseudomonas aeruginosa*
PfPIS, CDP-diacylglycerol--inositol 3-phosphatidyltransferase
Pf60RPL18a, 60S ribosomal protein L18a
PfRPL28, ribosomal protein L28
(ITDR)-CETSA, (isothermal dose response)- cellular thermal shift assay
AaRS, amino-acyl-tRNA synthetases
tRNA, transfer ribonucleic acid

## ■ REFERENCES

(1) World Health Organization. *World Malaria Report*; World Health Organization, 2023.
(2) Cowman, A. F.; Healer, J.; Marapana, D.; Marsh, K. Malaria: Biology and Disease. *Cell* **2016**, *167* (3), 610−624.
(3) Burrows, J. N.; Duparc, S.; Gutteridge, W. E.; Hooft van Huijsduijnen, R.; Kaszubska, W.; Macintyre, F.; Mazzuri, S.; Möhrle, J. J.; Wells, T. N. C. New Developments in Anti-Malarial Target Candidate and Product Profiles. *Malar. J.* **2017**, *16* (1), 26.
(4) Kamala, T.; Van, H. N.; Anna, R.-U.; Quang, P. B.; Do Manh, H.; Evi, P.; Pieter, G.; Van, V. N.; Thanh, D. T.; Alfred, A.-N.; Umberto, D.; Annette, E. Delayed Parasite Clearance after Treatment with Dihydroartemisinin-Piperaquine in Plasmodium Falciparum Malaria Patients in Central Vietnam. Antimicrob. *Agents Chemother.* **2014**, *58* (12), 7049−7055.
(5) Van der Pluijm, R. W.; Tripura, R.; Hoglund, R. M.; Pyae Phyo, A.; Lek, D.; ul Islam, A.; Anvikar, A. R.; Satpathi, P.; Satpathi, S.; Behera, P. K.; Tripura, A.; Baidya, S.; Onyamboko, M.; Chau, N. H.; Sovann, Y.; Suon, S.; Sreng, S.; Mao, S.; Oun, S.; Yen, S.; Amaratunga, C.; Chutasmit, K.; Saelow, C.; Runcharern, R.; Kaewmok, W.; Hoa, N. T.; Thanh, N. V.; Hanboonkunupakarn, B.; Callery, J. J.; Mohanty, A. K.; Heaton, J.; Thant, M.; Gantait, K.; Ghosh, T.; Amato, R.; Pearson, R. D.; Jacob, C. G.; Gonçalves, S.; Mukaka, M.; Waithira, N.; Woodrow, C. J.; Grobusch, M. P.; van Vugt, M.; Fairhurst, R. M.; Cheah, P. Y.; Peto, T. J.; von Seidlein, L.; Dhorda, M.; Maude, R. J.; Winterberg, M.; Thuy-Nhien, N. T.; Kwiatkowski, D. P.; Imwong, M.; Jittamala, P.; Lin, K.; Hlaing, T. M.; Chotivanich, K.; Huy, R.; Fanello, C.; Ashley, E.; Mayxay, M.; Newton, P. N.; Hien, T. T.; Valecha, N.; Smithuis, F.; Pukrittayakamee, S.; Faiz, A.; Miotto, O.; Tarning, J.; Day, N. P. J.; White, N. J.; Dondorp, A. M.; van der Pluijm, R. W.; Tripura, R.; Hoglund, R. M.; Phyo, A. P.; Lek, D.; ul Islam, A.; Anvikar, A. R.; Satpathi, P.; Satpathi, S.; Behera, P. K.; Tripura, A.; Baidya, S.; Onyamboko, M.; Chau, N. H.; Sovann, Y.; Suon, S.; Sreng, S.; Mao, S.; Oun, S.; Yen, S.; Amaratunga, C.; Chutasmit, K.; Saelow, C.; Runcharern, R.; Kaewmok, W.; Hoa, N. T.; Thanh, N. V.; Hanboonkunupakarn, B.; Callery, J. J.; Mohanty, A. K.; Heaton, J.; Thant, M.; Gantait, K.; Ghosh, T.; Amato, R.; Pearson, R. D.; Jacob, C. G.; Gonçalves, S.; Mukaka, M.; Waithira, N.; Woodrow, C. J.; Grobusch, M. P.; van Vugt, M.; Fairhurst, R. M.; Cheah, P. Y.; Peto, T. J.; von Seidlein, L.; Dhorda, M.; Maude, R. J.; Winterberg, M.; Thuy-Nhien, N. T.; Kwiatkowski, D. P.; Imwong, M.; Jittamala, P.; Lin, K.; Hlaing, T. M.; Chotivanich, K.; Huy, R.; Fanello, C.; Ashley, E.; Mayxay, M.; Newton, P. N.; Hien, T. T.; Valeche, N.; Smithuis, F.; Pukrittayakamee, S.; Faiz, A.; Miotto, O.; Tarning, J.; Day, N. P. J.; White, N. J.; Dondorp, A. M. Triple Artemisinin-Based Combination Therapies versus Artemisinin-Based Combination Therapies for Uncomplicated Plasmodium Falciparum Malaria: A Multicentre, Open-Label, Randomised Clinical Trial. *Lancet* **2020**, *395* (10233), 1345−1360.
(6) Dondorp, A. M.; Yeung, S.; White, L.; Nguon, C.; Day, N. P. J.; Socheat, D.; von Seidlein, L. Artemisinin Resistance: Current Status and Scenarios for Containment. *Nat. Rev. Microbiol.* **2010**, *8* (4), 272−280.

(7) Flannery, E. L.; Fidock, D. A.; Winzeler, E. A. Using Genetic Methods To Define the Targets of Compounds with Antimalarial Activity. *J. Med. Chem.* **2013**, *56* (20), 7761−7771.
(8) Allman, E. L.; Painter, H. J.; Samra, J.; Carrasquilla, M.; Llinás, M. Metabolomic Profiling of the Malaria Box Reveals Antimalarial Target Pathways. *Antimicrob. Agents Chemother.* **2016**, *60* (11), 6635−6649.
(9) Creek, D. J.; Chua, H. H.; Cobbold, S. A.; Nijagal, B.; MacRae, J. I.; Dickerman, B. K.; Gilson, P. R.; Ralph, S. A.; McConville, M. J. Metabolomics-Based Screening of the Malaria Box Reveals Both Novel and Established Mechanisms of Action. *Antimicrob. Agents Chemother.* **2016**, *60* (11), 6650−6663.
(10) Pradhan, A.; Siwo, G. H.; Singh, N.; Martens, B.; Balu, B.; Button-Simons, K. A.; Tan, A.; Zhang, M.; Udenze, K. O.; Jiang, R. H. Y.; Ferdig, M. T.; Adams, J. H.; Kyle, D. E. Chemogenomic Profiling of Plasmodium Falciparum as a Tool to Aid Antimalarial Drug Discovery. *Sci. Rep.* **2015**, *5* (1), 15930.
(11) Bowman, J. D.; Merino, E. F.; Brooks, C. F.; Striepen, B.; Carlier, P. R.; Cassera, M. B. Antiapicoplast and Gametocytocidal Screening To Identify the Mechanisms of Action of Compounds within the Malaria Box. *Antimicrob. Agents Chemother.* **2014**, *58* (2), 811−819.
(12) Hu, G.; Cabrera, A.; Kono, M.; Mok, S.; Chaal, B. K.; Haase, S.; Engelberg, K.; Cheemadan, S.; Spielmann, T.; Preiser, P. R.; Gilberger, T.-W.; Bozdech, Z. Transcriptional Profiling of Growth Perturbations of the Human Malaria Parasite Plasmodium Falciparum. *Nat. Biotechnol.* **2010**, *28* (1), 91−98.
(13) Luth, M. R.; Gupta, P.; Ottilie, S.; Winzeler, E. A. Using in Vitro Evolution and Whole Genome Analysis To Discover Next Generation Targets for Antimalarial Drug Discovery. *ACS Infect. Dis.* **2018**, *4* (3), 301−314.
(14) Cowell, A. N.; Istvan, E. S.; Lukens, A. K.; Gomez-Lorenzo, M. G.; Vanaerschot, M.; Sakata-Kato, T.; Flannery, E. L.; Magistrado, P.; Owen, E.; Abraham, M.; LaMonte, G.; Painter, H. J.; Williams, R. M.; Franco, V.; Linares, M.; Arriaga, I.; Bopp, S.; Corey, V. C.; Gnädig, N. F.; Coburn-Flynn, O.; Reimer, C.; Gupta, P.; Murithi, J. M.; Moura, P. A.; Fuchs, O.; Sasaki, E.; Kim, S. W.; Teng, C. H.; Wang, L. T.; Akidil, A.; Adjalley, S.; Willis, P. A.; Siegel, D.; Tanaseichuk, O.; Zhong, Y.; Zhou, Y.; Llinás, M.; Ottilie, S.; Gamo, F.-J.; Lee, M. C. S.; Goldberg, D. E.; Fidock, D. A.; Wirth, D. F.; Winzeler, E. A. Mapping the Malaria Parasite Druggable Genome by Using in Vitro Evolution and Chemogenomics. *Science (1979)* **2018**, *359* (6372), 191−199.
(15) Dharia, N. V.; Sidhu, A. B. S.; Cassera, M. B.; Westenberger, S. J.; Bopp, S. E. R.; Eastman, R. T.; Plouffe, D.; Batalov, S.; Park, D. J.; Volkman, S. K.; Wirth, D. F.; Zhou, Y.; Fidock, D. A.; Winzeler, E. A. Use of High-Density Tiling Microarrays to Identify Mutations Globally and Elucidate Mechanisms of Drug Resistance in Plasmodium Falciparum. *Genome Biol.* **2009**, *10* (2), R21.
(16) White, J.; Dhingra, S. K.; Deng, X.; El Mazouni, F.; Lee, M. C. S.; Afanador, G. A.; Lawong, A.; Tomchick, D. R.; Ng, C. L.; Bath, J.; Rathod, P. K.; Fidock, D. A.; Phillips, M. A. Identification and Mechanistic Understanding of Dihydroorotate Dehydrogenase Point Mutations in Plasmodium Falciparum That Confer in Vitro Resistance to the Clinical Candidate DSM265. *ACS Infect. Dis.* **2019**, *5* (1), 90−101.
(17) Paquet, T.; Le Manach, C.; Cabrera, D. G.; Younis, Y.; Henrich, P. P.; Abraham, T. S.; Lee, M. C. S.; Basak, R.; Ghidelli-Disse, S.; Lafuente-Monasterio, M. J.; Bantscheff, M.; Ruecker, A.; Blagborough, A. M.; Zakutansky, S. E.; Zeeman, A.-M.; White, K. L.; Shackleford, D. M.; Mannila, J.; Morizzi, J.; Scheurer, C.; Angulo-Barturen, I.; Martínez, M. S.; Ferrer, S.; Sanz, L. M.; Gamo, F. J.; Reader, J.; Botha, M.; Dechering, K. J.; Sauerwein, R. W.; Tungtaeng, A.; Vanachayangkul, P.; Lim, C. S.; Burrows, J.; Witty, M. J.; Marsh, K. C.; Bodenreider, C.; Rochford, R.; Solapure, S. M.; Jiménez-Díaz, M. B.; Wittlin, S.; Charman, S. A.; Donini, C.; Campo, B.; Birkholtz, L.-M.; Hanson, K. K.; Drewes, G.; Kocken, C. H. M.; Delves, M. J.; Leroy, D.; Fidock, D. A.; Waterson, D.; Street, L. J.; Chibale, K. Antimalarial Efficacy of MMV390048, an Inhibitor of Plasmodium Phosphatidylinositol 4-Kinase. *Sci. Transl. Med.* **2017**, *9* (387), No. eaad9735.
(18) Rottmann, M.; McNamara, C.; Yeung, B. K. S.; Lee, M. C. S.; Zou, B.; Russell, B.; Seitz, P.; Plouffe, D. M.; Dharia, N. V.; Tan, J.; Cohen, S. B.; Spencer, K. R.; González-Páez, G. E.; Lakshminarayana, S. B.; Goh, A.; Suwanarusk, R.; Jegla, T.; Schmitt, E. K.; Beck, H. P.; Brun, R.; Nosten, F.; Renia, L.; Dartois, V.; Keller, T. H.; Fidock, D. A.; Winzeler, E. A.; Diagana, T. T. Spiroindolones, a Potent Compound Class for the Treatment of Malaria. *Science (1979)* **2010**, *329* (5996), 1175−1180.
(19) Magistrado, P. A.; Corey, V. C.; Lukens, A. K.; LaMonte, G.; Sasaki, E.; Meister, S.; Wree, M.; Winzeler, E.; Wirth, D. F. Plasmodium Falciparum Cyclic Amine Resistance Locus (PfCARL), a Resistance Mechanism for Two Distinct Compound Classes. *ACS Infect. Dis.* **2016**, *2* (11), 816−826.
(20) Fidock, D. A.; Nomura, T.; Talley, A. K.; Cooper, R. A.; Dzekunov, S. M.; Ferdig, M. T.; Ursos, L. M. B.; bir Singh Sidhu, A.; Naudé, B.; Deitsch, K. W.; et al. Mutations in the P. Falciparum Digestive Vacuole Transmembrane Protein PfCRT and Evidence for Their Role in Chloroquine Resistance. *Mol. Cell* **2000**, *6* (4), 861−871.
(21) Cowell, A. N.; Winzeler, E. A. Advances in Omics-Based Methods to Identify Novel Targets for Malaria and Other Parasitic Protozoan Infections. *Genome Med.* **2019**, *11* (1), 63.
(22) Wright, M. H.; Sieber, S. A. Chemical Proteomics Approaches for Identifying the Cellular Targets of Natural Products. *Nat. Prod. Rep.* **2016**, *33* (5), 681−708.
(23) Kolb, H. C.; Finn, M. G.; Sharpless, K. B. Click Chemistry: Diverse Chemical Function from a Few Good Reactions. *Angew. Chem. Int. Ed.* **2001**, *40* (11), 2004−2021.
(24) Dziekan, J. M.; Wirjanata, G.; Dai, L.; Go, K. D.; Yu, H.; Lim, Y. T.; Chen, L.; Wang, L. C.; Puspita, B.; Prabhu, N.; Sobota, R. M.; Nordlund, P.; Bozdech, Z. Cellular Thermal Shift Assay for the Identification of Drug−Target Interactions in the Plasmodium Falciparum Proteome. *Nat. Protoc.* **2020**, *15* (6), 1881−1921.
(25) Dziekan, J. M.; Yu, H.; Chen, D.; Dai, L.; Wirjanata, G.; Larsson, A.; Prabhu, N.; Sobota, R. M.; Bozdech, Z.; Nordlund, P. Identifying Purine Nucleoside Phosphorylase as the Target of Quinine Using Cellular Thermal Shift Assay. *Sci. Transl. Med.* **2019**, *11* (473), No. eaau3174.
(26) Yu, C.; Chen, X.; Xu, W.; Li, S.; Chai, Q.; Zhang, Y. Solvent-Induced Proteome Profiling for Proteomic Quantitation and Target Discovery of Small Molecular Drugs. *Proteomics* **2023**, *23*, 1−10.
(27) Zhang, X.; Wang, Q.; Li, Y.; Ruan, C.; Wang, S.; Hu, L.; Ye, M. Solvent-Induced Protein Precipitation for Drug Target Discovery on the Proteomic Scale. *Anal. Chem.* **2020**, *92* (1), 1363−1371.
(28) Molina, D. M.; Jafari, R.; Ignatushchenko, M.; Seki, T.; Larsson, E. A.; Dan, C.; Sreekumar, L.; Cao, Y.; Nordlund, P. Monitoring Drug Target Engagement in Cells and Tissues Using the Cellular Thermal Shift Assay. *Science (1979)* **2013**, *341* (6141), 84−87.
(29) Jafari, R.; Almqvist, H.; Axelsson, H.; Ignatushchenko, M.; Lundbäck, T.; Nordlund, P.; Molina, D. M. The Cellular Thermal Shift Assay for Evaluating Drug Target Interactions in Cells. *Nat. Protoc.* **2014**, *9* (9), 2100−2122.
(30) Pai, M. Y.; Lomenick, B.; Hwang, H.; Schiestl, R.; McBride, W.; Loo, J. A.; Huang, J. Drug Affinity Responsive Target Stability (DARTS) for Small-Molecule Target Identification. In *Chemical Biology. Methods in Molecular Biology*; Hempel, J., Williams, C., Hong, C., Eds.; Humana Press: New York, 2015; Vol. *1263*; pp 287−298..
(31) Sun, W.; Tanaka, T. Q.; Magle, C. T.; Huang, W.; Southall, N.; Huang, R.; Dehdashti, S. J.; McKew, J. C.; Williamson, K. C.; Zheng, W. Chemical signatures and new drug targets for gametocytocidal drug development. *Sci. Rep.* **2014**, *4* (1), 3743.
(32) Reinhard, F. B. M.; Eberhard, D.; Werner, T.; Franken, H.; Childs, D.; Doce, C.; Savitski, M. F.; Huber, W.; Bantscheff, M.; Savitski, M. M.; Drewes, G. Thermal Proteome Profiling Monitors Ligand Interactions with Cellular Membrane Proteins. *Nat. Methods* **2015**, *12* (12), 1129−1131.


https://doi.org/10.1021/acsinfecdis.4c00418
ACS Infect. Dis. XXXX, XXX, XXX−XXX

(33) Thommen, B. T.; Dziekan, J. M.; Achcar, F.; Tjia, S.; Passecker, A.; Buczak, K.; Gumpp, C.; Schmidt, A.; Rottmann, M.; Grüring, C.; Marti, M.; Bozdech, Z.; Brancucci, N. M. B. Genetic Validation of PfFKBP35 as an Antimalarial Drug Target. *eLife* **2023**, *12*, RP86975.
(34) Van Vranken, J. G.; Li, J.; Mitchell, D. C.; Navarrete-Perea, J.; Gygi, S. P. Assessing Target Engagement Using Proteome-Wide Solvent Shift Assays. *eLife* **2021**, *10*, 1−21.
(35) Gaetani, M.; Sabatier, P.; Saei, A. A.; Beusch, C. M.; Yang, Z.; Lundström, S. L.; Zubarev, R. A. Proteome Integral Solubility Alteration: A High-Throughput Proteomics Assay for Target Deconvolution. *J. Proteome Res.* **2019**, *18* (11), 4027−4037.
(36) Bizzarri, L.; Steinbrunn, D.; Quennesson, T.; Lacour, A.; Bianchino, G. I.; Bravo, P.; Chaignon, P.; Lohse, J.; Mäser, P.; Seemann, M.; Van Calenbergh, S.; Hirsch; Hahne, H. Studying Target−Engagement of Anti-infectives by Solvent-Induced Protein Precipitation and Quantitative Mass Spectrometry. *ACS Infect. Dis.* **2024**, DOI: 10.1021/acsinfecdis.4c00417.
(37) Florens, L.; Washburn, M. P.; Raine, J. D.; Anthony, R. M.; Grainger, M.; Haynes, J. D.; Moch, J. K.; Muster, N.; Sacci, J. B.; Tabb, D. L.; Witney, A. A.; Wolters, D.; Wu, Y.; Gardner, M. J.; Holder, A. A.; Sinden, R. E.; Yates, J. R.; Carucci, D. J. A Proteomic View of the Plasmodium Falciparum Life Cycle. *Nature* **2002**, *419* (6906), 520−526.
(38) Milne, R.; Wiedemar, N.; Corpas-Lopez, V.; Moynihan, E.; Wall, R. J.; Dawson, A.; Robinson, D. A.; Shepherd, S. M.; Smith, R. J.; Hallyburton, I.; Post, J. M.; Dowers, K.; Torrie, L. S.; Gilbert, I. H.; Baragaña, B.; Patterson, S.; Wyllie, S. Toolkit of Approaches To Support Target-Focused Drug Discovery for Plasmodium Falciparum Lysyl TRNA Synthetase. *ACS Infect. Dis.* **2022**, *8* (9), 1962−1974.
(39) Savitski, M. M.; Reinhard, F. B. M.; Franken, H.; Werner, T.; Savitski, M. F.; Eberhard, D.; Molina, D. M.; Jafari, R.; Dovega, R. B.; Klaeger, S.; Kuster, B.; Nordlund, P.; Bantscheff, M.; Drewes, G. Tracking Cancer Drugs in Living Cells by Thermal Profiling of the Proteome. *Science (1979)* **2014**, *346* (6205), 1255784.
(40) Jarzab, A.; Kurzawa, N.; Hopf, T.; Moerch, M.; Zecha, J.; Leijten, N.; Bian, Y.; Musiol, E.; Maschberger, M.; Stoehr, G.; Becher, I.; Daly, C.; Samaras, P.; Mergner, J.; Spanier, B.; Angelov, A.; Werner, T.; Bantscheff, M.; Wilhelm, M.; Klingenspor, M.; Lemeer, S.; Liebl, W.; Hahne, H.; Savitski, M. M.; Kuster, B. Meltome Atlas-Thermal Proteome Stability across the Tree of Life. *Nat. Methods* **2020**, *17* (5), 495−503.
(41) Huang, D. W.; Sherman, B. T.; Lempicki, R. A. Systematic and Integrative Analysis of Large Gene Lists Using DAVID Bioinformatics Resources. *Nat. Protoc.* **2009**, *4* (1), 44−57.
(42) Sherman, B. T.; Hao, M.; Qiu, J.; Jiao, X.; Baseler, M. W.; Lane, H. C.; Imamichi, T.; Chang, W. DAVID: A Web Server for Functional Enrichment Analysis and Functional Annotation of Gene Lists (2021 Update). *Nucleic Acids Res.* **2022**, *50* (W1), W216−W221.
(43) Lyons, F. M. T.; Gabriela, M.; Tham, W.-H.; Dietrich, M. H. Plasmodium 6-Cysteine Proteins: Functional Diversity, Transmission-Blocking Antibodies and Structural Scaffolds. *Front. Cell. Infect. Microbiol.* **2022**, *12*, 945924.
(44) Pei, X.; Guo, X.; Coppel, R.; Bhattacharjee, S.; Haldar, K.; Gratzer, W.; Mohandas, N.; An, X. The Ring-Infected Erythrocyte Surface Antigen (RESA) of Plasmodium Falciparum Stabilizes Spectrin Tetramers and Suppresses Further Invasion. *Blood* **2007**, *110* (3), 1036−1042.
(45) Singh, S.; Soe, S.; Mejia, J.-P.; Roussilhon, C.; Theisen, M.; Corradin, G.; Druilhe, P. Identification of a Conserved Region of Plasmodium Falciparum MSP3 Targeted by Biologically Active Antibodies to Improve Vaccine Design. *J. Infect. Dis.* **2004**, *190* (5), 1010−1018.
(46) Li, J.; Van Vranken, J. G.; Paulo, J. A.; Huttlin, E. L.; Gygi, S. P. Selection of Heating Temperatures Improves the Sensitivity of the Proteome Integral Solubility Alteration Assay. *J. Proteome Res.* **2020**, *19* (5), 2159−2166.
(47) Peterson, D. S.; Walliker, D.; Wellems, T. E. Evidence That a Point Mutation in Dihydrofolate Reductase-Thymidylate Synthase Confers Resistance to Pyrimethamine in Falciparum Malaria. *Proc. Natl. Acad. Sci. U.S.A.* **1988**, *85* (23), 9114−9118.
(48) Cowman, A. F.; Morry, M. J.; Biggs, B. A.; Cross, G. A.; Foote, S. J. Amino Acid Changes Linked to Pyrimethamine Resistance in the Dihydrofolate Reductase-Thymidylate Synthase Gene of Plasmodium Falciparum. *Proc. Natl. Acad. Sci. U.S.A.* **1988**, *85* (23), 9109−9113.
(49) Baldwin, J.; Michnoff, C. H.; Malmquist, N. A.; White, J.; Roth, M. G.; Rathod, P. K.; Phillips, M. A. High-Throughput Screening for Potent and Selective Inhibitors of Plasmodium Falciparum Dihydroorotate Dehydrogenase. *J. Biol. Chem.* **2005**, *280* (23), 21847−21853.
(50) Gujjar, R.; Marwaha, A.; El Mazouni, F.; White, J.; White, K. L.; Creason, S.; Shackleford, D. M.; Baldwin, J.; Charman, W. N.; Buckner, F. S.; Charman, S.; Rathod, P. K.; Phillips, M. A. Identification of a Metabolically Stable Triazolopyrimidine-Based Dihydroorotate Dehydrogenase Inhibitor with Antimalarial Activity in Mice. *J. Med. Chem.* **2009**, *52* (7), 1864−1872.
(51) Kokkonda, S.; Deng, X.; White, K. L.; Coteron, J. M.; Marco, M.; de las Heras, L.; White, J.; El Mazouni, F.; Tomchick, D. R.; Manjalanagara, K.; Rudra, K. R.; Chen, G.; Morizzi, J.; Ryan, E.; Kaminsky, W.; Leroy, D.; Martínez-Martínez, M. S.; Jimenez-Diaz, M. B.; Bazaga, S. F.; Angulo-Barturen, I.; Waterson, D.; Burrows, J. N.; Matthews, D.; Charman, S. A.; Phillips, M. A.; Rathod, P. K. Tetrahydro-2-Naphthyl and 2-Indanyl Triazolopyrimidines Targeting Plasmodium Falciparum Dihydroorotate Dehydrogenase Display Potent and Selective Antimalarial Activity. *J. Med. Chem.* **2016**, *59* (11), 5416−5431.
(52) Jomaa, H.; Wiesner, J.; Sanderbrand, S.; Altincicek, B.; Weidemeyer, C.; Hintz, M.; Türbachova, I.; Eberl, M.; Zeidler, J.; Lichtenthaler, H. K.; Soldati, D.; Beck, E. Inhibitors of the Nonmevalonate Pathway of Isoprenoid Biosynthesis as Antimalarial Drugs. *Science (1979)* **1999**, *285* (5433), 1573−1576.
(53) Zhang, B.; Watts, K. M.; Hodge, D.; Kemp, L. M.; Hunstad, D. A.; Hicks, L. M.; Odom, A. R. A Second Target of the Antimalarial and Antibacterial Agent Fosmidomycin Revealed by Cellular Metabolic Profiling. *Biochemistry* **2011**, *50* (17), 3570−3577.
(54) Sibley, C. H.; Hyde, J. E.; Sims, P. F. G.; Plowe, C. V.; Kublin, J. G.; Mberu, E. K.; Cowman, A. F.; Winstanley, P. A.; Watkins, W. M.; Nzila, A. M. Pyrimethamine−Sulfadoxine Resistance in Plasmodium Falciparum: What Next? *Trends Parasitol.* **2001**, *17* (12), 582−588.
(55) Wong, W.; Bai, X.-C.; Sleebs, B. E.; Triglia, T.; Brown, A.; Thompson, J. K.; Jackson, K. E.; Hanssen, E.; Marapana, D. S.; Fernandez, I. S.; et al. Mefloquine Targets the Plasmodium Falciparum 80S Ribosome to Inhibit Protein Synthesis. *Nat. Microbiol.* **2017**, *2* (6), 17031−17039.
(56) Calic, P. P. S.; Mansouri, M.; Scammells, P. J.; McGowan, S. Driving Antimalarial Design through Understanding of Target Mechanism. *Biochem. Soc. Trans.* **2020**, *48*, 2067−2078.
(57) Pham, J. S.; Dawson, K. L.; Jackson, K. E.; Lim, E. E.; Pasaje, C. F. A.; Turner, K. E. C.; Ralph, S. A. Aminoacyl-TRNA Synthetases as Drug Targets in Eukaryotic Parasites. *Int. J. Parasitol. Drugs Drug Resist.* **2014**, *4* (1), 1−13.
(58) Baragaña, B.; Forte, B.; Choi, R.; Nakazawa Hewitt, S.; Bueren-Calabuig, J. A.; Pisco, J. P.; Peet, C.; Dranow, D. M.; Robinson, D. A.; Jansen, C.; Norcross, N. R.; Vinayak, S.; Anderson, M.; Brooks, C. F.; Cooper, C. A.; Damerow, S.; Delves, M.; Dowers, K.; Duffy, J.; Edwards, T. E.; Hallyburton, I.; Horst, B. G.; Hulverson, M. A.; Ferguson, L.; Jiménez-Díaz, M. B.; Jumani, R. S.; Lorimer, D. D.; Love, M. S.; Maher, S.; Matthews, H.; McNamara, C. W.; Miller, P.; O'Neill, S.; Ojo, K. K.; Osuna-Cabello, M.; Pinto, E.; Post, J.; Riley, J.; Rottmann, M.; Sanz, L. M.; Scullion, P.; Sharma, A.; Shepherd, S. M.; Shishikura, Y.; Simeons, F. R. C.; Stebbins, E. E.; Stojanovski, L.; Straschil, U.; Tamaki, F. K.; Tamjar, J.; Torrie, L. S.; Vantaux, A.; Witkowski, B.; Wittlin, S.; Yogavel, M.; Zuccotto, F.; Angulo-Barturen, I.; Sinden, R.; Baum, J.; Gamo, F.-J.; Mäser, P.; Kyle, D. E.; Winzeler, E. A.; Myler, P. J.; Wyatt, P. G.; Floyd, D.; Matthews, D.; Sharma, A.; Striepen, B.; Huston, C. D.; Gray, D. W.; Fairlamb, A. H.; Pisliakov, A. V.; Walpole, C.; Read, K. D.; Van Voorhis, W. C.; Gilbert, I. H. Lysyl-TRNA Synthetase as a Drug Target in Malaria and

Cryptosporidiosis. *Proc. Natl. Acad. Sci. U.S.A.* **2019**, *116* (14), 7015−7020.
(59) Yadavalli, S. S.; Ibba, M. Chapter 1 - Quality Control in Aminoacyl-TRNA Synthesis: Its Role in Translational Fidelity. *Adv. Protein Chem. Struct. Biol.* **2012**, *86*, 1−43.
(60) Boura, E.; Nencka, R. Phosphatidylinositol 4-Kinases: Function, Structure, and Inhibition. *Exp. Cell Res.* **2015**, *337* (2), 136−145.
(61) Wengelnik, K.; Vial, H. J. Characterisation of the Phosphatidylinositol Synthase Gene of Plasmodium Species. *Res. Microbiol.* **2007**, *158* (1), 51−59.
(62) Bibo-Verdugo, B.; Jiang, Z.; Caffrey, C. R.; O'Donoghue, A. J. Targeting Proteasomes in Infectious Organisms to Combat Disease. *FEBS J.* **2017**, *284* (10), 1503−1517.
(63) Khare, S.; Nagle, A. S.; Biggart, A.; Lai, Y. H.; Liang, F.; Davis, L. C.; Barnes, S. W.; Mathison, C. J. N.; Myburgh, E.; Gao, M.-Y.; Gillespie, J. R.; Liu, X.; Tan, J. L.; Stinson, M.; Rivera, I. C.; Ballard, J.; Yeh, V.; Groessl, T.; Federe, G.; Koh, H. X. Y.; Venable, J. D.; Bursulaya, B.; Shapiro, M.; Mishra, P. K.; Spraggon, G.; Brock, A.; Mottram, J. C.; Buckner, F. S.; Rao, S. P. S.; Wen, B. G.; Walker, J. R.; Tuntland, T.; Molteni, V.; Glynne, R. J.; Supek, F. Proteasome Inhibition for Treatment of Leishmaniasis, Chagas Disease and Sleeping Sickness. *Nature* **2016**, *537* (7619), 229−233.
(64) Gandolfi, S.; Laubach, J. P.; Hideshima, T.; Chauhan, D.; Anderson, K. C.; Richardson, P. G. The Proteasome and Proteasome Inhibitors in Multiple Myeloma. *Cancer Metastasis Rev.* **2017**, *36* (4), 561−584.
(65) Le Manach, C.; Scheurer, C.; Sax, S.; Schleiferböck, S.; Cabrera, D. G.; Younis, Y.; Paquet, T.; Street, L.; Smith, P.; Ding, X. C.; Waterson, D.; Witty, M. J.; Leroy, D.; Chibale, K.; Wittlin, S. Fast in Vitro Methods to Determine the Speed of Action and the Stage-Specificity of Anti-Malarials in Plasmodium Falciparum. *Malar. J.* **2013**, *12*, 424.
(66) Dieckmann, A.; Jung, A. Stage-Specific Sensitivity of Plasmodium Falciparum to Antifolates. *Z. Parasitenkd.* **1986**, *72* (5), 591−594.
(67) Wilson, D. W.; Langer, C.; Goodman, C. D.; McFadden, G. I.; Beeson, J. G. Defining the Timing of Action of Antimalarial Drugs against Plasmodium Falciparum. *Antimicrob. Agents Chemother.* **2013**, *57* (3), 1455−1467.
(68) Duffy, S.; Loganathan, S.; Holleran, J. P.; Avery, V. M. Large-Scale Production of Plasmodium Falciparum Gametocytes for Malaria Drug Discovery. *Nat. Protoc.* **2016**, *11* (5), 976−992.
(69) Mikolajczak, S. A.; Vaughan, A. M.; Kangwanrangsan, N.; Roobsoong, W.; Fishbaugher, M.; Yimamnuaychok, N.; Rezakhani, N.; Lakshmanan, V.; Singh, N.; Kaushansky, A.; et al. Plasmodium Vivax Liver Stage Development and Hypnozoite Persistence in Human Liver-Chimeric Mice. *Cell Host Microbe* **2015**, *17* (4), 526−535.
(70) Snyder, C.; Chollet, J.; Santo-Tomas, J.; Scheurer, C.; Wittlin, S. In Vitro and in Vivo Interaction of Synthetic Peroxide RBx11160 (OZ277) with Piperaquine in Plasmodium Models. *Exp. Parasitol.* **2007**, *115* (3), 296−300.
(71) Wickham, H.; François, R.; Henry, L.; Müller, K.; Vaughan, D. dplyr: A Grammar of Data Manipulation. R package version 1.1.4, 2023.
(72) Wickham, H. *ggplot2: Elegant Graphics for Data Analysis*; Springer: Cham, 2016.
(73) Blighe, K.; Rana, S.; Lewis, M. *EnhancedVolcano: Publication-Ready Volcano Plots with Enhanced Colouring and Labeling*. R package, 2021..


https://doi.org/10.1021/acsinfecdis.4c00418
*ACS Infect. Dis.* XXXX, XXX, XXX−XXX

# Integral solvent-induced protein precipitation for target-engagement studies in *Plasmodium falciparum*

Patricia Bravo[1,2], Lorenzo Bizzarri[3,4], Dominik Steinbrunn[3,5], Jonas Lohse[3], Anna K. H. Hirsch,[4,6] Pascal Mäser[1,2], Matthias Rottmann[1,2], Hannes Hahne[3*]

[1] Swiss Tropical and Public Health Institute, Kreuzstrasse 2, 4123 Allschwil, Switzerland
[2] Universität Basel Petersplatz 1, 4003 Basel, Switzerland
[3] OmicScouts GmbH, Lise-Meitner-Straße 30, D-85354 Freising, Germany
[4] Saarland University, Department of Pharmacy, Campus E8.1, D-66123 Saarbrücken, Germany
[5] TUM School of Natural Sciences, Department of Bioscience, Technical University of Munich, Center for Functional Protein Assemblies (CPA), D-85748 Garching bei München, Germany
[6] Helmholtz Institute for Pharmaceutical Research (HIPS), Helmholtz Centre for Infection Research (HZI), Saarland University, Campus E8.1, D-66123 Saarbrücken, Germany

**Correspondence to:* Hannes Hahne (hannes.hahne@omicscouts.com)

**Supporting Information**

Supporting Information – Figure S1

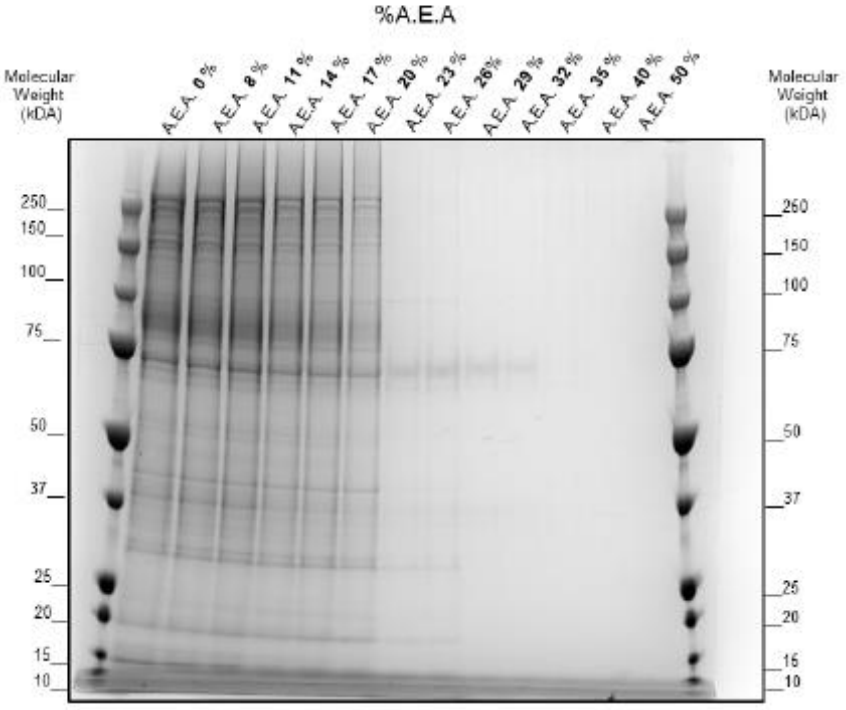


**Figure S1. Solvent proteome profiling of *Plasmodium falciparum* by SDS-PAGE readout.**
*P. falciparum* lysate aliquots were exposed to the A.E.A (v/v) gradient range 0-50%. The soluble fractions were then resolved by SDS-PAGE. The result shows a substantial fraction of proteins precipitating at A.E.A > 20%.

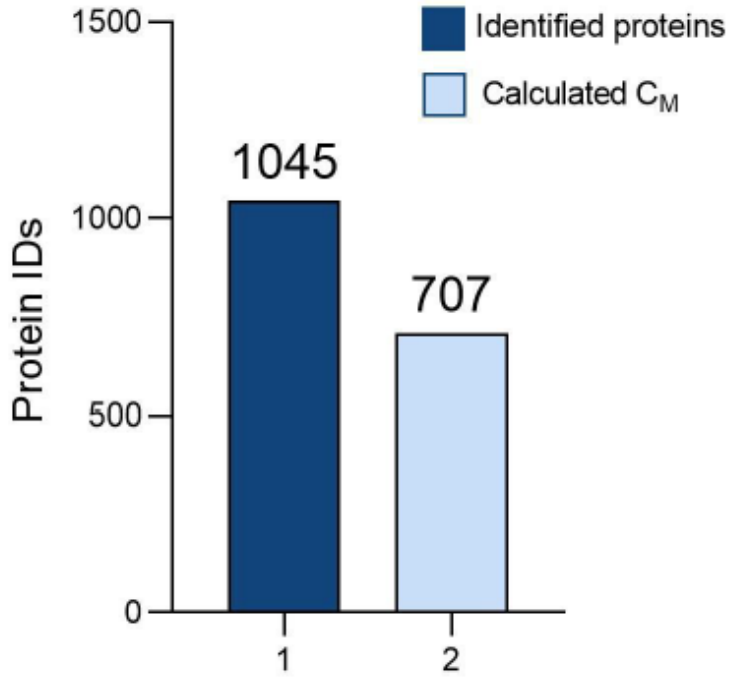


**Figure S2. High confidence $C_M$ values calculated for low abundant proteins**
Comparison between IDs of low-abundant proteins (dark blue) and the corresponding calculated $C_M$ values. High-quality melting curves and $C_M$ values were fitted to 68% of low-abundant proteins. Proteins classified as low-abundance (n=1045 protein IDs) fell in the lowest 30th percentile of all quantified proteins in the experiment, sorted by abundance.

Supporting Information – Figure S3

**A.**

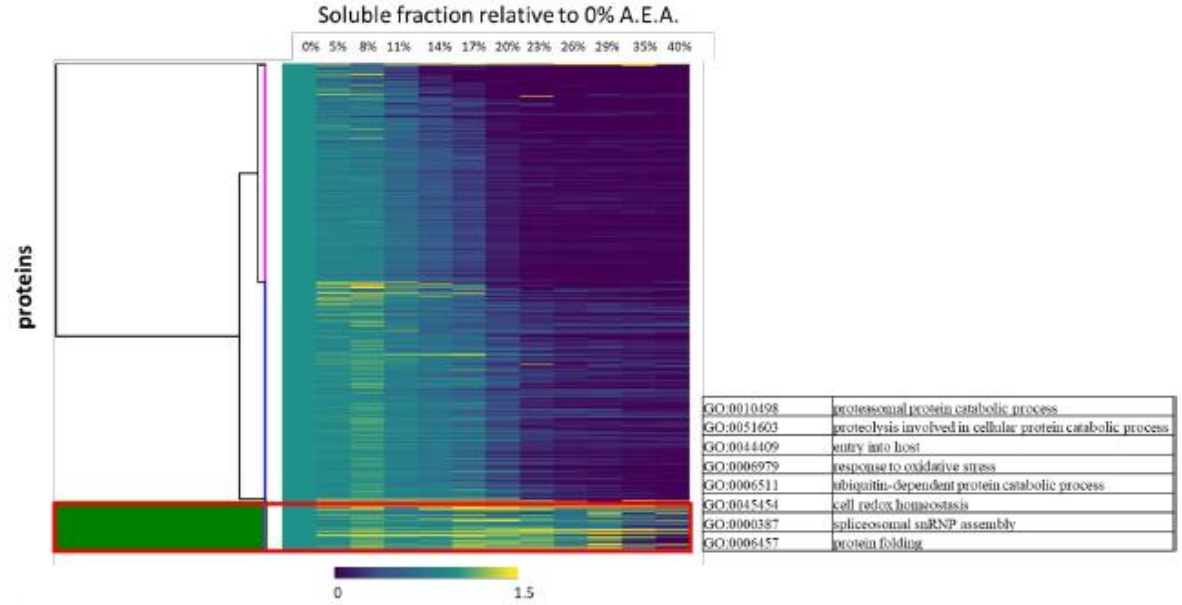


| | |
|---|---|
| GO:0010498 | proteasomal protein catabolic process |
| GO:0051603 | proteolysis involved in cellular protein catabolic process |
| GO:0044409 | entry into host |
| GO:0006979 | response to oxidative stress |
| GO:0006511 | ubiquitin-dependent protein catabolic process |
| GO:0045454 | cell redox homeostasis |
| GO:0000387 | spliceosomal snRNP assembly |
| GO:0006457 | protein folding |

**B.**

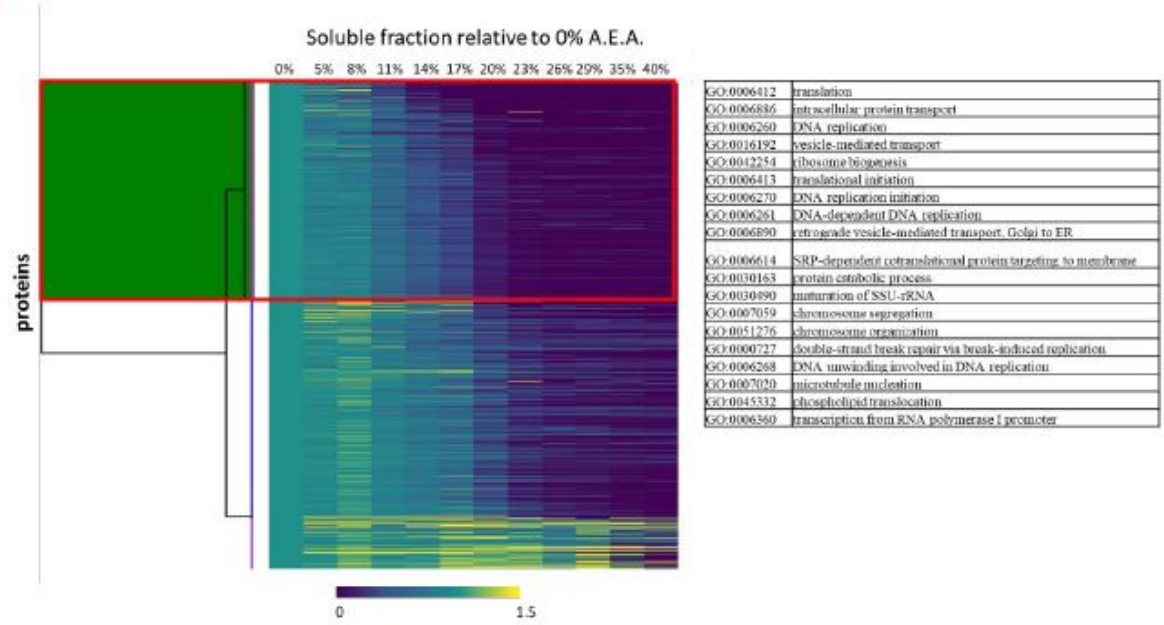


| | |
|---|---|
| GO:0006412 | translation |
| GO:0006886 | intracellular protein transport |
| GO:0006260 | DNA replication |
| GO:0016192 | vesicle-mediated transport |
| GO:0042254 | ribosome biogenesis |
| GO:0006413 | translational initiation |
| GO:0006270 | DNA replication initiation |
| GO:0006261 | DNA-dependent DNA replication |
| GO:0006890 | retrograde vesicle-mediated transport, Golgi to ER |
| GO:0006614 | SRP-dependent cotranslational protein targeting to membrane |
| GO:0030163 | protein catabolic process |
| GO:0030490 | maturation of SSU-rRNA |
| GO:0007059 | chromosome segregation |
| GO:0051276 | chromosome organization |
| GO:0000727 | double-strand break repair via break-induced replication |
| GO:0006268 | DNA unwinding involved in DNA replication |
| GO:0007020 | microtubule nucleation |
| GO:0045332 | phospholipid translocation |
| GO:0006360 | transcription from RNA polymerase I promoter |

**Figure S3 The proteasomal complex and its subunits have a high tolerance towards organic solvents, whereas ribosomal subunits and proteins involved in ribosomal biogenesis precipitate at lower %A.E.A.**

Hierarchical clustering was performed in Perseus (v.2.0.10.0) on the normalized median LFQ-DIA intensities of unique proteins in the eight gradient points of % A.E.A. The intensities were then normalized relative to 0% A.E.A. Proteins from each cluster were then isolated and GO terms analysis was performed with DAVID for each cluster (DAVID Functional Annotation Bioinformatics Microarray Analysis (ncifcrf.gov); A) Protein cluster with high tolerance towards %A.E.A. and B) Low tolerance towards %A.E.A.

Supporting Information – Figure S4

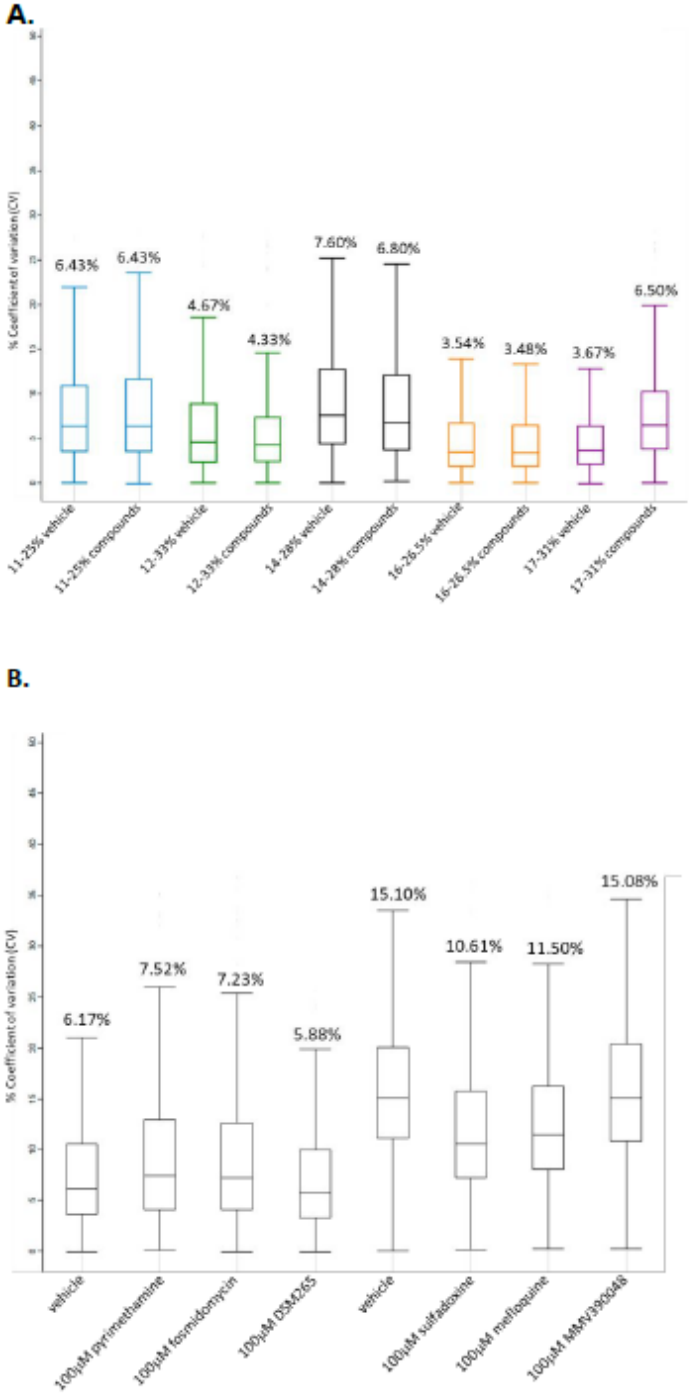


**Figure S4. Coefficient of variations (CV) within replicates of each condition in all iSPP experiments performed in this study.** A) CVs of the initial iSPP profiling experiments for %A.E.A. (v/v) gradients establishment. B) CV of iSPP validation experiments.

Supporting Information – Figure S5

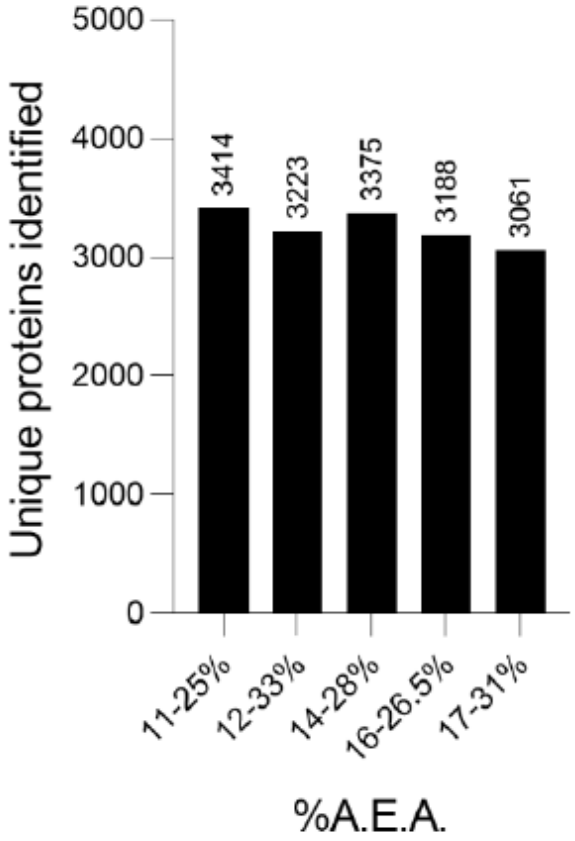


**Figure S5. Identified protein IDs across the %A.E.A. (v/v) solvent gradients tested in the iSPP experiments.**
The comparison revealed a decrease in the number of unique protein IDs identified with increasing concentrations of AEA (v/v). Specifically, higher AEA concentration gradients corresponded to lower numbers of identified proteins.

Supporting Information – Figure S6

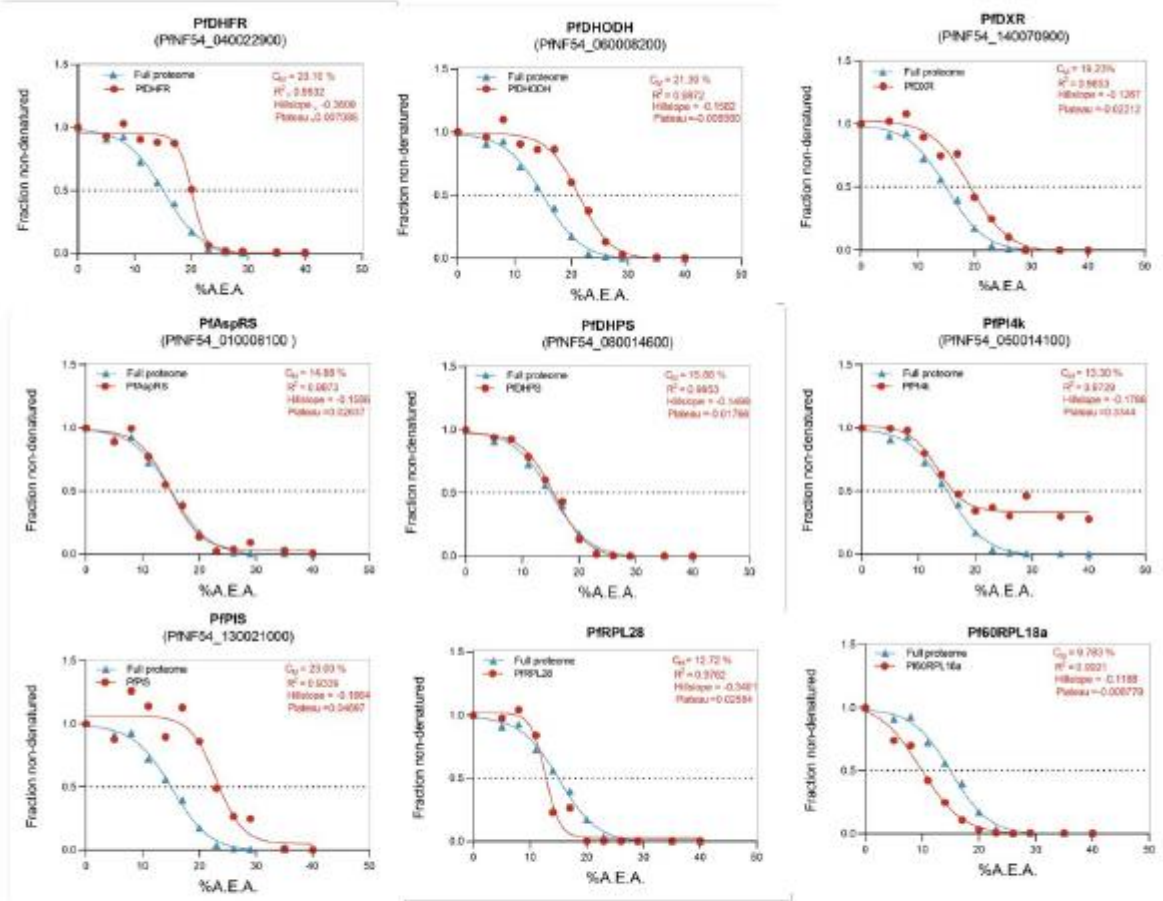


**Figure S6. Denaturation curves and corresponding $C_M$ values for the expected target proteins of the antimalarials employed in the iSPP experiments.**

# 4. FINAL DISCUSSION

The overarching goal of this thesis was to establish a reliable and highly effective quantitative MS-based proteomics method capable of characterizing MEP-pathway inhibitors in critical human pathogens. As described in the introduction, the MEP pathway is the exclusive source of the universal isoprenoid building blocks IDP and DMADP in green algae, pathogenic bacteria, and apicomplexan protozoa, including major human pathogens such as *M. tuberculosis*, *K. pneumoniae*, *P. aeruginosa*, and *P. falciparum*. Given the critical role of the MEP pathway in these organisms and its absence in humans, its enzymes represent prime drug targets for developing new anti-infective therapies. The success of fosmidomycin,[29] a potent DXR inhibitor, in clinical trials as part of antimalarial combination therapies further highlights the pathway's potential as a target for novel therapeutic interventions against infectious diseases.

Target identification and validation are crucial steps in drug discovery, as they are critical for understanding and confirming a drug's MoA and its viability as an anti-infective agent. Failure to adequately characterize drug targets during the early stages of discovery can result in expensive and time-consuming clinical trial failures. Thus, precise characterization of compounds at the initial stages of drug discovery is crucial to mitigate risks and streamline the development process. However, the traditional target-identification methods outlined in the introduction, despite past successes, face several limitations in modern drug discovery. Genetic approaches, which rely on the identification of resistance-conferring mutations, are often constrained by the challenges associated with pathogens that are difficult to genetically manipulate. Furthermore, alternative resistance mechanisms, such as the overexpression of efflux pumps, can obscure the true drug target. Macromolecular assays, although useful in detecting broad inhibitory effects on major cellular processes like DNA, RNA, or protein synthesis, are inherently low-resolution and may fail to uncover novel MoA. These challenges underscore the need for more versatile and higher-throughput approaches in identifying drug targets.

In contrast, (chemo-)proteomics approaches, such as those employed in this thesis, offer a more comprehensive and versatile alternative for target identification and validation. By leveraging quantitative mass spectrometry, these methods enable the direct identification of compound–protein interactions in native proteomes. The ability to unveil compound–target interactions on a proteome-wide scale can reveal novel therapeutic opportunities and elucidate mechanisms of resistance that would otherwise remain undetected through conventional approaches.

## 4.1 Proteomic Characterization of Pathogenic Microorganisms

Proteomics provides a comprehensive snapshot of pathogen physiology and cellular processes, offering invaluable insights into the molecular landscape of organisms under various conditions. This approach is particularly advantageous for drug discovery and development, as it facilitates the assessment of both the abundance and detectability of potential protein targets by LC-MS/MS. In the context of this project, proteomics enabled the comprehensive characterization of the acid-fast bacillus *M. tuberculosis*, the three Gram-negative bacteria—*E. coli*, *K. pneumoniae*, and *P. aeruginosa*—the Gram-positive bacterium *S. aureus* and the protozoan parasite *P. falciparum*. A key finding was the successful identification and quantification of all seven enzymes involved in the MEP pathway across species that utilize this pathway, establishing a robust foundation for future proteomics-driven inhibitor-discovery efforts targeting these essential enzymes.

A notable finding was the lower abundance of 2-*C*-methyl-D-erythritol 4-phosphate cytidylyltransferase (IspD) in *P. falciparum*, which might complicate efforts to demonstrate effective target–engagement in cells, potentially making it more challenging to validate small-molecule inhibitors against this enzyme. Moreover, IspD exhibited a relatively low number of detected peptides (n=4) by LC-MS/MS. While this number is sufficient to obtain reliable and robust quantification, it remains quite limited and reflects the inherent challenges in identifying this protein in complex proteomic samples, such as in enrichment assays. This finding underscores the broader implications of low-abundance proteins in proteomics studies, highlighting the necessity for enhanced analytical techniques and enrichment strategies to improve the detection and quantification of such proteins. The limitations of bottom-up proteomics can lead to inaccurate detection and quantification of peptides, particularly those with poor ionization properties or chromatographic separation issues, as well as incomplete digestion. These limitations can particularly impact low-abundance proteins like IspD, leading to underrepresentation in proteomic analyses. Addressing these challenges provides an opportunity to explore potential technological improvements in the field.

The extensive proteome coverage achieved across all species, including *M. tuberculosis*, displays the efficacy of the quantitative proteomics strategy employed. The application of harsher lysis methods in *M. tuberculosis* markedly improved protein recovery, especially for membrane-bound and low-abundance proteins, while adhering to biosafety requirements within a BSL3 laboratory. For the remaining species, native lysis conditions were preserved to maintain protein functionality for downstream biochemical analyses. This dual approach allowed for both comprehensive proteomic profiling and CRISPR interference (CRISPRi)-based target validation.

Through integration with CRISPRi, proteomics further enabled the quantitative assessment of protein levels in response to gene knockdown.[203] Specifically, CRISPRi-mediated repression of *rpoB*, *dxs1*, and *dxr* in *M. tuberculosis* resulted in a dose-dependent reduction in the corresponding protein abundance, as measured by mass spectrometry. Our findings also unveiled broader proteomic shifts that provide valuable insights into the metabolic reprogramming occurring in response to gene repression. Importantly, CRISPRi-mediated downregulation of *dxs1* and *dxr*, enzymes essential for isoprenoid biosynthesis, provides a valuable tool for future studies aimed at validating inhibitors targeting these proteins.

In conclusion, the proteomic methodologies applied in this work offered a detailed understanding of pathogen biology, while providing a valuable resource for future drug-discovery efforts. The successful integration of proteomics with CRISPRi validates this combined approach as a powerful platform for drug-target identification and the exploration of essential metabolic pathways, thereby contributing to the development of new strategies to tackle antimicrobial resistance.

## 4.2 Chemoproteomics Approaches and Their Challenges

Chemoproteomics, particularly affinity-based proteome profiling (e.g., pull-down assays), has emerged as a powerful tool in drug discovery for understanding target–engagement and inhibitor profiling. However, the technique is not without limitations, which can complicate the identification of true targets and hinder the full exploitation of its potential in certain biological contexts. This chapter outlines the major challenges associated with chemoproteomics, using examples from our studies with *P. falciparum* and *E. coli* as case studies to illustrate these issues.

One of the major challenges in chemoproteomics is the detection and enrichment of low-abundance proteins. Pull-down assays, for example, rely on the ability of a chemical probe to bind its target protein

and subsequently allow for its enrichment and detection. However, when the target protein is expressed at low levels, it may fall below the detection limit. In our experiments, we aimed to validate the engagement of IspD in *P. falciparum* using an affinity matrix based on the urea-based inhibitor (compound **1**) in a pull-down assay. Despite our efforts, IspD was not detected in either the samples treated with the affinity matrix nor in the background control, likely due to its low abundance in the parasite proteome. Our previous studies have shown that IspD is present at very low levels in *P. falciparum*, which likely hindered its detection. Although compound **1** demonstrated strong in vitro activity (*Pf*IspD $IC_{50}$ of 0.45 μM), the pull-down assay failed to enrich IspD, suggesting that low protein abundance is a critical limiting factor in such assays.

Despite the challenges with IspD, our pull-down experiments with compound **1** in *P. falciparum* successfully enriched several proteins, including actin-1 (Act1), glyceraldehyde-3-phosphate dehydrogenase (GAPDH), ornithine aminotransferase (OAT), and S-adenosylmethionine synthase (MAT). These proteins play important roles in the parasite's cellular processes, and their enrichment provides insights into the broader interaction profile of compound **1**. Since compound **1** exhibits potent antiplasmodial activity ($IC_{50}$ of 2 μM), these off-targets may contribute to its overall growth-inhibitory effects on the parasite.

Another critical challenge involves the design of chemical probes. Chemical probes need to be functionalized with tags or reactive groups to enable immobilization on affinity matrices. While these modifications are essential for the pull-down approach, they can inadvertently affect the binding affinity or selectivity of the compounds, leading to decreased efficacy in capturing the intended targets. This makes SAR studies necessary to maintain the biological activity of the probes post-functionalization. In the case of compound **1**, given its relatively strong in vitro activity, this explanation is less likely, but it remains a possibility.

In our profiling of the pyrazole class inhibitors in *E. coli*, an affinity matrix based on compound **2** was generated. However, the putative target IspE was not enriched, likely due to the weak inhibitory potency of the probe ($IC_{50}$ = 40 μM), which underscores the need for careful optimization of chemical probes to ensure that functionalization does not impair activity. While several other proteins, such as FMN-dependent NADH-quinone reductase (AzoR) and glutamine synthetase (GS), were enriched, this case demonstrates how suboptimal probe design can limit the detection of the intended target. Nevertheless, the enriched proteins can represent a starting point for follow-up studies.

Kinase-focused chemoproteomics approaches, such as the Kinobeads technology, have been widely used for kinase profiling in human cells. However, adapting these methods for bacterial kinases poses several challenges due to the structural differences between bacterial and human kinases. To improve the enrichment of the kinase IspE in *E. coli*, we employed the Kinobeads approach with various affinity matrices designed for human kinase profiling. Unfortunately, IspE was not enriched, likely due to the structural differences between bacterial and human kinases.[204] While both IspE and human kinases transfer phosphate groups, their substrates and functional contexts differ significantly. IspE acts on small molecules within a biosynthetic pathway, whereas human kinases primarily regulate cellular processes through the phosphorylation of proteins, phosphorylating specific amino- acid residues such as serine, threonine, or tyrosine. A small subset of human kinases, however, phosphorylate non-protein substrates, including lipids, nucleosides, and sugars, playing unique roles in metabolism and signaling. The catalytic site of IspE is adapted to accommodate the small, organic substrate (CDP-ME) and facilitate its phosphorylation. The enzyme utilizes ATP to transfer a phosphate group to the substrate, which involves specific interactions with the nucleotide and the organic molecule. Human kinases typically have more complex catalytic sites designed to accommodate larger protein substrates and

their specificity is often determined by the presence of a phosphorylation motif in the target protein, which interacts with the kinase's active site. The failure to capture IspE suggests that further optimization of the Kinobeads approach is necessary to tailor it for bacterial systems, as well as for kinases that phosphorylate non-protein substrates, including non-protein kinases. However, the successful enrichment of 46 other kinases demonstrates the potential of this method for studying bacterial kinases.

Another major limitation of chemoproteomics is the substantial amount of proteins required for enrichment assays, often in the milligram range per sample. For organisms like *P. falciparum*, characterized by slow growth rates and low protein yields, this can severely limit the number of conditions and replicates that can be tested, such as coupling densities, but also imposes restrictions on the throughput of the approach, limiting the number of compounds that can be efficiently profiled. This requirement arises from the inherent nature of affinity-based enrichment methods, which typically require robust input material to ensure sufficient capture of the target proteins and their potential interactors. In organisms with limited availability, like *P. falciparum*, generating enough protein for multiple experiments becomes labor-intensive and time-consuming, further reducing experimental flexibility. This challenge is particularly pronounced when profiling low-abundance proteins, which may already be underrepresented in the proteome and thus difficult to detect without extensive protein input. Additionally, the low yields of proteins in such organisms also affect the ability to optimize experimental parameters, such as testing different affinity matrices or varying concentrations of probes and competitors. These optimization steps are often crucial for fine-tuning the chemoproteomics workflow to enhance the specificity and sensitivity of target enrichment.

Given the limitations of chemoproteomics, alternative approaches that require less protein input and avoid the need for probe functionalization offer promising solutions. Methods such as TPP and iSPP allow for the assessment of compound–target interactions without chemical modification of the ligand, making them more suitable for low-yield organisms.

In summary, chemoproteomics is a valuable tool for studying target–engagement and inhibitor profiling but comes with several inherent limitations. These challenges, including the detection of low-abundance proteins, the effects of probe functionalization, incomplete target–engagement, poor probe affinity, and the substantial protein input required, were all encountered in our studies of *P. falciparum* and *E. coli*. The case studies presented here illustrate these challenges and underscore the need for alternative approaches to address these limitations.

## 4.3 iSPP Advantages and Challenges in Target–Engagement studies for AMR-Related Pathogens

In this thesis, we demonstrated the potential of iSPP as a robust biophysical method for studying target–engagement and target deconvolution in several human pathogens. iSPP relies on the stabilization of target proteins upon ligand binding and lysate exposure to organic solvents, providing a direct readout of target–engagement without necessitating any chemical modification of the ligand. This characteristic represents an advantage over traditional chemoproteomics methods. By eliminating the requirement for chemical modification, iSPP streamlines the experimental workflow, reducing both time and resource investment associated with probe development. This efficiency allows researchers to focus on evaluating the interactions between small molecules and their targets more rapidly and effectively. Furthermore, the absence of probe design and synthesis mitigates the potential for introducing biases that can arise from probe-specific interactions, thereby enhancing the reliability of

the data obtained. This versatility positions iSPP as an attractive tool in the drug-discovery pipeline, particularly in scenarios where the development of probes may be impractical or where target validation is critical.

The foundation of iSPP was laid by Zhang et al.[200] and further adapted by Van Vranken and colleagues[201] in human cell lysates, transitioning from traditional SPP assays relying on the generation of complete denaturation curves to a compressed format that pools multiple aliquots of lysate exposed to varying organic solvent concentrations. Our study led to the adaption and optimization of the workflow obtaining a comprehensive iSPP assay for target–engagement across the three Gram-negative bacteria *E. coli*, *K. pneumoniae* and *P. aeruginosa*, the Gram-positive bacterium *S. aureus*, and the parasite *P. falciparum*. We used asynchronous cultures of *P. falciparum* in our studies; however, the iSPP method can be adapted for synchronized cultures to investigate stage-specific compound activities.

By employing DIA quantitative MS, we achieved high-coverage proteome quantification in a cost-effective manner, distinguishing our approach from previous SPP studies that primarily relied on TMT labeling.[117,119] While TMT labeling has been widely used for quantitative proteomics due to its ability to multiplex samples, it entails significant drawbacks, including high reagent costs and increased hands-on labor in the laboratory. The financial implications of TMT labeling can be substantial, particularly for large-scale studies or those with limited budgets. The costs associated with TMT reagents may restrict the number of experiments that can be feasibly conducted, thereby potentially hindering the exploration of diverse conditions or compound libraries. Additionally, the labeling process requires additional steps, which increases the complexity of the workflow and introduces opportunities for variability and errors, ultimately affecting the reproducibility and reliability of the results. In contrast, our use of DIA mass spectrometry circumvents these limitations by enabling direct quantification without the need for complex labeling strategies. Moreover, TMT-labeled samples necessitate prior fractionation before MS analysis, adding another layer of complexity and time to the experimental workflow. Fractionation is crucial for TMT samples to reduce sample complexity and improve the detection. In contrast, samples prepared for DIA can be measured immediately in a single-shot analysis. This measurement capability streamlines the workflow, allowing for rapid data-acquisition without the need for extensive sample manipulation. The single-shot nature of DIA not only enhances throughput but also preserves sample integrity, minimizing the risk of peptides loss that can occur during fractionation. Therefore, DIA not only reduces the overall experimental cost but also simplifies the workflow.

Another hallmark of our iSPP method is its minimal input requirement, utilizing only 20 µg of total protein per data point. This optimization greatly enhances its applicability to studies involving slow-growing or hard-to-culture pathogens, characterized by low protein yields. This feature was particularly crucial in establishing the approach in *P. falciparum*, a notoriously challenging organism to culture and study due to its complex life cycle and growth conditions. By minimizing the protein input amount, the iSPP method allows for higher-throughput analyses, enabling the evaluation of multiple compounds while consuming a comparatively low amount of protein. This reduction in input not only streamlines the workflow but also expands the potential for target–engagement studies across a diverse range of biological systems, particularly those with limited protein availability.

In our studies, we investigated the ability of iSPP to confirm protein targets, as detailed in Chapters 3.3 and 3.4. By conducting target–engagement studies with multiple antibiotics and antimalarial drugs, we effectively demonstrated that iSPP can confirm the MoA of these compounds. Furthermore, we highlighted the critical role of AEA gradient selection. By employing windows tailored to the regions

exhibiting the most substantial solubility changes for the corresponding target proteins, we enhanced the observed effect size in stability, facilitating the identification of these targets among the top hits. These results simultaneously highlight a limitation of the iSPP approach. Conducting target deconvolution studies and obtaining a comprehensive target profile often necessitates the use of multiple solvent range windows and/or various compound concentrations. This added complexity stems from the need to optimize conditions for different proteins, making it challenging to capture all potential target interactions in a single experimental setup. Thus, while iSPP offers valuable insights into target–engagement, fully unraveling the target landscape may require an expanded experimental design to accommodate these variables.

Additionally, our studies highlighted other limitations associated with the compressed format of iSPP. Achieving robust stabilization of target proteins upon certain compound–protein interactions can be challenging. This was evident in the case of DXR in *P. aeruginosa* lysate following incubation with fosmidomycin, and similarly for the proteins DHPS and DHODH in *P. falciparum* when targeted by sulfadoxine and DSM265, respectively. Furthermore, we encountered known target proteins that did not exhibit any detectable stabilization, suggesting that target–engagement might not always be observable. A specific example is *Pf*DXR, for which we did not detect significant stabilization in the presence of fosmidomycin. One plausible explanation is that the protein may become partially unfolded during the extraction process, rendering it less responsive to ligand-induced stabilization. This highlights potential protein-specific limitations in using iSPP for target validation. We also observed the presence of multiple (de)stabilized proteins alongside the designated targets in certain experimental conditions. It is important to note that this (de)stabilization does not necessarily indicate target–engagement; rather, it may arise from artifacts associated with a low signal-to-noise ratio, which could lead to false positive hits. Additionally, destabilization may occur when ligands bind to a (partially) unfolded state of a protein, thereby reducing its stability. This phenomenon has been previously documented in TSA, as highlighted by Cimmperman and colleagues.[205] Such considerations underscore the necessity for cautious interpretation of destabilization data within the context of iSPP in cell lysates.

Notably, our findings, following *E. coli* incubation with ampicillin, revealed stabilization of PBP1a (MrcA) and PBP4 (DacB), aligning with results reported by Mateus et al. [184] in their 2D-TPP study. This consistency underscores the validity of iSPP as a target–engagement assay for bacteria, demonstrating its capability to confirm key protein targets identified through alternative methodologies. iSPP emerges as a valuable complementary approach to TPP. Certain proteins that may not exhibit drug-binding stabilization during thermal denaturation could, in contrast, respond to organic solvent-induced denaturation, and vice versa. This complementary was also highlighted by Van Vranken and colleagues,[201] who conducted a comparative analysis between SPP and TPP in human cell lysates. Their results suggested that while both methods are capable of generating overlapping sets of putative targets, their lists are not entirely congruent. These findings show the complementary nature of SPP and TPP: not only they enable independent corroboration of targets, but each method may also identify targets missed by the other. This mutual exclusivity enriches the repertoire of protein targets that can be reliably detected, thereby enhancing the robustness of target–engagement studies and providing a more comprehensive landscape of drug-protein interactions.

Collectively, these results underscore the versatility and utility of iSPP in confirming the MoA of novel anti-infectives, facilitating the advancement of drug-discovery efforts. By leveraging its capabilities in both target–engagement and deconvolution studies, we can enhance the drug discovery process, leading to the identification of more effective therapeutic strategies.

## 4.4 Outlook

The results presented in this thesis underscore the critical role of (chemo-)proteomics in advancing early-stage drug discovery, particularly for antimicrobial and antimalarial therapies. Specifically, by leveraging iSPP, researchers can more rapidly and accurately assess compound–protein interactions. The iSPP assay method developed here provides a robust and adaptable platform for characterizing inhibitors in key human pathogens, paving the way for the discovery of next-generation anti-infective agents.

We envision several potential steps to further advance these projects. First, expanding the characterization of promising lead compounds using the iSPP platform will be crucial for elucidating the binding interactions and potential off-target effects of inhibitors. Validating the additional stabilized proteins observed in our iSPP experiments, beyond the known targets, will provide further insights. For instance, AspRS, stabilized by fosmidomycin across multiple species, warrants deeper investigation in further assays. Moreover, conducting iSPP analysis in live bacterial cells is another important investigation. Since our current experiments were performed in lysates, downstream effects of compound incubation may differ in metabolically active cells, and such studies have the potential to reveal key insights into compound effects in live bacterial systems. Establishing the iSPP approach in *M. tuberculosis* cells within a BSL3 laboratory is also a priority. In addition, employing affinity matrices based on broad-spectrum bacterial kinase inhibitors could enhance the enrichment of bacterial kinases in pull-down assays. Finally, performing global proteomic profiling of *M. tuberculosis* will help validate targets following CRISPRi-mediated gene repression, enabling more comprehensive target validation.

# 5. REFERENCES


[1] Armstrong GL, Conn LA, Pinner RW. Trends in Infectious Disease Mortality in the United States During the 20th Century. JAMA 1999;281:61–6. https://doi.org/10.1001/JAMA.281.1.61.

[2] Cook MA, Wright GD. The past, present, and future of antibiotics. Sci Transl Med 2022;14. https://doi.org/10.1126/scitranslmed.abo7793.

[3] WHO World Health Organization. World malaria report. 2023.

[4] Rosenthal PJ, Asua V, Bailey JA, Conrad MD, Ishengoma DS, Kamya MR, et al. The emergence of artemisinin partial resistance in Africa: how do we respond? Lancet Infect Dis 2024;0. https://doi.org/10.1016/S1473-3099(24)00141-5.

[5] Li J, Docile HJ, Fisher D, Pronyuk K, Zhao L. Current Status of Malaria Control and Elimination in Africa: Epidemiology, Diagnosis, Treatment, Progress and Challenges. Journal of Epidemiology and Global Health 2024 2024:1–19. https://doi.org/10.1007/S44197-024-00228-2.

[6] Gauba A, Rahman KM. Evaluation of Antibiotic Resistance Mechanisms in Gram-Negative Bacteria. Antibiotics 2023;12:1590. https://doi.org/10.3390/antibiotics12111590.

[7] Okeke IN, de Kraker MEA, Van Boeckel TP, Kumar CK, Schmitt H, Gales AC, et al. The scope of the antimicrobial resistance challenge. The Lancet 2024;403:2426–38.

[8] Murray CJ, Ikuta KS, Sharara F, Swetschinski L, Robles Aguilar G, Gray A, et al. Global burden of bacterial antimicrobial resistance in 2019: a systematic analysis. The Lancet 2022;399:629–55. https://doi.org/10.1016/S0140-6736(21)02724-0.

[9] Tacconelli E, Carrara E, Savoldi A, Harbarth S, Mendelson M, Monnet DL, et al. Discovery, research, and development of new antibiotics: the WHO priority list of antibiotic-resistant bacteria and tuberculosis. Lancet Infect Dis 2018;18:318–27. https://doi.org/10.1016/S1473-3099(17)30753-3.

[10] Lewis K. Platforms for antibiotic discovery. Nature Reviews Drug Discovery 2013 12:5 2013;12:371–87. https://doi.org/10.1038/nrd3975.

[11] Lipsitch M, Samore MH. Antimicrobial Use and Antimicrobial Resistance: A Population Perspective. Emerg Infect Dis 2002;8:347. https://doi.org/10.3201/EID0804.010312.

[12] Muñoz KA, Ulrich RJ, Vasan AK, Sinclair M, Wen P-C, Holmes JR, et al. A Gram-negative-selective antibiotic that spares the gut microbiome. Nature 2024 2024:1–8. https://doi.org/10.1038/s41586-024-07502-0.

[13] Lange K, Buerger M, Stallmach A, Bruns T. Effects of Antibiotics on Gut Microbiota. Digestive Diseases 2016;34:260–8. https://doi.org/10.1159/000443360.

[14] Owens RC, Donskey CJ, Gaynes RP, Loo VG, Muto CA. Antimicrobial-Associated Risk Factors for Clostridium difficile Infection. Clinical Infectious Diseases 2008;46:S19–31. https://doi.org/10.1086/521859.

[15] Poon SSB, Hung LY, Wu Q, Parathan P, Yalcinkaya N, Haag A, et al. Neonatal antibiotics have long term sex-dependent effects on the enteric nervous system. J Physiol 2022;600:4303–23. https://doi.org/10.1113/JP282939.

[16] Iizumi T, Battaglia T, Ruiz V, Perez Perez GI. Gut Microbiome and Antibiotics. Arch Med Res 2017;48:727–34. https://doi.org/10.1016/J.ARCMED.2017.11.004.

[17] Endo T, Takemae H, Sharma I, Furuya T. Multipurpose Drugs Active Against Both Plasmodium spp. and Microorganisms: Potential Application for New Drug Development. Front Cell Infect Microbiol 2021;11. https://doi.org/10.3389/fcimb.2021.797509.

[18] Belete TM. Novel targets to develop new antibacterial agents and novel alternatives to antibacterial agents. Hum Microb J 2019;11:100052. https://doi.org/10.1016/J.HUMIC.2019.01.001.

[19] Frank A, Groll M. The Methylerythritol Phosphate Pathway to Isoprenoids. Chem Rev 2017;117:5675–703. https://doi.org/10.1021/acs.chemrev.6b00537.

[20] Rohmer M. The discovery of a mevalonate-independent pathway for isoprenoid biosynthesis in bacteria, algae and higher plants. Nat Prod Rep 1999;16:565–74. https://doi.org/10.1039/A709175C.

[21] Rohmer M, Seemann M, Horbach S, Bringer-Meyer S, Sahm H. Glyceraldehyde 3-Phosphate and Pyruvate as Precursors of Isoprenic Units in an Alternative Non-mevalonate Pathway for Terpenoid Biosynthesis. J Am Chem Soc 1996;118:2564–6. https://doi.org/10.1021/JA9538344.

[22] Arigoni D, Sagner S, Latzel C, Eisenreich W, Bacher A, Zenk MH. Terpenoid biosynthesis from 1-deoxy-D-xylulose in higher plants by intramolecular skeletal rearrangement. Proc Natl Acad Sci U S A 1997;94:10600–5.

[23] Lange BM, Rujan T, Martin W, Croteau R. Isoprenoid biosynthesis: The evolution of two ancient and distinct pathways across genomes. Proc Natl Acad Sci U S A 2000;97:13172–7.

[24] Masini T, Hirsch AKH. Development of inhibitors of the 2C-methyl-D-erythritol 4-phosphate (MEP) pathway enzymes as potential anti-infective agents. J Med Chem 2014;57:9740–63. https://doi.org/10.1021/jm5010978.

[25] Wang X, Dowd CS. The Methylerythritol Phosphate Pathway: Promising Drug Targets in the Fight against Tuberculosis. ACS Infect Dis 2018;4:278–90. https://doi.org/10.1021/acsinfecdis.7b00176.

[26] Rodriguez-Concepcion M. The MEP Pathway: A New Target for the Development of Herbicides, Antibiotics and Antimalarial Drugs. Curr Pharm Des 2005;10:2391–400. https://doi.org/10.2174/1381612043384006.

[27] Zhu D, Johannsen S, Masini T, Simonin C, Haupenthal J, Illarionov B, et al. Discovery of novel drug-like antitubercular hits targeting the MEP pathway enzyme DXPS by strategic application of ligand-based virtual screening. Chem Sci 2022;13:10686–98. https://doi.org/10.1039/d2sc02371g.

[28] Lell B, Ruangweerayut R, Wiesner J, Missinou MA, Schindler A, Baranek T, et al. Fosmidomycin, a Novel Chemotherapeutic Agent for Malaria. Antimicrob Agents Chemother 2003;47:735. https://doi.org/10.1128/AAC.47.2.735-738.2003.

[29] Knak T, Abdullaziz MA, Höfmann S, Alves Avelar LA, Klein S, Martin M, et al. Over 40 Years of Fosmidomycin Drug Research: A Comprehensive Review and Future Opportunities. Pharmaceuticals 2022;15:1553. https://doi.org/10.3390/ph15121553.
[30] Umeda T, Tanaka N, Kusakabe Y, Nakanishi M, Kitade Y, Nakamura KT. Molecular basis of fosmidomycin's action on the human malaria parasite Plasmodium falciparum. Sci Rep 2011;1. https://doi.org/10.1038/srep00009.
[31] Mombo-Ngoma G, Remppis J, Sievers M, Zoleko Manego R, Endamne L, Kabwende L, et al. Efficacy and Safety of Fosmidomycin–Piperaquine as Nonartemisinin-Based Combination Therapy for Uncomplicated Falciparum Malaria: A Single-Arm, Age De-escalation Proof-of-Concept Study in Gabon. Clin Infect Dis 2018;66:1823. https://doi.org/10.1093/CID/CIX1122.
[32] Borrmann S, Adegnika AA, Matsiegui PB, Issifou S, Schindler A, Mawili-Mboumba DP, et al. Fosmidomycin-clindamycin for Plasmodium falciparum infections in African children. Journal of Infectious Diseases 2004;189:901–8.
[33] Ruangweerayut R, Looareesuwan S, Hutchinson D, Chauemung A, Banmairuroi V, Na-Bangchang K. Assessment of the pharmacokinetics and dynamics of two combination regimens of fosmidomycin-clindamycin in patients with acute uncomplicated falciparum malaria. Malar J 2008;7:225. https://doi.org/10.1186/1475-2875-7-225.
[34] Mallick P, Kuster B. Proteomics: a pragmatic perspective. Nature Biotechnology 2010 28:7 2010;28:695–709. https://doi.org/10.1038/nbt.1658.
[35] Meissner F, Geddes-McAlister J, Mann M, Bantscheff M. The emerging role of mass spectrometry-based proteomics in drug discovery. Nat Rev Drug Discov 2022. https://doi.org/10.1038/s41573-022-00409-3.
[36] Schirle M, Bantscheff M, Kuster B. Mass spectrometry-based proteomics in preclinical drug discovery. Chem Biol 2012;19:72–84. https://doi.org/10.1016/j.chembiol.2012.01.002.
[37] Larance M, Lamond AI. Multidimensional proteomics for cell biology. Nature Reviews Molecular Cell Biology 2015 16:5 2015;16:269–80. https://doi.org/10.1038/nrm3970.
[38] Aebersold R, Mann M. Mass-spectrometric exploration of proteome structure and function. Nature 2016;537:347–55. https://doi.org/10.1038/nature19949.
[39] Picotti P, Bodenmiller B, Mueller LN, Domon B, Aebersold R. Full Dynamic Range Proteome Analysis of S. cerevisiae by Targeted Proteomics. Cell 2009;138:795–806. https://doi.org/10.1016/j.cell.2009.05.051.
[40] Ebhardt HA, Sabidó E, Hüttenhain R, Collins B, Aebersold R. Range of protein detection by selected/multiple reaction monitoring mass spectrometry in an unfractionated human cell culture lysate. Proteomics 2012;12:1185–93. https://doi.org/10.1002/PMIC.201100543.
[41] Ebhardt HA, Root A, Sander C, Aebersold R. Applications of targeted proteomics in systems biology and translational medicine. Proteomics 2015;15:3193–208. https://doi.org/10.1002/pmic.201500004.
[42] Macek B, Forchhammer K, Hardouin J, Weber-Ban E, Grangeasse C, Mijakovic I. Protein post-translational modifications in bacteria. Nat Rev Microbiol 2019;17:651–64. https://doi.org/10.1038/s41579-019-0243-0.
[43] Leng SX, McElhaney JE, Walston JD, Xie D, Fedarko NS, Kuchel GA. ELISA and Multiplex Technologies for Cytokine Measurement in Inflammation and Aging Research. The Journals of Gerontology: Series A 2008;63:879–84. https://doi.org/10.1093/GERONA/63.8.879.
[44] Wik L, Nordberg N, Broberg J, Björkesten J, Assarsson E, Henriksson S, et al. Proximity Extension Assay in Combination with Next-Generation Sequencing for High-throughput Proteome-wide Analysis. Mol Cell Proteomics 2021;20. https://doi.org/10.1016/J.MCPRO.2021.100168.
[45] Duo J, Chiriac C, Huang RYC, Mehl J, Chen G, Tymiak A, et al. Slow Off-Rate Modified Aptamer (SOMAmer) as a Novel Reagent in Immunoassay Development for Accurate Soluble Glypican-3 Quantification in Clinical Samples. Anal Chem 2018;90:5162–70.
[46] Aksel T, Qian H, Hao P, Indermuhle PF, Inman C, Paul S, et al. High-density and scalable protein arrays for single-molecule proteomic studies. BioRxiv 2022:2022.05.02.490328. https://doi.org/10.1101/2022.05.02.490328.
[47] Egertson JD, DiPasquo D, Killeen A, Lobanov V, Patel S, Mallick P. A theoretical framework for proteome-scale single-molecule protein identification using multi-affinity protein binding reagents. BioRxiv 2021:2021.10.11.463967. https://doi.org/10.1101/2021.10.11.463967.
[48] Sabidó E, Selevsek N, Aebersold R. Mass spectrometry-based proteomics for systems biology. Curr Opin Biotechnol 2012;23:591–7. https://doi.org/10.1016/j.copbio.2011.11.014.
[49] Müller JB, Geyer PE, Colaço AR, Treit P V., Strauss MT, Oroshi M, et al. The proteome landscape of the kingdoms of life. Nature 2020;582:592–6. https://doi.org/10.1038/s41586-020-2402-x.
[50] Linscheid N, Santos A, Poulsen PC, Mills RW, Calloe K, Leurs U, et al. Quantitative proteome comparison of human hearts with those of model organisms. PLoS Biol 2021;19:e3001144. https://doi.org/10.1371/JOURNAL.PBIO.3001144.
[51] Kelstrup CD, Jersie-Christensen RR, Batth TS, Arrey TN, Kuehn A, Kellmann M, et al. Rapid and deep proteomes by faster sequencing on a benchtop quadrupole ultra-high-field orbitrap mass spectrometer. J Proteome Res 2014;13:6187–95.
[52] Schessner JP, Voytik E, Bludau I. A practical guide to interpreting and generating bottom-up proteomics data visualizations. Proteomics 2022:1–18. https://doi.org/10.1002/pmic.202100103.
[53] Lenčo J, Jadeja S, Naplekov DK, Krokhin O V., Khalikova MA, Chocholouš P, et al. Reversed-Phase Liquid Chromatography of Peptides for Bottom-Up Proteomics: A Tutorial. J Proteome Res 2022;21:2846–92.
[54] Meier F, Park MA, Mann M. Trapped ion mobility spectrometry and parallel accumulation–serial fragmentation in proteomics. Molecular and Cellular Proteomics 2021;20:100138.
[55] Hebert AS, Prasad S, Belford MW, Bailey DJ, McAlister GC, Abbatiello SE, et al. Comprehensive Single-Shot Proteomics with FAIMS on a Hybrid Orbitrap Mass Spectrometer. Anal Chem 2018;90:9529–37.

[56] Helm D, Vissers JPC, Hughes CJ, Hahne H, Ruprecht B, Pachl F, et al. Ion mobility tandem mass spectrometry enhances performance of bottom-up proteomics. Molecular and Cellular Proteomics 2014;13:3709–15. https://doi.org/10.1074/mcp.M114.041038.
[57] Gillet LC, Navarro P, Tate S, Röst H, Selevsek N, Reiter L, et al. Targeted Data Extraction of the MS/MS Spectra Generated by Data-independent Acquisition: A New Concept for Consistent and Accurate Proteome Analysis. Molecular & Cellular Proteomics 2012;11:O111.016717. https://doi.org/10.1074/MCP.O111.016717.
[58] Messner CB, Demichev V, Bloomfield N, Yu JSL, White M, Kreidl M, et al. Ultra-fast proteomics with Scanning SWATH. Nat Biotechnol 2021;39:846–54. https://doi.org/10.1038/s41587-021-00860-4.
[59] Tiwary S, Levy R, Gutenbrunner P, Salinas Soto F, Palaniappan KK, Deming L, et al. High-quality MS/MS spectrum prediction for data-dependent and data-independent acquisition data analysis. Nat Methods 2019;16:519–25. https://doi.org/10.1038/s41592-019-0427-6.
[60] Li J, Smith LS, Zhu HJ. Data-independent acquisition (DIA): An emerging proteomics technology for analysis of drug-metabolizing enzymes and transporters. Drug Discov Today Technol 2021;39:49–56. https://doi.org/10.1016/j.ddtec.2021.06.006.
[61] Guzman UH, Martinez-Val A, Ye Z, Damoc E, Arrey TN, Pashkova A, et al. Ultra-fast label-free quantification and comprehensive proteome coverage with narrow-window data-independent acquisition. Nat Biotechnol 2024. https://doi.org/10.1038/s41587-023-02099-7.
[62] Kong AT, Leprevost F V., Avtonomov DM, Mellacheruvu D, Nesvizhskii AI. MSFragger: ultrafast and comprehensive peptide identification in mass spectrometry–based proteomics. Nat Methods 2017;14:513–20. https://doi.org/10.1038/nmeth.4256.
[63] Demichev V, Messner CB, Vernardis SI, Lilley KS, Ralser M. DIA-NN: neural networks and interference correction enable deep proteome coverage in high throughput. Nat Methods 2020;17:41–4. https://doi.org/10.1038/s41592-019-0638-x.
[64] Gessulat S, Schmidt T, Zolg DP, Samaras P, Schnatbaum K, Zerweck J, et al. Prosit: proteome-wide prediction of peptide tandem mass spectra by deep learning. Nat Methods 2019;16:509–18. https://doi.org/10.1038/s41592-019-0426-7.
[65] Patrie SM. Top-Down Mass Spectrometry: Proteomics to Proteoforms. Adv Exp Med Biol 2016;919:171–200. https://doi.org/10.1007/978-3-319-41448-5_8.
[66] Bhuyan AK. On the mechanism of SDS-induced protein denaturation. Biopolymers 2010;93:186–99. https://doi.org/10.1002/BIP.21318.
[67] Peach M, Marsh N, Miskiewicz EI, MacPhee DJ. Solubilization of Proteins: The Importance of Lysis Buffer Choice. Western Blotting: Methods and Protocols 2015:49–60. https://doi.org/10.1007/978-1-4939-2694-7_8.
[68] Rundlett KL, Armstrong DW. Mechanism of Signal Suppression by Anionic Surfactants in Capillary Electrophoresis-Electrospray Ionization Mass Spectrometry. Anal Chem 1996;68:3493–7.
[69] Smith PK, Krohn RI, Hermanson GT, Mallia AK, Gartner FH, Provenzano MD, et al. Measurement of protein using bicinchoninic acid. Anal Biochem 1985;150:76–85. https://doi.org/10.1016/0003-2697(85)90442-7.
[70] Shuken SR. An Introduction to Mass Spectrometry-Based Proteomics. J Proteome Res 2023. https://doi.org/10.1021/acs.jproteome.2c00838.
[71] Giansanti P, Aye TT, van den Toorn H, Peng M, van Breukelen B, Heck AJR. An Augmented Multiple-Protease-Based Human Phosphopeptide Atlas. Cell Rep 2015;11:1834–43. https://doi.org/10.1016/j.celrep.2015.05.029.
[72] Shevchenko A, Tomas H, Havliš J, Olsen J V., Mann M. In-gel digestion for mass spectrometric characterization of proteins and proteomes. Nature Protocols 2007 1:6 2007;1:2856–60. https://doi.org/10.1038/nprot.2006.468.
[73] Havliš J, Shevchenko A. Absolute Quantification of Proteins in Solutions and in Polyacrylamide Gels by Mass Spectrometry. Anal Chem 2004;76:3029–36. https://doi.org/10.1021/AC035286F.
[74] Hailemariam M, Eguez RV, Singh H, Bekele S, Ameni G, Pieper R, et al. S-Trap, an Ultrafast Sample-Preparation Approach for Shotgun Proteomics. J Proteome Res 2018;17:2917–24. https://doi.org/10.1021/ACS.JPROTEOME.8B00505.
[75] Hughes CS, Foehr S, Garfield DA, Furlong EE, Steinmetz LM, Krijgsveld J. Ultrasensitive proteome analysis using paramagnetic bead technology. Mol Syst Biol 2014;10.
[76] Müller T, Kalxdorf M, Longuespée R, Kazdal DN, Stenzinger A, Krijgsveld J. Automated sample preparation with SP 3 for low-input clinical proteomics. Mol Syst Biol 2020;16:e9111. https://doi.org/10.15252/msb.20199111.
[77] Moggridge S, Sorensen PH, Morin GB, Hughes CS. Extending the Compatibility of the SP3 Paramagnetic Bead Processing Approach for Proteomics. J Proteome Res 2018;17:1730–40.
[78] Dieters-Castator DZ, Manzanillo P, Yang HY, Modak R V., Rardin MJ, Gibson BW. Magnetic Bead-Based Workflow for Sensitive and Streamlined Cell Surface Proteomics. J Proteome Res 2023. https://doi.org/10.1021/acs.jproteome.3c00432.
[79] Cavanagh J, Benson LM, Thompson R, Naylor S. In-Line Desalting Mass Spectrometry for the Study of Noncovalent Biological Complexes. Anal Chem 2003;75:3281–6. https://doi.org/10.1021/AC030182Q.
[80] Wilm M. Principles of Electrospray Ionization. Molecular & Cellular Proteomics 2011;10:M111.009407. https://doi.org/10.1074/MCP.M111.009407.
[81] Gomez A, Tang K. Charge and fission of droplets in electrostatic sprays. Physics of Fluids 1994;6:404–14. https://doi.org/10.1063/1.868037.
[82] Jarnuczak AF, Lee DCH, Lawless C, Holman SW, Eyers CE, Hubbard SJ. Analysis of Intrinsic Peptide Detectability via Integrated Label-Free and SRM-Based Absolute Quantitative Proteomics. J Proteome Res 2016;15:2945–59.
[83] Yuan L, Zhang D, Jemal M, Aubry AF. Systematic evaluation of the root cause of non-linearity in liquid chromatography/tandem mass spectrometry bioanalytical assays and strategy to predict and extend the linear standard curve range. Rapid Communications in Mass Spectrometry 2012;26:1465–74. https://doi.org/10.1002/RCM.6252.
[84] Meier F, Brunner AD, Koch S, Koch H, Lubeck M, Krause M, et al. Online parallel accumulation–serial fragmentation (PASEF) with a novel trapped ion mobility mass spectrometer. Molecular and Cellular Proteomics 2018;17:2534–45. https://doi.org/10.1074/mcp.TIR118.000900.

[85] Meier F, Beck S, Grassl N, Lubeck M, Park MA, Raether O, et al. Parallel accumulation-serial fragmentation (PASEF): Multiplying sequencing speed and sensitivity by synchronized scans in a trapped ion mobility device. J Proteome Res 2015;14:5378–87.
[86] Boesl U. Time-of-flight mass spectrometry: Introduction to the basics. Mass Spectrom Rev 2017;36:86–109. https://doi.org/10.1002/MAS.21520.
[87] Eliuk S, Makarov A. Evolution of Orbitrap Mass Spectrometry Instrumentation. Annual Review of Analytical Chemistry 2015;8:61–80.
[88] Hu Q, Noll RJ, Li H, Makarov A, Hardman M, Cooks RG. The Orbitrap: a new mass spectrometer. Journal of Mass Spectrometry 2005;40:430–43. https://doi.org/10.1002/JMS.856.
[89] Heil LR, Damoc E, Arrey TN, Pashkova A, Denisov E, Petzoldt J, et al. Evaluating the Performance of the Astral Mass Analyzer for Quantitative Proteomics Using Data-Independent Acquisition. J Proteome Res 2023;22:3290–300.
[90] Dumas T, Martinez Pinna R, Lozano C, Radau S, Pible O, Grenga L, et al. The astounding exhaustiveness and speed of the Astral mass analyzer for highly complex samples is a quantum leap in the functional analysis of microbiomes. Microbiome 2024;12:1–15. https://doi.org/10.1186/S40168-024-01766-4/FIGURES/6.
[91] Savaryn JP, Toby TK, Kelleher NL. A researcher's guide to mass spectrometry-based proteomics. Proteomics 2016;16:2435–43. https://doi.org/10.1002/PMIC.201600113.
[92] Beck S, Michalski A, Raether O, Lubeck M, Kaspar S, Goedecke N, et al. The Impact II, a Very High-Resolution Quadrupole Time-of-Flight Instrument (QTOF) for Deep Shotgun Proteomics *. Molecular & Cellular Proteomics 2015;14:2014–29. https://doi.org/10.1074/MCP.M114.047407.
[93] Scheltema RA, Hauschild JP, Lange O, Hornburg D, Denisov E, Damoc E, et al. The Q exactive HF, a benchtop mass spectrometer with a pre-filter, high-performance quadrupole and an ultra-high-field orbitrap analyzer. Molecular and Cellular Proteomics 2014;13:3698–708. https://doi.org/10.1074/mcp.M114.043489.
[94] Lai YH, Wang YS. Advances in high-resolution mass spectrometry techniques for analysis of high mass-to-charge ions. Mass Spectrom Rev 2023;42:2426–45. https://doi.org/10.1002/MAS.21790.
[95] Nolting D, Malek R, Makarov A. Ion traps in modern mass spectrometry. Mass Spectrom Rev 2019;38:150–68. https://doi.org/10.1002/MAS.21549.
[96] Makarov A. Electrostatic Axially Harmonic Orbital Trapping: A High-Performance Technique of Mass Analysis. Anal Chem 2000;72:1156–62. https://doi.org/10.1021/AC991131P.
[97] Roepstorff P, Fohlman J. Proposal for a common nomenclature for sequence ions in mass spectra of peptides. Biomed Mass Spectrom 1984;11:601–601. https://doi.org/10.1002/BMS.1200111109.
[98] Johnson RS, Martin SA, Biemann K, Stults JT, Watson JT. Novel Fragmentation Process of Peptides by Collision-Induced Decomposition in a Tandem Mass Spectrometer: Differentiation of Leucine and Isoleucine. Anal Chem 1987;59:2621–5.
[99] Olsen J V., Macek B, Lange O, Makarov A, Horning S, Mann M. Higher-energy C-trap dissociation for peptide modification analysis. Nature Methods 2007 4:9 2007;4:709–12. https://doi.org/10.1038/nmeth1060.
[100] Chapman JD, Goodlett DR, Masselon CD. Multiplexed and data-independent tandem mass spectrometry for global proteome profiling. Mass Spectrom Rev 2014;33:452–70. https://doi.org/10.1002/mas.21400.
[101] Deutsch EW. File formats commonly used in mass spectrometry proteomics. Molecular and Cellular Proteomics 2012;11:1612–21. https://doi.org/10.1074/mcp.R112.019695.
[102] Oveland E, Muth T, Rapp E, Martens L, Berven FS, Barsnes H. Viewing the proteome: How to visualize proteomics data? Proteomics 2015;15:1341–55. https://doi.org/10.1002/PMIC.201400412.
[103] Bittremieux W, Valkenborg D, Martens L, Laukens K. Computational quality control tools for mass spectrometry proteomics. Proteomics 2017;17:1600159. https://doi.org/10.1002/PMIC.201600159.
[104] Rudnick PA, Clauser KR, Kilpatrick LE, Tchekhovskoi D V., Neta P, Blonder N, et al. Performance metrics for liquid chromatography-tandem mass spectrometry systems in proteomics analyses. Molecular and Cellular Proteomics 2010;9:225–41. https://doi.org/10.1074/mcp.M900223-MCP200.
[105] Noga M, Sucharski F, Suder P, Silberring J. A practical guide to nano-LC troubleshooting. J Sep Sci 2007;30:2179–89. https://doi.org/10.1002/JSSC.200700225.
[106] Tyanova S, Temu T, Cox J. The MaxQuant computational platform for mass spectrometry-based shotgun proteomics. Nat Protoc 2016;11:2301–19. https://doi.org/10.1038/nprot.2016.136.
[107] Orsburn BC. Proteome Discoverer—A Community Enhanced Data Processing Suite for Protein Informatics. Proteomes 2021, Vol 9, Page 15 2021;9:15. https://doi.org/10.3390/PROTEOMES9010015.
[108] Pearson WR, Lipman DJ. Improved tools for biological sequence comparison. Proceedings of the National Academy of Sciences 1988;85:2444–8. https://doi.org/10.1073/PNAS.85.8.2444.
[109] Downloads | UniProt help | UniProt n.d. https://www.uniprot.org/help/downloads.
[110] Tang WH, Shilov I V., Seymour SL. Nonlinear fitting method for determining local false discovery rates from decoy database searches. J Proteome Res 2008;7:3661–7.
[111] Elias JE, Gygi SP. Target-Decoy Search Strategy for Mass Spectrometry-Based Proteomics. Methods Mol Biol 2010;604:55. https://doi.org/10.1007/978-1-60761-444-9_5.
[112] Grossmann J, Roschitzki B, Panse C, Fortes C, Barkow-Oesterreicher S, Rutishauser D, et al. Implementation and evaluation of relative and absolute quantification in shotgun proteomics with label-free methods. J Proteomics 2010;73:1740–6. https://doi.org/10.1016/J.JPROT.2010.05.011.
[113] Arul AB, Robinson RAS. Sample Multiplexing Strategies in Quantitative Proteomics. Anal Chem 2019;91:178–89.
[114] Ong SE, Blagoev B, Kratchmarova I, Kristensen DB, Steen H, Pandey A, et al. Stable isotope labeling by amino acids in cell culture, SILAC, as a simple and accurate approach to expression proteomics. Mol Cell Proteomics 2002;1:376–86. https://doi.org/10.1074/mcp.M200025-MCP200.

[115] Hoedt E, Zhang G, Neubert TA. Stable Isotope Labeling by Amino Acids in Cell Culture (SILAC) for Quantitative Proteomics. Adv Exp Med Biol 2019;1140:531–9. https://doi.org/10.1007/978-3-030-15950-4_31.
[116] Bantscheff M, Schirle M, Sweetman G, Rick J, Kuster B. Quantitative mass spectrometry in proteomics: a critical review. Anal Bioanal Chem 2007;389:1017–31. https://doi.org/10.1007/S00216-007-1486-6.
[117] Li J, Cai Z, Bomgarden RD, Pike I, Kuhn K, Rogers JC, et al. TMTpro-18plex: The Expanded and Complete Set of TMTpro Reagents for Sample Multiplexing. J Proteome Res 2021;20:2964–72.
[118] McAlister GC, Huttlin EL, Haas W, Ting L, Jedrychowski MP, Rogers JC, et al. Increasing the multiplexing capacity of TMTs using reporter ion isotopologues with isobaric masses. Anal Chem 2012;84:7469–78. https://doi.org/10.1021/AC301572T.
[119] Werner T, Becher I, Sweetman G, Doce C, Savitski MM, Bantscheff M. High-resolution enabled TMT 8-plexing. Anal Chem 2012;84:7188–94.
[120] Werner T, Sweetman G, Savitski MF, Mathieson T, Bantscheff M, Savitski MM. Ion coalescence of neutron encoded TMT 10-plex reporter ions. Anal Chem 2014;86:3594–601.
[121] Savitski MM, Mathieson T, Zinn N, Sweetman G, Doce C, Becher I, et al. Measuring and managing ratio compression for accurate iTRAQ/TMT quantification. J Proteome Res 2013;12:3586–98.
[122] Karp NA, Huber W, Sadowski PG, Charles PD, Hester S V., Lilley KS. Addressing accuracy and precision issues in iTRAQ quantitation. Molecular and Cellular Proteomics 2010;9:1885–97. https://doi.org/10.1074/mcp.M900628-MCP200.
[123] Sun D, Gao W, Hu H, Zhou S. Why 90% of clinical drug development fails and how to improve it? Acta Pharm Sin B 2022;12:3049–62. https://doi.org/10.1016/j.apsb.2022.02.002.
[124] Lee J, Bogyo M. Target deconvolution techniques in modern phenotypic profiling. Curr Opin Chem Biol 2013;17:118–26. https://doi.org/10.1016/J.CBPA.2012.12.022.
[125] Schenone M, Dančík V, Wagner BK, Clemons PA. Target identification and mechanism of action in chemical biology and drug discovery. Nat Chem Biol 2013;9:232–40. https://doi.org/10.1038/nchembio.1199.
[126] Miethke M, Pieroni M, Weber T, Brönstrup M, Hammann P, Halby L, et al. Towards the sustainable discovery and development of new antibiotics. Nat Rev Chem 2021;5:726–49. https://doi.org/10.1038/s41570-021-00313-1.
[127] Tommasi R, Brown DG, Walkup GK, Manchester JI, Miller AA. ESKAPEing the labyrinth of antibacterial discovery. Nat Rev Drug Discov 2015;14:529–42. https://doi.org/10.1038/nrd4572.
[128] Farha MA, Brown ED. Strategies for target identification of antimicrobial natural products. Nat Prod Rep 2016;33:668–80. https://doi.org/10.1039/C5NP00127G.
[129] Terstappen GC, Schlüpen C, Raggiaschi R, Gaviraghi G. Target deconvolution strategies in drug discovery. Nat Rev Drug Discov 2007;6:891–903. https://doi.org/10.1038/nrd2410.
[130] Siqueira-Neto JL, Wicht KJ, Chibale K, Burrows JN, Fidock DA, Winzeler EA. Antimalarial drug discovery: progress and approaches. Nature Reviews Drug Discovery 2023 22:10 2023;22:807–26. https://doi.org/10.1038/s41573-023-00772-9.
[131] Chughlay MF, El Gaaloul M, Donini C, Campo B, Berghmans PJ, Lucardie A, et al. Chemoprotective Antimalarial Activity of P218 against Plasmodium falciparum: A Randomized, Placebo-Controlled Volunteer Infection Study. Am J Trop Med Hyg 2021;104:1348. https://doi.org/10.4269/AJTMH.20-1165.
[132] Agarwal A, Paliwal S, Mishra R, Sharma S, Kumar Dwivedi A, Tripathi R, et al. Discovery of a selective, safe and novel anti-malarial compound with activity against chloroquine resistant strain of Plasmodium falciparum. Sci Rep 2015;5:1–8. https://doi.org/10.1038/srep13838.
[133] Pavadai E, El Mazouni F, Wittlin S, De Kock C, Phillips MA, Chibale K. Identification of New Human Malaria Parasite Plasmodium falciparum Dihydroorotate Dehydrogenase Inhibitors by Pharmacophore and Structure-Based Virtual Screening. J Chem Inf Model 2016;56:548–62.
[134] Uddin A, Gupta S, Mohammad T, Shahi D, Hussain A, Alajmi MF, et al. Target-Based Virtual Screening of Natural Compounds Identifies a Potent Antimalarial With Selective Falcipain-2 Inhibitory Activity. Front Pharmacol 2022;13:850176.
[135] Dascombe MJ, Drew MGB, Morris H, Wilairat P, Auparakkitanon S, Moule WA, et al. Mapping antimalarial pharmacophores as a useful tool for the rapid discovery of drugs effective in vivo: Design, construction, characterization, and pharmacology of metaquine. J Med Chem 2005;48:5423–36.
[136] de Sousa ACC, Combrinck JM, Maepa K, Egan TJ. Virtual screening as a tool to discover new β-haematin inhibitors with activity against malaria parasites. Sci Rep 2020;10:1–10. https://doi.org/10.1038/s41598-020-60221-0.
[137] Ruggeri C, Drinkwater N, Sivaraman KK, Bamert RS, McGowan S, Paiardini A. Identification and Validation of a Potent Dual Inhibitor of the P. falciparum M1 and M17 Aminopeptidases Using Virtual Screening. PLoS One 2015;10:e0138957. https://doi.org/10.1371/JOURNAL.PONE.0138957.
[138] Fishman MC, Porter JA. A new grammar for drug discovery. Nature 2005;437:491–3. https://doi.org/10.1038/437491a.
[139] Mak PA, Rao SPS, Ping Tan M, Lin X, Chyba J, Tay J, et al. A high-throughput screen to identify inhibitors of ATP homeostasis in non-replicating mycobacterium tuberculosis. ACS Chem Biol 2012;7:1190–7.
[140] Hudson MA, Lockless SW. Elucidating the Mechanisms of Action of Antimicrobial Agents. MBio 2022;13:1–9. https://doi.org/10.1128/mbio.02240-21.
[141] Telenti A, Imboden P, Marchesi F, Matter L, Schopfer K, Bodmer T, et al. Detection of rifampicin-resistance mutations in Mycobacterium tuberculosis. The Lancet 1993;341:647–51. https://doi.org/10.1016/0140-6736(93)90417-F.
[142] Fujimoto-Nakamura M, Ito H, Oyamada Y, Nishino T, Yamagishi JI. Accumulation of mutations in both gyrB and parE genes is associated with high-level resistance to novobiocin in Staphylococcus aureus. Antimicrob Agents Chemother 2005;49:3810–5.
[143] Andries K, Verhasselt P, Guillemont J, Göhlmann HWH, Neefs JM, Winkler H, et al. A diarylquinoline drug active on the ATP synthase of Mycobacterium tuberculosis. Science (1979) 2005;307:223–7.

[144] Metzker ML. Sequencing technologies — the next generation. Nat Rev Genet 2009;11:31–46. https://doi.org/10.1038/nrg2626.
[145] Hartkoorn RC, Sala C, Neres J, Pojer F, Magnet S, Mukherjee R, et al. Towards a new tuberculosis drug: pyridomycin - nature's isoniazid. EMBO Mol Med 2012;4:1032–42. https://doi.org/10.1002/EMMM.201201689.
[146] Schalkwijk J, Allman EL, Jansen PAM, De Vries LE, Verhoef JMJ, Jackowski S, et al. Antimalarial pantothenamide metabolites target acetyl-coenzyme A biosynthesis in Plasmodium falciparum. Sci Transl Med 2019;11:9917.
[147] Summers RL, Pasaje CFA, Pisco JP, Striepen J, Luth MR, Kumpornsin K, et al. Chemogenomics identifies acetyl-coenzyme A synthetase as a target for malaria treatment and prevention. Cell Chem Biol 2022;29:191-201.e8. https://doi.org/10.1016/j.chembiol.2021.07.010.
[148] Nikaido H. Preventing drug access to targets: cell surface permeability barriers and active efflux in bacteria. Semin Cell Dev Biol 2001;12:215–23. https://doi.org/10.1006/SCDB.2000.0247.
[149] Marcusson LL, Frimodt-Møller N, Hughes D. Interplay in the Selection of Fluoroquinolone Resistance and Bacterial Fitness. PLoS Pathog 2009;5:e1000541. https://doi.org/10.1371/JOURNAL.PPAT.1000541.
[150] Grzesiuk E, Janion C. Some aspects of EMS-induced mutagenesis in Escherichia coli. Mutation Research/Reviews in Genetic Toxicology 1993;297:313–21. https://doi.org/10.1016/0165-1110(93)90022-F.
[151] Ljosa V, Caie PD, Ter Horst R, Sokolnicki KL, Jenkins EL, Daya S, et al. Comparison of methods for image-based profiling of cellular morphological responses to small-molecule treatment. J Biomol Screen 2013;18:1321–9. https://doi.org/10.1177/1087057113503553.
[152] Canepari P, Boaretti M, Del Mar Lleo M, Satta G. Lipoteichoic acid as a new target for activity of antibiotics: mode of action of daptomycin (LY146032). Antimicrob Agents Chemother 1990;34:1220–6. https://doi.org/10.1128/AAC.34.6.1220.
[153] Oliva B, Maiese WM, Greenstein M, Borders DB, Chopra I. Mode of action of the cyclic depsipeptide antibiotic LL-AO341 beta 1 and partial characterization of a Staphylococcus aureus mutant resistant to the antibiotic. J Antimicrob Chemother 1993;32:817–30. https://doi.org/10.1093/JAC/32.6.817.
[154] Singh MP, Petersen PJ, Jacobus N V., Maiese WM, Greenstein M, Steinberg DA. Mechanistic studies and biological activity of bioxalomycin alpha 2, a novel antibiotic produced by Streptomyces viridodiastaticus subsp. "litoralis" LL-31F508. Antimicrob Agents Chemother 1994;38:1808. https://doi.org/10.1128/AAC.38.8.1808.
[155] Fanti RC, Vasconcelos SNS, Catta-Preta CMC, Sullivan JR, Riboldi GP, Dos Reis C V., et al. A Target Engagement Assay to Assess Uptake, Potency, and Retention of Antibiotics in Living Bacteria. ACS Infect Dis 2022;8:1449–67. https://doi.org/10.1021/acsinfecdis.2c00073.
[156] Bantscheff M, Drewes G. Chemoproteomic approaches to drug target identification and drug profiling. Bioorg Med Chem 2012;20:1973–8. https://doi.org/10.1016/J.BMC.2011.11.003.
[157] Jones LH, Neubert H. Clinical chemoproteomics—Opportunities and obstacles. Sci Transl Med 2017;9. https://doi.org/10.1126/SCITRANSLMED.AAF7951.
[158] Niphakis MJ, Cravatt BF. Ligand discovery by activity-based protein profiling. Cell Chem Biol 2024;31:1636–51. https://doi.org/10.1016/J.CHEMBIOL.2024.08.006.
[159] Krysiak J, Sieber SA. Activity-based protein profiling in bacteria. Methods in Molecular Biology, vol. 1491, Humana Press Inc.; 2017, p. 57–74. https://doi.org/10.1007/978-1-4939-6439-0_5.
[160] Sharifzadeh S, Shirley JD, Carlson EE. Activity-based protein profiling methods to study bacteria: The power of small-molecule electrophiles. Curr Top Microbiol Immunol, vol. 420, Springer Verlag; 2019, p. 23–48. https://doi.org/10.1007/82_2018_135.
[161] Keller LJ, Babin BM, Lakemeyer M, Bogyo M. Activity-based protein profiling in bacteria: Applications for identification of therapeutic targets and characterization of microbial communities. Curr Opin Chem Biol 2020;54:45–53. https://doi.org/10.1016/j.cbpa.2019.10.007.
[162] Rostovtsev V V., Green LG, Fokin V V., Sharpless KB. A Stepwise Huisgen Cycloaddition Process: Copper(I)-Catalyzed Regioselective "Ligation" of Azides and Terminal Alkynes. Angewandte Chemie International Edition 2002;41:2596–9. https://doi.org/10.1002/1521-3773(20020715)41:14<2596::AID-ANIE2596>3.0.CO;2-4.
[163] Sadaghiani AM, Verhelst SH, Bogyo M. Tagging and detection strategies for activity-based proteomics. Curr Opin Chem Biol 2007;11:20–8. https://doi.org/10.1016/J.CBPA.2006.11.030.
[164] Weerapana E, Wang C, Simon GM, Richter F, Khare S, Dillon MBD, et al. Quantitative reactivity profiling predicts functional cysteines in proteomes. Nature 2010;468:790–5. https://doi.org/10.1038/nature09472.
[165] Hacker SM, Backus KM, Lazear MR, Forli S, Correia BE, Cravatt BF. Global profiling of lysine reactivity and ligandability in the human proteome. Nat Chem 2017;9:1181–90. https://doi.org/10.1038/nchem.2826.
[166] Bak DW, Bechtel TJ, Falco JA, Weerapana E. Cysteine reactivity across the subcellular universe. Curr Opin Chem Biol 2019;48:96–105. https://doi.org/10.1016/J.CBPA.2018.11.002.
[167] Deng X, Weerapana E, Ulanovskaya O, Sun F, Liang H, Ji Q, et al. Proteome-wide quantification and characterization of oxidation-sensitive cysteines in pathogenic bacteria. Cell Host Microbe 2013;13:358. https://doi.org/10.1016/J.CHOM.2013.02.004.
[168] Li Z, Hao P, Li L, Tan CYJ, Cheng X, Chen GYJ, et al. Design and synthesis of minimalist terminal alkyne-containing diazirine photo-crosslinkers and their incorporation into kinase inhibitors for cell- and tissue-based proteome profiling. Angewandte Chemie - International Edition 2013;52:8551–6. https://doi.org/10.1002/anie.201300683.
[169] Homan RA, Lapek JD, Woo CM, Niessen S, Jones LH, Parker CG. Photoaffinity labelling with small molecules. Nature Reviews Methods Primers 2024;4:30. https://doi.org/10.1038/s43586-024-00308-4.
[170] Eirich J, Orth R, Sieber SA. Unraveling the protein targets of vancomycin in living S. aureus and E. faecalis cells. J Am Chem Soc 2011;133:12144–53.

[171] Sinha Roy R, Yang P, Kodali S, Xiong Y, Kim RM, Griffin PR, et al. Direct interaction of a vancomycin derivative with bacterial enzymes involved in cell wall biosynthesis. Chem Biol 2001;8:1095–106. https://doi.org/10.1016/S1074-5521(01)00075-8.
[172] Blumberg PM, Strominger JL. Isolation by Covalent Affinity Chromatography of the Penicillin-Binding Components from Membranes of Bacillus subtilis. Proceedings of the National Academy of Sciences 1972;69:3751–5. https://doi.org/10.1073/PNAS.69.12.3751.
[173] Sheldrick GM, Jones PG, Kennard O, Williams DH, Smith GA. Structure of vancomycin and its complex with acetyl-D-alanyl-D-alanine. Nature 1978;271:223–5. https://doi.org/10.1038/271223a0.
[174] Sinha Roy R, Yang P, Kodali S, Xiong Y, Kim RM, Griffin PR, et al. Direct interaction of a vancomycin derivative with bacterial enzymes involved in cell wall biosynthesis. Chem Biol 2001;8:1095–106. https://doi.org/10.1016/S1074-5521(01)00075-8.
[175] Tabana Y, Babu D, Fahlman R, Siraki AG, Barakat K. Target identification of small molecules: an overview of the current applications in drug discovery. BMC Biotechnol 2023;23:1–19. https://doi.org/10.1186/s12896-023-00815-4.
[176] Molina DM, Jafari R, Ignatushchenko M, Seki T, Larsson EA, Dan C, et al. Monitoring drug target engagement in cells and tissues using the cellular thermal shift assay. Science (1979) 2013;341:84–7. https://doi.org/10.1126/science.1233606.
[177] Jafari R, Almqvist H, Axelsson H, Ignatushchenko M, Lundbäck T, Nordlund P, et al. The cellular thermal shift assay for evaluating drug target interactions in cells. Nat Protoc 2014;9:2100–22. https://doi.org/10.1038/nprot.2014.138.
[178] Pantoliano MW, Petrella EC, Kwasnoski JD, Lobanov VS, Myslik J, Graf E, et al. High-density miniaturized thermal shift assays as a general strategy for drug discovery. J Biomol Screen 2001;6:429–40. https://doi.org/10.1177/108705710100600609.
[179] Savitski MM, Reinhard FBM, Franken H, Werner T, Savitski MF, Eberhard D, et al. Tracking cancer drugs in living cells by thermal profiling of the proteome. Science (1979) 2014;346. https://doi.org/10.1126/science.1255784.
[180] Franken H, Mathieson T, Childs D, Sweetman GMA, Werner T, Tögel I, et al. Thermal proteome profiling for unbiased identification of direct and indirect drug targets using multiplexed quantitative mass spectrometry. Nat Protoc 2015;10:1567–93. https://doi.org/10.1038/nprot.2015.101.
[181] Savitski MM, Zinn N, Faelth-Savitski M, Poeckel D, Gade S, Becher I, et al. Multiplexed Proteome Dynamics Profiling Reveals Mechanisms Controlling Protein Homeostasis. Cell 2018;173:260-274.e25. https://doi.org/10.1016/j.cell.2018.02.030.
[182] Reinhard FBM, Eberhard D, Werner T, Franken H, Childs D, Doce C, et al. Thermal proteome profiling monitors ligand interactions with cellular membrane proteins. Nat Methods 2015;12:1129–31. https://doi.org/10.1038/nmeth.3652.
[183] Becher I, Andrés-Pons A, Romanov N, Stein F, Schramm M, Baudin F, et al. Pervasive Protein Thermal Stability Variation during the Cell Cycle. Cell 2018;173:1495-1507.e18. https://doi.org/10.1016/J.CELL.2018.03.053.
[184] Mateus A, Bobonis J, Kurzawa N, Stein F, Helm D, Hevler J, et al. Thermal proteome profiling in bacteria: probing protein state in vivo. Mol Syst Biol 2018;14. https://doi.org/10.15252/msb.20188242.
[185] Dobrescu I, Hammam E, Dziekan JM, Claës A, Halby L, Preiser P, et al. Plasmodium falciparum Eukaryotic Translation Initiation Factor 3 is Stabilized by Quinazoline-Quinoline Bisubstrate Inhibitors. ACS Infect Dis 2023;9:1257–66.
[186] Mateus A, Kurzawa N, Becher I, Sridharan S, Helm D, Stein F, et al. Thermal proteome profiling for interrogating protein interactions. Mol Syst Biol 2020;16:e9232. https://doi.org/10.15252/msb.20199232.
[187] Tan CSH, Go KD, Bisteau X, Dai L, Yong CH, Prabhu N, et al. Thermal proximity coaggregation for system-wide profiling of protein complex dynamics in cells. Science (1979) 2018;359:1170–7. https://doi.org/10.1126/science.aan0346.
[188] Becher I, Werner T, Doce C, Zaal EA, Tögel I, Khan CA, et al. Thermal profiling reveals phenylalanine hydroxylase as an off-target of panobinostat. Nat Chem Biol 2016;12:908–10. https://doi.org/10.1038/nchembio.2185.
[189] Gaetani M, Sabatier P, Saei AA, Beusch CM, Yang Z, Lundström SL, et al. Proteome Integral Solubility Alteration: A High-Throughput Proteomics Assay for Target Deconvolution. J Proteome Res 2019;18:4027–37. https://doi.org/10.1021/acs.jproteome.9b00500.
[190] Van Vranken JG, Li J, Mintseris J, Gadzuk-Shea M, Gygi SP, Schweppe DK. Large-scale characterization of drug mechanism of action using proteome-wide thermal shift assays. Elife 2024. https://doi.org/10.7554/eLife.95595.1.
[191] Figueroa-Navedo AM, Ivanov AR. Experimental and data analysis advances in thermal proteome profiling. Cell Reports Methods 2024;4:100717. https://doi.org/10.1016/J.CRMETH.2024.100717.
[192] Peng H, Guo H, Pogoutse O, Wan C, Hu LZ, Ni Z, et al. An Unbiased Chemical Proteomics Method Identifies FabI as the Primary Target of 6-OH-BDE-47. Environ Sci Technol 2016;50:11329–36.
[193] Schopper S, Kahraman A, Leuenberger P, Feng Y, Piazza I, Müller O, et al. Measuring protein structural changes on a proteome-wide scale using limited proteolysis-coupled mass spectrometry. Nat Protoc 2017;12:2391–410. https://doi.org/10.1038/nprot.2017.100.
[194] Piazza I, Kochanowski K, Cappelletti V, Fuhrer T, Noor E, Sauer U, et al. A Map of Protein-Metabolite Interactions Reveals Principles of Chemical Communication. Cell 2018;172:358-372.e23. https://doi.org/10.1016/J.CELL.2017.12.006.
[195] Peng H, Guo H, Pogoutse O, Wan C, Hu LZ, Ni Z, et al. An Unbiased Chemical Proteomics Method Identifies FabI as the Primary Target of 6-OH-BDE-47. Environ Sci Technol 2016;50:11329–36.
[196] Leuenberger P, Ganscha S, Kahraman A, Cappelletti V, Boersema PJ, Von Mering C, et al. Cell-wide analysis of protein thermal unfolding reveals determinants of thermostability. Science (1979) 2017;355. https://doi.org/10.1126/SCIENCE.AAI7825.
[197] Strickland EC, Geer MA, Tran DT, Adhikari J, West GM, Dearmond PD, et al. Thermodynamic analysis of protein-ligand binding interactions in complex biological mixtures using the stability of proteins from rates of oxidation. Nat Protoc 2013;8:148–61. https://doi.org/10.1038/NPROT.2012.146.

[198] Cornwell O, Ault JR. Fast photochemical oxidation of proteins coupled with mass spectrometry. Biochimica et Biophysica Acta (BBA) - Proteins and Proteomics 2022;1870:140829. https://doi.org/10.1016/J.BBAPAP.2022.140829.
[199] Johnson DT, Di Stefano LH, Jones LM. Fast photochemical oxidation of proteins (FPOP): A powerful mass spectrometry–based structural proteomics tool. Journal of Biological Chemistry 2019;294:11969–79. https://doi.org/10.1074/JBC.REV119.006218.
[200] Zhang X, Wang Q, Li Y, Ruan C, Wang S, Hu L, et al. Solvent-Induced Protein Precipitation for Drug Target Discovery on the Proteomic Scale. Anal Chem 2020;92:1363–71. https://doi.org/10.1021/acs.analchem.9b04531.
[201] Van Vranken JG, Li J, Mitchell DC, Navarrete-Perea J, Gygi SP. Assessing target engagement using proteome-wide solvent shift assays. Elife 2021;10:1–21. https://doi.org/10.7554/eLife.70784.
[202] Yu C, Chen X, Xu W, Li S, Chai Q, Zhang Y. Solvent-induced proteome profiling for proteomic quantitation and target discovery of small molecular drugs. Proteomics 2023:1–10. https://doi.org/10.1002/pmic.202200281.
[203] Yimer SA, Birhanu AG, Kalayou S, Riaz T, Zegeye ED, Beyene GT, et al. Comparative proteomic analysis of Mycobacterium tuberculosis lineage 7 and lineage 4 strains reveals differentially abundant proteins linked to slow growth and virulence. Front Microbiol 2017;8:1–14. https://doi.org/10.3389/fmicb.2017.00795.
[204] Grangeasse C, Nessler S, Mijakovic I. Bacterial tyrosine kinases: Evolution, biological function and structural insights. Philosophical Transactions of the Royal Society B: Biological Sciences 2012;367:2640–55. https://doi.org/10.1098/rstb.2011.0424.
[205] Cimmperman P, Baranauskiene L, Jachimovičiute S, Jachno J, Torresan J, Michailoviene V, et al. A quantitative model of thermal stabilization and destabilization of proteins by ligands. Biophys J 2008;95:3222–31. https://doi.org/10.1529/biophysj.108.134973.